

# **On selective formation and transformation of amorphous solid and hydrate crystals**

Dissertation  
zur Erlangung des  
Doktorgrades der Ingenieurwissenschaften (Dr.-Ing.)  
der  
Naturwissenschaftlichen Fakultät I – Biowissenschaften –

der Martin-Luther-Universität  
Halle-Wittenberg,

vorgelegt  
von Herrn M.Sc. Jungsuk Kim  
geb. am 23. Juli 1986 in Daejeon, Süd Korea

Gutachter:

Prof. Dr.-Ing. habil. Dr. h.c. Joachim Ulrich

Prof. Dr.-Ing. René Androsch

Prof. Dr.-Ing. Ulrich Teipel

Datum der öffentlichen Verteidigung:

01.08.2023

## Acknowledgement

This Ph.D. study has been defended at Martin-Luther-University Halle-Wittenberg, Germany.

It was an infinite honor to study under the guidance of Professor Dr. Joachim Ulrich, who is world-renowned in the field of industrial crystallization. I am grateful for his enthusiasm for research, patience, advice and warm teaching. All of these motivated me to pursue a Ph.D. under his guidance. The support and encouragement he gave me will never be forgotten.

I wish to thank the referees of the thesis, Prof. Dr. Ulrich Teipel and Prof. Dr. Rene Androsch for a positive evaluation of the thesis. I would like to express my thanks to Prof. Dr. Milton Stubbs, Chairman of the doctoral promotion committee for his warm advice. I would also thank committee members, Prof. Dr. Jörg Kressler, PD Dr. Hauke Lilie, PD Dr. Annette Meister and Prof. Dr. Elke Hartmann for their valuable comments.

Also, I would like to thank Prof. Dr. K. J. Kim of the National Crystallization Research Laboratory for always supporting me to conduct experiments and analysis. I wish to thank the members of the TVT laboratory and the national crystallization laboratory for their support and assistance. Especially, I would like to give my special thanks to Frau Ulrich, who made me feel at home through her support and kindness, during my stay in Germany. I am very grateful to my colleagues and friends who always encourage me. In particular, I give thanks to Jeonghyeon, Jonggeol, Hyunseok, Jinyong, Sangwoo, and Hanmin for being friends while studying.

I was able to complete this thesis because of my family. I was able to overcome many difficulties with the support, patience and sacrifice of my parents and parents-in-law. My special gratitude goes to them. I would like to thank you Jungwon and Seong-Min for their support. I am also grateful to my brother-in-law and his wife. And I thank you grandparents for encouraging me. Above all, my beloved wife Bong-Sun, my sons Taeyool, and Doyool were a great source of strength for me throughout my studies. Without their love, patience and understanding, this study would not have been possible. I will become a wonderful husband and a perfect father. I would like to share this thesis with them.

Halle, August 2023

Jungsuk Kim

---

# Table of Content

<b>Acknowledgement .....</b>	<b>I</b>
<b>Table of Content .....</b>	<b>II</b>
<b>1. Introduction .....</b>	<b>1</b>
<b>2. State of Art .....</b>	<b>3</b>
<b>2.1 Phase Transformation.....</b>	<b>3</b>
<b>2.2 Crystallization of Polymorphs .....</b>	<b>4</b>
<b>2.3 Thermodynamics of Polymorph (or Solvate) Crystallization .....</b>	<b>8</b>
2.3.1 Thermodynamics of Phase Selection.....	8
2.3.2 Thermodynamic and Kinetic Factors of Polymorph (or Solvate) Crystallization.....	9
<b>2.4 Phase Transitions of Metastable Phases.....</b>	<b>10</b>
<b>2.5 Kinetics of Solution- and Liquid-Mediated Phase Transformation .....</b>	<b>12</b>
<b>2.6 Supersaturation and Nucleation .....</b>	<b>13</b>
2.6.1 Supersaturation and Metastable Zone Limit.....	13
2.6.2 Nucleation.....	15
<b>2.7 Transformation Kinetics by Dissolution and Growth .....</b>	<b>16</b>
<b>2.8 Substance Investigated .....</b>	<b>20</b>
<b>3. Motivation and Aim of Thesis .....</b>	<b>23</b>
<b>3.1 Motivation.....</b>	<b>23</b>
<b>3.2 Aim of Thesis .....</b>	<b>24</b>
<b>4. Materials and Methods.....</b>	<b>25</b>
<b>4.1 Materials .....</b>	<b>25</b>
4.1.1 Raw Materials and Solvents .....	25
4.1.2 Preparation of Amorphous GMP .....	25
4.1.3 Preparation of Tetrahydrate and Heptahydrate .....	25
<b>4.2 Methods.....</b>	<b>25</b>

---

4.2.1 Solubility Measurement Method .....	25
4.2.2 Crystallization Method .....	27
<b>4.3 Instrumental Analysis Methods .....</b>	<b>28</b>
4.3.1 Raman Spectroscopy .....	28
4.3.2 X-Ray Powder Diffraction.....	28
4.3.3 Focused Beam Reflectance Measurement.....	28
4.3.4 Particle Video Microscope.....	28
4.3.5 Thermal Analysis .....	29
4.3.6 Viscosity Measurement.....	29
<b>4.4 Calibration and Identification .....</b>	<b>29</b>
4.4.1 Characterization of Materials .....	29
4.4.2 Calibration and Analysis of Raman Spectroscopic Data .....	33
4.4.3 Calibration of Solution and Solid Concentrations.....	34
<b>4.5 Measuring Concentration of Solid Forms .....</b>	<b>37</b>
<b>5. Results .....</b>	<b>40</b>
<b>5.1 Solubilities and Metastable Zone Width of Solid Forms.....</b>	<b>40</b>
5.1.1 Solubilities of Solid Forms .....	40
5.1.2 Enthalpy and Entropy of Dissolution .....	42
5.1.3 Supersaturation and Metastable Zone Width.....	44
<b>5.2 Finding Conditions for Selective Formation of Solid Forms .....</b>	<b>46</b>
5.2.1 Selective Formation .....	46
5.2.2 Case study for Amorphous to Heptahydrate Transformation .....	48
5.2.3 Case Study for Heptahydrate to Tetrahydrate Transformation .....	49
5.2.4 Case Study for Tetrahydrate to Heptahydrate Transformation .....	51
<b>5.3 Nucleation in Anti-Solvent Crystallization .....</b>	<b>53</b>
5.3.1 Amorphous Formation and Transformation .....	53
5.3.2 Phase Transformation by Anti-solvent Crystallization.....	56
<b>5.4 Growth and Dissolution Kinetic and Rate Controlling Step .....</b>	<b>59</b>
5.4.1 Metastable Zone Limits for Amorphous and Heptahydrate Forms .....	59
5.4.2 Rate-Controlling Step of Phase Transformation.....	61
5.4.3 Data Analysis of Dissolution and Growth Kinetics.....	64
5.4.4 Calculation of Kinetic Parameters .....	67
5.4.5 Changes in Particle Number, Particle Size, and Particle Size Distribution.....	69
<b>6. Discussion.....</b>	<b>74</b>
<b>6.1 Solubility and Maximum Supersaturation .....</b>	<b>74</b>

---

6.1.1 Effect of the Solvent Fraction on the Maximum Supersaturation .....	74
6.1.2 Solubilities and Maximum Supersaturation of Solid Forms .....	76
<b>6.2 Finding Conditions of Phase Transformation .....</b>	<b>78</b>
6.2.1 Amorphous–Heptahydrate Transformation .....	78
6.2.2 Tetrahydrate–Heptahydrate Transformation .....	78
6.2.3 Heptahydrate–Tetrahydrate Transformation .....	79
6.2.4 Selective Preparation of Amorphous, Heptahydrate, and Tetrahydrate without Transformation .....	80
6.2.5 Effect of Anti-solvent Adding Rate .....	81
<b>6.3 Nucleation Study on Phase Transformation .....</b>	<b>84</b>
6.3.1 Metastable Zone Width and Supersaturation .....	84
6.3.2 Effect of the Initial Concentration .....	86
6.3.3 Effect of Methanol Fraction.....	90
6.3.4 Effect of the Addition Rate .....	92
6.3.5 Screening of Solid Forms and the Kinetic Effect on Transformation .....	93
<b>6.4 Dissolution, Growth Kinetics and Controlling Step .....</b>	<b>97</b>
6.4.1 Effect of Operating Parameters .....	97
6.4.2 Effect of Slurry Viscosity on Rate-Controlling Step .....	99
6.4.3 Model Presentation .....	104
<b>6.5 Summary of Results.....</b>	<b>106</b>
<b>7. Summary .....</b>	<b>112</b>
<b>8. Abbreviations, Symbols and Units.....</b>	<b>114</b>
<b>9. References .....</b>	<b>116</b>
<b>10. Appendix .....</b>	<b>126</b>
<b>Statement of Authorship.....</b>	<b>142</b>
<b>Curriculum Vitae .....</b>	<b>143</b>
<b>Publications.....</b>	<b>144</b>

## 1. Introduction

Different polymorphic or solvate forms of crystalline materials often show differences in physicochemical properties, such as, hygroscopicity, solubility, surface chemistry, stability, and processability [Bec01]. Selective manufacturing of desired products of polymorphs or solvates has been important problems in the chemical and pharmaceutical sectors for over a century. Thermodynamically, amorphous solids provide higher solubility and higher dissolution rates compared to crystalline forms. However, amorphous forms are often not wanted as they are not stable and can be transformed into crystalline forms during drying, processing, storage, or dissolution [Bab11,Pok06]. Hydrates, solvates with water can be described in terms of the stoichiometric ratio of water molecules to host molecules. They are either stoichiometric or non-stoichiometric [Tie16]. In general, amorphous and crystalline forms of a substance exhibit different physical properties such as compressibility, melting point, bioavailability and solubility, which can greatly affect the performance of the material thereafter [Kan15]. Therefore, it is important to control the manufacturing process to produce selectively the desired solid forms. Fig. 1-1 shows a classification scheme for the solid forms [Cui07,Ulr15,Hea17].

Solid forms can be classified as crystalline and amorphous forms according to the order of molecular packing. Long-range order in crystalline forms refers to the regularity or periodicity in which hundreds or thousands of molecules first assemble via neighbours (short ranges) and then propagate over perceivable distances to form phases [Ulr15]. On the other hand, the amorphous form presents only short-range order in molecular packing and no long-range order. Short-range order here refers to the way neighboring molecules sit next to each other (molecular coordination). As shown in Fig. 1-1, crystalline solids can also exist in several subphases such as polymorphs, solvates (or hydrates) and co-crystals [Cui07,Ulr15,Hea17]. Because of the different arrangements of molecular packing, polymorphs have different crystalline lattices of the same chemical substance (at different free energy states). On the other hand, solvates/hydrates and co-crystals are similar in that they all consist of more than one chemical substances. All types of chemical substances (main substance and the other) participate in the short-range and long-range order of one single crystal form, and the stoichiometric ratios between the involved substances and their coordination in these crystal forms are often highly ordered. Preparing crystalline forms from amorphous materials is difficult due to the potential for a selective formation and transformation of different solid forms.

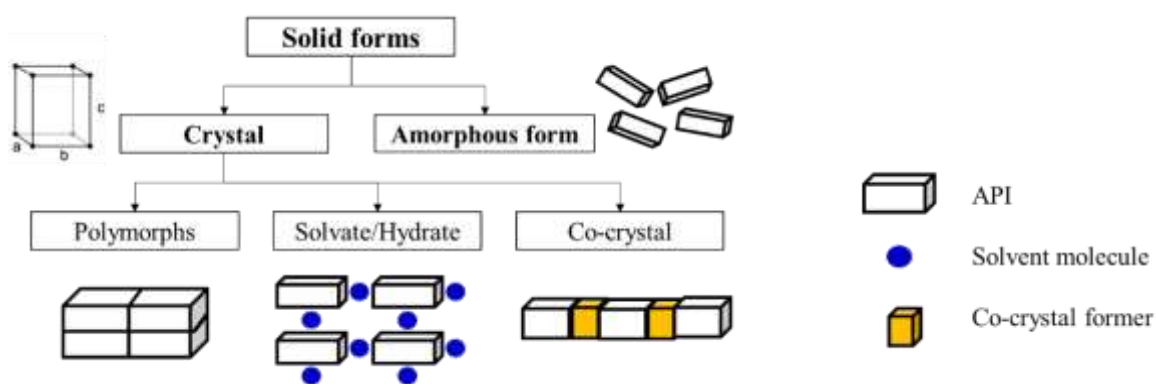


Fig. 1-1: Classification scheme for the solid forms [Ulr15].

The physical stability of a solid phase depends on the thermodynamic conditions (temperature, pressure, and concentration). One solid phase has the least free energy at any given condition. The molecular arrangement in crystals frequently influenced by the kinetic determines the functionality and properties (e.g. dissolution rate, morphology and purity) of many kinds of materials [Kit09]. Therefore, in order to obtain highly functional products in the industrial sector, advanced control technology for crystallization of polymorph (or solvated) crystals is required. Compounds in various solid-state forms, crystalline or amorphous, offer unique challenges in product development and manufacturing. In many cases metastable forms are not adopted because they are susceptible to transformation into more thermodynamically stable forms [Rod99, Kim15].

The theoretical studies on the transformation kinetics related to dissolution and growth and the formation of stable and unstable forms without transformation are necessary. It should be possible to crystallize the pure product in the desired polymorph (or solvate). The selective crystallization of polymorphs (or solvates) has been investigated by only a few researchers [Kit09, Jin10, Kim15], and supersaturation, solvent and temperature are known to be important. There is, however, little theoretical framework regarding the effects of these factors. Although theoretical considerations of the effect of supersaturation have been proposed [Car85], the theory fails to explain some observations for polymorph crystallization. The effect of supersaturation has been described by Ostwald's law of stages [Ost97]. This explains the spontaneous change from a metastable form to a stable form, but lacks a theoretical basis for the selectivity of the crystalline form. Since supersaturation affects the metastability of the phase, various types of polymorphs (or solvates) can be explored therefrom.

Previous studies on the selective manufacturing of solid forms depends on laboratory control of operating parameters and process analytical techniques [Her12, Mah14, Yan20, Hei12]. However, theoretical work on selection of solid forms is relatively rare. The screenings of solid form are a challenging task. The solubility of each polymorph is not the operational factor, however, the supersaturation of each polymorph is based on the solubility. Based on a selected case study of GMP (disodium guanosine 5'-monophosphate), the kinetic and thermodynamic properties of the selective formation and transformation from the amorphous form to the crystalline hydrate forms are systemically highlighted.

## 2. State of Art

### 2.1 Phase Transformation

Generally, the mechanisms of phase transformation are divided into solid state and solution state (Tab. 2-1). Solid state transformation can cause a polymorphic transformation, solvation/ and crystallization of amorphous solids during processing, storage, and preparation [Zha04]. Solution state transformation, as crystallization of polymorph takes place in solution, polymorphic transformation often occurs according to Ostwald's rule of stages [Ost97], whereby the metastable form is transformed into the stable form. It considers selective separation, co-crystal preparation, crystallization conditions, polymorph screening and polymorph crystallization.

**Tab. 2-1: History of phase transformations**

Year	States	Materials	Operation method	Solid form control
2002	Solid state	Caffeine	Wet granulation	Hydration [Jor02]
2004	Solid state	Carbamazepine	Process-induced phase transition (heating)	Anhydrate-dihydrate [Zha04]
2006	Solid state	Indomethacin	Surface crystallization	Amorphous formation [Wu06]
2007	Solid state	Chlorpropamide	Sheer-based	Polymorph [Wil06]
2010	Solid state	Astaxanthin	Thermal treatment	Polymorph transformation [Guo10]
2013	Solid state	Felodipine	Melt quenching	Amorphous formation [Kes13]
2016	Solid state	Caffeine	Process-induced phase transition (compression)	Phase transition of polymorph [Jub16]
2018	Solid state	Acetaminophen	Thermal gradient crystallization	Polymorph transformation [Cha18]
2019	Solid state	Chlorpropamide	Sheer-based	Polymorph transformation [Tha19]
2021	Solid state	DL-methionine	Milling	Polymorph transformation [Shi21]
2004	Solution	Paracetamol	Crystallization from liquid solutions	Selective crystallization [Mik04]
2007	Solution	Paracetamol	Anti-solvent crystallization	Supersaturation effect [Tak12]
2011	Solution	Sodium-2-ketogulonate monohydrate	Anti-solvent crystallization	Crystalline morphology [Sch11]
2013	Solution	Indomethacin	Evaporative crystallization	Kinetic study on polymorph [Hel13a]
2014	Solution	Theophylline - hydroxybenzoic acids	Solution crystallization	Co-crystal screening [Buc14]
2015	Solution	Paracetamol	Ultrasound assisted crystallization	Polymorph crystallization [Mor15]
2016	Solution	Clopidogrel	Anti-solvent crystallization	Polymorphic transition in ionic liquid [An16]
2017	Solution	Olmesartan medoxomil	Anti-solvent crystallization	Amorphous crystallization [Qi17]
2018	Solution	Acetaminophen	Evaporation crystallization	Solution shearing crystallization [Gut18]
2021	Solution	Carbamazepine	Rapid cooling	Solvent effect on polymorph [Ouy21]
2022	Solution	GMP	Supersaturation control	Amorphous crystallization [Kim22a]



the solution reaches a concentration saturated with the polymorph MS, and the solid does not dissolve in the saturated solution and can be set to point A (in Fig.2-3). Slurry solution composed of MS solids and saturated solution dissolves MS solid and moves from point B to point C, generating S solid by seed, surface activation, collision, mixing, etc.. The solution at this point is saturated with respect to polymorph MS and supersaturated with respect to polymorph S. The solute concentration varies between the solubility concentrations of the two polymorphs, in the region from point B to point C. During the nucleation and growth of polymorph S crystals, the solute concentration reduces continuously to the solubility of polymorph S,  $C_s^*$ .

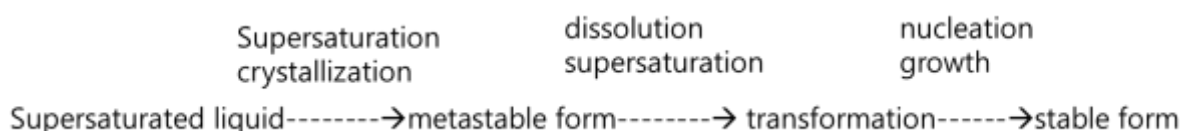
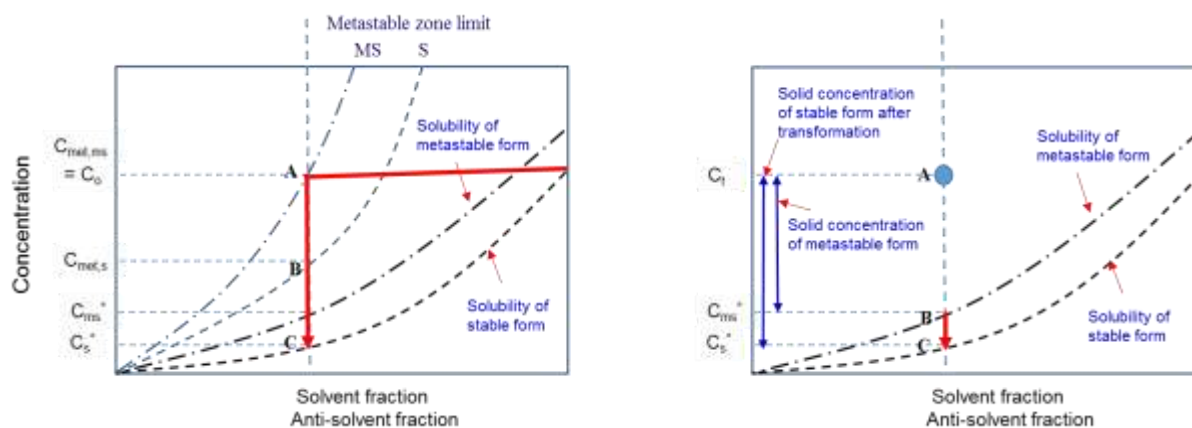


**Fig. 2-2: Processes of liquid-mediated phase transformation (LMPT).**

Fig. 2-2 shows the concept of liquid-mediated phase transformation process. Fig. 2-3b shows the solute concentration against anti-solvent fraction for monotropic systems. Metastable zone width and solubility of two forms are compared in different supersaturation region. If the anti-solvent fraction is increased from starting point of the horizontal solid line, the solution is supersaturated with respect to the polymorph (or solvates) MS, which is a metastable limit that metastable crystals may be crystallized (both nucleation and growth). Moreover, in point A at the end of the horizontal solid line (the solution at concentration  $C_0$ ), then the solution is supersaturated with respect to both polymorphs (or solvates), in which polymorph (or solvates) MS may first nucleate. The solute concentration starts to be decreased. During the nucleation and growth of polymorph MS crystals, the solute concentration  $C_0$  reduces continuously to the solubility of polymorph MS,  $C_{ms}^*$ . When the solute concentration decreases and reaches the metastable zone limit (point B) of the stable phase S, the metastable phase MS begins to transform into the stable phase S by means of dissolution and growth. The concentration decreases until the solubility of polymorph S.

Tab. 2-2 shows the historical background of studies on polymorph crystallization in solution. Cardew [Car85] predicted the change of solute concentration by modeling the SMPT process using dissolution and growth kinetics. Since then, a model of phase transformation with in-situ measurement of solute concentration [Wan00] and solid concentration [Cai08] has been verified. Most of the works were focused on the study of SMPT's operating condition effects and polymorph screening by crystallization. Recently, the theoretical modeling of the transformation process has been expanded by introducing amorphous solidification and dissolution, and crystal nucleation and growth, and the validity of the model has been proved by in-situ experimental results [Kim22].



(a) Liquid-mediated transformation

(b) Solution-mediated transformation

**Fig. 2-3: Comparison of liquid- and solution-mediated phase transformation using anti-solvent addition (the red lines are operating solution lines).**

In cases when the solution-mediated transformation occurs, the supersaturation of each polymorph contributes to the determination of polymorphic form. Fig. 2-3 shows the variation of concentration in liquid- and solution mediated transformation. The ratio of supersaturations for metastable form (ms) and stable form (s) can be calculated by:

$$\frac{S_{ms}}{S_s} = \frac{C_s^*}{C_{ms}^*} \quad (2-1)$$

where  $S$  is the supersaturation ratio ( $C/C^*$ ) and  $C^*$  the saturation concentration.

The supersaturation ratio for solution-mediated transformation is affected by solubility difference of the phases, which is a thermodynamic property.

**Tab. 2-2: Historical background of studies on polymorph crystallization in solution**

Year	Author	Materials	Process, idea or theory
1985	Cardew [Car85]	Copper phthalocyanine	SMPT model based on dissolution and growth
1988	Amathieu [Ama88]	Gypsum	Surface nucleation, dissolution rate, growth kinetic
1992	Boistelle [Boi92]	Pancreatic R-amylase isoenzymes	Transition temperature
1996	Beckmann [Bec96]	Abecarnil	Effect of temperature
2000	Wang [Wan00]	Progesterone	First Raman monitoring of the SMPT
2001	Lewiner [Lew01]	aKGA monohydrate	FTIR monitoring polymorph transformation
2002	Yamanobe [Yam02]	D,L-methionine	Qualitative modelling of the phase transition
2002	Jourani [Jou02]	Hydroxyapatite	Transformation kinetics by growth and dissolution
2002	Davey [Dav02]	Dihydroxy-2,6 benzoic acid	Monitoring of the transition by optical microscopy
2002	Garcia [Gar02]	Irbesartan	In-situ monitoring by conductimetry
2003	Veesler [Vee03]	Irbesartan	Dissolution controlled by the mass transfer
2003	Ferrari [Fer03]	Glycine	Limiting step analysis
2004	Ono [Ono04]	L-glutamic acid	Rate limiting step area of metastable crystals
2004	Fevotte [Fev04]	aC	In-situ near-IR spectroscopic
2005	Hu [Hu05]	Flufenamic acid	Monitoring of the solute concentration
2005	Stoica [Sto05]	Steroid API	Surface nucleation on metastable form
2006	Scholl [Sch06]	L-glutamic acid	In-situ monitoring using Raman, PVM, FTIR and FBRM probes the rate-controlling step
2006	Qu [Qu06]	Carbamazepine	Rate-controlling step on the transformation rate

2006	Omar [Oma06]	Paracetamol	Interfacial energy of polymorphic forms in different solvents
2007	Caillet[Cai08]	Citric acid	Simultaneous monitoring of the concentration of solid in suspension
2008	Barthe [Bar08]	Paracetamol	In-situ monitoring of the transformation by tracking habit modification
2008	Omar [Oma08]	Acetaminophen	Supersaturation effect on growth rate
2009	Kelly [Kel09]	Carbamazepine	Effect of solvent on induction time
2010	Guo [Guo10]	Astaxanthin	Polymorph screening by heat treatment
2010	Jin [Jin10]	Atorvastatin calcium	Solvate transformation
2011	Lee [Lee11]	Sulfamerazine	Transformation by A Couette–Taylor crystallizer
2012	Xu [Xu12]	HNIW	Crystallization mechanism and supersaturation in transformation
2013	Flood [Flo13]	DL-methionine	Dissolution, nucleation, and growth kinetics
2014	Munroe [Mun14]	Sulphathiazole	Dissolution-recrystallization mechanism
2015	Kim [Kim15]	Clopidogrel	Relationship between supersaturation and solubility
2015	Seidel [Sei15]	Salicylic acid	First concept on liquid-mediated phase transformation
2016	Dang [Dan16]	Taltirelin	Supersaturation effect
2016	Hartwig [Har16]	Xylitol	Crystallization in solution
2017	Wang [Wan17]	Argatroban	Ternary phase diagrams and rate controlling step
2018	Guo [Guo18]	Rifampicin	Mathematical model with kinetics of dissolution, nucleation and growth
2019	Zong [Zon19]	Lansoprazole	Thermodynamic and population balance models
2020	Tang [Tan20]	Tolfenamic Acid	Modeled by nucleation, growth, and dissolution
2021	Kim [Kim21]	GMP	Metastable limit, supersaturation and solubility
2022	Kim [Kim22]	GMP	Rate-controlling step, nucleation behavior

For liquid-mediated transformation:

$$\frac{S_{ms}}{S_s} = \frac{C_s^*/C_{ms}^*}{C_{met,s}/C_{met,ms}} \quad (2-2)$$

The supersaturation ratio for liquid-mediated transformation is affected by metastable limiting concentrations of the phases, which is a kinetic parameter influenced by supersaturation.

It is reported that the polymorph (or solvate) crystallization is affected by seeds, additives, solvents and interfaces [Tao07, Kit09, Kit13]. However, the quantitative comparisons between the operating factors and polymorph (or solvate) crystallization behavior is not yet understood. The crystallization of polymorphs and solvated crystals consists solely of competition between nucleation and growth rates, and transformation from a metastable state to a stable form. The nucleation process is practically the most important factor for the control of polymorph (or solvate) crystallization. However, selective crystallization of polymorphs (or solvates) requires elucidation of the mechanisms of each constituent step of the crystallization process and their relationship to operating conditions. Therefore, the controlling factors including molecular structure of polymorph (or solvate) crystallization and the crystallization mechanism in systems consisting of various crystal solvate forms and an amorphous form should be investigated.

According to Ostwald's rule of stages [Ost97], the solution-mediated crystallization process [Ngu08] frequently transforms the crystal form, allowing only a change from the metastable form to the stable form, making it difficult to prepare the metastable form. Therefore, it is important to grasp which operation factors influence the transformation. The transformation is caused by the difference in solubility between the two forms or various mechanisms depending

on the supersaturation conditions. The crystallization conditions for the production of the pure metastable forms can also be set according to the supersaturation conditions [Jun05]. Therefore, the generation of the amorphous form can also be established by this method [Kim15,Vau06]. When an amorphous form is suspended in a saturated solution, a transformation into a stable crystalline form can occur [Kim22b].

Solvent-mediated transformation studies can use a single measurement instrument, such as attenuated total reflectance Fourier transformed infra-red (ATR-FTIR) [Sal98], near infra-red (NIR) [Bla05], Raman [Ngu15] or focused beam reflectance measurement (FBRM) [Su13,Bar 08,Mos14], but in many cases use a combination of instruments to understand simultaneously complex mechanisms. To understand the hydrate formation and the transformation during operation, it is necessary to measure not only the solid form and concentration of the suspended solid state in solution, but also the change in solute concentration. Supersaturation is a non-equilibrium parameter affecting nucleation and crystal growth kinetics [Ulr02,Oma08,Oma06]. Supersaturation should be calculated from the difference between solubility and actual solution concentration, which is measured in real time by in-line instruments. Particle number, particle size distribution, and particle size are needed to be measured as they provide information on nucleation and growth during transformation. By analyzing the formation and transformation kinetics of substances composed of amorphous, heptahydrates and tetrahydrates with in-situ measuring devices, these solid forms can be selectively prepared. Supersaturation limits for polymorph (or solvate) crystallization with anti-solvent are established based on methanol/water ratio, initial concentration, anti-solvent addition rate and temperature.

## 2.3 Thermodynamics of Polymorph (or Solvate) Crystallization

### 2.3.1 Thermodynamics of Phase Selection

Solubility is an important parameter that determines the supersaturation, which is a non-equilibrium parameter to affect the nucleation rate, crystal growth and phase transformation kinetics [Tak12]. Therefore, it is important to be able to measure the solubility to understand selection of solid forms in the crystallization process. For the selective preparation of compounds with various solid forms, it is necessary to know their solubility differences.

The difference in solubility between solid forms results from differences in molecular configuration, or more precisely, in the balance between the attractive forces that hold solids together and the destructive forces that make solute molecules into solution. The solid form with the lowest solubility is necessarily the most stable at the temperature considered. In fact, the more soluble polymorph (or solvate) will eventually undergo solvent-mediated transformation as the system strives to reach equilibrium. It is generally recommended to formulate the most stable solid form to avoid transformation problems.

Solubility data for metastable phases of substances are rarely reported. The metastable form is easy to be transformed into the stable form during solubility measurement. To measure the solubility of the metastable form, an experiment is required to reach equilibrium and ensure that the solid form is still the metastable form. Therefore, to determine the solubility of metastable forms, the concentration of the solution phase and the forms of the solid phase must be simultaneously measured in-line. The solubility of metastable forms is measured to reach equilibrium at temperature. There are many methods of measuring solute concentration, such as gravimetric analysis [Pin05], titration [Buc98], spectroscopy [Har09], HPLC [Wol89] or solution density. Solubility is a thermodynamic property, and so its true value is certainly not affected by the time course of a phase transformation. Measurement of the solubility of solid

forms requires accuracy and precision to avoid problems associated with phase transformations in solution. The most stable polymorph always results in the lowest solubility and vice versa. The key for selection of solid form requires not only measuring the solubility of all forms in the solvent to be used, but also obtaining information on the metastable zone limit of forms according to supersaturation [Kim15].

### 2.3.2 Thermodynamic and Kinetic Factors of Polymorph (or Solvate) Crystallization

Fig. 2-4 shows the thermodynamic characteristics of polymorph (or solvate) crystallization in the case that the stable form is formed without transformation from the supersaturated solution and when the metastable form is formed and transformed into the stable form [Cro10]. Thermodynamically, a system is driving itself to the lowest possible free energy state ( $G_S$  in Fig. 2-4). This will correspond to the equilibrium state of the most stable polymorph (or solvate), form S in this example. However, the stable polymorph (or solvate) may have a higher activation energy (barrier to nucleation),  $E_S$ , than the metastable polymorph MS. This makes nucleation of the metastable polymorph (or solvate) more likely as there is less of a barrier to overcome in doing so. Nucleation of metastable forms can be occurred even when this is not the thermodynamically preferred phase. This is a kinetic effect: nucleation of the metastable phase can occur at a faster rate because it has less of a barrier to overcome. The metastable form will subsequently transform to the stable form provided it has enough time to do so ( $E_{S1}$  and  $E_{S2}$ ). In general, thermodynamics may be viewed to favor a stable polymorph (or solvate) formation and kinetics metastable polymorph (or solvate) formation. The situation can arise where two polymorphs (or solvates) are almost energetically equivalent and can nucleate simultaneously. This is a result of similar nucleation and growth rates for both polymorphs (or solvates), and the resulting polymorphs (or solvates) are termed “concomitant” polymorphs (or solvates) [Ber99]. Once a polymorph (or solvate) form is established in solution, the potential may exist for it to transform to a more stable form. The transformation options available to a polymorph (or solvate) are determined by the system being monotropic or enantiotropic.

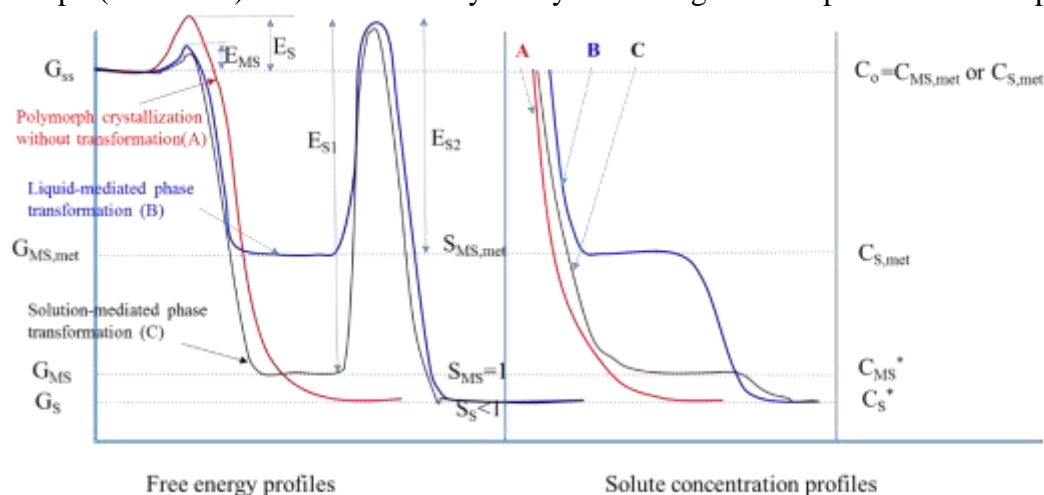


**Fig. 2-4: Free energy profiles and solute concentration profiles for polymorph (or solvate) crystallizations with and without transformation [Cro10].**

In polymorph (or solvate) crystallization, polymorph (or solvate) S crystals nucleate and grow because the solution is still supersaturated with respect to polymorph (or solvate) S (Plot A). In the liquid-mediated phase transformation (LMPT), after the metastable polymorph (or solvate) MS forms first at  $C_{MS,met}$ , a stable form S solid at  $S_{S,met}$  where the stable form S starts

to form (Plot B). It grows and decreases in concentration until solubility of the form S. In SMPT, the solute concentration drops below the solubility of polymorph (or solvate) MS, the supersaturation ratio of polymorph (or solvate) S becomes  $S_{S,met}$ , which leads to polymorph (or solvate) MS start dissolving (Plot C). This is the starting point for the phase transformation process in solution, which includes the nucleation and crystal growth of the stable polymorph (or solvate) S and the crystal dissolution of the metastable polymorph (or solvate) MS [Oma13, Wan17]. The solute concentration is still constant by the reduction of the solute concentration due to the growth of polymorph (or solvate) S crystals and the increment of the solute concentration due to the dissolution of polymorph (or solvate) MS crystals. Therefore, during the SMPT process, the dissolution of polymorph (or solvate) MS crystals is rapid enough to maintain the solute concentration  $C_o$  at or close to the solubility  $C_{MS}^*$  of polymorph (or solvate) MS. This concentration (or supersaturation ratio) will remain constant until polymorph (or solvate) MS crystals are completely dissolved. If the crystals of polymorph (or solvate) S are further grown, the solute concentration starts to reduce until the concentration reaches the solubility  $C_S^*$  of polymorph (or solvate) S. At this point, the whole SMPT process is complete, the supersaturation ratios  $S_{MS} = 1$  and  $S_S < 1$ . This coincides with Point B in Fig. 2-3b.

Form of the residual solid in the solubility measurement and analysis might be transformed. Therefore, in-situ measuring techniques are desirable, because it is difficult to monitor the metastable form with an off-line analysis [Zha11,Par19]. A focused beam reflectance measurement (FBRM) probe and a Raman spectroscopy are mounted on-line to measure the crystal size, the number of particles, the polymorph (or solvate) difference, and the solubility, simultaneously. In addition, off-line measurements using thermogravimetric analysis-differential scanning calorimetry (TGA-DSC), powder X-ray diffraction (PXRD), light microscopy, Raman spectroscopy, and scanning electron microscopy (SEM) can find out the thermal decomposition properties, structure and crystal form.

In previous studies, the solubility had been measured by the gravimetric method, but changes in the crystal form during the measurement process were not analyzed [Par19,Pan15,Oma13]. When the amorphous form is suspended in a saturated solution, a transformation to the stable form can occur. Thus, there can be difficulties in measuring the solubility of the unstable form. In anti-solvent crystallization, knowing the maximum supersaturation limit is also necessary for selective formation of polymorphs (or solvates).

#### 2.4 Phase Transitions of Metastable Phases

Unstable (or metastable) forms arise for kinetic reasons in the unstable (or metastable) phase. The unstable phases may remain in a metastable state for a period. The transformation of a metastable phase corresponding to the minimum free energy of the system into a stable phase is called a phase transition. A polymorph (or solvate) does not directly proceed towards equilibrium, but towards the closest metastable state [Ost89]. There are many examples that support this rule, but there are also many exceptions.

Fig. 2-5 shows the solubility curves of three solid phases at different anti-solvent fraction, the stable phase, the metastable phase, and unstable phase according to the monotropic solubility rule. Depending on the degree of supersaturation, the metastable zone limit at which each phase is formed is different at low supersaturation, the metastable zone limit is low and nucleation and growth of stable form occur without transformation. Since  $J_S > J_{MS}$ , it is stable phase S that is expected to nucleate. At middle and high supersaturations, the solution is supersaturated for three phases, which have the potential to nucleate. If the metastable phase nucleates before the stable phase according to the Oswald phase rule, this means that the kinetic factors that lead to

nucleation dominate the thermodynamic factors that lead to the final equilibrium. So,  $J_S > J_{MS} > J_{US}$ , which can only be described in two ways.

(1) the interfacial free energies among crystals of phases S, MS and US and solution are as follows:  $\gamma_S > \gamma_{MS} > \gamma_{US}$ , since crystals of different phases have different surface structures (even if the crystal chemical composition is the same) and since the higher the solubility the lower the interfacial energy, the inequality on the interfacial energy is verified [Gu01,Tey08].

(2) the kinetic factor  $K_0$  of a stable phase is higher than the kinetic factor of metastable phase,  $K_{0S} > K_{0MS} > K_{0US}$ , since the kinetic factor depends on the frequency factor and is thus higher than the unstable or metastable phase.

There are two possibilities for phase transformation: phase S is present in the solution (appears simultaneously with phase MS or by heterogeneous nucleation on phase MS) and phase S grows at the transformation of phase MS, which will disappear, or else only crystals of phase MS are present but are metastable [Dav86,Oma13]. The kinetics of transformation from phases MS to S is limited either by the kinetics of dissolution of the unstable phase or by the kinetics of growth of the metastable phase [Rod99]. Stable form S may directly nucleate and grow, and it can reach point F through the transformation process of metastable form MS and unstable form US.

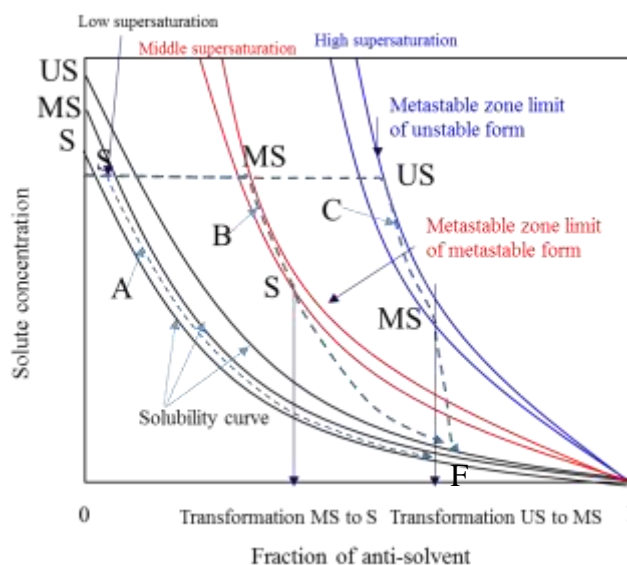


**Fig. 2-5: Schematic plots of the solubility curves of three phases in anti-solvent crystallization, in the case of a monotropic system [Thr00].**

The solubility curves of polymorphs (or solvates) are unchangeable due to a thermodynamic property, while their metastable zone limits are changeable, because of a kinetic property. The metastable zone limit depends on the degree of driving forces such as cooling, evaporation, and anti-solvent addition rates for cooling crystallization, evaporative crystallization, and anti-solvent crystallization, respectively.

Fig. 2-5 shows the schematic change of metastable zone limit with respect to supersaturation level. Plot A shows the case operated at low supersaturation. In this case, the stable form is only obtained in the nucleation point and is grown, because the other two forms are undersaturated. Thus, it is not possible to be transformed from the metastable form. However, as shown in Plot B, at a middle supersaturation, metastable form nucleates first, and then is transformed into a stable form. As shown in Plot C, at a very high supersaturation, unstable

form (like amorphous form) is formed and grown or transformed. The amorphous form can be transformed into a more stable form if the operation line passes through the metastable limits of stable form. In fact, to procure the amorphous form a very high supersaturation is necessary. This supports that the amorphous form was obtained by high-supersaturation techniques such as spray drying, rapid cooling and quenching [Vau06, Kim15, Yu14, Ryu12]. Finally, it is important to note that polymorph (or solvate) formation and phase transformation are associated with nucleation, growth, and dissolution processes. Therefore, the parameters affecting the kinetics of phase transformation are considered such as temperature, supersaturation, material, mixing, and solid property.

## 2.5 Kinetics of Solution- and Liquid-Mediated Phase Transformation

The basic phenomena involved in polymorph (or solvate) crystallization have already been described; a) primary nucleation of the more stable solid phase or the metastable phase, b) dissolution of the metastable solid phase, c) and growth of the more stable solid by mass transfer of solute in the solution. The phase transformation that accompanies polymorph (or solvate) crystallization includes solution-mediated and liquid-mediated transformation.

These three mechanisms can be activated. Therefore, nucleation of a stable polymorph (or solvate) or its seeding causes a phase transformation during crystallization. Primary nucleation may occur on the surface of a substrate such as a homologous impurity or crystals of the metastable polymorph [Cro10]. Many authors have reported the heterogeneous nucleation on the faces of a metastable phase during the crystallization [Man09, Sto05]. Once nucleation starts, the growth of the stable phase induces a decrease in solution concentration.

When this concentration falls below the solubility of the metastable polymorph (or solvate), it dissolves, thereby accelerating the growth of the more stable polymorph (or solvate). These dissolution and growth processes are often revealed by concentrations lying between the solubilities of the two forms (Fig. 2-6). The location of this plateau is due to competition between dissolution and growth kinetics.

In the case of LMPT, the MS form is generated and grown up to  $C_{S,met}$  in the A-B section, and the MS form is transformed in the B-C section  $C_{S,met}$ , and the S form is generated and grown, so that the supersaturation consumption is greatly reduced and reaches  $C_S^*$ . In the case of SMPT, it is in equilibrium with MS solid and solution  $C_{MS}^*$ , and MS solid dissolves and transforms, and the solution grows S form by the change of supersaturation between solubilities,  $C_{MS}^*$  and  $C_S^*$ .

When solute consumption by growth is slower than solute production by dissolution, the plateau is located near the solubility of the metastable polymorph (or solvate). Therefore, the growth mechanism of the stable polymorph (or solvate) is the rate-controlling step. When supersaturation dominates the growth rate and the rate of dissolution is slower, the concentration plateau is just above the solubility of the stable polymorph (or solvate). The dissolution mechanism of the metastable phase is the rate controlling step.

Normally, the solid concentration in industrial conditions is high. The presence of larger solid surfaces and/or increased interparticle collisions can activate the occurrence of secondary nucleation mechanisms of stable phases in suspension. This may be due to a surface contact mechanism [Kim21]. Thus, when their existence is favored by operating conditions, secondary mechanisms must be taken into account in addition to primary nucleation, dissolution, and growth mechanisms. For example, increasing the number of stable forms promotes SMPT. Due to secondary nucleation associated with transformation, the concentration plateau no longer exists. To generate different supersaturation levels with a given solvent, crystallization

experiments are performed using different techniques (cooling, evaporation, anti-solvent, or drowning out) and varying, in each case, the operating conditions (cooling or evaporation rate, flow-rate of the added anti-solvent). Crystallization operated at high supersaturations can produce mixtures of various polymorphs (or solvates) or amorphous forms. These unstable forms, held in suspension, are eventually transformed into the most stable polymorphs (or solvates). To determine the different polymorphs (or solvates), the suspension must be filtered very quickly or an in-situ measuring instrument must be used.

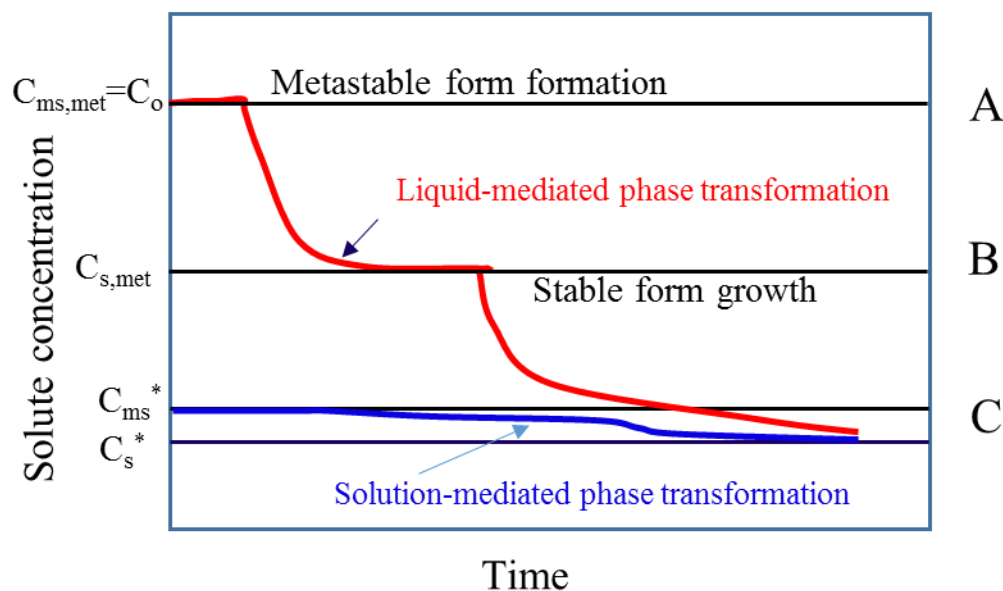


**Fig. 2-6: Limit profile of concentration against time during a phase transition in solution-mediated and liquid-mediated transformation,  $C_{met}$ ,  $C_{ms}^*$  and  $C_s^*$  are the metastable concentration and solubilities of the two phases [Car85,Wan18,Kim22b].**

In the biochemical industry, an anti-solvent addition mode is frequently utilized in crystallization processes. The anti-solvent crystallization is a technique employed in liquid-mediated phase transformation that is influenced by the concentration, solvent, temperature, anti-solvent composition, and anti-solvent addition rate, which affects supersaturation [Sei15].

## 2.6 Supersaturation and Nucleation

### 2.6.1 Supersaturation and Metastable Zone Limit

Knowledge of the driving forces of crystallization is essential not only to determine the kinetics but also to relate them to the parameters that control crystallization. The number of molecules required to form a critical nucleation cluster is inversely proportional to the degree of supersaturation. Therefore, as the supersaturation is increased, the probability of nucleation increases. However, nucleation is energetically more demanding than crystal growth, and there is a supersaturated region where crystal growth proceeds while nucleation is suppressed. [Mul93,Mer01].

A frequently used definition for the supersaturation of phase  $i$  is :

$$S_i = \frac{c}{c_i^*} \quad (2-8)$$

Supersaturation may be created by various methods that regulate the solute activity (concentration) or activity product. These include (a) removal of the solvent (evaporation or freezing), (b) addition of a salt unrelated to the ions participating in precipitation, and (c) dissolution of the metastable solid phase. Supersaturation can also be created by controlling solute solubility, such as changing temperature, changing pH, or adding anti-solvents that reduce solute solubility.

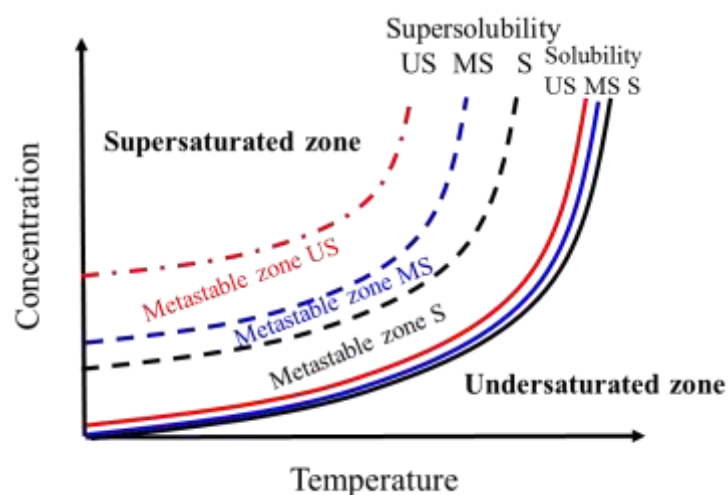


**Fig. 2-7: Solubility, supersolubility and metastable zone of solid forms [Thr00,Ulr04, Tit03,Reu06,Kim15].**

The solubility-temperature (or solvent fraction) diagram shown in Fig. 2-7 illustrates the conditions under which a cooling (or anti-solvent) crystallization is feasible. The metastable zone limit of the three phases with a small difference in solubility shows a large difference according to the degree of supersaturation. As shown in Fig. 2-7, the solubility and metastable zone limit of phases US, MS and S are compared. Therefore, it is essential to understand the metastable zone width, which is a kinetic property, for the nucleation, growth and transformation of a phase in the course of phase formation. Theoretically, supersaturation at a level can cause nucleation in solution. However, primary (homogeneous) nucleation from solution does not spontaneously occur usually until the supersaturation exceeds a certain threshold. The metastable limit is represented by the supersolubility curve. In the region between the solubility and supersolubility curves (i.e. the metastable zone), heterogeneous nucleation on surfaces or at interfaces of crystals (secondary nucleation), impurities or even dust particles can occur. A certain supersaturation needs to be maintained in the metastable zone for a crystallization to be controlled [Lu05].

When designing a crystallization process for a polymorphic system, the solubility curve of each crystal form must be considered. Solubility-temperature diagrams that illustrate the challenges encountered in selectively crystallizing monotropic polymorph (or solvate) pairs are shown in Fig. 2-7. It guides the formation and transformation according to the metastable region for each shape. Information in this metastable region is the key data for selective shape control.

The production of the most stable form of polymorph (or solvate) can only be guaranteed a priori if the solution can be supersaturated for a single polymorph (which is necessarily the most stable one) throughout the crystallization process.

## 2.6.2 Nucleation

Nucleation phenomena are equally important in the control of micromeritic properties and in the selective crystallization of a particular polymorph. Nucleation mechanisms can be divided into two main categories: homogeneous and surface or interface catalyzed [Mul93, Mes01].

Let us consider a pair of polymorphs, one stable (ST) and another one metastable (MS). The classical nucleation theory can help us to predict which polymorph crystallizes first as a function of the experimental conditions [Oma06,Ulr03]. It describes the nucleation rate as:

$$J = A \exp\left(\frac{-\Delta G_c^*}{RT}\right) \quad (2-9)$$

where  $\Delta G_c^*$  is the critical nucleation free energy,  $A$  is a pre-exponential constant,  $T$  is the temperature (in Kelvin), and  $R$  is the ideal gas constant. So, the polymorph that will nucleate first is the one with the highest nucleation rate or, in other words, the one with the lowest critical nucleation free energy. The critical nucleation free energy is calculated as:

$$\Delta G_c^* = \frac{16\pi N_A \gamma^3 v_m^2}{3k^2 T^2 \ln^2 S} \quad (2-10)$$

where  $\gamma$  is the interfacial energy,  $N_a$  is Avogadro's number,  $\kappa$  is the Boltzmann constant,  $v_m$  is the molar volume, and  $S$  is the supersaturation ratio.

By combining eqs. 2-9 and 2-10, the expression for the nucleation rate becomes:

$$J = A \exp\left(-\frac{16\pi N_A \gamma^3 v_m^2}{3k^2 T^2 \ln^2 S}\right) \quad (2-11)$$

Depending on the model used for describing the kinetics association [Kas95,Mer01], different expressions of the pre-exponential factor are available in the literature. Generally, this factor depends on a collision frequency between molecules (which can be related to solubility), the solid-liquid surface energy, and the energy barrier for diffusion of molecules from the solution to the crystal. The pre-exponential factor  $A$  in eq. 2-11 is expressed as [Kim01]:

$$A = \frac{3}{2} D d_m^2 (C N_a)^{7/3} \left(\frac{\gamma d_m^2}{kT}\right)^{1/2} \quad (2-12)$$

where  $D$  is the diffusion coefficient of the solute in the solvent,  $d_m$  is the molecular diameter of the molecule, and  $C$  is the solution concentration.

So, for a pair of polymorphs:

$$\frac{\Delta G_{c,MS}^*}{\Delta G_{c,ST}^*} = \left(\frac{\gamma_{MS}}{\gamma_{ST}}\right)^3 \frac{\ln^2 S_{ST}}{\ln^2 S_{MS}} \quad (2-13)$$

where the subscripts "ST" and "MS" refer to the stable and metastable polymorphs, respectively. The supersaturation ratio is defined with respect to the stable polymorph as

$$S_{ST} = \frac{C}{C_{ST}^*} \quad (2-14)$$

$$S_{MS} = S_{ST} \frac{C_{ST}^*}{C_{MS}^*} \quad (2-15)$$

where  $C$  is the concentration and  $C^*$  is the solubility. Hence, from combination of eqs. 2-13, 2-14 and 2-15:

$$\frac{\Delta G_{C,MS}^*}{\Delta G_{C,ST}^*} = \left(\frac{\gamma_{MS}}{\gamma_{ST}}\right)^3 \frac{\ln^2 S_{ST}}{\ln S_{ST} - \ln\left(\frac{C_{MS}^*}{C_{ST}^*}\right)} \quad (2-16)$$

The equilibrium solubility ratio,  $C_{MS}^*/C_{ST}^*$ , and the interfacial energy ratio,  $\gamma_{ST}/\gamma_{MS}$ , are specific for each pair of polymorphs, so the supersaturation will define which polymorph has the lowest critical nucleation free energy and therefore will nucleate first. If the supersaturation is lower, then  $\Delta G_{C,ST}^* < \Delta G_{C,MS}^*$  and the stable polymorph should nucleate first. On the other hand, if the supersaturation is higher, then  $\Delta G_{C,ST}^* > \Delta G_{C,MS}^*$  and the metastable polymorph should nucleate first.

However, even though some supersaturation conditions promote the nucleation of the metastable polymorph, it will hardly remain in contact with the solution without transforming into the stable polymorph. Ostwald [Ost97] proposed that the less stable polymorphs quickly redissolve and the solute may be renucleated as the more stable polymorph as the crystallization system moves from the original high-energy state through a transition state to the equilibrium with minimal loss of free energy. This low-energy route of transition between polymorphs occurs because the molecules of solute have torsional, rotational, and translational degrees of freedom and can rearrange and recrystallize to decrease the overall free energy of the system (Fig. 2-8). Therefore, metastable polymorphs should be isolated after their formation to avoid solvent-mediated polymorphic transformations.

Since forms MS and US exhibit better properties for drug formulation and performance than form S, several research groups (e.g. Babu [Bab11], Kanajia [Kan15] and Vaughn [Vau06]) have been developing a variety of methods to selectively crystallize and separate these polymorphs. A comprehensive study of these methods is necessary.

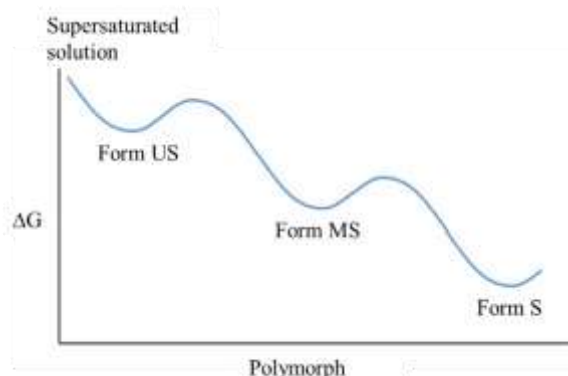


**Fig. 2-8: Gibbs free energy states of solid forms illustrating the Ostwald's rule of stages.  $\Delta G$  is the change in free energy (expressed by Ostwald's rule) [Ost97].**

## 2.7 Transformation Kinetics by Dissolution and Growth

Transformations in solution occur much faster than solid state transformations because it requires a large activation energy due to the kinetic resistance to the transformation in the solid state. This energy is associated with the nucleation and the growth of new forms, which occur through molecular diffusion and conformational changes at the contact interface formed between two phases. On the other hand, recrystallization of the more stable form at the expense of the less stable form through melting, dissolving, or interfacial phenomena can reduce the total activation energy for the polymorphic transformation compared to that for a solid state transformation.

Fig. 2-9 illustrates the process of amorphous-crystalline transformation. Crystalline phase grows from the interfacial layer saturated with amorphous phase. Because of the dissolution of amorphous and growth of crystalline form, there is a concentration profile across the interfacial layer. The solution-mediated mechanism for driving force of transformation is illustrated in Fig. 2-9a. For a given slurry temperature, both forms can exist either through seeded mode or supersaturation generation. In such a case, a solid-liquid boundary around both forms MS and S develops where each polymorph exerts its equilibrium solubility. As a result of the solubility difference, a concentration gradient develops across the liquid phase that leads to dissolution of form MS together with a simultaneous growth of form S. This solubility difference depends on temperature or anti-solvent fraction and becomes the driving force for transformation kinetics.

The liquid-mediated mechanism for the interconversion design is shown in Fig. 2-9b. After the generation of the MS at a given temperature, the slurry concentration and the liquid concentration are established and both forms can be present after the seeding or induction period. In this case, a solid-liquid boundary around the two forms MS and ST arises, taking into account the equilibrium solubility and metastable zone limits of each polymorph. As a result of the solubility differences and metastable zone limits of MS and ST, a concentration gradient occurs across the liquid phase leading to dissolution of form MS with growth of form ST. This difference in the limits of the metastable region depends on the degree of supersaturation or kinetic properties and is the driving force of the transformation kinetics.

A dissolution-crystallization model to explain transformation process was described first by Jakubiak [Jak16]. During transformation process, there are two steps: dissolution of solid phase, crystallization (nucleation and growth) of the stable phase. These processes allow us to present the kinetics of polymorphic transformations in solution. During crystal growth, individual molecules gradually accumulate into already existing particles. So, crystal growth rate is related to solution concentration and the amount of solid-state substance. The nucleation which is a process of an aggregate out of the dissolved compound can be supposed to be an encounter of many solute molecules. Additionally, the dissolution occurs during transformation and affects growth.

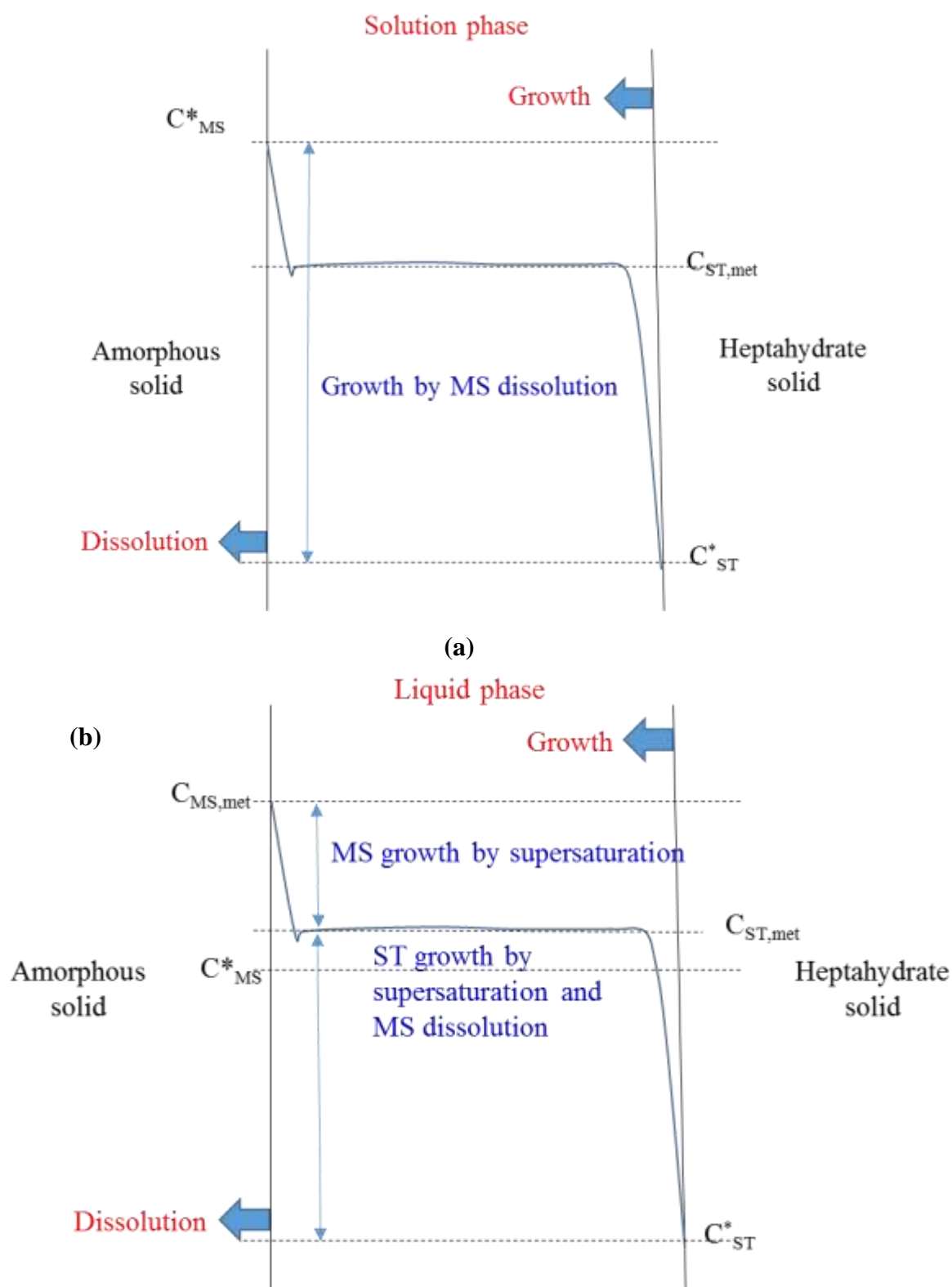


Fig. 2-9: Driving forces of (a) Solution-mediated phase transformation and (b) liquid-mediated phase transformation.

The transformation in solution is usually the most important process in polymorph crystallization. It is composed of the growth of the stable form (s) and the dissolution of the metastable form (ms). The growth (or dissolution) kinetics can be expressed as a function of supersaturation (or undersaturation) for each set of conditions by diffusion controlled model [Jib02,Wan17,Sot19].

$$G_i = \frac{dm_s}{dt} = k_G(C - C_s^*) \quad (2-17)$$

$$D_i = -\frac{dm_{ms}}{dt} = k_D(C_{ms}^* - C) \quad (2-18)$$

Where  $k_G$  and  $k_D$  are rate constants of the growth and dissolution,  $C_s$  and  $C_{ms}$  are solubilities of stable and metastable forms. Such relationship was applied to the change of mass of each form was measured in the transformation process.

The relationship between solution concentration and the amount of solid can be explained as follows:

$$\frac{dC}{dt} = G_i - D_i \quad (2-19)$$

where  $D_i$  stands for dissolution rate of the metastable form;  $G_i$  represents the crystal growth rate of the stable form;  $C$  is the solution concentration.

Models that explain the concentration-time profiles during a solution-mediated transformation have been developed [Car85]. Several studies have highlighted the importance of phase-transformation kinetics and the implications of their processes [Sot19,Zhu19,Tak16]. There are at least two mechanisms that control the transformation rates: either the growth-controlled process (growth of the stable form) or the dissolution-controlled process (dissolution of the metastable form) [Das10,Lok13,Jak16,Pan18]. When the metastable phase is formed first, the transformation of the metastable phase into the stable phase follows. Kinetic studies of transformation into an amorphous crystalline form are rarely reported, and the kinetic and rate-controlling steps of phase transformation of GMP are not reported at all, especially, for various different operating conditions. It is necessary to identify the rate-controlling processes, analyze mechanisms of dissolution and growth using various rate equation models, and determine how operating conditions affect the kinetics and mechanisms of the transformation. Dissolution and growth kinetics should be studied using zero-order, first-order, and surface reaction equations. In addition, factors influencing the transformation are also investigated.

The first study on the kinetics of solution-mediated phase transformation has been carried out by direct microscopic observation and was first given a quantitative analysis in 1985 by Cardew and Davey [Car85]. In their analysis, it was demonstrated that the kinetics of such a process is dominated by the relative growth and dissolution rate constants for the transformation. For this reason, physical information may only be derived through the measurement of the solution composition with time [Dav86]. Since 1985, several kinetic studies have been reported [Kit93, Wan17,Tur18,Tan20], and the analysis of this kinetic equation has followed.

Transformation analysis needs dynamic information using real-time and in-situ monitoring [Sal98,Bla05,Hel13b,Hel15]. Several in-situ analytical techniques such as IR spectroscopy [Bla05] and Raman spectroscopy [Ngu15,Su13,Kim22] have been applied to study systems undergoing phase transformations. When the metastable phase is formed first, the transformation of the metastable phase into the stable phase follows. Kinetic studies of transformation into an amorphous crystalline form are rarely reported, and the kinetic and rate-controlling steps of phase transformation of GMP are not reported at all, especially, for various different operating conditions.

## 2.8 Substance Investigated

Disodium guanosine 5'-monophosphate (GMP) is a component used in manufacturing of RNAs, as well as pharmaceutical intermediates and food additives. GMP is synthesized by fermentation and then purified by crystallizing the fermentation broth. Crystallization serves to control product qualities, such as the hydrate form and the purity. From thermal and PXRD analyses, GMP is known to crystallize both as the tetrahydrate and the heptahydrate form [Kam67]. However, due to the difficulty of crystallization caused by gel formation through tetramer stacking, only the crystal structure of the heptahydrate has been reported. Determination of the crystal structure of the tetrahydrate, and a powder X-ray diffraction analysis of the transformation into an anhydride through three intermediate phases were reported [Bar82,Kat80]. The crystal structure of the tetrahydrate was disclosed with intermediate phases [Tsu18]. An understanding of the selective crystallization of GMP hydrates requires solubility and supersaturation limits, and these have rarely been reported for the tetrahydrate, heptahydrate, and the amorphous solid [Che18,Zou17,Lie11].

GMP exists in several hydrate forms and one amorphous form [Zim76,Kat80]. The chemical structures of tetrahydrate and heptahydrate GMPs are shown in Fig. 2-10. In order to understand transformation of the hydrate forms in solution crystallization, it is necessary to grasp the effect of supersaturation according to the crystallization conditions. In addition, previous studies on GMP crystallization have mainly focused on the transformation of heptahydrate and amorphous forms [Zou15,Zou16]. Several papers have reported crystallization of GMP with variables, such as solvent, temperature, and pH [Zou17,Zha11]. However, studies on the relationship between supersaturation and the solid form, and the selective crystallization of tetrahydrate GMP are lacking. In GMP manufacturing, the analysis of the mechanisms of transformation between hydrate and amorphous states and between hydrate states is required. In addition, conditions must be established for the growth of the amorphous and the hydrates without transformation. Because physical properties of GMP depend on the solid forms, the solubility, supersaturation, induction times, nucleation, and growth rates are different in the crystallization process. Formation of the amorphous form requires just a supersaturation of the solution, whereas transformation into the crystalline form needs nucleation of the crystalline state from the amorphous state in solution. Although many cases of amorphous-to-crystalline transformation have been reported [Zou17,Qi17,Gre10,Kes13,Hea17], the kinetics of transformation and crystallization, and metastable zone limit of amorphous and heptahydrate solids for their selective formation has almost never been monitored, discussed, and reported in detail.

In the field of crystal engineering, variation in the number of crystal water molecules is known to affect the stability, dissolution rate and solubility. Examination of the transitions between hydrate and amorphous phases is therefore of particular interest, and control of the hydration degree is of importance in the fine chemical industry.

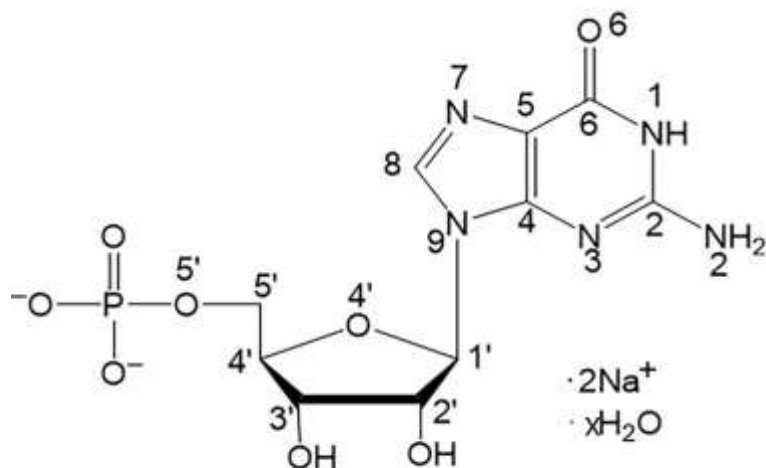


Fig. 2-10: Structure of GMP.

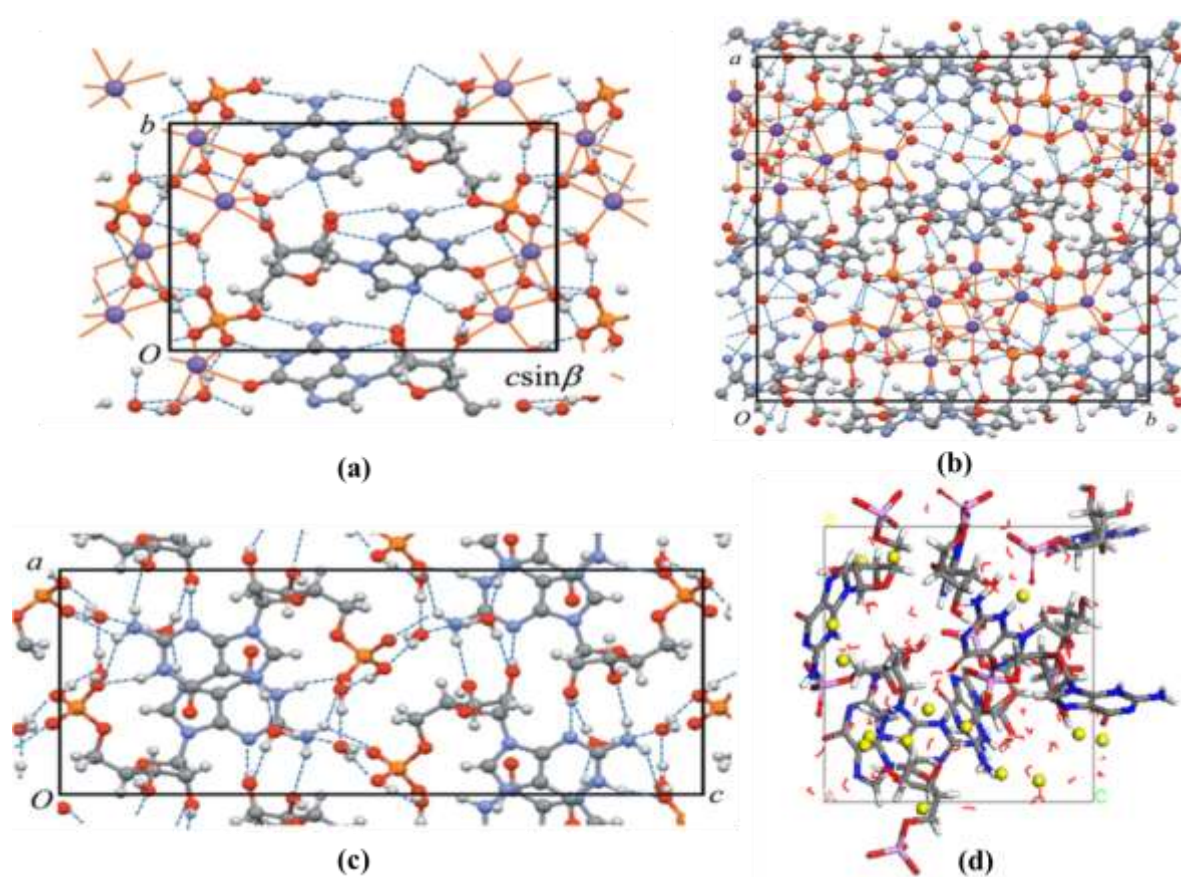


Fig. 2-11: Crystal structures of (a) tetrahydrate, (b) heptahydrate and (c) trihydrate and (d) amorphous [Bar82,Kat80,Zou17].

Among the various GMP salts found, the disodium salt of GMP is known to crystallize as the tetrahydrate and the heptahydrate [Kam67].

The crystal and molecular structures of the tetrahydrate, heptahydrate, trihydrate and amorphous are shown in Fig. 2-11. As shown in Figs. 2-11(a) and 2-11(b), the crystal packing of the tetrahydrate differs significantly from that of the heptahydrate. In the tetrahydrate, bases are unstacked in the molecular layers and sodium ions that bridge neighboring molecules play an important role in sustaining the layer structure. An expected example of amorphous product has a disordered structure with crystal water.

Few studies have focused on the transformation and selective crystallization of GMP, although the crystallographic and solubility data for GMP have been reported previously [Zou16,Zou17]. Studies of the as-yet-unreported metastable zone, the induction time, and the dissolution, the primary nucleation and growth mechanisms of GMP are necessary for its quality control. Understanding its polymorphic transformation will improve the quality of the final product and facilitate the scale up process. When improper processing conditions are used, the amorphous form is easily obtained, which is undesirable since it prolongs the operation time and lowers the product quality. The transformation of GMP in mixed solvent of methanol–water has been studied [Ngu11]. However, the mechanisms and kinetics of phase transformation were not investigated. Then, the next question is how to transform the amorphous form into a specific crystal form, such as certain metastable forms that sometimes have strong pharmaceutical effects.

### 3. Motivation and Aim of Thesis

#### 3.1 Motivation

Solution crystallization is the most used purification technique for high purity production in the fine chemicals industry [Ulr03]. It offers many advantages over other unit operations because it is simple, economical and energy efficient. In practice, most pharmaceutical manufacturing processes involve a series of crystallization processes, and product quality is often related to final crystal morphology (e.g. crystal habit, shape and size distribution). However, the crystallization process of polymorphs is still poorly understood, as it involves many complex mechanisms (e.g., dissolution, aggregation, fragmentation, dispersion, etc.) in addition to the main mechanisms (i.e., nucleation and growth). This presents a challenge to selective control of the desired polymorph.

In the chemical, pharmaceutical, and food industries, all substances may exist in both amorphous and crystalline forms [Bec01,Hea17,Sha06]. In the process of preparing compounds that exist in various solid forms, either crystalline or amorphous forms, the selective production of a solid form is of interest [Ulr03,Bec01]. Thermodynamically, amorphous solids provide higher solubility compared to crystalline forms. However, amorphous forms are often not wanted as they are not stable. They can transform during drying, processing, storage, or dissolution [Bab11,Var06,Kan15]. Intentional manufacturing of the amorphous form requires very high supersaturation. The amorphous form is prepared by high supersaturation techniques like spray drying, rapid cooling, supercritical fluids, etc. [Bro92,Bru95,Cri91,Lim13]. Since industrial crystallization favors high yields and high production rates, it operates at high supersaturation, so the formation of an amorphous form is inevitable. In crystallization of polymorphs or solvates operated with high supersaturation in solution, three stages are expected [Her12,Mah14,Kim15,Qi17]: generation of the amorphous form, dissolution of the amorphous form, and nucleation and growth of the crystalline form. Since each step can be the rate-determining step, it is necessary to understand which step governs the kinetics of the process. From this point of view, understanding the kinetics of transformation from the amorphous form to the crystalline form is necessary for producing selectively the desired solid forms. According to Ostwald's rule of stages [Ost97], a solution crystallization [Ngu08] frequently transforms the crystalline forms and only allows changes from metastable forms to stable forms, making it difficult to prepare metastable forms. Therefore, it is important to grasp which operation factors influence the transformation. The first study on the kinetics of solution-mediated phase transformation has been performed by observation of microscopic data, and quantitative analysis was first provided by Cardew and Davey in 1985 [Car85]. Several kinetic studies have been reported since then, followed by analysis of kinetic equations [Kit93,Wan17,Tur18,Tan20]. On the other hand, liquid-mediated phase transformation occurs in non-equilibrium operations performed at high supersaturation. Compared to SMPT (solution-mediated phase transformation), studies on LMPT (liquid-mediated phase transformation) are very rare. Kinetic studies of transformation from amorphous to crystalline forms are rarely reported, and so are the kinetic and rate-controlling steps of phase transformation.

The variations in physical properties of solid products make polymorphism an important issue for the food, specialty chemical and pharmaceutical industries, where products are specified not only by the chemical composition, but also by their performance [Ulr02,Ulr03]. As a result, controlling polymorphism to ensure consistent production of the desired polymorph is very crucial in those industries, including drug manufacturing industry. Encouraged by the importance of polymorphism in pharmaceutical industries, this study investigates the

modelling and control of solvate crystallization and phase transformation of GMP as a case study, which consists of amorphous form and three crystalline hydrates.

### 3.2 Aim of Thesis

Due to the hard-to-predict nature of amorphous to crystalline transformation, the control of solid design remains challenging in functional solid manufacturing. In this work, the main objective is to systematically study the selective production of the solid forms including amorphous and crystalline solids in crystallization processes based on the study of thermodynamic properties, supersaturation effect, metastable limit, phase transformation kinetics, polymorph formation and process analytic techniques. This study should be conducted as a case study for the material GMP, because it is necessary to selectively form various solid forms of amorphous and crystalline forms. Difficulties in product quality control due to various formation routes and phase transformation processes during the process have been proven.

The detailed objectives of this thesis are:

1. Study the thermodynamic properties that are fundamental information for the solvate (or polymorph forming) crystallization process modeling and control and the supersaturation to control the crystallization of solid forms.
2. Study solubility of amorphous form and crystalline hydrates using in-situ Raman spectroscopy with calibration plots and the effects of the temperature and the solvent fraction on the solubility of solid forms.
3. Develop a simple analytical method to quantitatively measure the solution concentration and slurry density to implement the in-situ monitoring of the solvate crystallization process.
4. Interpret various patterns of kinetics of liquid-mediated phase transformation including amorphous formation and transformation to crystalline phase.
5. Study the controlling steps in the transformation of amorphous-to-hydrate solids and hydrate-to-hydrate crystals.
6. Study the impact of transformation kinetics of amorphous-crystalline system on the solvate outcome, and provide a general approach to determine the optimal crystallization operation to prepare the desired solid forms.
7. Design a selective solvate manufacturing method by understanding the supersaturation and metastable zone limits for the formation of each solid phases of substance.
8. Study the formation of the amorphous form, transformation of the amorphous form, and the nucleation of the crystalline heptahydrate of GMP in a methanol–water solvent.
9. Study a clear understanding of the phase transformation kinetics of GMP and an important information to control the manufacturing process of crystalline hydrate products.
10. Develop a good understanding of the kinetics of phase transformation and offers critical information controlling the manufacturing processes of hydrate products.
11. Study dissolution and growth kinetics, and rate-controlling step in transformation of amorphous state to crystalline state using anti-solvent crystallization.
12. Study the impacts of operating conditions on the product properties in anti-solvent crystallization, and offer general guidance for designing a crystallization process.

## 4. Materials and Methods

### 4.1 Materials

#### 4.1.1 Raw Materials and Solvents

GMP was supplied by Wako Pure Chemical Industries with a purity of 99.9 wt %. In this study, the heptahydrate GMP used was prepared by recrystallization by adding methanol to the GMP solution dissolved in water at 20 °C. Methanol was of analytical grade and purchased from Aldrich, USA. Distilled water was used.

#### 4.1.2 Preparation of Amorphous GMP

An amorphous form was produced by anti-solvent crystallization using water and methanol. After 25 g of the hydrate crystals was dissolved in 100 g water at 20 °C, the solution was supersaturated by adding 50 g methanol for 10 s. During the experiments, the Raman peaks were recorded at intervals of 5 s to monitor the amorphous form. Before transformation, the solids were separated by using a solid-liquid separator with a glass filter, washed with methanol, and dried at 30 °C for 2 h. PXRD and Raman spectroscopy were used to confirm the hydrate forms of the product. The purity of the prepared amorphous form was above 0.95 in the mass fraction from the Raman peak.

#### 4.1.3 Preparation of Tetrahydrate and Heptahydrate

Tetrahydrate crystal was obtained under the conditions of 15wt% solute concentration and 70 wt% methanol/30 wt% water at 50 °C. Heptahydrate crystals were prepared by anti-solvent crystallization at 10 wt% solute concentration, 50 wt% methanol + 50 wt% water and 30 °C. Raman spectroscopy was used to monitor the hydrate forms in situ at intervals of 5 s. The crystals were separated by using a solid-liquid separator with a glass filter and dried at 30 °C for 2 h. It was confirmed that the hydrate crystals were not transformed during drying. XRD and Raman spectroscopy were used to confirm the solvate form of the product. The purity of the prepared hydrate was above 0.99 in the mass fraction from the Raman peak.

### 4.2 Methods

#### 4.2.1 Solubility Measurement Method

The gravimetric method was used to measure the solubility. During the measurement of the solvate solubility, the crystalline form of the residual solid can undergo transformation. A phase transition of the metastable form in the solution phase may occur during the solubility measurement process [Par19,Qu06]. The solubility of the metastable form cannot be measured by an off-line method. Therefore, an on-line measurement is desirable since it is impossible to monitor the transformation of the crystalline form during off-line analysis.

The measuring device consists of a FBRM probe (Mettler-Toledo, Switzerland) and a Raman spectrometer (Kaiser Optical Systems, Ann Arbor MI, USA), which are in-situ measuring instruments. In-situ Raman measurements of the solid solvate concentration and the solution concentration were used to measure simultaneously the solubility, the solid concentration, and a potential change in the solvate of GMP with elapsed time. The equilibrium point was finally obtained. At the same time, the solvate of the residual solid was measured in situ. The GMP solids, solution, and solvent have characteristic Raman spectra, from which the Raman spectra of the solution that did not overlap with others were selected to develop the calibration curve

for the solution concentration.

The setup of the solubility measurement apparatus is shown in Fig. 4-1. It consists of a Raman spectrometer and a FBRM probe, used in conjunction with a temperature controller ( $\pm 0.1$  K) in a jacketed vessel. The double-jacket glass was connected with a thermostat (RAUDA, K-4/R) with an accuracy of 0.1 K and kept at a constant temperature. The vessel was equipped with a magnetic driver and condenser to prevent any vapor leakage. In-situ measurements of the solid and solution concentrations were used to obtain the solubility measurements. In the in-situ Raman method, it is necessary to search for the point of equilibrium under isothermal conditions, where the concentration is varied for different conditions. Linear relationships between the concentration of the solution and the Raman intensity were used to measure the solubility of the GMP in binary solvent mixtures.

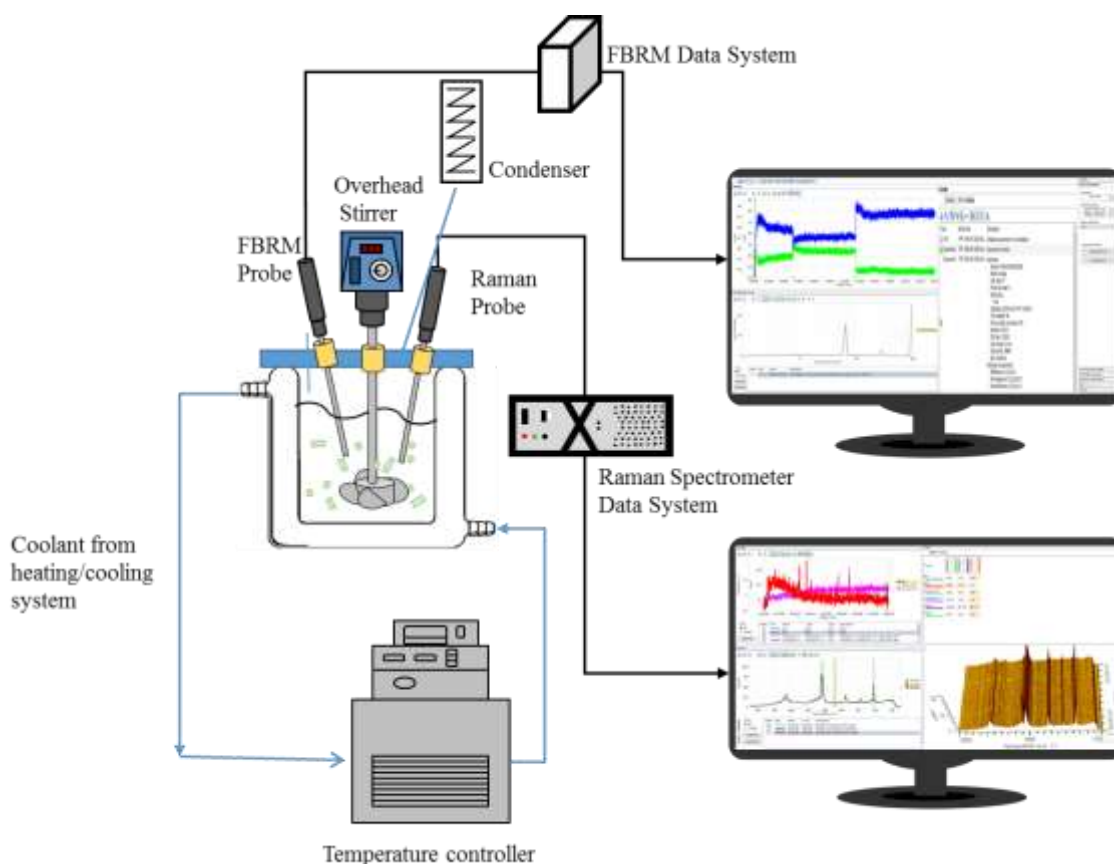


**Fig. 4-1: Setup of the experimental apparatus.**

Solute was added step by step until saturation was reached. Then, an additional 5–10 g of extra solute was added per 100 g of saturated solution. The solubility of the solute at a given temperature was calculated from the weight of the dissolved solute in the solvent. The temperature was set in the range from 20 to 60 °C. Off-line analysis of the final sample was carried out with an in-situ measurement. After 48 h, the remaining solid was filtered and weighed, and the concentration calculated as gram of dissolved solute per gram of solvent. The off-line data were confirmed by the Raman data. Unstable forms such as the amorphous form changed easily into a stable form during the solubility measurement. Some of the experiments were conducted in triplicate to check the reproducibility. The solubility for a given temperature

was reproducible within 0.001 g of solute per 100 g of solution. The off-line measurements were performed twice and compared with the in-line measurement result. Thus, the accuracy for the solubility measurement was in the range of 99.9–99.99 %.

#### 4.2.2 Crystallization Method

The experimental setup consisted of a 400 mL double jacketed crystallizer, 3-blade propeller mechanical stirrer, Raman system, FBRM, PVM, thermostat, vacuum filter, and drying equipment (Fig. 4-2). A stirring speed of 400 rpm, which was sufficient to keep the solid in suspension, was used. The temperature of the crystallizer was controlled by a heating and refrigeration circulator (Jeio Tech, HTRC-30) with a programmable controller.

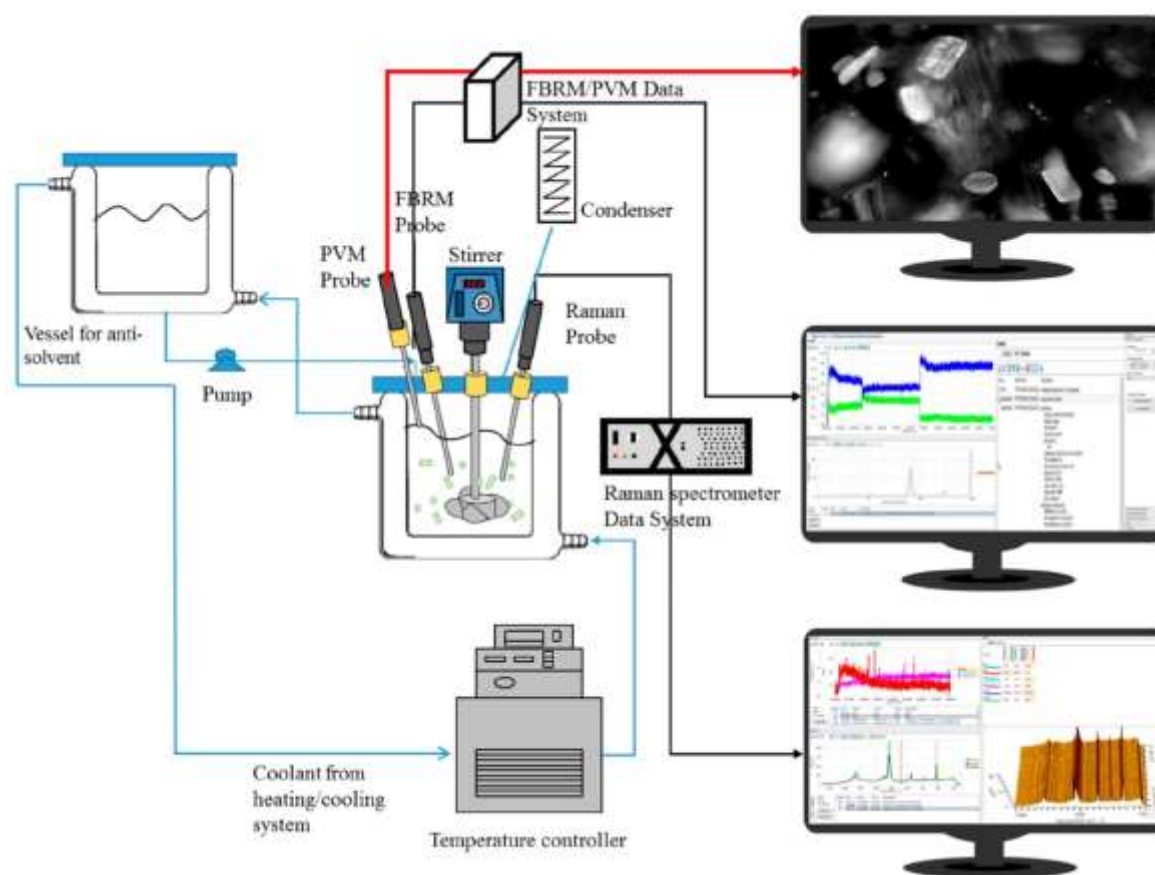


**Fig. 4-2: Anti-solvent crystallization equipment.**

Experiments were performed in batch crystallization mode. After dissolving the GMP crystals in a solvent (water) at 10 K higher than the saturation temperature, the GMP solution was cooled to a set temperature. The temperature of methanol was set to be the same as the crystallization temperature using a thermostat. Then, methanol was fed to the stirred solution at a constant rate. In all experiments, the Raman spectra, FBRM data, PVM data, and temperature were recorded at 10 s intervals. Crystals were sampled at regular intervals using a solid–liquid separator with glass filters and dried for 24 h at 30 °C for analysis. The initial concentration of the GMP solution was set at 10–30% by mass. The temperature was 20 °C, and the methanol mass fraction of the solvent mixture ranged from 0.3 to 0.8 (methanol g/solvent mixture g). The addition rate ranged from 0.7 to 40 g/min. Products were identified

using a Raman spectrometer (Kaiser Optical Systems, Ann Arbor, MI, USA) equipped with a light-emitting diode laser (785 nm, 450 mW) as an excitation source. The crystal morphology was investigated once every minute by the HNK250 PVM (Mettler Toledo, Switzerland). The measurement range of the FBRM probe (model M400LF) is 0.5 to 1000  $\mu\text{m}$ .

### 4.3 Instrumental Analysis Methods

#### 4.3.1 Raman Spectroscopy

The Raman spectra were recorded using RXN Systems (Kaiser Optical Systems, USA) equipped with a light-emitting diode laser (785 nm, 450 mW) as the excitation source. A one-fold objective lens with a probe was used to collect the spectra. The spectra ranged from 100 to 1890  $\text{cm}^{-1}$  and were acquired with 4  $\text{cm}^{-1}$  of spectral width and 5 s of exposure. The iCRaman software (Mettler-Toledo, Switzerland) was used to calibrate the concentrations of solids and solution. Analysis of the Raman data was performed by the absence and occurrence of peaks originally found in spectra of the single components. To calibrate the concentrations of the solids and solution, a multivariate partial least square (PLS) model was used. In this study, the noncontact PhAT probe was used to collect offline the spectra of the isolated solid materials, while the MR probe was employed in solution and in a suspended state for the online measurement. To confirm the identity of the forms, PXRD patterns of the polymorphs were compared.

#### 4.3.2 X-Ray Powder Diffraction

For PXRD, a PXRD pattern of the solid was calculated using a Smart Lab X-ray diffractometer (Rigaku, Japan) with  $\text{CuK}\alpha$  radiation generated at 200 mA and 45 kV. The sample was placed on a silicone plate at room temperature. Data were collected from 3° to 45° ( $2\theta$ ) at a step size of 0.02° and a scan rate of 5°  $\text{min}^{-1}$ .

#### 4.3.3 Focused Beam Reflectance Measurement

The FBRM tools used in this study were manufactured by Mettler-Toledo, USA. A FBRM probe (model M400LF) was used to characterize both the nucleation and dissolution of the material. FBRM measures a chord length distribution (CLD) and thereby the number and the measured count data can be split into specific population regions in the size range, as the chord length is converted into particle sizes. As the FBRM was carried out over a 10-s period, the number of counts in the range of 0.1–990  $\mu\text{m}$  was used as an indication of nucleation. The process of crystalline transformation was also monitored by monitoring the changes in the size and number of particles. The solubilities of the amorphous and hydrate forms, which can change into a more stable form, were determined by FBRM. iCFBRM software was utilized during the experiment.

#### 4.3.4 Particle Video Microscope

Particle video microscopy (PVM) provides in-situ digital grayscale images and can examine the shape of droplets or particles in addition to measuring droplet size. A high-resolution CCD camera and six independent laser sources, arranged in a circle at an angle of 60° around the objective, enable high-quality pictures to be taken even in relatively dark slurries. The PVM probe (model 800L) was operated at an image update rate of two images per second.

#### 4.3.5 Thermal Analysis

TGA and DSC of the solid forms were carried out by using a thermogravimetric analyzer (TGA 2050, DSC 2010; TA Instruments, USA) at up to 573 K (300 °C) with dried nitrogen and at a flow rate of 70 mL min<sup>-1</sup> and a heating rate of 10 K min<sup>-1</sup>.

#### 4.3.6 Viscosity Measurement

Viscosity was determined by a Brookfield DVEELVTJO viscometer (Middleborough, MA, USA) at 20 °C using an LV2-62 spindle at 100 rpm. The viscosities of the GMP solution and the amorphous slurry were measured under the same conditions as in all of the experiment runs. The measurement was carried out by putting 500 mL of the test material into the measurement vessel at 20 °C. The viscosities of the water–GMP solution and the amorphous slurry under the same conditions of each run were measured separately.

### 4.4 Calibration and Identification

#### 4.4.1 Characterization of Materials

PXRD (D / MAX 2500H, Rigaku) patterns of GMP obtained in this study are shown in Fig. 4-3. Based on comparing the PXRD pattern of GMP used in this study with the literature [Tsu18], the PXRD pattern of tetrahydrate GMP was 5.7, 10.0, 14.0, 17.4, 17.8, 18.2, 23.1, and 24.4 °. In addition, a comparison of the PXRD pattern of heptahydrate GMP used in this study with the pattern in the literature [Che18] showed that it had the same characteristic peaks at 2θ of 7.9, 12.7, 15.9, 20.4, 22.6, and 37.9 °. The characteristic peak of amorphous GMP was only at 27.6 °, which is consistent with the reference [Zou17].

The Raman spectrum of the GMP measured by a Raman spectrometer (Kaiser Optical Systems, Ann, Michigan, USA) equipped with a light emitting diode laser (785 nm, 450 mW) is shown in Fig. 4-4. The Raman spectrum of the tetrahydrate is 367, 431, 502, 593, 680, 882, 984, 1326, 1495, 1632, and 1705 cm<sup>-1</sup>; and 882cm<sup>-1</sup> was chosen as the characteristic peak of tetrahydrate crystal. The Raman spectrum of heptahydrate is 355, 387, 470, 592, 652, 832, 867, 974, 1009, 1057, 1090, 1185, 1418, 1495, and 1670 cm<sup>-1</sup>; and the characteristic peaks of heptahydrate selected were 893 cm<sup>-1</sup> and 976 cm<sup>-1</sup>. Also the Raman spectrum of the amorphous is 1741, 1587, 1480, 1372, 1328, 1025, 983, 880, 582, 503, 380, and 327 cm<sup>-1</sup>; and the characteristic peaks selected were 380 cm<sup>-1</sup> and 1480 cm<sup>-1</sup>. Raman spectra of GMP dissolved in a solvent show distinct peaks at 876, 977, 1077, 1487, and 1581 cm<sup>-1</sup>, while those of water are characterized at 373, 418, and 1742 cm<sup>-1</sup>. Therefore, multiple intrinsic peaks of 876 and 977 cm<sup>-1</sup> were selected for the peaks of the GMP solution to obtain the calibration curve.

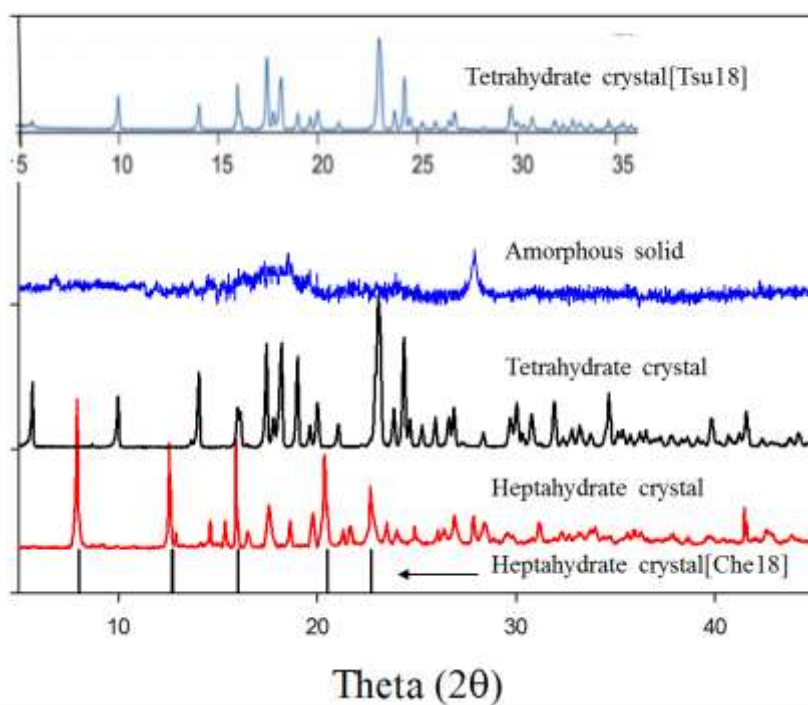
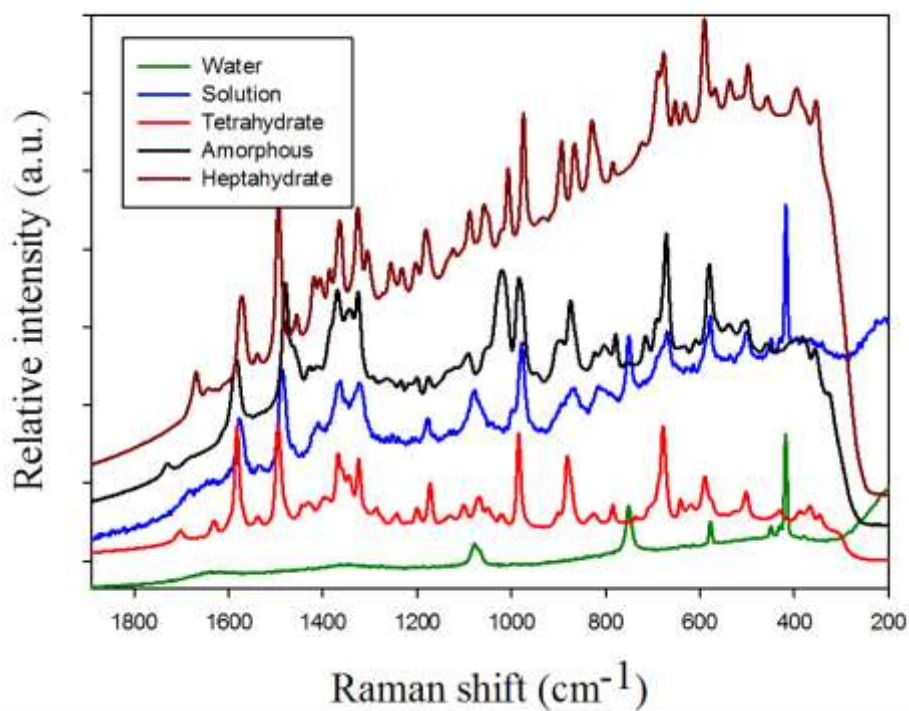


**Fig. 4-3:** PXRD patterns of amorphous, tetrahydrate and heptahydrate forms of GMP, which are compared with the references [Tsu18,Che18].



(a)

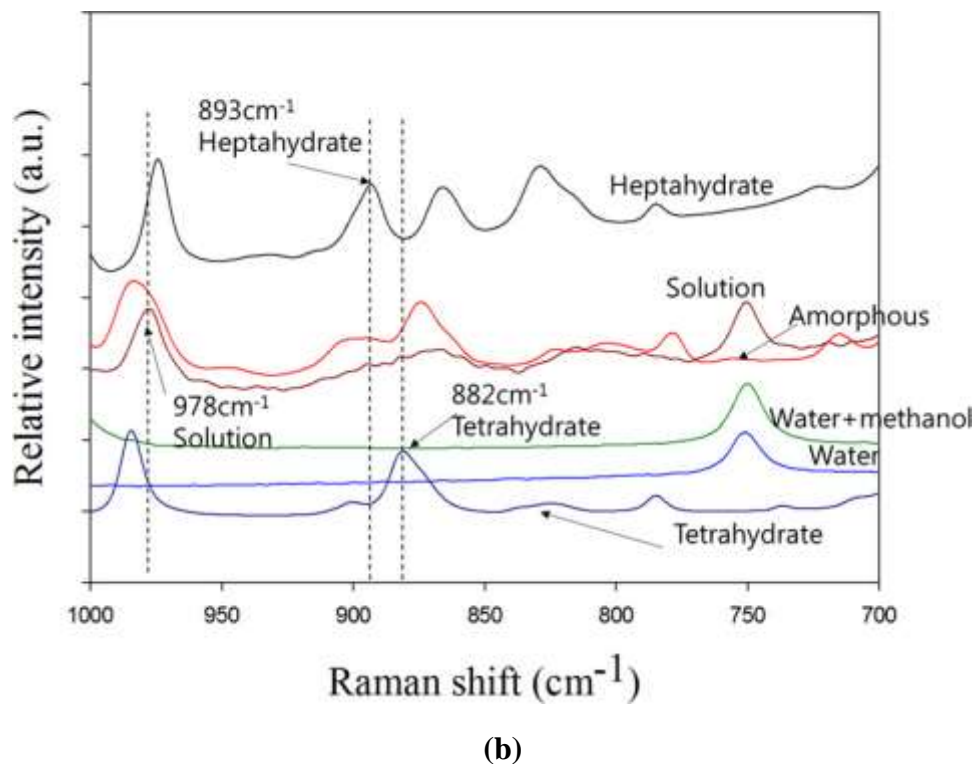
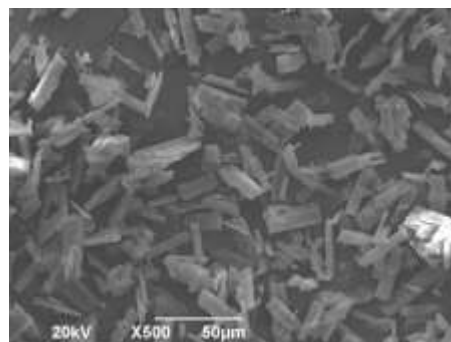
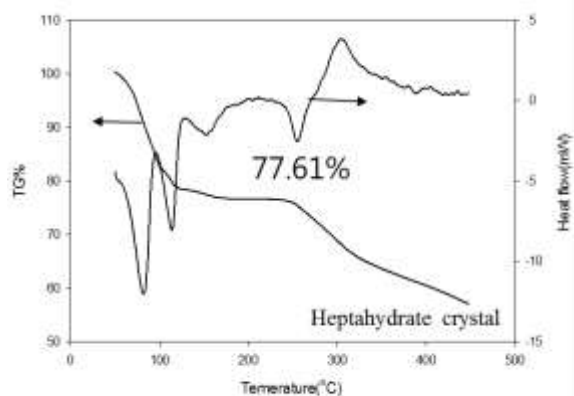


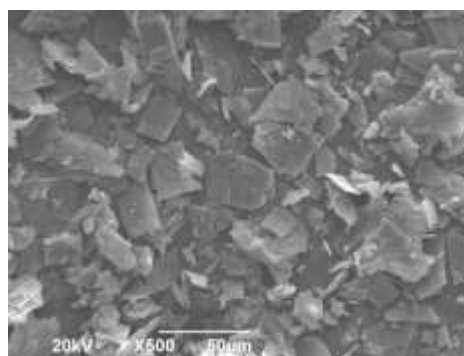
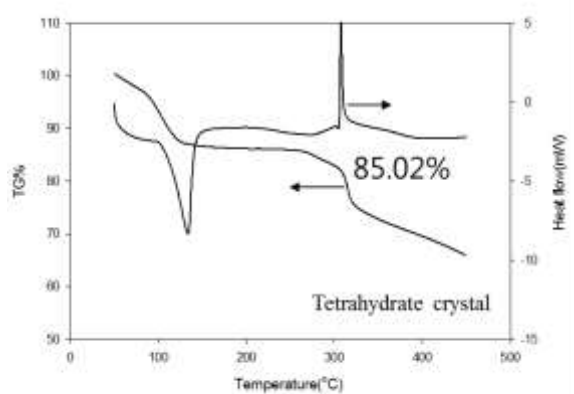
**Fig. 4-4: (a) Raman spectra of amorphous solid, tetrahydrate crystal, heptahydrate crystal, solution and solvent in range of 200 to 2000. (b) Characteristic Raman spectra of the amorphous solid, tetrahydrate crystal, heptahydrate crystal, solution and solvent ranging from 700 to 1000  $\text{cm}^{-1}$ .**

The tetrahydrate, heptahydrate, and amorphous forms of GMP were confirmed by TGA-DSC and are shown in Fig. 4-5(a). The TGA-DSC results show the different thermodynamic characteristics of the three solid forms. The TGA curve of the crystalline form of tetrahydrate and heptahydrate shows a stepwise loss of crystal water molecules, giving a total water content of 22.39% and 14.98%, respectively, which are consistent with the literature data [Zou17,Che18]. The curve of the amorphous form is smoother, with a total water content of 12.98%, which is similar to the data given in reference [Che18]. From the DSC pattern, it can be seen that the different molecular arrangements brought about the different heat absorption and release behaviors, and the response signal of the endothermic peak of hydrate GMP was obviously higher than that of amorphous GMP.

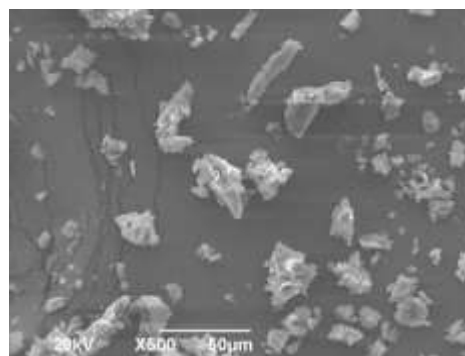
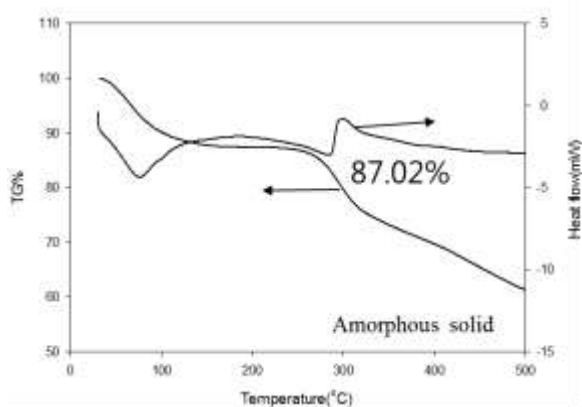
Morphologies of the solid samples were observed by means of SEM (JEOL, JSM-6390) and optical microscopy. The morphology of the crystals is shown in Fig. 4-5(b) as taken with scanning electron microscope. The amorphous and hydrate forms clearly exhibited different morphologies. The forms also had different appearance morphologies in the SEM images: the heptahydrate form appeared as regular rectangles and tetrahydrate crystals appeared to have distorted facets, while the amorphous form was constructed from disordered irregular shapes [Che18]. Combined with the results of PXRD, Raman spectroscopy, SEM, and TG-DSC, it was concluded that amorphous GMP, tetrahydrate GMP, and heptahydrate GMP were well characterized.



(Heptahydrate crystals)



(Tetrahydrate crystals)



(Amorphous solids)

(a)

(b)

**Fig. 4-5: TG-DSC analysis and scanning electron microscopy photos of amorphous, tetrahydrate and heptahydrate forms of GMP.**

#### 4.4.2 Calibration and Analysis of Raman Spectroscopic Data

Raman spectra of solvents, solution, amorphous solid, tetrahydrate crystal, and heptahydrate crystal are shown in Fig. 4-4. Raman spectra of GMP dissolved in solvent show distinct peaks at 876, 977, 1077, 1487, and 1581  $\text{cm}^{-1}$ ; while those of water are characterized at 373, 418, and 1742  $\text{cm}^{-1}$ . Therefore, multiple intrinsic peaks of 867 and 977  $\text{cm}^{-1}$  were selected for the peak of the GMP solution to obtain the calibration curve. This PLS technique was used to calculate the solubility of GMP.

The calibration of solution concentration at the peak of 977  $\text{cm}^{-1}$  is shown in Figs. 4-6(a) and (b), while the Raman intensity of solution concentration for peaks of 867 and 977  $\text{cm}^{-1}$  is shown in Fig. 4-6(a). The Raman spectrum of the solution was measured in a solution in which a range of 0-80 g of GMP was completely dissolved in 100 g of solvent. Raman spectra were collected at various fractions of solute/solvent for a solute concentration range of 0-0.8 (GMP g/water g). Solution concentration was calculated using the intensity of the Raman peak of the GMP dissolved in the solution per peak of the solvent. A distinct peak of the solvent is at 418  $\text{cm}^{-1}$ . PLS technology can neglect the weak effects of temperature, crystal size, solution density, or unpredictable variables. The calibration plot of GMP concentration in solution against peak ratio of GMP/solvent are well matching with the correlation coefficient of 0.9997 (Fig.4-6(b)). From the results of the calibration curve for concentrations of solution, amorphous solid, tetrahydrate crystal, and heptahydrate crystal (Fig. 4-6(b)), it was found that the predicted concentration and actual concentration were well matched. Calibration lines of solids using Raman spectra were developed for solids suspended in saturated solution. However, transformation in the Raman spectrum was found during crystalline measurements. A solid fraction was determined using the Raman spectrum of slurry before transformation occurred. The validity of the calibration line for in-situ measurements was confirmed by the comparison with the off-line Raman measurement. The spectra were normalized to 418  $\text{cm}^{-1}$  each with the difference in strength of the solvent peak and the valley. The calibration curve of the concentration of solids shows the correlation coefficient as 0.9971-09998.

Since the solution concentration and the solid concentrations can be measured simultaneously using this Raman calibration, the solubility of the materials accompanying a potential solvate transformation can be easily obtained using in-line Raman measurement.

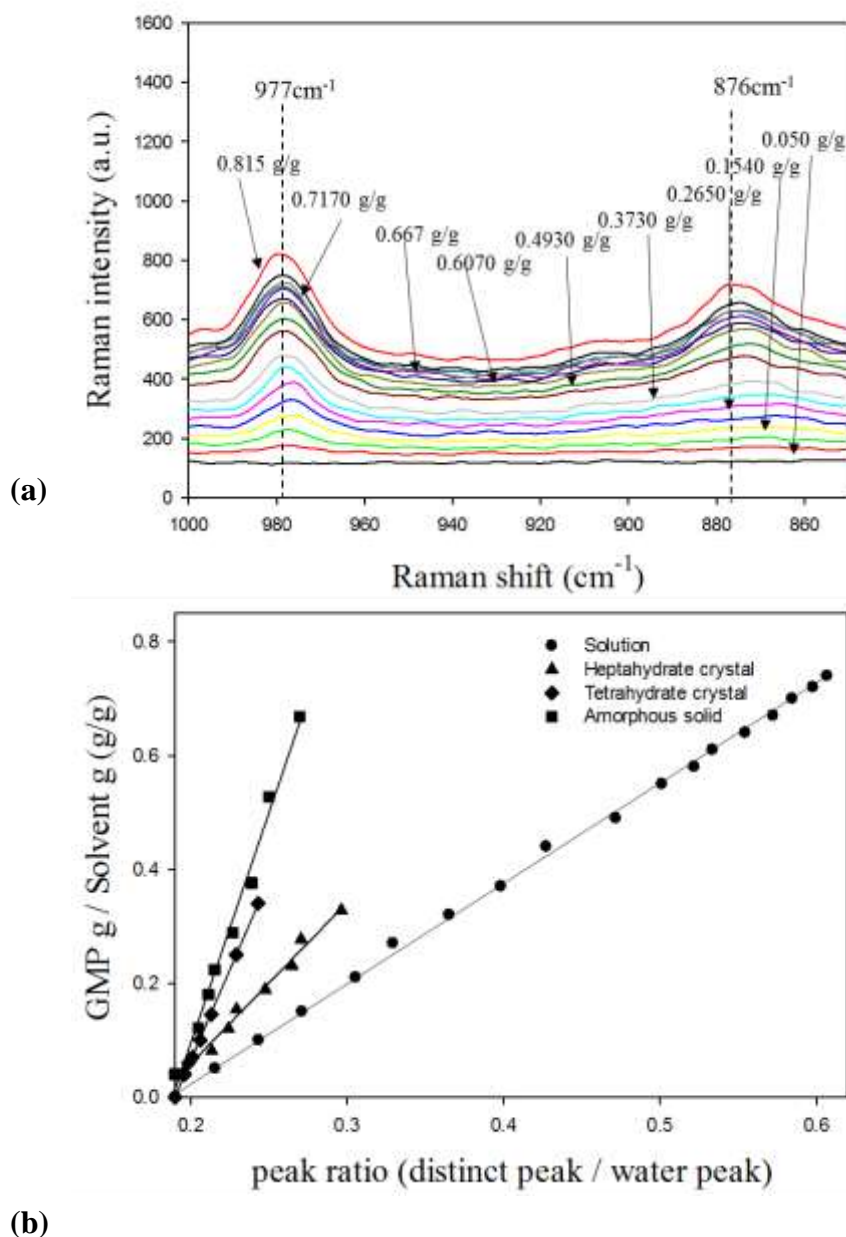
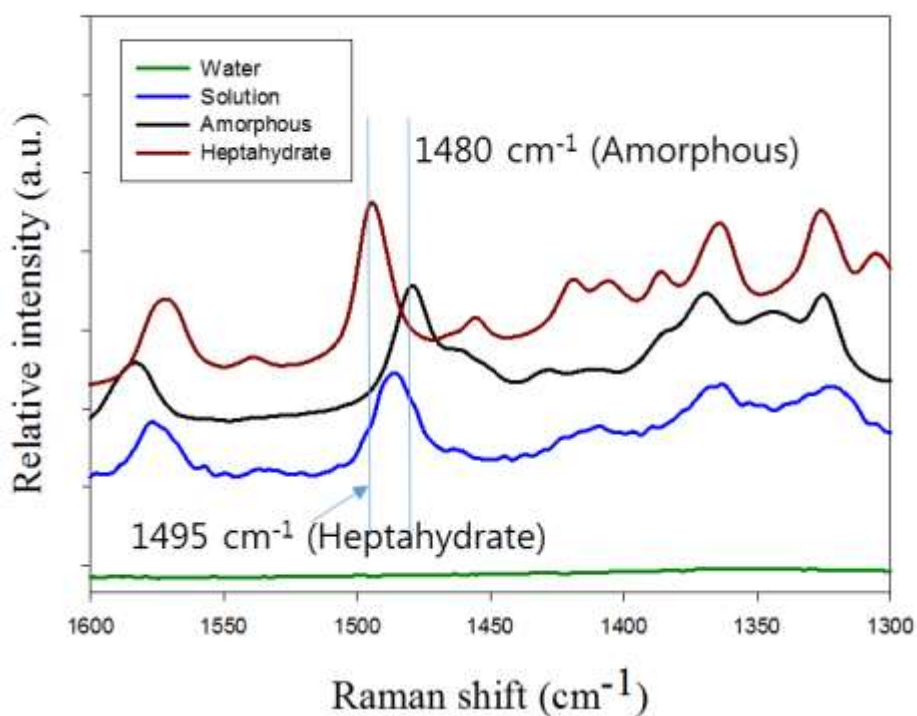


**Fig. 4-6: Calibration of concentration by PLS method using Raman spectra. (a) Raman intensity against solution concentration at 876 and 977  $\text{cm}^{-1}$  and (b) calibration of amorphous solid ( $380 \text{ cm}^{-1}$ ), tetrahydrate crystal ( $802 \text{ cm}^{-1}$  and  $984 \text{ cm}^{-1}$ ), heptahydrate crystal ( $867$  and  $974 \text{ cm}^{-1}$ ) and solution. The calibration curve of GMP concentration in solution is developed using relative Raman intensity, which is GMP solute peaks ( $876$  and  $977 \text{ cm}^{-1}$ )/solvent peak ( $418 \text{ cm}^{-1}$ ).**

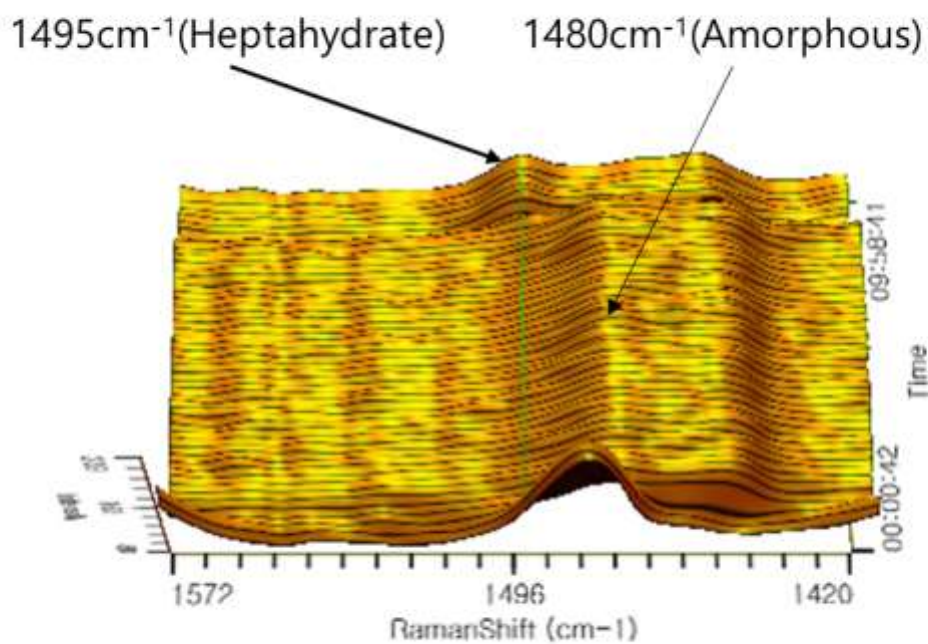
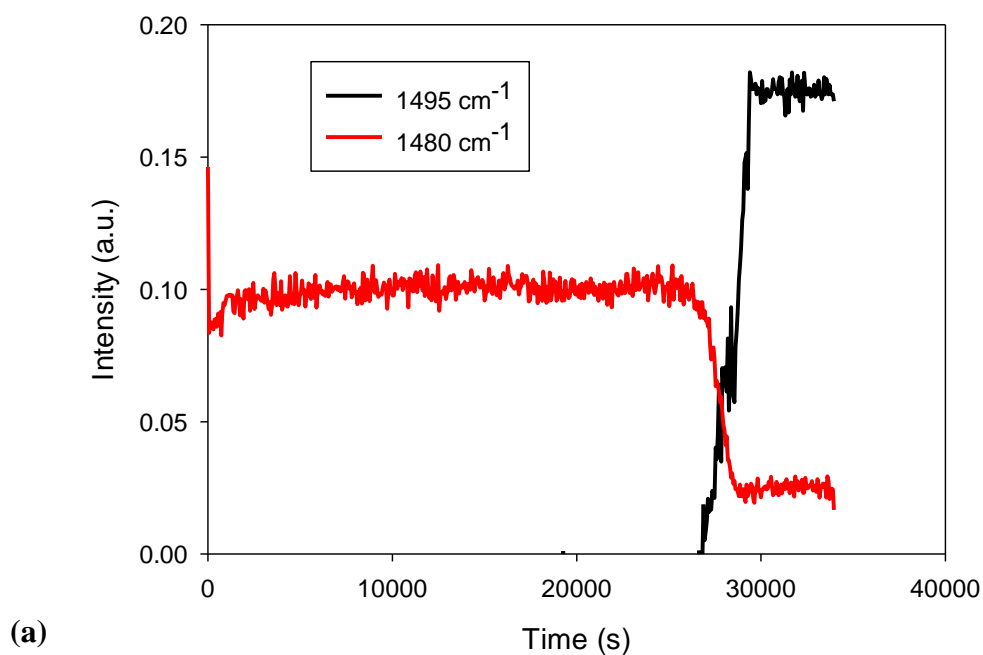
#### 4.4.3 Calibration of Solution and Solid Concentrations

Fig. 4-7 shows the Raman shift values of solvents (water), GMP solutions, amorphous solids and heptahydrate solids found in Raman spectra in the range of  $1300$  to  $1600 \text{ cm}^{-1}$ . Fig. 4-8a is a result of in-situ measurement by Raman spectroscopy, comparing the intensities of  $1480$

$\text{cm}^{-1}$  (amorphous solid) and  $1495 \text{ cm}^{-1}$  (heptahydrate solid) peaks. Fig. 4-8b is a waterfall diagram of the formation and extinction of amorphous and heptahydrate. They can find the concentration of each solid through calibration. The calibration of amorphous solid, heptahydrate solid and solute concentration using Raman spectra has been presented in Fig. 4-6b. Fig. 4-6a shows the Raman intensity against solution concentration at the peaks of  $876 \text{ cm}^{-1}$  and  $977 \text{ cm}^{-1}$ . Fig. 4-8b shows the calibration results for solution, amorphous solid and heptahydrate solid. The correlation coefficient of the calibration curve for the solid concentration is 0.9971-0.9998. The calibrated concentration of the mixed solids was consistent with the actual concentration.



**Fig. 4-7: Raman spectra of the amorphous form and the crystalline heptahydrate in the range of 1300 to 1600  $\text{cm}^{-1}$ .**



Kaiser Optical Systems / METTLER TOLEDO

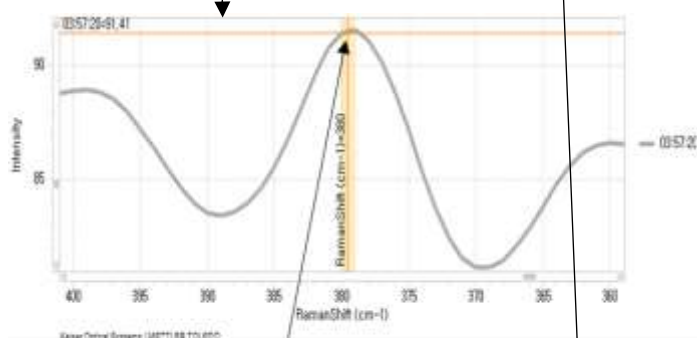
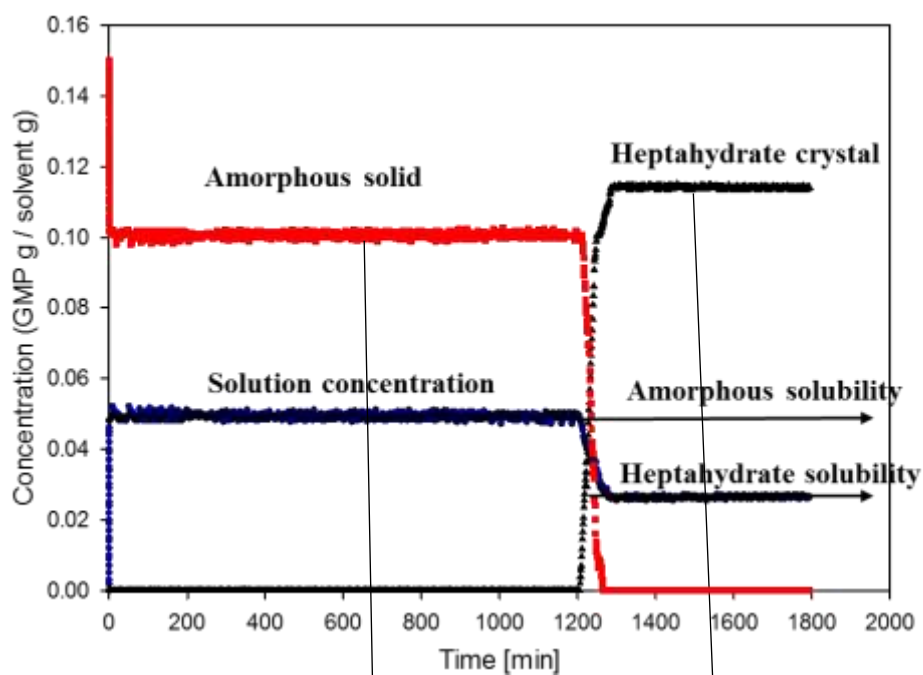
(b)

**Fig. 4-8: Formation of amorphous and transformation to heptahydrate. (a) variation of Raman intensity, (b) 3D waterfall diagram.**

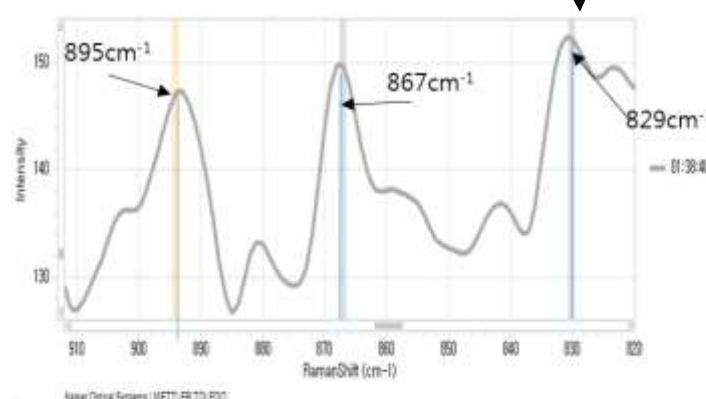
#### 4.5 Measuring Concentration of Solid Forms

Solubility (equilibrium state) is a very important thermodynamic parameter for determining the crystallization mode, supersaturation, phase diagram, and yields [Su10,Ngu08]. The solubility is the concentration at which no crystalline state change can be observed. In addition, it can also be needed for determination of the kinetics of crystallization and the particle size and shape, which are controlled by the supersaturation. The solubility measured by the off-line gravimetric method was compared with the solubility measured by Raman spectroscopy. Raman spectroscopy in-situ monitored the measurement by the gravimetric method. In the final data of the experimental runs, the results of the Raman spectroscopy were well matching with those of the solubility measured off-line. This method was then repeated to measure the amorphous, heptahydrate, and tetrahydrate equilibrium solubilities at different temperatures. Solubility and transformation were easily detected from the Raman peak and FBRM data. The solid concentration, solution concentration, and solubility were measured in the binary solvent mixture in situ by Raman spectroscopy.

The solubilities of the amorphous and heptahydrate particles/crystals measured by Raman spectroscopy are shown in Fig. 4-9a with its waterfall diagram. To measure the solubility of the heptahydrate solid, an excess amount was added. After measurement, Raman spectroscopy at 20 °C and a methanol mass fraction of 0.5 (methanol g/solvent mixture g) were used to confirm the form of the residue. A change in solid form during measurement was observed. 15 g of amorphous solid was added to 100 g of solvent. After the addition, the amorphous solid started to dissolve. At equilibrium, 4.954 g of solid was dissolved and 10.045 g of solid did not dissolve. After about 20 h, the amount of the amorphous solid started to decrease sharply as it was transformed into heptahydrate crystals. With an increase in the amount of heptahydrate crystals in the transformation process, the solution concentration decreased to 0.0263 (GMP g/ water g). As a result, the solubility of the amorphous form was 0.04951 (GMP g/ water g), and the solubility of the heptahydrate was 0.0263 (GMP g/ water g). This is because the heptahydrate is more thermodynamically stable than the amorphous solid in these solvents. The solubilities of the heptahydrate and tetrahydrate crystals measured by Raman spectroscopy at 50 °C and a methanol mass fraction of 0.7 (methanol g/solvent mixture g) are shown in Figs. 4-9b and c. Of the heptahydrate solid, 20 g was added to 100 g of solvent. At equilibrium, 4.205 g of heptahydrate had dissolved in 100 g of solvent. At about 6844 s, the heptahydrate crystal started to be transformed into the tetrahydrate crystal. The Raman waterfall at the same condition shows that the Raman shift of 893  $\text{cm}^{-1}$  (heptahydrate) disappeared at 8238 s and the one of 882  $\text{cm}^{-1}$  (tetrahydrate) appeared at 6844 s. This indicates that the heptahydrate in binary solvent mixtures (methanol + water) was transformed to the tetrahydrate for 1394 s. As the tetrahydrate crystals increase in the transformation process, the solution concentration decreases to 0.04205 g. As a result, the solubilities of the heptahydrate and tetrahydrate are almost the same. However, the tetrahydrate is a little more thermodynamically stable than the heptahydrate in methanol/water.

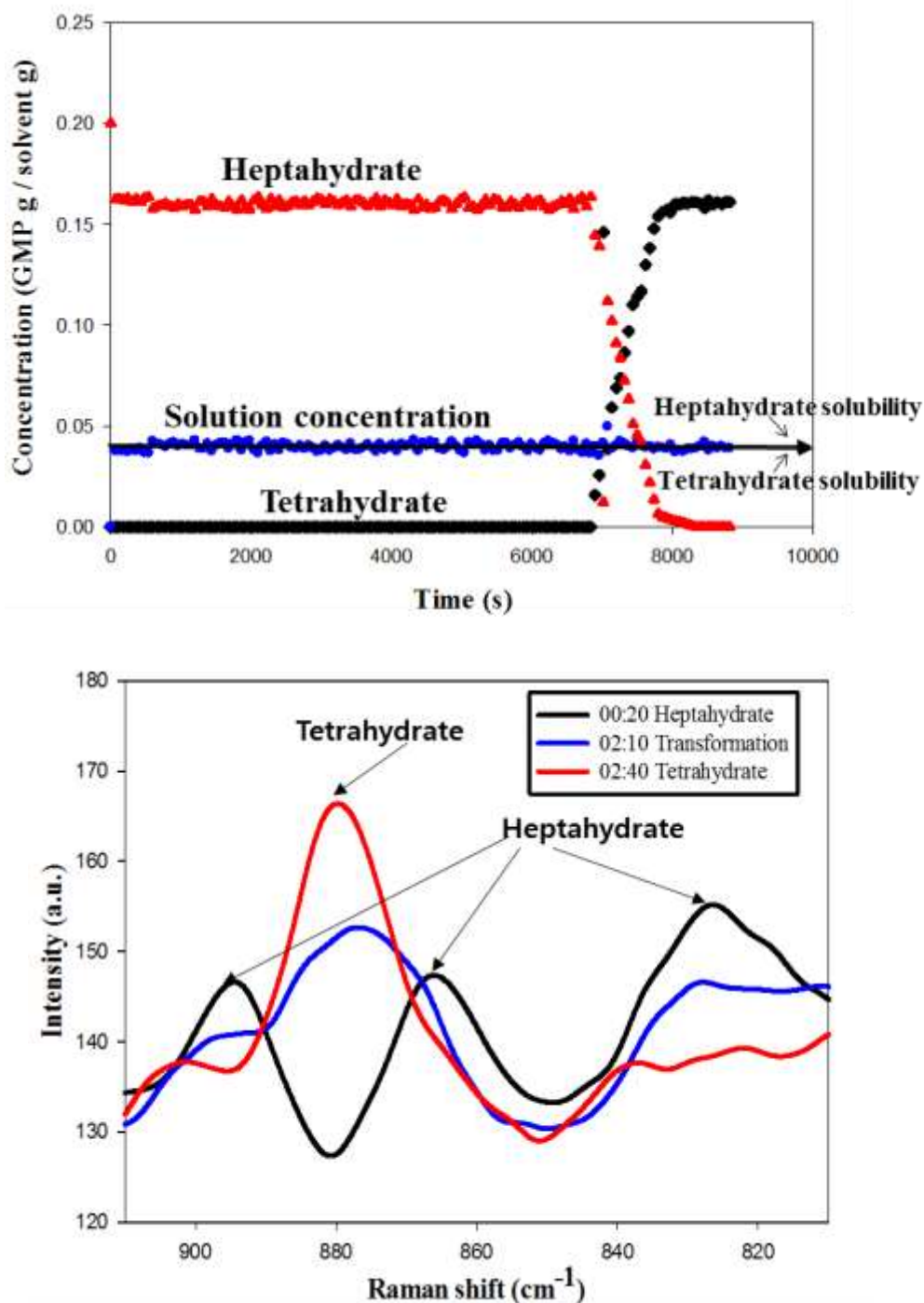


380cm<sup>-1</sup> peak (amorphous)



895cm<sup>-1</sup>, 867cm<sup>-1</sup>, 829cm<sup>-1</sup> (heptahydrate)

(a)



(b)

**Fig. 4-9:** (a) Solubility measurement of the amorphous solid (metastable form) and heptahydrate (stable form) in binary solvent mixtures measured by Raman spectroscopy at 293.15 K and a methanol fraction of 0.5 with Raman spectra. (b) Solubility measurement of the heptahydrate (metastable form) and the tetrahydrate (stable form) in binary solvent mixtures measured by Raman spectroscopy at 323.15 K and a methanol fraction of 0.7 with Raman spectra of the solid forms.

## 5. Results

### 5.1 Solubilities and Metastable Zone Width of Solid Forms

#### 5.1.1 Solubilities of Solid Forms

The solubility of the stable form for the amorphous, tetrahydrate, and heptahydrate solids in water/methanol was determined in the range of 20–60 °C and a methanol mass fraction of 0.1–0.9 (methanol g/solvent mixture g). Experiments for the stable form solubility were carried out for about 48 h. The experimental data are listed in Tab. 5-1 and plotted in Fig. 5-1, in which the solubility of GMP is expressed as the mass of GMP per mass of solvent [Kim22a]. According to a previous work [Lie11], the solubility of the heptahydrate in a methanol fraction of 0.3 (methanol g/solvent mixture g) was found to be 0.0395 (GMP g/water g) at 20 °C. This is similar to the data measured in this study. The solubility increased slightly with increasing temperature, as shown in Fig. 5-1, because the solubility strongly depends on the solvent fraction in water and methanol. Anti-solvent crystallization using methanol can be applied to a selective preparation of GMP. Furthermore, the solubility curve is divided into two zones: at 50–60 °C and  $0.15 < \text{methanol fraction (methanol g/solvent mixture g)} < 0.9$ , the tetrahydrate is stable, while below 40 °C and at  $0.15 < \text{methanol fraction (methanol g/solvent mixture g)} < 0.6$ , the heptahydrate is stable. At 20–60 °C and a methanol fraction (methanol g/solvent mixture g) of 0.8–0.9, the tetrahydrate is stable. At methanol fractions (methanol g/solvent mixture g)  $< 0.1$  and all temperatures, the amorphous form was found, even though heptahydrate solids were added in the experiment. Crystals of the tetrahydrate were obtained at temperatures  $> 45$  °C. At high temperatures, crystals with low hydration numbers are easily formed, and ionic groups are not fully hydrated under these conditions. The solubility of the amorphous solid is highest at the temperatures investigated. The amorphous solids were formed at the temperatures investigated and a water fraction (water g/solvent mixture g)  $> 0.9$ , and the solubility of the amorphous solids was highest within this temperature range.

**Tab. 5-1: Solubility of the stable form as a function of the temperature and solvent fraction. A, amorphous; H, heptahydrate; T, tetrahydrate. Errors of measurements were less than 0.1 %**

Temperature (°C)	Methanol mass fraction (-)								
	0.1	0.2	0.3	0.4	0.5	0.6	0.7	0.8	0.9
20	0.3102	0.07255	0.05103	0.04563	0.02634	0.01792	0.01213	0.01022	0.00612
	(A)	(H)	(H)	(H)	(H)	(H)	(H)	(T)	(T)
25	0.3287	0.08315	0.06051	0.05055	0.03010	0.02153	0.01642	0.01312	0.00745
	(A)	(H)	(H)	(H)	(H)	(H)	(H)	(T)	(T)
30	0.3418	0.09891	0.06263	0.06018	0.03421	0.02647	0.02086	0.01546	0.00953
	(A)	(H)	(H)	(H)	(H)	(H)	(T)	(T)	(T)
35	0.3435	0.1172	0.07758	0.07070	0.03844	0.03046	0.02355	0.01878	0.01123
	(A)	(H)	(H)	(H)	(H)	(T)	(T)	(T)	(T)

40	0.3488 (A)	0.1291 (H)	0.08445 (H)	0.07840 (H)	0.04491 (T)	0.03523 (T)	0.03027 (T)	0.02316 (T)	0.01333 (T)
45	0.3606 (A)	0.1432 (T)	0.09965 (T)	0.08935 (T)	0.04965 (T)	0.03985 (T)	0.03582 (T)	0.02812 (T)	0.01658 (T)
50	0.3771 (A)	0.1602 (T)	0.11510 (T)	0.09431 (T)	0.05548 (T)	0.04312 (T)	0.04240 (T)	0.03218 (T)	0.01887 (T)
55	0.3968 (A)	0.1789 (T)	0.12840 (T)	0.1044 (T)	0.06032 (T)	0.04915 (T)	0.04673 (T)	0.03665 (T)	0.02375 (T)
60	0.4125 (A)	0.1945 (T)	0.14010 (T)	0.1157 (T)	0.06680 (T)	0.05543 (T)	0.05325 (T)	0.04223 (T)	0.02682 (T)

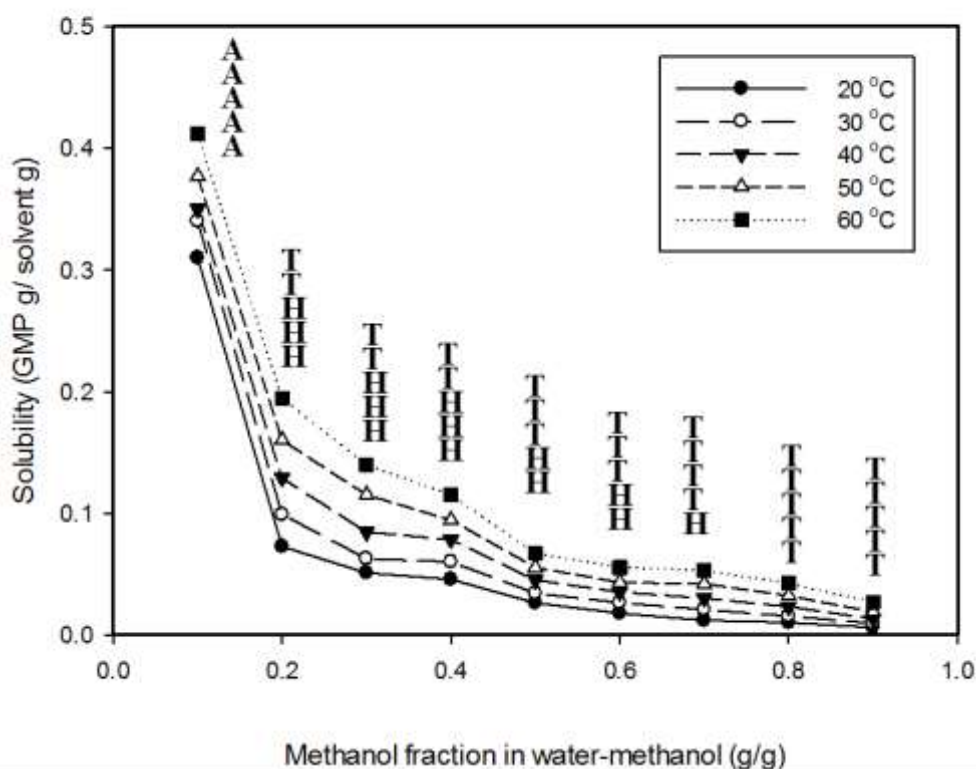


**Fig. 5-1: Solubility of GMP in water-methanol at various temperatures and methanol fractions. (A, H and T stand for amorphous, heptahydrate and tetrahydrate, respectively. Errors of measurements was less than 0.1%.**

As a result, the solubility (equilibrium) and the concentration at which solids start to form (metastable zone limit) are found by simultaneously measuring the solution concentration and the concentrations of the tetrahydrate, heptahydrate, and amorphous solids. This equilibrium water activity value depends greatly on the temperature. The lower the temperature, the smaller

is the water activity value needed to attain equilibrium between the hydrates. The obtained results are useful for determining the crystallization parameters to achieve the desired hydrates. The approach can be applied to other amorphous and hydrate (or solvate) systems.

Intermediate phases were detected during transformation from the amorphous to the hydrate form. Amorphous solids are dissolved because of the solubility difference, and the hydrates are crystallized. In addition, the water molecules of the heptahydrate are desorbed below about 40 °C, and the heptahydrate is transformed into the tetrahydrate because of hydration loss. This supports our understanding that a single intermediate state composed of tetrahydrate was observed with the dehydration test [Kam67].

### 5.1.2 Enthalpy and Entropy of Dissolution

From the solubility data, the enthalpy of dissolution,  $\Delta H_d$ , and the entropy of dissolution,  $\Delta S_d$ , can be calculated [Wan11, Kim22a]:

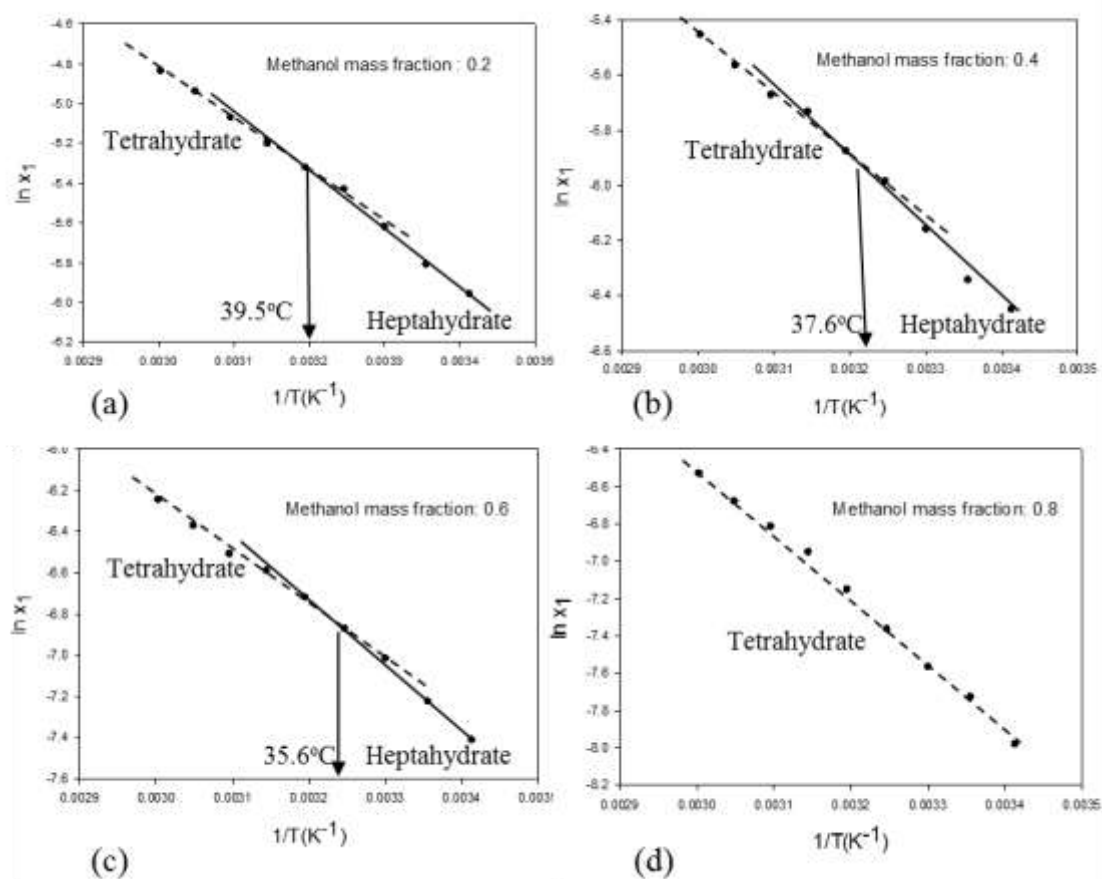
$$\ln x = -\frac{\Delta H_d}{RT} + \frac{\Delta S_d}{R}, \quad (5-1)$$

where  $R$  is the gas constant,  $\Delta H_d$  and  $\Delta S_d$  are the dissolution enthalpy and the entropy, respectively, and  $T$  is the absolute temperature.

Examples of the solubilities of the tetrahydrate and heptahydrate, which are plotted as  $\ln x$  versus  $1/T$  for solvent fractions, are shown in Fig. 5-2. The values of the enthalpy and entropy of dissolution of both forms were obtained from the slope and the intercept of the plots and are listed in Tab. 5-2. The values of the enthalpy and entropy of dissolution of the heptahydrate were higher than those of the tetrahydrate. A similar result was reported for the anhydrate/monohydrate of carbamazepine in water-methanol mixtures [Mur02]. However, the enthalpy and entropy of dissolution of both the tetrahydrate and heptahydrate decreased with increasing water fraction in the solvent mixture. The enthalpy and entropy of dissolution also increased with increasing methanol fraction in the solvent, as the solubility in water was much higher than that in methanol. The relative stabilities of the tetrahydrate and heptahydrate can be obtained from Fig. 5-2, and enantiotropic behavior is exhibited. For a solvent fraction, the stable form must have a lower solubility than the metastable form.

**Tab. 5-2: Enthalpy and entropy of dissolution of the heptahydrate and tetrahydrate**

Methanol fraction (-)	Heptahydrate		Tetrahydrate		Transition temperature (°C)
	$\Delta H_d(\text{kJ/mol})$	$\Delta S_d(\text{kJ/mol K})$	$\Delta H_d(\text{kJ/mol})$	$\Delta S_d(\text{kJ/mol K})$	
0.2	21.7	0.0526	20.7	0.0491	39.5
0.3	22.0	0.0503	20.8	0.0464	39.1
0.4	22.1	0.0500	20.8	0.0448	37.6
0.5	21.0	0.0411	20.2	0.0386	37.4
0.6	24.6	0.0508	22.2	0.0429	35.6
0.7	29.8	0.0660	24.7	0.0499	30.1
0.8	-	-	27.9	0.0574	-
0.9	-	-	30.4	0.0612	-

**Fig. 5-2: Plot of  $\ln(x_1)$  versus  $1/T$  from the solubility of GMP at methanol fractions of (a) 0.2, (b) 0.4, (c) 0.6, and (d) 0.8. The  $R^2$  of linear regression analyses is 0.994.**

The intercept in the extrapolation of the plots of the two forms represents the point where the solubilities of the tetrahydrate and heptahydrate are identical. In other words, the tetrahydrate

and heptahydrate are in equilibrium. Thus, it is referred to as the transition temperature in the specified solvent system. The tetrahydrate is the stable form at temperatures higher than the transition point. The heptahydrate is the stable form if the temperature is lower than the transition point. A smaller water fraction (water g/solvent mixture g) leads to a lower transition temperature between heptahydrate and tetrahydrate, but the tetrahydrate exists without a transition point at a methanol mass fraction (methanol g/solvent mixture g)  $> 0.8$ .

### 5.1.3 Supersaturation and Metastable Zone Width

In solution crystallization, supersaturation is the main parameter affecting the solid form that crystallizes [Kim15,Oma08]. Previous studies have presented the solubility of heptahydrate, tetrahydrate, and amorphous forms of GMP as a function of a water–methanol fraction [Kim22a]. The amorphous solubility was highest in the whole range of the solvent fraction. Below 45 °C, the solubilities of tetrahydrate and heptahydrate were close together with heptahydrate as somewhat lower one, while at 45 °C or higher, tetrahydrate was the slightly lower one. At 20 °C and a methanol fraction (methanol g/solvent mixture g)  $> 0.2$ , the solubility is in the order of amorphous  $>$  heptahydrate  $>$  tetrahydrate. At a methanol fraction (methanol g/solvent mixture g) of 0.3, the solubility difference between amorphous and heptahydrate and between heptahydrate and tetrahydrate are 0.0105 and 0.0065 solute g/solvent g, respectively, and the solubility difference decreases as the methanol fraction increases. The supersaturation difference between the amorphous and the hydrates is clear. Thus, selective preparation of solid forms can be carried out by adjusting the temperature and the methanol/water ratio, based on the solubility and the supersaturation.

Although the solubility differences between the three forms are not very large, the metastable zone widths differ significantly. The metastable zone width depends on the supersaturation as a kinetic property. The solubility, on the other hand, is a thermodynamic property. Figs. 5-3a and 3b shows schematic changes in metastable zone width with respect to methanol fraction and time in anti-solvent crystallization, respectively [Kim22b]. It serves as a guide for the formation and transformation of metastable forms. Therefore, from the understanding of the difference between saturation and supersaturation, a method for preparing selectively either a stable form or a metastable form without transformation can be proposed.

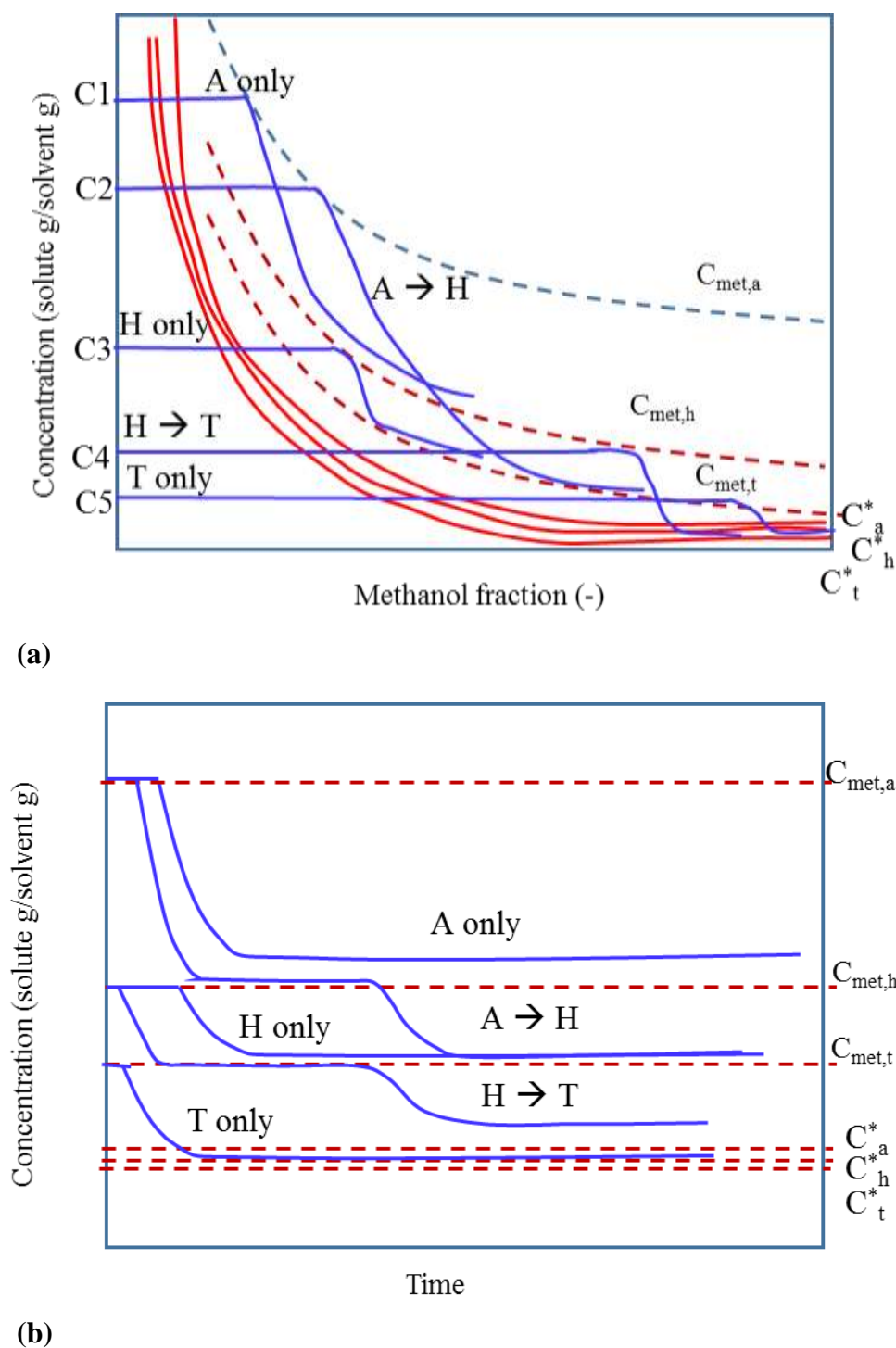


**Fig. 5-3: a) Schematic concentration changes with respect to methanol fraction. b) Schematic concentration changes with respect to time in anti-solvent crystallization (A, H and T stand for amorphous, heptahydrate and tetrahydrate, respectively.).**

Supersaturation depends, besides the temperature, on the feed rate, initial concentration, and fraction of anti-solvent in anti-solvent crystallization. Therefore, amorphous, heptahydrate, and tetrahydrate forms can be selectively controlled by adjusting these variables. Fig. 5-3a shows the metastable supersaturation limits  $C_{met,a}$ ,  $C_{met,h}$ , and  $C_{met,t}$  arbitrarily in the plots of solute

concentration against methanol fraction. From this figure, during anti-solvent crystallization at the initial concentration  $C1$ , the operating line meets  $C_{\text{met,a}}$  to form an amorphous form. The concentration decreases and an amorphous form is produced without transformation. At the initial concentration of  $C2$ , amorphous is first formed in  $C_{\text{met,a}}$ , and after a certain induction period, it meets  $C_{\text{met,h}}$ , in which amorphous form is transformed into heptahydrate. At the initial concentration of  $C3$ , only the formation and growth of heptahydrate take place under the condition that it meets the limit line of the metastable zone of heptahydrate,  $C_{\text{met,h}}$ . At the initial concentration of  $C4$ , heptahydrate is first formed at  $C_{\text{met,h}}$  and is transformed into tetrahydrate at  $C_{\text{met,t}}$ . At the initial concentration  $C5$ , only the formation and growth of tetrahydrate occurs under the condition that it meets the limit line of the metastable zone of tetrahydrate,  $C_{\text{met,t}}$ . In addition, at the same concentration, a higher addition rate of the anti-solvent leads to a greater supersaturation. Fig. 5-3b shows the selective formation and transformation of the solid forms from the plot of concentration versus time corresponding to Fig. 5-3a.

## 5.2 Finding Conditions for Selective Formation of Solid Forms

### 5.2.1 Selective Formation

There are various routes for formation of crystalline hydrates and the amorphous form. Anti-solvent crystallization at an initial concentration of 0.1–0.3 (GMP g/water g) and addition rates of 0.9–38 g min<sup>-1</sup> were carried out [Kim22b]. Supersaturation was generated by adding anti-solvent into the solution. In-situ monitoring was observed by Raman spectroscopy. Raman spectra of eight cases are presented as 3D surface waterfalls in Fig. 5-4. Raman spectra with elapsed time are dramatically different in the range of 1890–200 cm<sup>-1</sup>. As can be seen in Fig. 5-4, the nucleation, the growth, and the transformation of amorphous, heptahydrate and tetrahydrate were shown by Raman spectra in the range of 300–412, 760–932, and 302–414 cm<sup>-1</sup>, respectively.

In Fig. 5-4a, Raman spectra of solids, during operation, at a feed concentration of 0.3 (GMP g/water g), a temperature of 20 °C and an anti-solvent fraction (methanol g/solvent mixture g) of 0.5 are presented as a 3D surface waterfall plot. The amorphous peak at 380 cm<sup>-1</sup> was formed, and no transformation was observed for about 24 h. Fig. 5-4b shows heptahydrate peaks at 893 and 973 cm<sup>-1</sup>, which were formed without transformation for 10 h. Fig. 5-4c shows the amorphous peak at 380 cm<sup>-1</sup>, which was formed first and transformed into heptahydrate with peaks at 893 and 973 cm<sup>-1</sup>. Fig. 5-4d shows the amorphous peak at 380 cm<sup>-1</sup>, which was formed first and transformed into heptahydrate with a peak at 355 cm<sup>-1</sup>. Raman spectra of heptahydrate peaks at 893 and 973 cm<sup>-1</sup> were changed into that of the tetrahydrate peak at 882 cm<sup>-1</sup> after 1.9 h (Fig. 5-4e). Raman spectra of the tetrahydrate peak at 882 cm<sup>-1</sup> were changed into that of the heptahydrate in the solid state at 1.5 h (see Fig. 5-4f). At a feed concentration of 0.1 (GMP g/water g), the tetrahydrate was directly nucleated without any transformation, which was evidenced by the appearance of the 882 cm<sup>-1</sup> peak in Raman spectra. Raman spectra of this case are depicted in Fig. 5-4g. Fig. 5-4h shows Raman peaks of the solution concentrations at 867 and 977 cm<sup>-1</sup>.

Therefore, it can be seen that the formation and transformation of the solid phase during the crystallization process can be quantified by Raman spectra. In this study, two in-line tools, Raman spectral analysis and FBRM, can clearly identify the solution-mediated transformation mechanism. Six case studies were conducted to prepare various forms of solids [Kim22b].

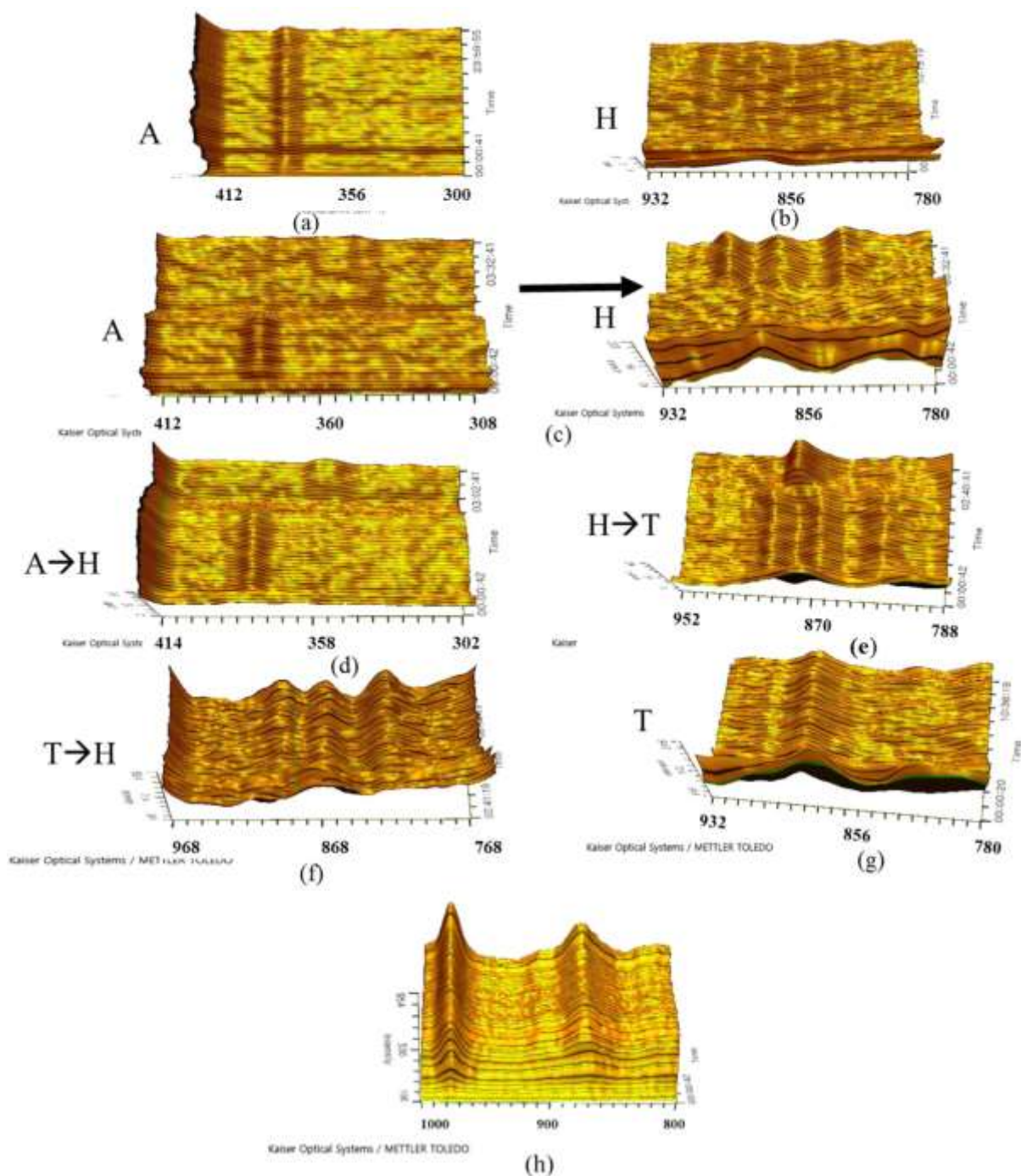


**Fig. 5-4: 3D surface waterfall Raman spectra in the regions of 300–412, 760–932, 302–414, and 800–1000  $\text{cm}^{-1}$ , and during a) formation of the amorphous, b) formation of the heptahydrate, c and d) formation of the amorphous and transformation into the heptahydrate, e) formation of the heptahydrate and transformation into the tetrahydrate, f) formation of the tetrahydrate and transformation into the heptahydrate, g) crystallization of the tetrahydrate, and h) solution. (A, H and T stand for amorphous, heptahydrate and tetrahydrate, respectively.)**

### 5.2.2 Case study for Amorphous to Heptahydrate Transformation

Fig. 5-5 shows Raman and FBRM data for the case of amorphous-to-heptahydrate transformation. It was carried out by anti-solvent crystallization at 20 °C with a GMP/water ratio of 0.2, a methanol fraction of 0.33 (methanol g/solvent mixture g) in the solvent, and a methanol feed rate of 38 g min<sup>-1</sup>. In this case, the results of Raman spectroscopy and FBRM can be divided into four sections: precipitation of amorphous material, dissolution of amorphous solid, heptahydrate nucleation and transformation into heptahydrate, and heptahydrate growth.

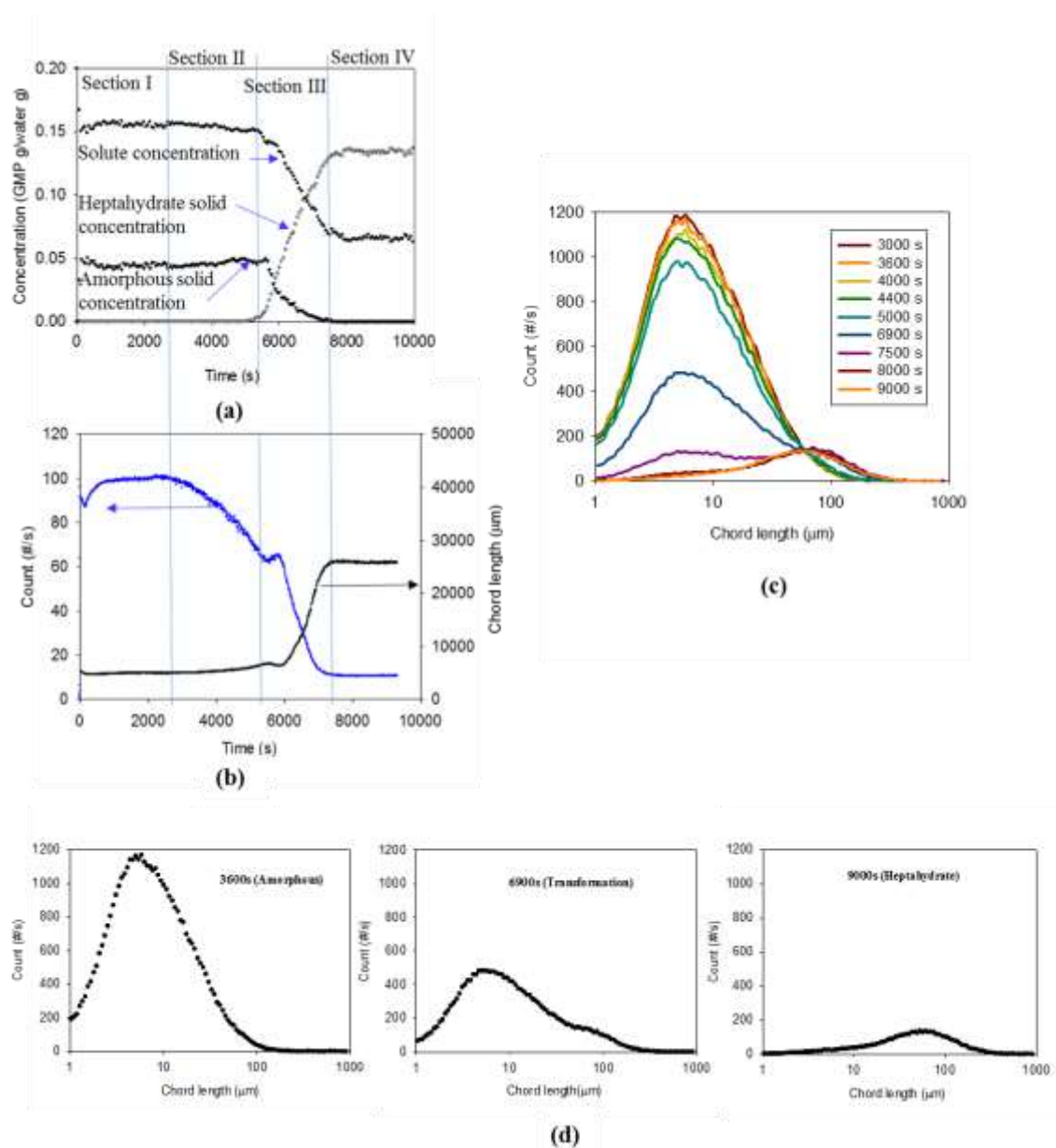


**Fig. 5-5: Raman and FBRM data for amorphous-to-heptahydrate transformation. a) Time-concentration profiles for solution, and amorphous, and heptahydrate solids. b) Counts and chord length from FBRM. c) Chord length distributions (CLDs) over time. d) CLDs during transformation.**

Section I is the amorphous formation section. Solid formation is accomplished by adding methanol into the solution. The change of particle size is reflected in the FBRM's unweighted CLD, as shown in Fig. 5-5b. The number of particles increased rapidly after generating supersaturation by methanol addition and then remained constant. The particle size also increased rapidly at the same time as the methanol added, and kept constant at about 11  $\mu\text{m}$ . The width of the particle size distribution remained without change. It is clear that there were a large number of fine particles between 1 and 20  $\mu\text{m}$  initially in the unweighted CLD. The amorphous concentration of 0.048 (amorphous GMP g/water g), the solute concentration of 0.152 (GMP g/water g) in the solution (see Fig. 5-5a), the number of counts, and the chord length were constant until 2800 s.

Section II is the pre-transformation section. After 2900 s, the width of the particle size distribution did not change, and the peak began to decrease slightly. Accordingly, the number of particles decreased and the mean particle size was not changed (see Fig. 5-5b). In addition, the number of fine particles between 1 and 20  $\mu\text{m}$  underwent a relatively small change in the transformable form to prepare for the subsequent crystallization of the heptahydrate form (see Fig. 5-5b,c). The concentrations of the solution and the amorphous solid were 0.152 and 0.048 solute g/solvent g, respectively. Additionally, the pretransformation section is a step to prepare the supersaturation conditions to generate the heptahydrate nuclei.

Section III is the transformation section. The number of particles decreases rapidly, and the particle size increases due to the decrease in supersaturation and dissolution of the amorphous form with a higher solubility compared to the solubility of heptahydrate (see Fig. 5-5b). For this reason, there is a moment at 5200 s in which the particle number increased slightly, and hence the particle size decreased slightly. At the same time, the concentration of the solution began to decrease. No dissolution of the amorphous solid was initially observed. After that, dissolution of amorphous solids and a sharp decrease in solution concentration occurred near 5900 s, and the solution supersaturation for heptahydrate steadily decreased, causing nucleation of heptahydrate. In the CLDs (see Fig. 5-5c,d), a bimodal distribution curve was created as another peak appeared near 67  $\mu\text{m}$  during the transformation process at 6900 and 7500 s. As a result, a bimodal distribution with peaks at 8.9 and 67  $\mu\text{m}$  was shown. Therefore, the number of small particles (0–50  $\mu\text{m}$ ), which were amorphous solids, first increased, and then decreased due to the dissolution, which activated the crystal growth of heptahydrates.

In Section IV, due to the dissolution of the amorphous form and the growth of heptahydrate in the previous section, the particle number gradually decreased and the particle size increased to 67  $\mu\text{m}$ . The increase in size was due to crystal growth of heptahydrate. In the particle size distribution, the amorphous particles disappeared completely, the bimodal distribution disappeared, and only crystals of heptahydrate around 67  $\mu\text{m}$  existed (see Fig. 5-5c,d). The solution concentration decreased from 0.2 to 0.069 (GMP g/water g). In summary, this case consisted of amorphous formation, amorphous dissolution, amorphous to hydrate transformation, and hydrate crystal growth. Characteristically, an amorphous dissolution was discovered before transformation, and then the transformation process by nucleation of heptahydrate was revealed.

### 5.2.3 Case Study for Heptahydrate to Tetrahydrate Transformation

Fig. 5-6 shows Raman and FBRM data for the case of heptahydrate-to-tetrahydrate transformation. It was carried out by anti-solvent crystallization at 50 °C at a GMP/water ratio of 0.2, a methanol fraction of 0.5 (methanol g/solvent mixture g) in solvent, and a methanol feed rate of 38 g  $\text{min}^{-1}$ . In this case, the results of FBRM and Raman spectroscopy can be

divided into three sections: nucleation and growth of heptahydrate, transformation from heptahydrate to tetrahydrate, and growth of tetrahydrate.

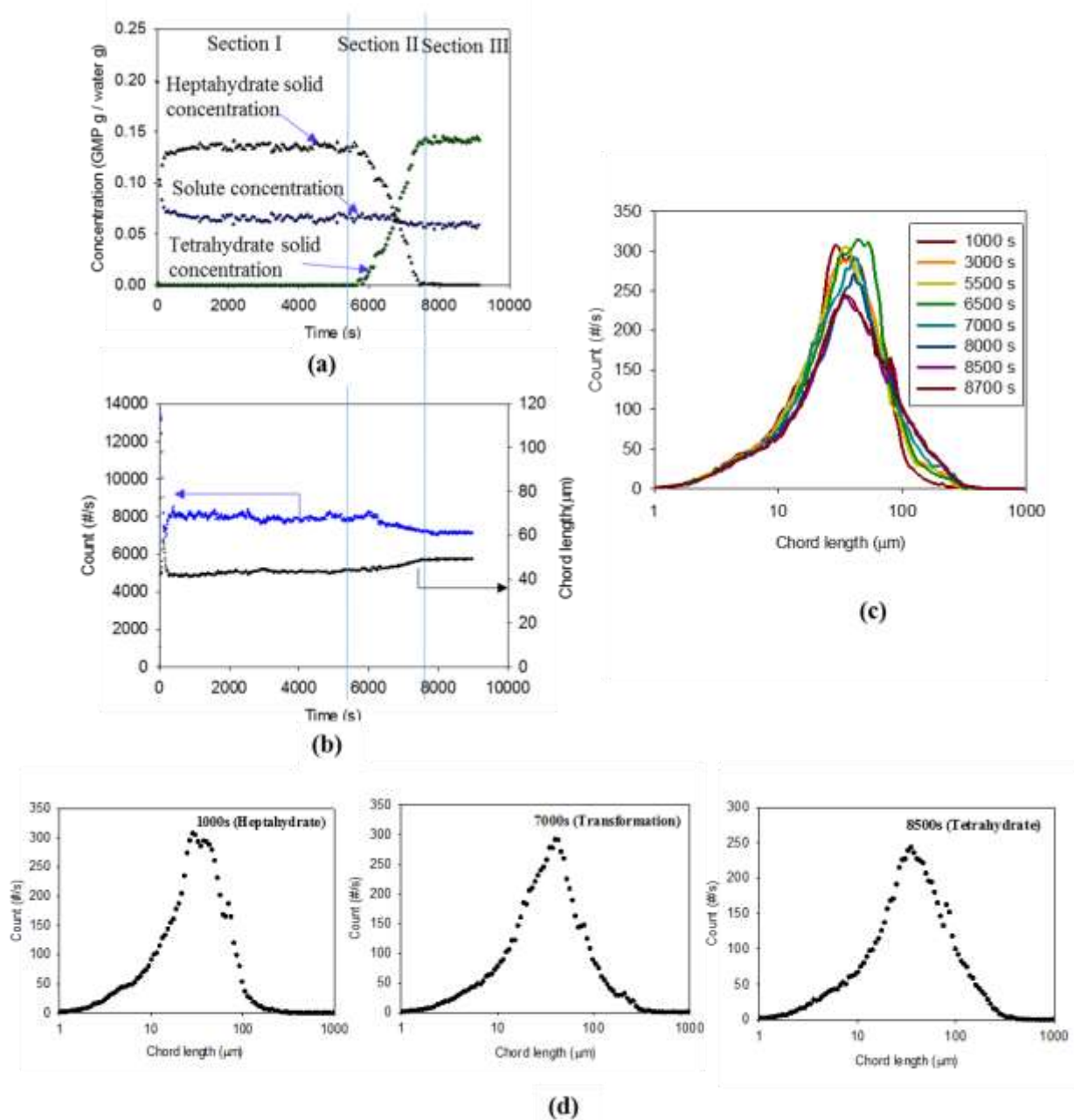


**Fig. 5-6: Raman and FBRM data for heptahydrate-to-tetrahydrate transformation. a) Time–concentration profiles for solution, and heptahydrate and tetrahydrate solids. b) Counts and chord length from FBRM. c) Chord length distributions (CLDs) over time. d) CLDs for transformation.**

Section I represents the heptahydrate nucleation and growth. In crystallization, crystals of heptahydrate nucleate and grow by adding methanol into the solution. Upon the addition of methanol, supersaturation was achieved, and the number of particles increased rapidly and then remained at  $8023 \text{ \# s}^{-1}$ . The particle size also increased sharply at the same time as methanol

addition and remained constant at about 43  $\mu\text{m}$ . It was found that the width of the particle size distribution was not changed significantly in the range of 10–100  $\mu\text{m}$ . The solution concentration decreased from 0.2 to 0.058 solute g/solvent g when heptahydrate was formed, and the concentration of heptahydrate crystals increased to 0.142 solute g/solvent g.

Section II represents nucleation of tetrahydrate and dissolution of heptahydrate (see Fig. 5-6a,b). As shown in the solute concentration–time profile in Fig. 5-6a, the solubilities of heptahydrate and tetrahydrate are similar, but the solubility of tetrahydrate is lower by 0.0052 solute g/solvent g. After the induction period, the nucleation of tetrahydrate occurred rapidly as a result of the dissolution of heptahydrate due to the slightly higher solubility. For this reason, the particle number started to decrease suddenly at 5700 s and the particle size started to increase. According to the FBRM results, the crystal size increased from 43 to 48  $\mu\text{m}$  during the transformation process (see Fig. 5-6c,d). In the process, the number of particles decreased from 8023 # to 7600 #  $\text{s}^{-1}$ . Due to a small solubility difference, the solution concentration decreased by about 0.0071 solute g/solvent g. No formation of an amorphous solid was observed.

Thereafter, the supersaturation for tetrahydrate formation steadily decreased, causing the growth of tetrahydrate in the state, where the dissolution of the heptahydrate near 6800 s does not result in a change in the solute concentration. Then the solute concentration decreased. In the particle size distribution, the peak near 43  $\mu\text{m}$  was maintained without change during the transformation process. Therefore, the particle size distribution of heptahydrate was initially shown, but no change in the number of particles was observed by the nucleation of tetrahydrate in the fine particles (1–20  $\mu\text{m}$ ). Since there is a little difference in solubility between two hydrated crystals, the transformation process is driven by dissolution of heptahydrate crystals and growth of tetrahydrate crystals. Therefore, the number of transformed particles decreased, and the size increased by 5  $\mu\text{m}$  (about 10%).

No clear change in particle size distribution was observed during the transformation process. Therefore, the nucleation of heptahydrate was not reflected in the distribution. In addition, crystal growth caused the distribution to broaden to the right and the peak height to decrease slightly. From this phenomenon, transformation due to dissolution appears to be large and accompanied by crystal growth of tetrahydrate.

Section III is the tetrahydrate growth section. Due to the dissolution of the heptahydrate and the growth of the tetrahydrate, the particle number decreased slightly and the particle size increased up to 48  $\mu\text{m}$ . The CLDs become gradually wider and indicate the growth of the tetrahydrate. In this case, nucleation of heptahydrate, transformation from heptahydrate to tetrahydrate, and growth of tetrahydrate were identified. Characteristically, there was a slight change in crystal size and little change in particle size distribution during the transformation process.

#### 5.2.4 Case Study for Tetrahydrate to Heptahydrate Transformation

Fig. 5-7 shows Raman and FBRM data for the case of tetrahydrate-to-heptahydrate transformation. It was carried out by anti-solvent crystallization at 50  $^{\circ}\text{C}$  with a GMP/water ratio of 0.2, a methanol fraction of 0.333 (methanol g/solvent mixture g), and a methanol feed rate of 38  $\text{g min}^{-1}$ . In this case, the results of FBRM and Raman spectroscopy can be divided into three sections: tetrahydrate nucleation and growth, heptahydrate nucleation and transformation, and heptahydrate growth.

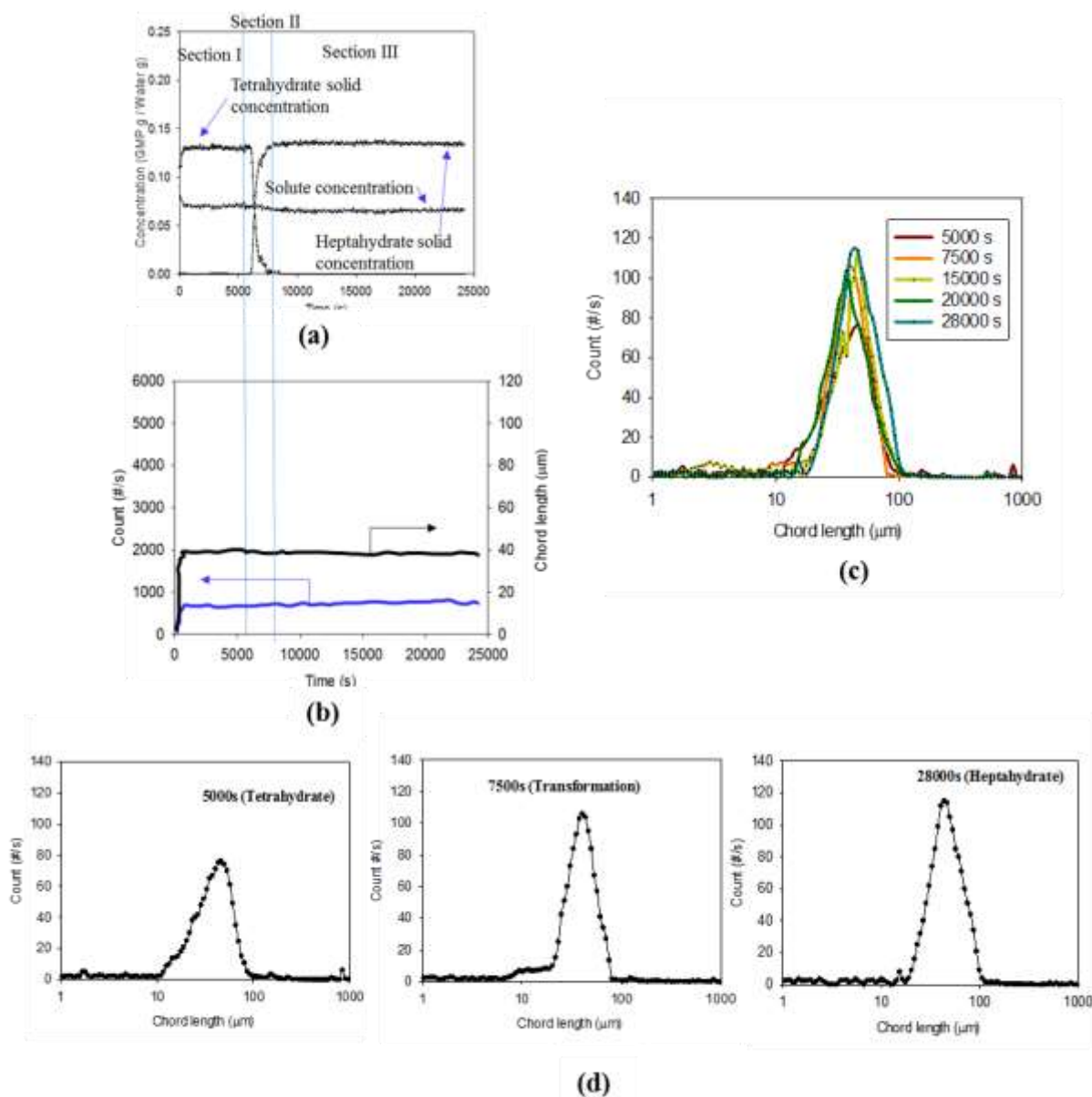


**Fig. 5-7: Raman and FBRM data for tetrahydrate-to-heptahydrate transformation. a) Time–concentration profiles for solution, and tetrahydrate and heptahydrate solids. b) Counts and chord length from FBRM over time. c) Chord length distributions (CLDs) over time. d) CLDs for transformation.**

Section I is the nucleation and growth of tetrahydrate section. The crystallization of tetrahydrate is achieved by adding methanol into the solution. After the addition of methanol to generate supersaturation, the number of particles increased rapidly and then was maintained at  $2230 \text{ \# s}^{-1}$ . The particle size also increased rapidly at the same time as methanol addition and was kept at about  $41 \text{ \mu m}$ . The width of the particle size distribution did not change significantly before 5100 s (see Fig. 5-7c). The crystal distribution width of heptahydrate is narrower than that of tetrahydrate (see Fig. 5-7d). The concentration of the solution decreased from 0.2 to 0.07 solute g/solvent g, and the concentration of heptahydrate crystals was 0.13 solute g/solvent g.

Section II is the section on nucleation of heptahydrate and dissolution of tetrahydrate (see Fig. 5-7a,b). As can be seen in Fig. 5-7a, crystallization of heptahydrate occurs rapidly due to the dissolution of tetrahydrate. It results from the slightly higher solution concentration compared to the solubility of the stable form (heptahydrate). For this reason, heptahydrate nucleation occurred instantaneously at 6000 s, and the particle number and particle size did not change. The concentration of the solution did not change either. No dissolution of the tetrahydrate solid was observed in the particle size distribution. After that, the crystal growth of tetrahydrate was induced in the state where no change in solution concentration was detected near 6000 s. The particle size distribution was maintained without changing the peak near 40  $\mu\text{m}$  during the transformation process. Therefore, the particle size distribution of tetrahydrate appeared at first, but the number of particles increased in the fine particles (1–20  $\mu\text{m}$ ) due to nucleation of heptahydrate. Despite the dissolution of tetrahydrate and the growth of heptahydrate, the particle number and particle size did not change, and the number of coarse chord lengths (50–150  $\mu\text{m}$ ) was constant. In this process, nucleation of tetrahydrate, transformation from tetrahydrate to heptahydrate, and growth of heptahydrate were identified. Characteristically, the transformation process occurred with little change in particle size distribution, particle size, and number of particles.

According to the FBRM results, the particle size was almost constant at 40  $\mu\text{m}$  during the transformation. There was little change in the number of particles. The reason is that the solubilities of heptahydrate and tetrahydrate are similar. The change in solution concentration had little effect with a decrease of about 0.001 solute g/solvent g. There was no obvious change in the particle size distribution during the transformation. Therefore, the tetrahydrate crystals did not appear after transformation (see Fig. 5-7c,d). It was observed that the particle size distribution was slightly widened to the right due to growth of heptahydrate crystals. From this phenomenon, it is expected that transformation by dissolution occurs on the solid surface and is accompanied by crystal growth.

### 5.3 Nucleation in Anti-Solvent Crystallization

#### 5.3.1 Amorphous Formation and Transformation

Characteristic peaks of the amorphous form at 380, 582 and 880  $\text{cm}^{-1}$ , and peaks of heptahydrate crystals at 893, 829 and 865  $\text{cm}^{-1}$  were selected. Fig. 5-8 shows the Raman data with elapsed time for Run 1 (given in Tab. 5-3) as an example. The time-dependent spectral change in the range of 300–500  $\text{cm}^{-1}$  (Fig. 5-8a) reveals that an amorphous peak at 380  $\text{cm}^{-1}$  appears when the anti-solvent is introduced. It disappears after about 8 h, and then the crystalline heptahydrate form appears at 893  $\text{cm}^{-1}$  (Fig. 5-8b). This implies that the amorphous form was generated first and then completely transformed into the crystalline heptahydrate via liquid-mediated phase transformation.

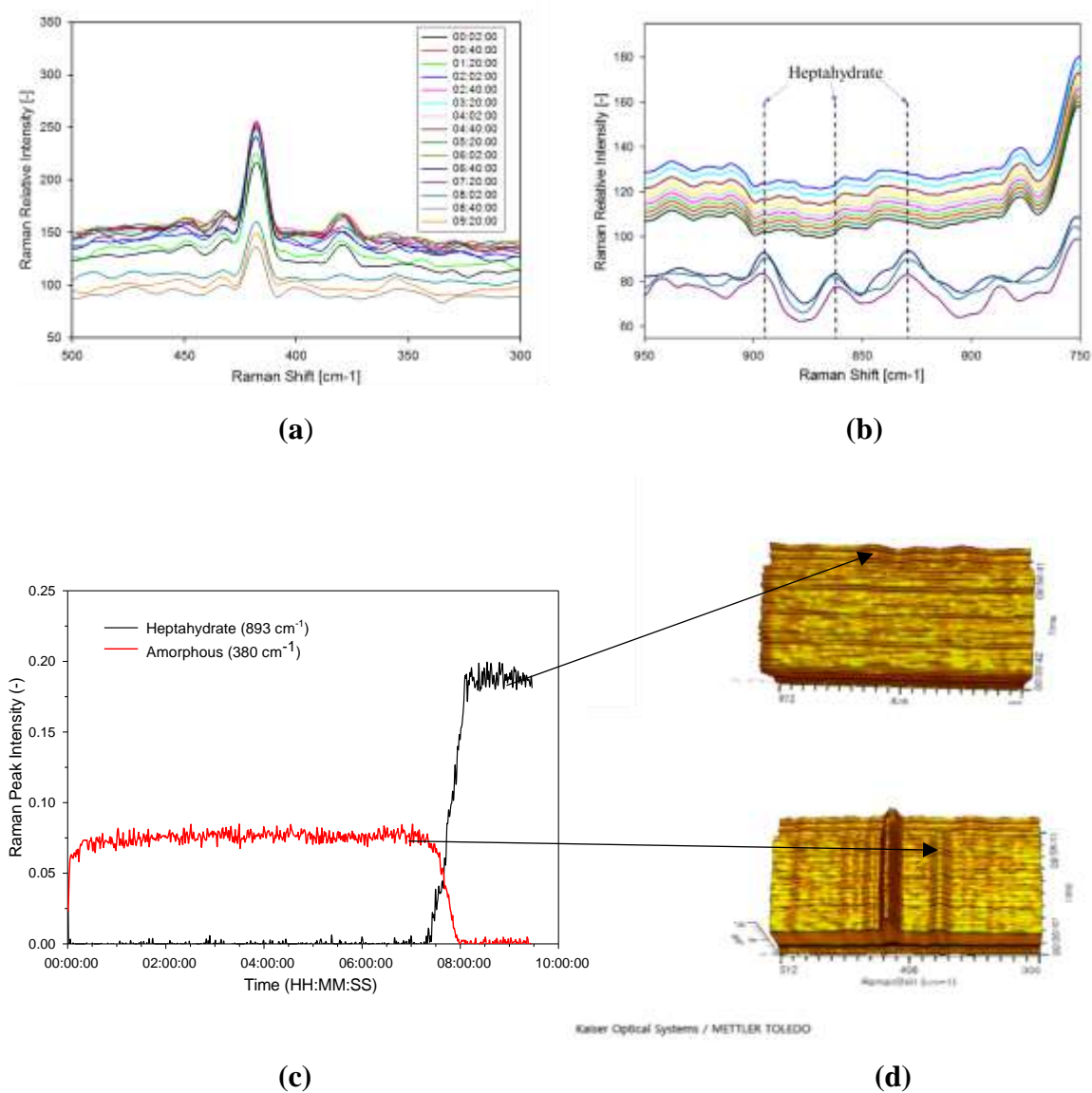


**Fig. 5-8: Variation of Raman peaks with elapsed time for Run 1: (a) an amorphous peak at 380 cm<sup>-1</sup>, (b) the heptahydrate peaks at 893, 829 and 865 cm<sup>-1</sup>, (c) comparison of intensity of peaks at 380 and 893 cm<sup>-1</sup>, and (d) a waterfall diagram of amorphous and heptahydrate peaks according to time.**

**Tab. 5-3: Experimental Conditions and Results**

Run #	Initial concentration (GMP g/water g)	Methanol fraction (-)	Methanol Addition rate or time (g/min or min)	Solid form	$S_H$	$S_A$	$\eta_{sol} \times 10^3$ (Pa s)	$\eta_{sul} \times 10^3$ (Pa s)
1	0.3	0.50	<1 min	A-->H	1.397	2.467	4.26	98.0
2	0.25	0.50	<1 min	A-->H	1.343	2.350	3.62	67.0
3	0.2	0.50	<1 min	A-->H	1.339	2.134	3.04	21.0
4	0.15	0.50	<1 min	A-->H	1.332	1.745	2.51	14.5
5	0.1	0.50	<1 min	H only	1.297		2.05	
6	0.2	0.50	0.94 g/min	H only	1.227		3.04	
7	0.2	0.50	1.25 g/min	A-->H	1.377	1.681	3.04	6.1
8	0.2	0.50	1.88 g/min	A-->H	1.371	1.886	3.04	7.4
9	0.2	0.50	3.75 g/min	A-->H	1.363	1.686	3.04	6.4
10	0.2	0.60	1.25 g/min	A-->H	1.360	1.867	3.04	10.1
11	0.2	0.67	1.67 g/min	A-->H	1.361	2.114	3.04	17.9
12	0.2	0.71	2.08 g/min	A-->H	1.300	2.220	3.04	36.3
13	0.2	0.33	0.63 g/min	H only	1.285		3.04	
14	0.2	0.71	<1 min	A-->H	1.302	12.579	3.04	74.1
15	0.2	0.67	<1 min	A-->H	1.319	12.415	3.04	47.7
16	0.2	0.60	<1 min	A-->H	1.334	10.309	3.04	44.4
17	0.2	0.33	<1 min	A-->H	1.364	3.279	3.04	17.3
18	0.2	0.50	<1 min	A-->H	1.345	5.731	3.04	26.2

Fig. 5-8c compares the intensity of peaks at  $380 \text{ cm}^{-1}$  (amorphous) and  $893 \text{ cm}^{-1}$  (heptahydrate), as measured in situ by Raman spectroscopy. Fig. 5-8d is a waterfall diagram of the amorphous formation-dissolution and the heptahydrate nucleation (see the peak at  $380 \text{ cm}^{-1}$  for amorphous and peaks at 893, 829, and  $865 \text{ cm}^{-1}$  for heptahydrate). Thus, formation and dissolution of the amorphous form and nucleation of heptahydrate crystals were analyzed. Tab. 5-3 shows the operational conditions for these experiments such as the initial concentration, anti-solvent fraction, and anti-solvent addition rate.

### 5.3.2 Phase Transformation by Anti-solvent Crystallization

When the supersaturation is generated by adding the anti-solvent, the nucleation occurs at the upper limit of the metastable zone, which is the maximum supersaturation achievable [Kim22c]. Therefore, maximum supersaturation is one of the key variables in batch experiments. Tab. 5-3 lists the solid form, supersaturation, viscosity of solution ( $\eta_{sol}$ ), and viscosity of the amorphous slurry ( $\eta_{sul}$ ) under various operating conditions. Tab. 5-4 lists the induction time (amorphous, crystalline), transformation time, methanol fraction at an amorphous induction time, methanol fraction at a crystalline induction time, plateau amorphous slurry concentration (In Fig. 5-9 and appendix), the plateau indicates a steady situation, not the started or finished transformation process.), solute concentration, metastable zone width ( $\Delta A_{a,max}$ ), particle size, and plateau solute concentration (see Fig. 5-9).

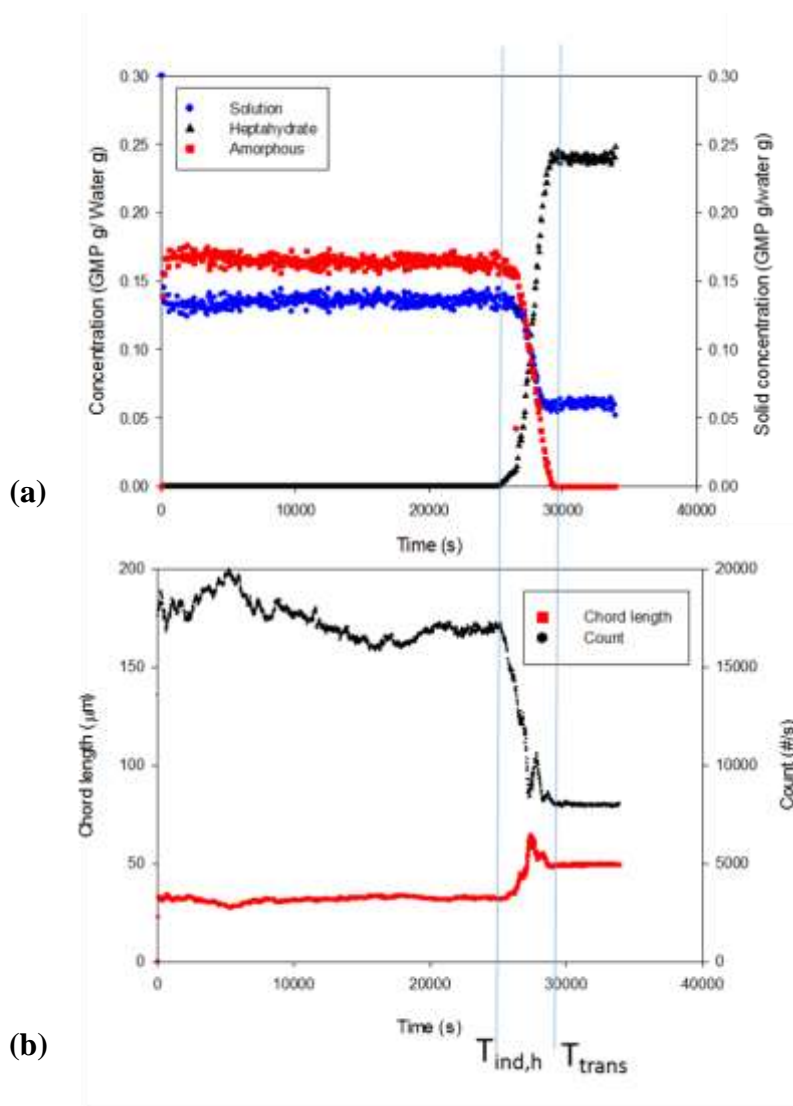


**Fig. 5-9: Measurement by in-situ Raman spectroscopy and FBRM at the experimental conditions of Run 1: (a) time dependence on the solute concentration and solid form concentration and (b) time dependence on particle size and counts.**

**Tab. 5-4: Experimental Data**

Run #	$t_{ind,A}$ (s)	$t_{ind,H}$ (s)	$t_{trans}$ (s)	$A_a$ in $t_{ind,a}$	$A_a$ in $t_{ind,h}$	Plateau amorphous slurry conc. (g/g)	Plateau conc. (g/g)	$\Delta A_{a,max}$ (-)	Amorphous size ( $\mu\text{m}$ )	Heptahydrate size ( $\mu\text{m}$ )
1	56	25352	29579	0.157	0.500	0.1648	0.1352	0.447	35	55
2	65	3745	5820	0.178	0.500	0.136	0.114	0.436	39	51
3	76	3598	5665	0.202	0.500	0.0903	0.1097	0.401	28	46
4	85	1853	3383	0.221	0.500	0.0659	0.1017	0.407	35	49
5	-	75	-	-	0.200	-	-	0.072		37
6	-	1821		-	0.105	-	-	0.026		150
7	688	1577	1916	0.160	0.304	0.012	0.188	0.226	20	40
8	522	1200	1448	0.179	0.333	0.0221	0.1779	0.254	21	38
9	288	1031	1148	0.194	0.462	0.0142	0.1858	0.383	11	58
10	487	1977	2638	0.169	0.452	0.0395	0.1605	0.373	23	48
11	420	19300	28738	0.189	0.667	0.0705	0.1295	0.588	25	38
12	401	11024	23406	0.218	0.714	0.109	0.0882	0.635	18	35
13	-	1045	8800		0.127			0.048		88
14	21	6902	9614	0.412	0.714	0.148	0.052	0.635	29	43
15	25	5300	9614	0.510	0.667	0.124	0.076	0.588	25	58
16	23	8400	11340	0.434	0.600	0.12	0.084	0.521	19	56
17	20	4120	8017	0.333	0.333	0.0686	0.135	0.254	14	61
18	28	3450	6200	0.384	0.500	0.0913	0.1087	0.421	20	40

Fig. 5-9a shows the formation of the amorphous solid and the transformation from amorphous states into heptahydrate crystals using concentration–time profiles of solution and solid phases for Run 1 at 400 g scale. The concentration of the solution and the solid was measured using the Raman peak calibration developed in our earlier works [Kim22a,Kim22b]. To generate the supersaturation, the anti-solvent was quickly injected within 1 min at a methanol fraction of 0.5 (methanol g/solvent mixture g) and 300 g/L solutions. The data were reproducible. Three regions were identified [Kim 22c].

In the first region, the supersaturation was created by adding the anti-solvent into the solution. The amorphous form was produced after a brief time (within 1 min). While the solute concentration corresponded to the supersaturation concentration of the amorphous form, no

heptahydrate crystals were formed. However, the particle size, number of particles, solid concentration, and solute concentration were all constant.

In the second region, an induction time of 25352 s (about 7 h) elapsed to nucleate heptahydrate crystals. The amount of the amorphous form decreased, while the amount of the crystalline heptahydrate rapidly increased as the solute concentration decreased for about 2250 s (37.5 min). This phenomenon refers to the transformation of the solid form in which the amorphous form dissolves, and simultaneously the crystalline form nucleates and grows.

In the third region, the content of the heptahydrate crystal is maximized by completing the amorphous dissolution while maintaining the solute concentration consistent with the saturated concentration of the heptahydrate crystals. Based on these observations, the amorphous slurry reaches a maximum at a plateau solute concentration in the early stage, and the heptahydrate crystal content reached a maximum when the solute concentration approached the ultimate saturation in the final stage.

Fig. 5-9b shows changes in the number and the particle size of the solid phase obtained at the experimental conditions of Run 1. The particle number and the particle size were held constant throughout the amorphous formation stage, but as the amorphous dissolution and heptahydrate crystal growth progressed, the particle number decreased, and the particle size increased. It indicated that the solid form was transforming. Some scattering in the number and the size of particles in the initial stage of the process is mainly due to aggregation and breakage of the amorphous solid. In both Raman and FBRM data, the time points for generation and transformation were almost identical.

The solute concentration initially lowers as an amorphous form is formed by introducing an anti-solvent and then maintains a stable plateau concentration before decreasing again when transformation begins. The solid concentration first maintains a steady plateau concentration of the amorphous slurry and eventually exhibits a plateau concentration of heptahydrate crystals following transformation. The dissolution rate of the amorphous form and the growth rate of the heptahydrate crystals can be briefly calculated from the concentration of the solid form and transformation time per 1 g of solvent. According to the results of Run 1 (see Fig. 5-9a), the growth rate of heptahydrate crystals ( $5.7 \times 10^{-5}$  g/s) is faster than the dissolution rate of amorphous solids ( $5.0 \times 10^{-5}$  g/s), which is limiting the transformation. The supersaturation can be calculated from the difference between the solute concentration and the saturation concentration. In addition, the metastable zone width based on the methanol fraction can be obtained from the maximum supersaturation at the nucleation point. The induction times,  $t_{\text{ind,A}}$  and  $t_{\text{ind,H}}$ , are defined as the time when the amorphous form and heptahydrate crystal are first observed in the solid phase, respectively. The transformation time,  $t_{\text{trans}}$ , is the entire time required to complete the transformation following the addition of the methanol.

Fig. 5-10 illustrates the morphological changes of GMP in the pictures captured by PVM during the operation at the experimental conditions of Run 1. At the start of the process, the cloud-like amorphous form dominated the solution. After about 25200 s (7 h), a few needle-shaped heptahydrate crystals emerged in the solution. The transformation process increases the number of needle-shaped heptahydrate crystals and their crystal size. At 4500 s after the induction time, massive rod-shaped heptahydrate crystals were primarily collected. The change in crystal shape during the transformation provided by PVM is consistent with the FBRM data discussed above. It denoted that the transformation process consists of dissolution of metastable forms and nucleation and growth of the heptahydrate form. Eventually, Raman analysis, FBRM data, and PVM data were all consistent at the time points of the generation-consumption of the amorphous form and the nucleation-transformation of the crystalline form.

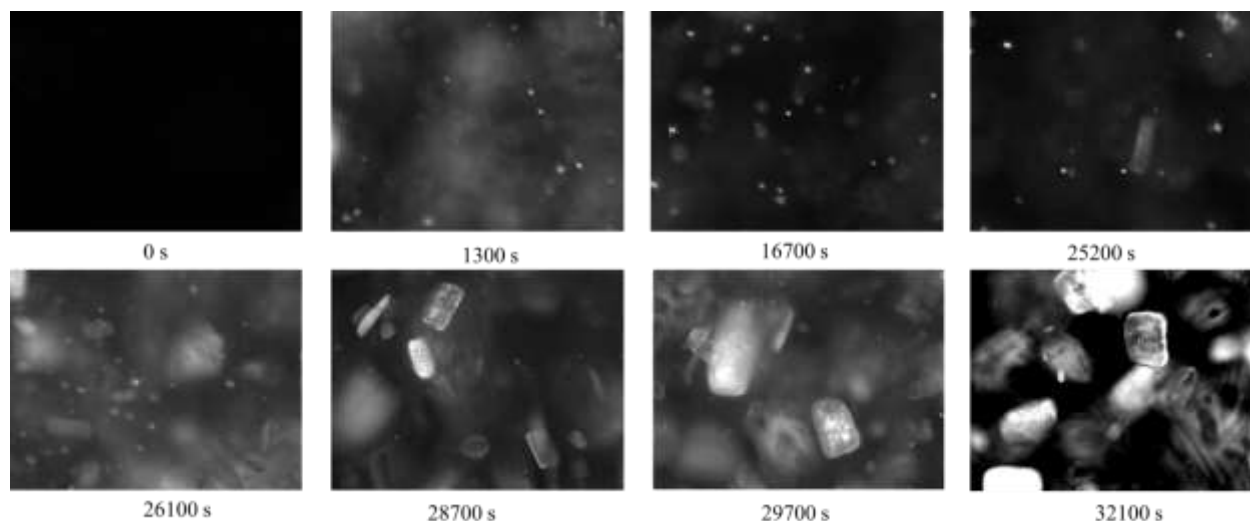


**Fig. 5-10: Change of morphological pictures captured by PVM according to time at the experimental conditions of Run 1.**

#### 5.4 Growth and Dissolution Kinetic and Rate Controlling Step

##### 5.4.1 Metastable Zone Limits for Amorphous and Heptahydrate Forms

Previous work has presented the effect of water–methanol fraction on the solubility of heptahydrate, tetrahydrate, and amorphous substances in GMP [Kim22a]. Although the difference in solubility between the three forms is not very large, the metastable zone widths are significantly different.

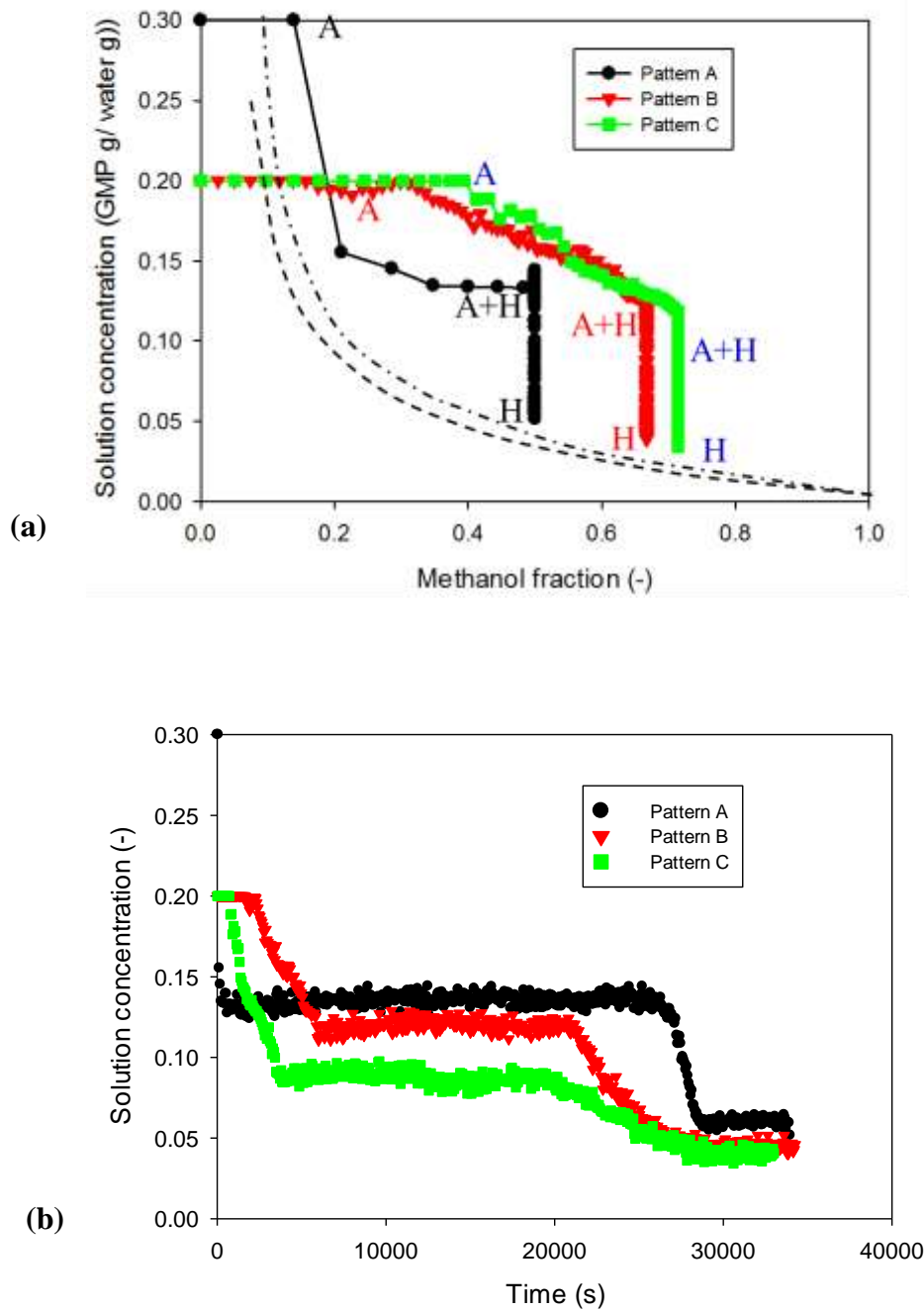
The metastable zone width is dependent on supersaturation as a kinetic property [Ulr02, Oma08, Oma06]. However, solubility is a thermodynamic property. The metastable zone widths of each form serve as information on the formation and transformation of metastable forms. Therefore, the solid forms can be selectively produced by adjusting these parameters. In a previous study [Kim22a], the metastable zone limits representing regions producing amorphous and heptahydrate forms by unseeded anti-solvent crystallization were determined. As a result, the production conditions of the amorphous form are determined by the initial supersaturation, and the environment of the amorphous slurry affects the transformation process to heptahydrate.

Fig. 5-11a shows the metastable zone limits and the respective solubility of the amorphous and heptahydrate forms in a plot of solute concentration versus mass fraction of methanol in the mixed solvent. The metastable zone limits are defined as the fraction of methanol at the onset of nucleation of the solid forms. For example, if the solute concentration is plotted against the anti-solvent fraction in the anti-solvent crystallization for Patterns A–C, the formation and disappearance of the amorphous phase and the formation process of the heptahydrate phase are clearly shown [Kim22d].

The maximum supersaturation of the three patterns is expressed as a solution concentration for the metastable zone width. The maximum supersaturation in Patterns A–C is 0.172, 0.0832, and 0.101 GMP g/water g, respectively. It contributes to the nucleation of the amorphous form, and the slurry content of the formed amorphous phase affects the transformation process. Therefore, it is a key variable in the transformation process.

Fig. 5-11b shows the profile of solution concentration and time for the three patterns. From the solution concentration profile, the concentration change in the process of formation and transformation of amorphous material is shown. Also, the induction period and the

transformation time of the amorphous to heptahydrate phase are provided. As a result, the degree of supersaturation affects the formation of amorphous forms and also has a great influence on the rate-controlling step for dissolution of amorphous forms and the growth of heptahydrate. Fig. 5-11c shows the concentration profile of amorphous solid for the three patterns. The process of formation and disappearance of the amorphous form is shown over time. After the amorphous solid is formed, a plateau of amorphous solid concentration is maintained for a certain period of time and dissolved for transformation.



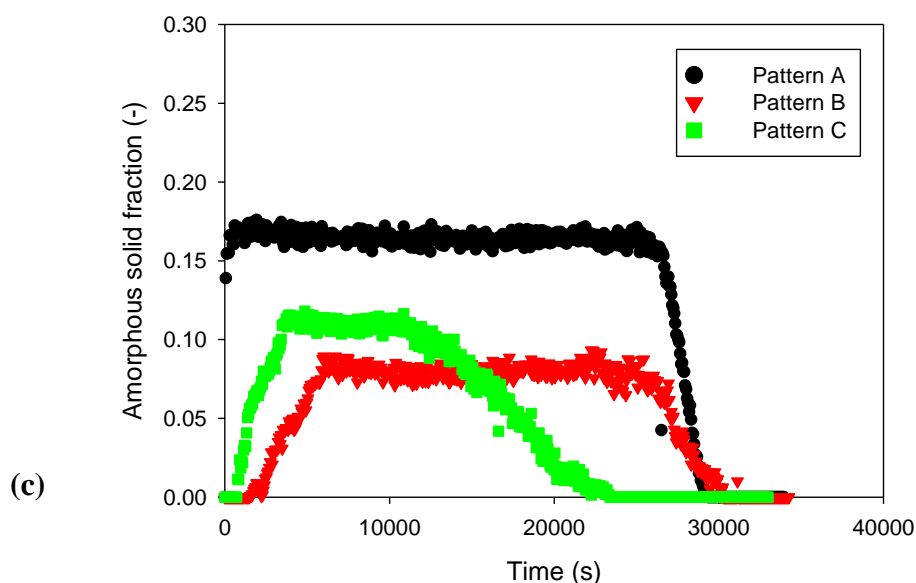


**Fig. 5-11: Variation of solution concentration (a) against methanol fraction, where A and H stand for amorphous phase and heptahydrate phase, respectively (b) against operation time, and (c) variation of amorphous solid concentration against time.**

#### 5.4.2 Rate-Controlling Step of Phase Transformation

O'Mahony et al. [Oma13] demonstrated how it is possible to identify the rate-controlling step of solution-mediated phase transformation when both solution and solid phase concentrations are recorded. Four scenarios are sketched with plots of the solution and solid-state data over time via schematic diagrams. In this study, the phase transformation process of GMP was analyzed in more detail using in-situ Raman spectroscopy and FBRM. Thirteen operating runs were carried out with different conditions of initial concentration, addition rate, and anti-solvent fraction. The liquid-mediated phase transformation (the formation of the amorphous phase by generating the supersaturation and the transformation to the heptahydrate phase by the dissolution and growth) was carried out by adding anti-solvent into the water-GMP solution at 20 °C.

Transformation from the amorphous slurry is affected by the conditions of the amorphous state of the suspension, such as viscosity, concentration, supersaturation, and temperature [Kim22c]. For the formation of the amorphous forms, anti-solvent addition rate, anti-solvent/solvent ratio, and initial concentration were applied as variables for supersaturation. Solution-mediated phase transformation occurs between the solubility curves of the two forms based on the solution concentration and is reported to be controlled by dividing it into dissolution and growth-controlled steps [Guo18,Wan15,Mar99,Pan18]. On the other hand, in this liquid-mediated phase transformation study, the metastable or stable form is first prepared by supersaturation of the liquid phase [Kim22a and b]. For the metastable form, transformation occurs in a slurry state, and the transformation process takes place in the form of a mixture of dissolution and growth-controlled steps. If the stable form nucleates first, growth of the stable form follows without transformation. As suggested in the previous study [Kim22c], the transformation process is a nonequilibrium operation, so that supersaturation does not occur between the equilibrium concentrations of the two forms.

Fig. 5-12 shows the concentration–time profiles of liquid and solid for the process of amorphous formation and its transformation. Here, the metastable form is the amorphous phase, whereas the heptahydrate solid is defined as the stable form. In this study, three different patterns of the transformation were found, each divided into two sections [Kim22d].

Pattern A is typically shown in the experimental results of Run 1. As shown in Fig. 5-12a, the transformation process is divided into two sections. From this figure, the rate constants of dissolution and growth in the transformation phase can be calculated. In the first section of the transformation section (I), the amount of the heptahydrate form increases, whereas the amount of the amorphous phase and the solute concentration decrease simultaneously. It indicates that the dissolution rate of the amorphous form is slightly smaller than the growth rate of the heptahydrate form. Thus, the dissolution of the amorphous form is the controlling step in the initial section. However, in the latter section of the phase transformation section (II), the solute concentration of the solution is constant, and the dissolution of amorphous increases. Thus, the growth of the heptahydrate form is the controlling step in the latter section. The combination of two sections is necessary for grasping the overall rate-limited determined step.

Fig. 5-12b shows the experimental results of Run 7 (Tab. 6-1), which is a typical curve of Pattern B. At the initial section of the transformation section (I), the amount of heptahydrate solid increases and the solute concentration decreases, whereas the amount of amorphous maintains at a plateau. It suggests that the dissolution rate of the amorphous form is slower than the nucleation and growth rate of the heptahydrate form. Thus, the dissolution of the amorphous form is the controlling step in the initial section. However, in the latter section of the phase transformation section (II), the solute concentration of the solution is constant and the solid concentration of the amorphous form decreases, which suggests that the dissolution rate of the amorphous form is faster than the growth of the heptahydrate form. Thus, the growth of the heptahydrate form is the controlling step in the latter section.

Fig. 5-12c shows the experimental results of Run 8 (Tab. 6-1), which is a typical curve of Pattern C. In the initial period of transformation (I), the amount of the heptahydrate form increases and the amount of the amorphous form decreases, while the solute concentration remains at a plateau. It indicates that the dissolution rate of the amorphous form is faster than the nucleation and growth rate of the heptahydrate form. Thus, the nucleation and growth of the heptahydrate form is the controlling step in the initial section. However, in the latter section of the phase transformation section (II), the solute concentration decreases, which supports that the dissolution rate of the amorphous form is lower than the nucleation and growth of the heptahydrate form because of the decrease in the solid concentration of the amorphous form. Thus, the dissolution of the amorphous form is the controlling step in the final section.

The rate-controlling step for the three patterns in this study should be analyzed considering both the rate-controlling steps of both sections of the transformation process. Davey and Cardew [Dav86] insisted that the rate-controlling step of a transformation process is determined by solute concentration behavior. The dissolution-controlled process shows that the supersaturation decreases quickly from its initial value to a low value, while the growth-limited process indicates that the supersaturation remains close to the initial value due to dissolution of the metastable phase. Therefore, qualitative identification based on the solution concentration is difficult to interpret because of the complex phenomenon consisting of the two-section transformation for rate-controlling steps. For quantitative analysis, suitable kinetic equations were derived by comparing the kinetics of the dissolution rate equation and the crystal growth rate equation.

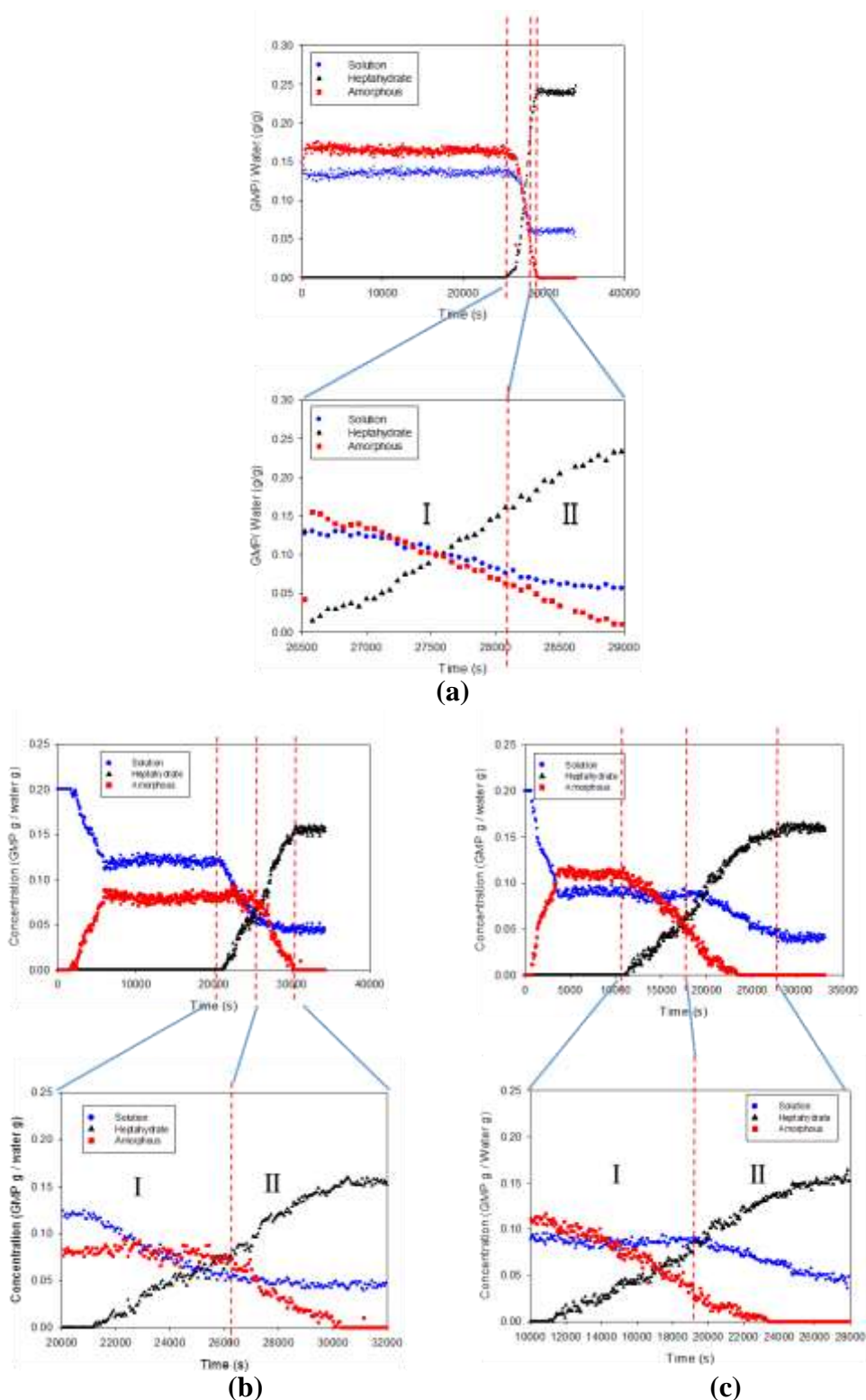


**Fig. 5-12:** The concentration–time profiles for solution, amorphous solid and heptahydrate solid in liquid-mediated phase transformation from amorphous phase to heptahydrate phase at 20 °C in-situ monitored by Raman for (a) Patterns A, (b) Pattern B and (c) Pattern C.

### 5.4.3 Data Analysis of Dissolution and Growth Kinetics

Raman and FBRM data provide a concentration and particle characteristic profile over time by providing solid concentration and liquid concentration, particle number, particle size, and particle size distribution during the transformation process.

The dissolution and growth processes in slurry for the two solid states were analyzed by using simple equation models [Kim22d]. This was achieved by converting the measured concentration into fractional conversion of solids for each phase using eqs. 5-2 and 5-3:

$$X_a = 1 - c_a(t)/c_a(i) \quad (5-2)$$

$$X_h = c_h(t)/c_h(f) \quad (5-3)$$

where  $c_a(t)$  and  $c_h(t)$  are the solid concentrations of the respective phases with elapsed time in the transformation,  $c_h(f)$  and  $c_a(i)$  are the concentration of the heptahydrate phase formed at the end of the transformation, and the starting concentration of the amorphous phase, respectively, and  $X_a$  and  $X_h$  are the fractional conversions of the amorphous and heptahydrate phases, respectively.

The dissolution and growth profiles were fitted by a zero-order, a first-order, and a surface reaction equations [Tur18, Das10, Lok13, Jak16, Zon19, Sha14, Kit13, Dan09, Dha08]. In the case of the zero-order equation, the dissolution rate and growth rate are independent of the concentration and the particle surface. The kinetic expressions of the zero-order equation for the dissolution of the amorphous and growth of the heptahydrate are as follows:

$$k_{da,0}t = X_a \quad (5-4)$$

$$k_{gh,0}t = X_h \quad (5-5)$$

From eqs. 5-4 and 5-5, the slopes of linear plots of  $X_a$  and  $X_h$  versus time ( $t$ ) give the kinetic constants  $k_{da,0}$  and  $k_{gh,0}$ , respectively.

If the dissolution and growth rates are proportional to the concentration [Dan09, Dha08, Zhu19], a first-order equation is expressed as follows:

$$k_{da,1}t = -\ln(1 - X_a) \quad (5-6)$$

$$k_{gh,1}t = \ln X_h \quad (5-7)$$

From eqs. 5-6 and 5-7, the slopes of linear plots of  $-\ln(1 - X_a)$  and  $\ln X_h$  versus time ( $t$ ) give kinetic constants  $k_{da,1}$  and  $k_{gh,1}$ , respectively.

If the dissolution and growth rates depend on the surface of the particle, they are expressed by the surface reaction model equations in eqs. 5-8 and 5-9, respectively [Kit93, Mar99, Sha14, Hix31]:

$$k_{da,s}t = 1 - X_a^{1/3} \quad (5-8)$$

$$k_{gh,s}t = X_h^{1/3} \quad (5-9)$$

From eqs. 5-8 and 5-9, the slopes of linear plots of  $1 - X_a^{1/3}$  and  $X_h^{1/3}$  versus time ( $t$ ) give kinetic constants  $k_{da,s}$  and  $k_{gh,s}$ .

As highlighted in eqs. 5-5, 5-7, and 5-9,  $k_{gh,0}$ ,  $k_{gh,1}$ , and  $k_{gh,s}$  are the growth rate constants of zero-order, first-order, and surface reaction equations with respect to the heptahydrate phase, respectively. As expressed in eqs. 5-4, 5-6, and 5-8,  $k_{da,0}$ ,  $k_{da,1}$ , and  $k_{da,s}$  are the dissolution rate constants of zero order, first order, and surface reaction equations with respect to the amorphous phase, respectively. This analysis was carried out for each isothermal experiment at 20 °C. The dissolution of the amorphous phase and the growth of the heptahydrate phase were compared with three order equation models investigated in this study using eqs. 5-4 to 5-9.

The dissolution of the amorphous form and the growth of the heptahydrate form together with the zero-order, first-order, and surface reaction equations fitting profiles are highlighted in Fig. 5-13, respectively. The calculated values of growth and dissolution rate constants at the

isothermal temperature are provided in Tab. 5-5. From the overall dissolution rate constant and the growth rate constant, the rate-limiting step of the entire transformation process can be determined. As shown in Tab. 5-5, it can be seen that  $k_{da} < k_{gh}$  for Pattern A, while  $k_{da} > k_{gh}$  for Patterns B and C. Therefore, from the comparison of the rate constants, Pattern A is the dissolution rate control step, and Patterns B and C are the growth rate control steps.

**Tab. 5-5: Overall dissolution rate constants and overall growth rate constants for zero-order, first-order and surface reaction models**

Rate equation	Unit	Overall $k_{da} \times 10^4$			Overall $k_{gh} \times 10^4$		
		Pattern A	Pattern B	Pattern C	Pattern A	Pattern B	Pattern C
Zero	g/g s	2.66	0.82	6.89	4.15	0.68	3.60
First	1/s	6.22	4.17	1.71	9.56	3.12	1.27
Surface	$\text{g}^{1/3}/\text{g}^{1/3}\text{s}$	2.02	0.254	0.43	2.10	0.211	0.237

Fig. 5-13 compares the accuracy of the three dissolution and growth kinetic equations with that of the experimental results of the three patterns of transformation processes investigated. It was fitted with zero-order, first-order, and surface reaction equations. Tab. 5-6 shows the correlation coefficient  $r^2$  calculated through linear regression of the kinetic equation and the experimental data. The plots obtained in this study were explained best by the zero-order model because the plots showed the highest linearity, and the determination coefficient ( $r^2$ ) was in the range of 0.988 to 0.992, followed by the surface reaction model ( $r^2$  ranged from 0.813 to 0.981). The growth and dissolution were best explained by the first-order equation ( $r^2$  ranged from 0.865 to 0.933).

The accuracy of the dissolution kinetic equations was in the order of zero-order > surface reaction > first-order equations. The accuracy of the growth kinetic equations was in the order of zero-order > first-order > surface reaction equations. The zero-order kinetic equation has the best correlation in this table. Therefore, the calculation of the kinetic constants,  $k_{da,0}$ , and  $k_{gh,0}$  for dissolution and growth were obtained through the linear regression of the experimental data and eqs. 5-4 and 5-5 using the zero-order equation, respectively.

**Tab. 5-6: Correlation coefficient between experiments and models for zero-order, first-order and surface reaction models**

Equation	Dissolution			Growth		
	Pattern A	Pattern B	Pattern C	Pattern A	Pattern B	Pattern C
Zero	0.990	0.988	0.992	0.989	0.990	0.991
First	0.865	0.882	0.923	0.931	0.933	0.928
Surface	0.981	0.933	0.942	0.835	0.863	0.813



#### 5.4.4 Calculation of Kinetic Parameters

Fig. 5-14 shows the fraction of solids over time for three different types of slurry transformation processes. The use of a zero-order model to fit the growth and dissolution profiles allows extrapolation of the rate constants associated with each step to discover which is rate-limiting in the transformation kinetics. Figures corresponding to Runs 10–12 (Tab. 6-1) are shown in the Appendix. For 13 experiments (Tab. 6-1), three transformation patterns were classified, and rate constants for dissolution and growth were calculated by applying the zero-order rate equation.

For the zero-order rate constant,  $k_{d,I}$  and  $k_{g,I}$  of section (I) and  $k_{d,II}$  and  $k_{g,II}$  of section (II) were calculated from the slope, as shown in Fig. 5-14, and the overall  $k_d$  and  $k_g$  of the overall section were calculated from the following equations [Kim22d].

$$\text{Overall } k_d = \frac{\text{time of section I} \times k_{d,I} + \text{time of section II} \times k_{d,II}}{\text{Total transformation time}} \quad (5-10)$$

$$\text{Overall } k_g = \frac{\text{time of section I} \times k_{g,I} + \text{time of section II} \times k_{g,II}}{\text{Total transformation time}} \quad (5-11)$$

The kinetic constants evaluated for the dissolution and growth stages of the transformation processes are shown in Tab. 5-7. The growth profile of the heptahydrate phase highlighted in Fig. 5-14 indicates that although a simple zero-order model fits this curve well, there are some deviations from the model, especially at the beginning and end of the experiment.

In the case of Pattern A, the  $k_d$  value is smaller than the  $k_g$  value in sections (I) and (II), so the overall  $k_d$  is smaller than the overall  $k_g$  value in the entire section. As a result, the dissolution rate controls the overall controlling step of the process. In the case of Pattern B, the  $k_d$  value is smaller than the  $k_g$  value in section (I) and vice versa in section (II). Overall  $k_g$  is lower than overall  $k_d$  in the whole section. Therefore, the overall controlling step of the process is determined by the growth rate. Heptahydrate crystal growth is induced by a rapid decrease in supersaturation without a change in the concentration of amorphous solids at the initial section. In the next section, the amorphous dissolution rate is fast, and the supersaturated concentration is almost constant. This phenomenon is the same as the result shown by the magnitude of the rate constant. In the case of Pattern C, the  $k_g$  value in section (I) is smaller than the  $k_d$  value and vice versa in section (II). Overall  $k_g$  is less than overall  $k_d$  in the whole section. Therefore, the controlling step of the process is governed by the growth rate. In the initial section, there was a large change in the concentration of amorphous solids without a change in supersaturation. As the amorphous dissolution rate increased, the heptahydrate crystal growth rate also increased. In the next section, the dissolution rate of the amorphous substance is almost constant, and the supersaturation concentration decreases. This phenomenon is also the same as the magnitude of the rate constant.

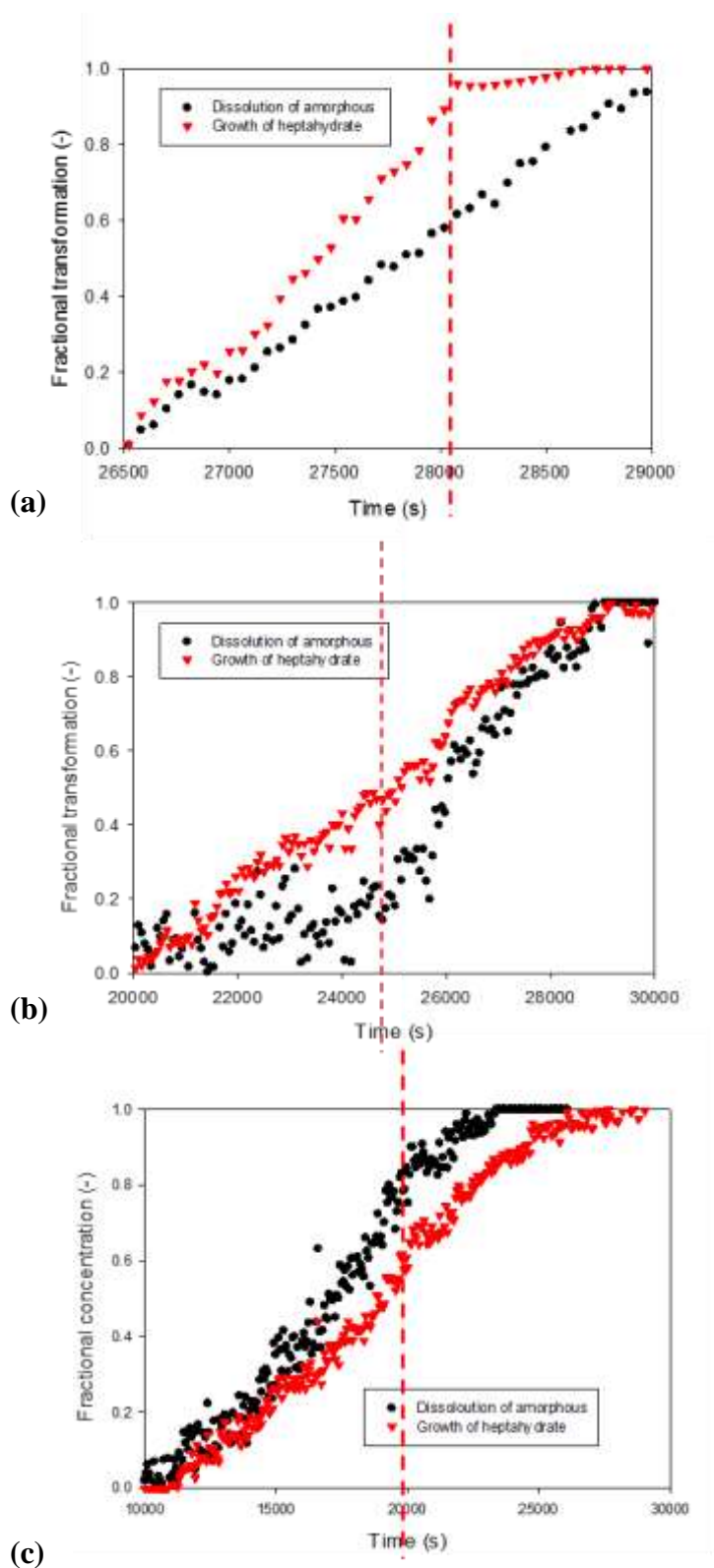


**Fig. 5-14: Calculation of rate constants of dissolution and growth from plot of fractional concentration against time during transformation for (a) Pattern A, (b) Pattern B and (c) Pattern C.**

**Tab. 5-7: Calculated dissolution and growth rate constants and their ratios for the isothermal experiments**

## a) Operating conditions

Pattern	Feed concentration	Methanol fraction	Addition time
	(GMP g/water g)	(g/g)	(min)
A	0.3	0.5	0.5
B	0.2	0.667	60
C	0.2	0.71	60

## b) Rate constant for Sections I and II

Pattern	Section I		Section II	
	$k_d \times 10^4$ [g/g s]	$k_g \times 10^4$ [g/g s]	$k_d \times 10^4$ [g/g s]	$k_g \times 10^4$ [g/g s]
A	0.425	0.524	3.783	5.970
B	0.672	0.549	1.004	0.842
C	5.682	0.550	7.067	4.052

## c) Rate constant for overall stage and controlled step

Pattern	Overall stage		Controlled step		
	$k_d \times 10^4$ [g/g s]	$k_g \times 10^4$ [g/g s]	Section I	Section II	Overall
A	2.664	4.155	D	D	D
B	0.822	0.682	D	G	G
C	6.889	3.600	G	G	G

## 5.4.5 Changes in Particle Number, Particle Size, and Particle Size Distribution

As the growth of heptahydrate crystals is revealed by the solid concentration, the growth kinetics are related to the overall mass transfer into the heptahydrate phase, which causes a change in the particle size distribution over time. Changes in particle size, the number of particles, and particle size distribution with time were noted during the transformation process. FBRM data do not provide quantitative information on crystalline transformation, but they do provide information on nucleation and crystal growth rate during transformation. In this study, Raman data were measured as quantitative data such as concentration and the solid form, and the correlation with FBRM data was investigated.

The FBRM CLDs underline the change in particle system dynamics caused by the phase transition. Fig. 5-15 depicts the time-elapsing trend of particle size distributions. Fig. 5-15 shows a gradual decrease in counts and peak changes in the distribution model from the CLD as the transformation process progresses, which accounts for phase transformation processes in the solution. The peaks of the amorphous form from the particle size distribution were 6.7, 4.5, and 4.4  $\mu\text{m}$  for Patterns A–C, respectively. The peaks of the final distribution of heptahydrate after the transformation were 51, 44, and 47  $\mu\text{m}$  for Patterns A–C, respectively.

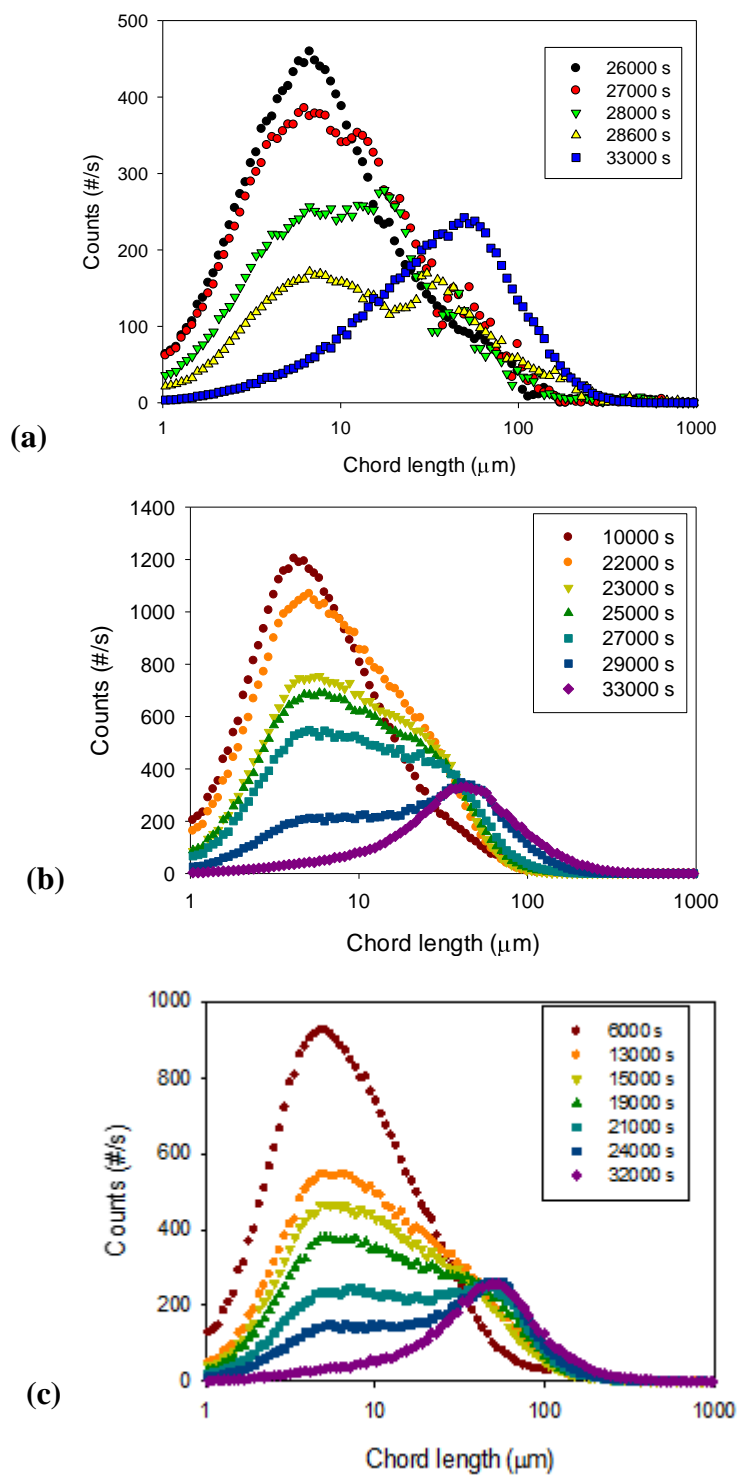


**Fig. 5-15: Variation of chord length distributions for (a) Pattern A, (b) Pattern B and (c) Pattern C.**

For patterns A–C, the mean square-weighted chord lengths for the amorphous were 25, 17, and 22  $\mu\text{m}$  and for the heptahydrate, 50, 51, and 59  $\mu\text{m}$ , respectively (see Fig. 5-16). Under the operating conditions of the three patterns, the amorphous size was 4.4–6.7  $\mu\text{m}$ , and the heptahydrate size after conversion was 50–59  $\mu\text{m}$ , with no significant difference. The amorphous obtained in the three different operating conditions had similar sizes, but the number of particles varied greatly. This is because supersaturation influences the number of particles in the amorphous formation. Solubility, supersaturation, and amorphous dissolution rates all influence the rate of heptahydrate formation, thus affecting the number of particles.

In Pattern A (see Fig. 5-15a and Fig. 5-16a), the particle size at the peak of the generated amorphous particle distribution is 6.7  $\mu\text{m}$ , and a heptahydrate peak is formed at the same time as the peak height is decreased, thereby forming a bimodal particle distribution and its shift occurs simultaneously. The mean square-weighted particle size attained throughout the amorphous formation process was 25  $\mu\text{m}$ . As the transformation occurs, supersaturation decreases, and the amorphous form dissolves simultaneously, thereby increasing the driving force. As a result, heptahydrates were rapidly generated to form a bimodal distribution, and a particle size distribution with a mean square-weighted size of 51  $\mu\text{m}$  was formed.

In Pattern B (see Fig. 5-15b and Fig. 5-16b), the mean square-weighted particle size of the amorphous phase formed was 17  $\mu\text{m}$ , and the dissolution rate was fast during the initial transformation process. The particle size at the peak is 4.5  $\mu\text{m}$ , and the peak height was first lowered. Following that, as the growth rate increases, the particle size distribution widens to the right, and finally, a shift occurs in the particle size distribution with a mean square-weighted particle size of 54  $\mu\text{m}$ . According to the Raman data in Fig. 5-11, transformation happens in this manner when supersaturation diminishes, but the concentration of the amorphous solid remains almost constant. Pattern B's heptahydrate phase grows at a slower rate than Pattern A's.

In Pattern C (see Fig. 5-15c and Fig. 5-16c), the mean square-weighted size of the formed amorphous was 22  $\mu\text{m}$ , and the peak size of the particle size distribution was 5  $\mu\text{m}$ . It decreases rapidly during the transformation process, and then, the growth of 44  $\mu\text{m}$ -sized heptahydrate particles occurs. From the comparison with the Raman results in Fig. 5-11, it is expected that transformation occurs as the amorphous content decreases rapidly at a plateau where the supersaturation concentration is constant. Compared to B, the width of the CLD is much smaller, so the growth rate is expected to be small in the later section.

In all patterns, the number of particles with a size of 1–5  $\mu\text{m}$  and the number of particles with a size of 6–50  $\mu\text{m}$  increased initially, and the number of particles with a size of 51–100  $\mu\text{m}$  remained unchanged (see Fig. 5-16). As the transformation started, the number of particles of 1–5  $\mu\text{m}$  and 6–50  $\mu\text{m}$  decreased, and the number of particles of 51–100  $\mu\text{m}$  size increased slightly. Compared with Patterns A–C, remarkable differences in the variations of the FBRM counts were found. The FBRM counts change from the amorphous to the heptahydrate at 293 K during transformation is graphically presented in Fig. 5-16. From Fig. 5-16a, there was a relatively quick transformation process within 28,100 s. The counts in all ranges measured by FBRM decreased, as there was an abrupt decline in FBRM counts in the first 28,100 s. Particle counts (1–5  $\mu\text{m}$ ) decreased rapidly, which was followed by 6–50  $\mu\text{m}$ . Counts of 51–100  $\mu\text{m}$  particles increased slightly after 28,100 s. The changes in the FBRM data were consistent with the change in concentration.

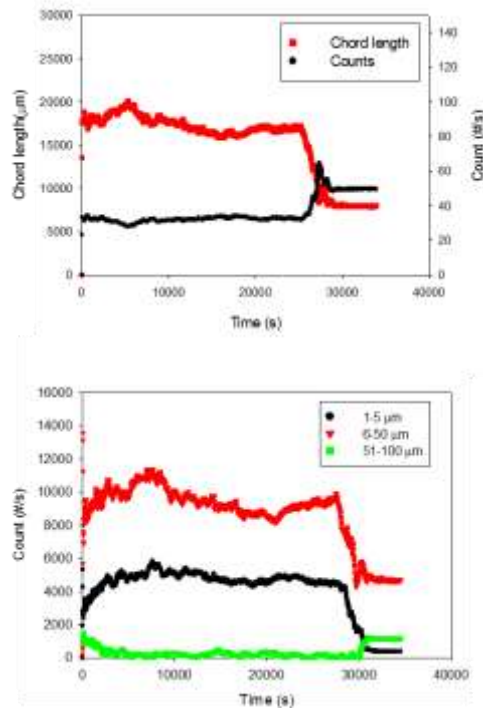
As shown in Fig. 5-16b, particle counts of all population ranges decline in the first 25,000 s, with particle counts of the 1–5  $\mu\text{m}$  range decreasing significantly. The dissolution rate of small particles is believed to be faster than that of big particles. The supersaturation of the fluid

---

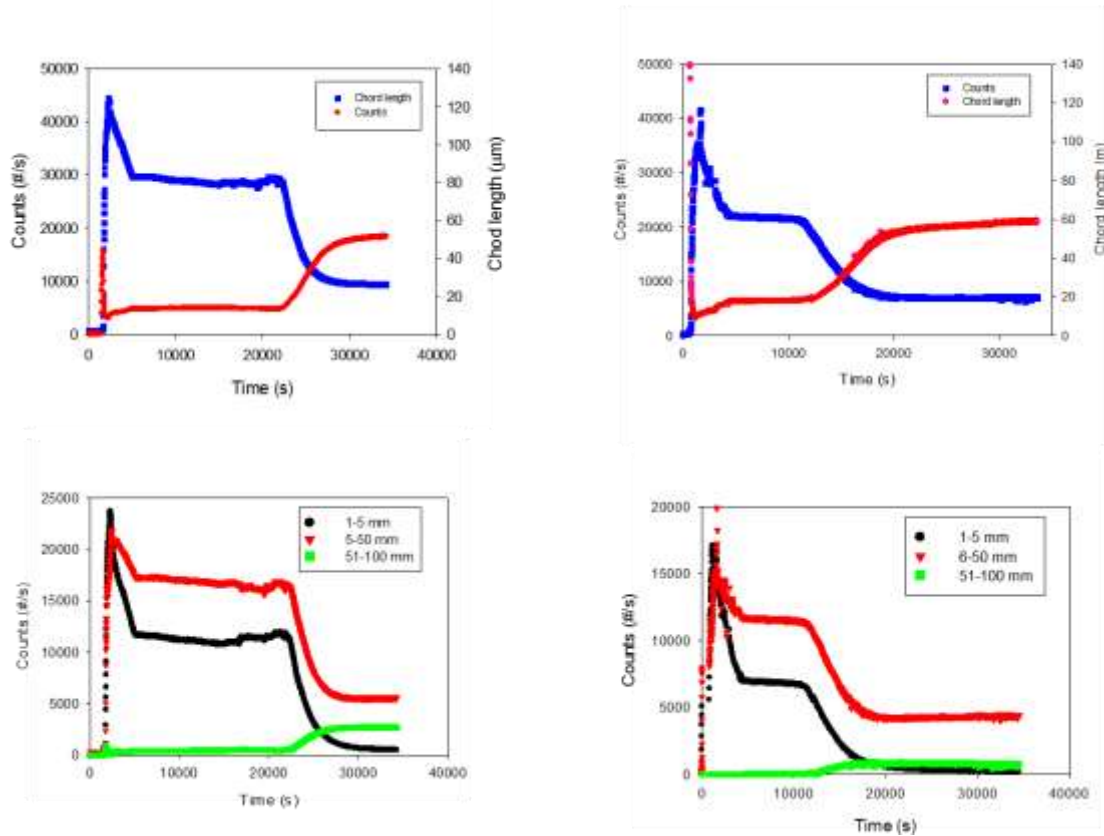
increased when amorphous particles dissolved. After 25,000 s, particle counts in the 51–100  $\mu\text{m}$  range rapidly increased, owing to heptahydrate formation. This can be confirmed by the history of different chord length distributions at different times shown in Fig. 5-15b. Chord length distributions decreased in the first 25,000 s, followed by a change in the peak of the chord length distribution, indicating an amorphous to heptahydrate transformation.

As shown in Fig. 5-16, the amorphous size of Pattern A, 35  $\mu\text{m}$ , is the largest compared to those of Patterns B and C, 10–15  $\mu\text{m}$ . Counts of the amorphous phase, 15,000 #/s, are the lowest compared to Patterns B and C, 22,000–30,000 #/s. From the highlight of Pattern A, the decrease in solute concentration is expected to be mainly due to the situation when the interfacial solid–liquid surface area of the metastable form is much smaller than that of the stable form over most of the transformation time. This can occur when the metastable form consists of a relatively large number of small crystals and nucleation results in a significant number of nuclei in the stable form.

Patterns B and C are more prevalent than Pattern A because the intrinsic growth rate is predicted to be lower than the intrinsic dissolution rate. Otherwise, the same considerations concerning the influence of the solid–liquid interface surface area apply in this arrangement. While the initial total surface area of the metastable form is defined by the supersaturation conditions that produce the amorphous form, the total surface area of the stable form is entirely controlled by the number of nucleated crystals of the heptahydrate. Even though the current state of knowledge has very little control over this, earlier research has shown that the formation conditions of the amorphous form and the physical features of the amorphous slurry might have contributed to it.



(a)



(b)

(c)

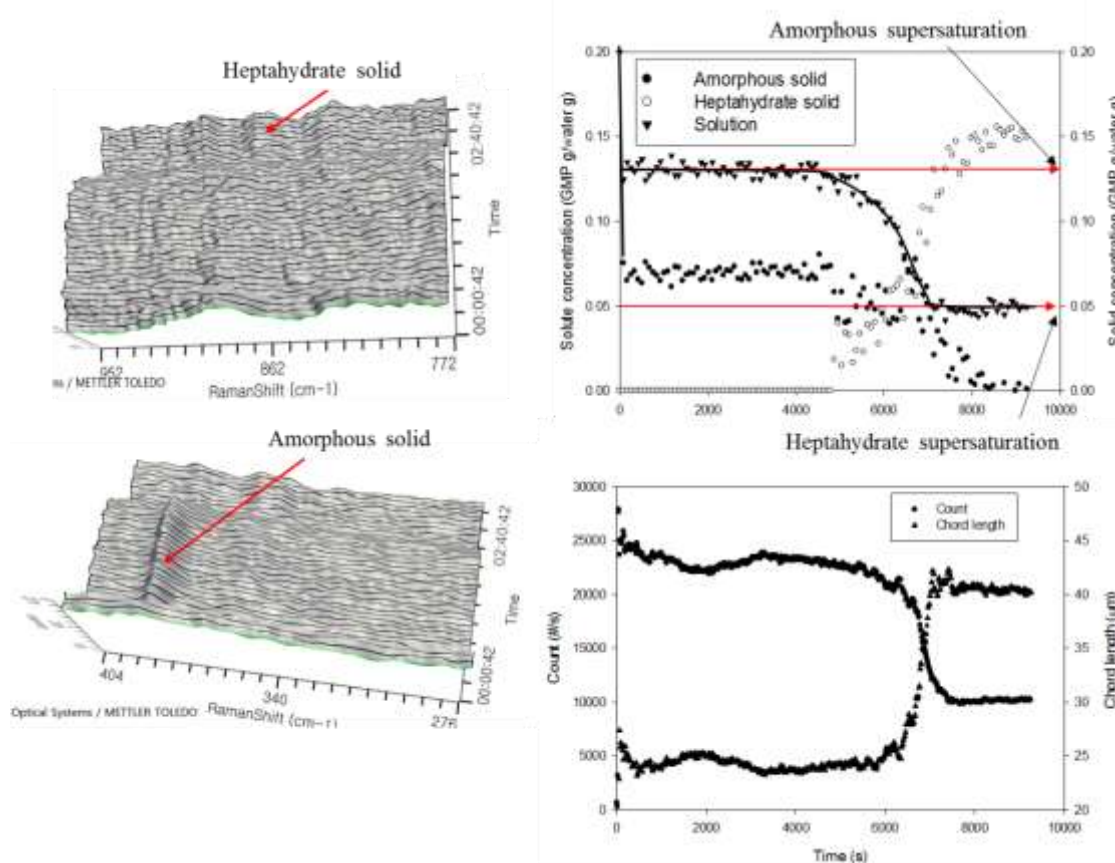
**Fig. 5-16: Variation of the chord length and counts (total, 1–5  $\mu\text{m}$  range, 6–50  $\mu\text{m}$  range and 51–100  $\mu\text{m}$  range) for (a) Pattern A, (b) Pattern B and (c) Pattern C.**

## 6. Discussion

### 6.1 Solubility and Maximum Supersaturation

#### 6.1.1 Effect of the Solvent Fraction on the Maximum Supersaturation

Examples of maximum supersaturated concentrations measured by Raman spectroscopy and FBRM in anti-solvent crystallization are shown in Fig. 6-1, which presents the concentrations of the solution and the concentrations of the solid forms. The transformation of the amorphous form to the heptahydrate can be clearly observed from the Raman shift, as shown in Fig. 6-1a. The operation was performed by adding methanol (methanol/water ratio of 1:1) for 10 s to a solution at a GMP/solvent ratio of 0.2 and 20 °C. The formation of amorphous GMP was observed first, as soon as the methanol was added. After 4607 s, transformation into a heptahydrate crystal started, and the transformation was finished at 8354 s. The supersaturated concentrations of the amorphous and heptahydrate solids were 0.1263 and 0.0503 (GMP g/water g), respectively. An instant addition resulted in maximum supersaturation in anti-solvent crystallization. In these experiments, the number of particles increased rapidly during nucleation and the particle size was 5–10  $\mu\text{m}$ , but the number of particles decreased and the particle size increased when the heptahydrate was formed.



(a)

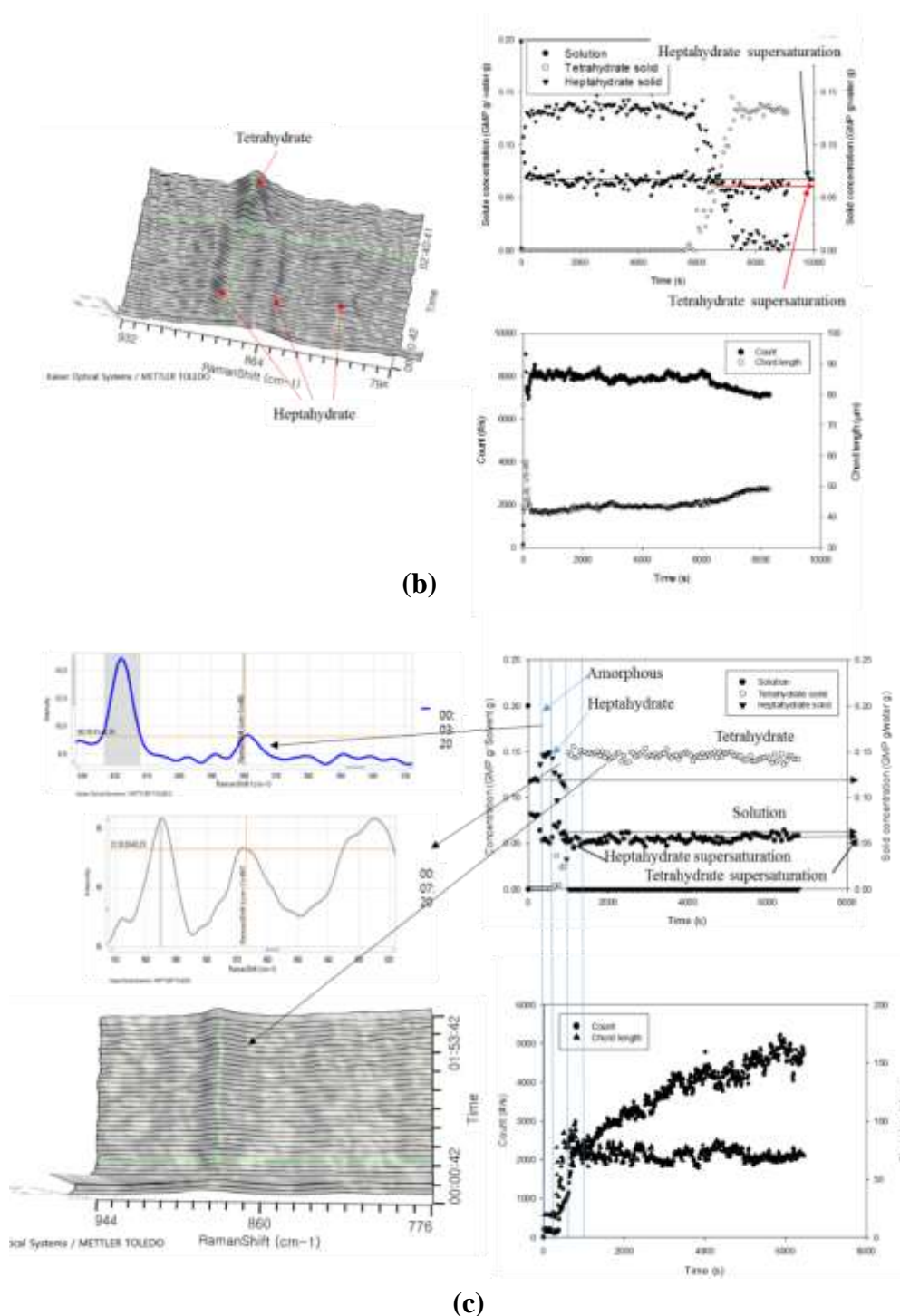


**Fig. 6-1: Measurement of the maximum supersaturated concentrations of (a) the amorphous and heptahydrate forms using anti-solvent crystallization by Raman spectroscopy and FBRM at 20 °C and a methanol fraction of 0.5 (methanol g/solvent mixture g); (b) the tetrahydrate and heptahydrate using anti-solvent crystallization by Raman spectroscopy and FBRM at 50 °C and a methanol fraction of 0.5 (methanol g/solvent mixture g); (c) the amorphous form, tetrahydrate, and heptahydrate using anti-solvent crystallization by Raman spectroscopy and FBRM at 50 °C and a methanol fraction of 0.7(methanol g/solvent mixture g).**

The transformation of the heptahydrate into the tetrahydrate was clearly observed from the Raman spectra results, as depicted in Fig. 6-1b. The operation was performed by adding methanol (methanol/water ratio of 1:1) for 10 s in the solution concentration (GMP/solvent of 0.2) at 50 °C. Heptahydrate GMP was first formed after 3 s and then transformation into tetrahydrate crystals started after 5290 s and was completed at 7231 s. The supersaturated concentrations of the heptahydrate and tetrahydrate crystals were 0.0646 and 0.0532 (GMP g/water g), respectively. The average of the points where the concentration was stable before the phase transition started was considered as the metastable form solubility. The metastable region (concentration) was measured at a constant temperature and mass fraction of methanol. The metastable region had the largest supersaturation for the amorphous form and there was only little difference between tetrahydrate and heptahydrate. It was observed that, when the mass fraction of methanol is greater than 0.8 (methanol g/solvent mixture g), the supersaturated concentrations of the tetrahydrate and heptahydrate are almost the same.

In another example, the operation was performed at 50 °C with a methanol mass fraction of 0.7 (methanol g/solvent mixture g) and a GMP/solvent ratio of 0.2 by adding methanol instantly (Fig. 6-1c), and the results show that amorphous GMP was generated instantly after methanol addition. Transformation into a heptahydrate crystal started after 280 s, followed by transformation into the tetrahydrate after 698 s. The maximum supersaturation of the amorphous, heptahydrate, and tetrahydrate solids was measured as the difference between the actual concentration and the equilibrium concentration (saturation). This supersaturated concentration represents a characteristic value for each form and is: amorphous  $\gg$  heptahydrate  $>$  tetrahydrate. The stability is: tetrahydrate  $>$  heptahydrate  $\gg$  amorphous, and the solubility tends to be reversed so that it can be assumed that the supersaturation of the solid forms is generated.

The amorphous solid form was expected to be detected during rapid addition, and the heptahydrate or tetrahydrate crystals, by slow addition. Under intermediate conditions, polymorphic transformation was confirmed. The mixing of all polymorphic forms was not detected in any experiment, except for transformation. It is recognized that the Raman method is very likely to detect less than 1 % of solid state impurities. There was some delay between the nucleation point and the reaction of the Raman probe at a slow input rate, but the trend was clearly analyzed. This was due to the time required for sufficient solids to accumulate in the solution. The off-line X-ray diffraction results of the solids recovered at the end of the crystallization were consistent with the Raman results for the different solid forms. The concentration at that time was also consistent with the Raman results.

### 6.1.2 Solubilities and Maximum Supersaturation of Solid Forms

The solubilities and maximum supersaturation concentrations of the three solids, which were measured by anti-solvent crystallization, are shown in Fig. 6-2, with the solubility and maximum supersaturation against the methanol mass fraction at 20 and 50 °C being shown in Figs. 6-2a and b, respectively. The amorphous solubility was highest over the entire solvent fraction range. On the other hand, the solubilities of the tetrahydrate and heptahydrate were similar, with that of the tetrahydrate being slightly lower. The maximum supersaturation was highest in the amorphous form, followed by the heptahydrate and tetrahydrate. From these results, the solubility and maximum supersaturation values to selectively produce the amorphous, heptahydrate, and tetrahydrate forms were clearly provided. The amorphous solid form was generated at the highest supersaturation compared to the hydrates. Heptahydrate crystallization was possible at 20–40 °C and a methanol fraction of 0.15–0.6 (methanol

g/solvent mixture g). The tetrahydrate was obtained in the entire solvent fraction range at 45–60 °C and, especially, was crystallized when the methanol fraction was 0.8 (methanol g/solvent mixture g) or higher, even in the range of 20–40 °C.

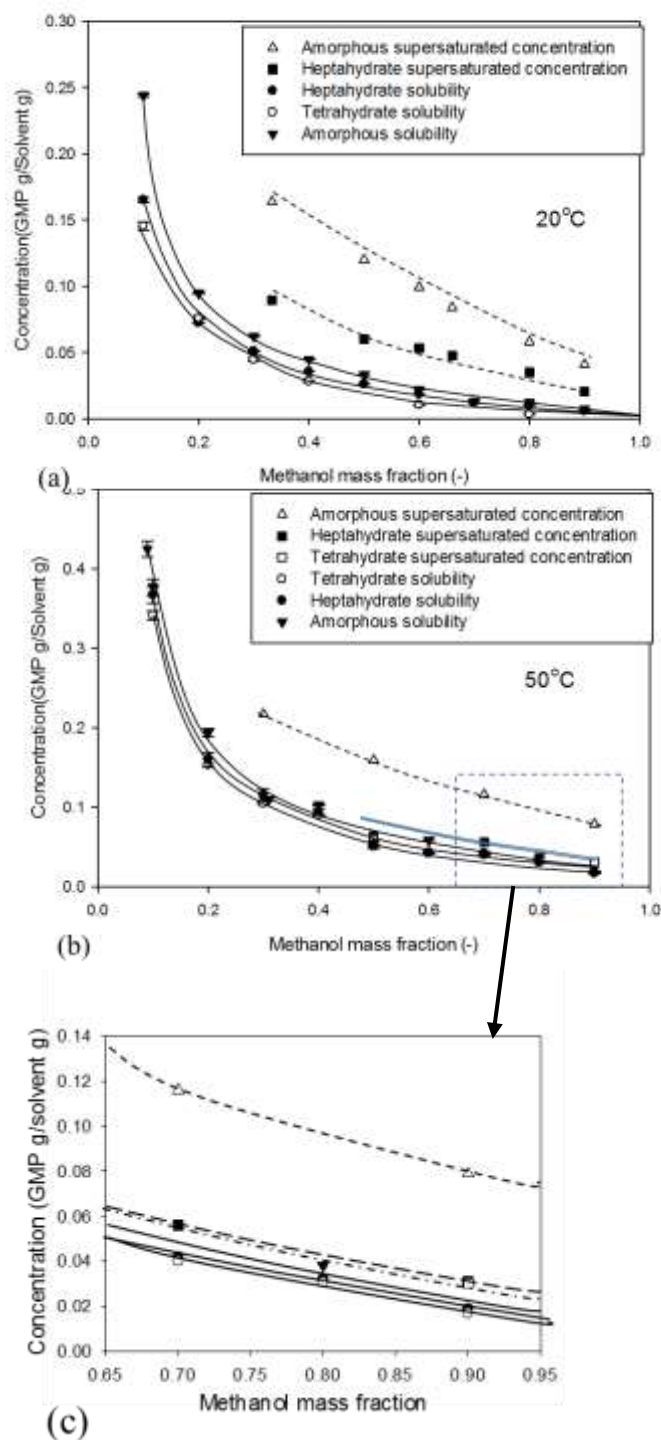


**Fig. 6-2: Solubility and maximum supersaturated concentration of the amorphous, heptahydrate, and tetrahydrate forms at (a) 20 and (b, c) 50 °C.**

Solubility is a thermodynamic property, but the maximum supersaturation or upper limit of the metastable zone is a kinetic property. The actual supersaturation depends on the rate of crystallization, since the metastable limit, i.e. the difference between solubility and actual supersaturation, depends on crystallization conditions. Information on the metastable limit is essential for the selective formation of hydrates and amorphous forms. In this study, it is revealed that crystalline selectivity can be identified by in-situ measuring the metastable limit. The kinetic studies are necessary for control of the crystal size, purity, shape, etc. Crystallization starts when the solution reaches supersaturation, and the crystal size, purity, shape, etc. are controlled according to the degree of this supersaturation. Therefore, supersaturation can be calculated using the solubility data established in this study, and crystalline and amorphous forms can be selectively produced by anti-solvent crystallization operation. Therefore, supersaturation can be predicted using the solubility data established in this study, and crystalline and amorphous forms can be selectively produced by anti-solvent crystallization operation.

## 6.2 Finding Conditions of Phase Transformation

### 6.2.1 Amorphous–Heptahydrate Transformation

As shown in Fig. 5-5, the concentrations of solution, amorphous solid, and heptahydrate solid were presented. It was changed due to the formation of heptahydrate, a more stable form, and the solution concentration was reduced to 0.065 solute g/solvent g. The concentration of the amorphous solid is 0.048 solute g/solvent g. In the process of transformation, the supersaturation consumption rate by dissolution of the amorphous solid was 0.048 solute g/solvent g per transformation time (2024 s), whereas the total formation–growth rate of heptahydrate was 0.135 solute g/solvent g per transformation time (2024 s). The supersaturation consumption rate of the solution is 0.087 solute g/solvent g per transformation time (2024 s). It is calculated as the difference between the solubility of the amorphous (0.152 solute g/solvent g) and that of the heptahydrate (0.065 solute g/solvent g). Therefore, this transformation process can be considered a dissolution-controlled transformation (frequently also called liquid-mediated phase change), because the nucleation-growth rate by supersaturation reduction is much higher than the amorphous dissolution rate. In the dissolution and growth mechanism, the overall dissolution and growth rate depends on the driving force, supersaturation. It is determined by the total surface area of the solid–liquid interface and the mass transfer rate constant from solution to crystal. In general, the growth rate is considered higher than the dissolution rate because there are both mass transfer resistances involved in the diffusion and surface integration steps [Oma07,Oma08]. As shown in Fig. 5-5b, the surface area of the amorphous solid–liquid interface is much higher than that of the heptahydrate during transformation. This is due to the fact that the amorphous form has a relatively large number of particles while relatively few crystals of heptahydrate are produced. This result supports the polymorphic transformation of methionine in batch crystallization [Wan13,Oma12].

### 6.2.2 Tetrahydrate–Heptahydrate Transformation

As shown in Fig. 5-6, heptahydrate is formed after an induction period of 6000 s and tetrahydrate disappears at 8450 s. When heptahydrate was formed, the measured solubility was 0.067 solute g/solvent g. Therefore, the concentration consumed by crystal growth of the heptahydrate is about 0.132 solute g/solvent g. The supersaturated consumption of the solution is 0.004 solute g/solvent g. Therefore, the supersaturation rate in the solution was much lower

than the consumption rate by dissolution of the tetrahydrate. There is also a plateau region of solution concentration of tetrahydrate. The solution concentration decreased when nucleation of heptahydrates started before solution concentration decreased and most of the tetrahydrates were dissolved. Therefore, this transformation can be considered a nucleation-growth-controlled transformation.

The solution concentration maintained the solubility of the tetrahydrate for 5850 s and remained constant until almost no solid form of the tetrahydrate remained in suspension. In the transformation, the supersaturation rate by crystal growth of heptahydrate was 0.137 solute g/solvent g per 2735 s, and the total dissolution rate of the tetrahydrate was 0.132 solute g/solvent g per 1527 s. Therefore, the rate of supersaturation consumption by nucleation growth is smaller than that by dissolution. This case demonstrates a nucleation-growth-controlling transformation step. The intrinsic growth rate is lower than the intrinsic dissolution rate. Most transformations expect this situation to be more common. Otherwise, the same considerations for the effect of surface area in the solid-liquid interface would be applied to this case. However, the initial total surface area of tetrahydrate is similar to that of heptahydrate and is estimated from the particle size distribution. Therefore growth-controlled transformation can explain this case.

### 6.2.3 Heptahydrate-Tetrahydrate Transformation

As shown in Fig. 5-7, after an induction period of 5650 s, tetrahydrate is formed and the concentration decreases to 0.060 solute g/solvent g. The supersaturation consumption by dissolution of heptahydrate was about 0.0139 solute g/solvent g, which was less than the total growth of tetrahydrate of 0.143 solute g/solvent g.

There is a plateau region in the concentration of heptahydrate solid. As soon as the nucleation of the tetrahydrate started after the induction period, it behaved similarly to tetrahydrate-heptahydrate transformation. The solution concentration maintained the solubility of heptahydrate for 6800 s. In this transformation, the supersaturation consumed by crystal growth of tetrahydrate was 0.143 solute g/solvent g per 1990 s, and the total dissolution of heptahydrate was 0.139 solute g/solvent g per 1689 s. Therefore the rate of supersaturation consumption by nucleation growth is smaller than that by dissolution. This case appears as a nucleation-growth-controlled transformation. From the viewpoint of the transformation mechanism, there is no change in particle size, number of particles, or particle size distribution over the entire period, and the transformation from heptahydrate to tetrahydrate occurs. This phenomenon requires a driving force for nucleation of tetrahydrate, because the difference in solubility between the two hydrates is very small. One possibility of explaining it is a surface nucleation. The presence of a surface may be necessary to reduce the energy barrier for nucleation and to promote nucleation of the tetrahydrate. At this point, a higher concentration appears on the surface of the dissolved heptahydrate crystals compared to the solution, and, as a result, nucleation of tetrahydrate on the surface of the heptahydrate may be activated. A higher concentration of heptahydrate surface cannot induce nucleation of tetrahydrate on the same surface, because there is no driving force for heptahydrate dissolution prior to tetrahydrate nucleation. The transformation of the hydrate is energetically more likely to form nuclei at the interface. Similar results were reported in hydrate-anhydrate transformation [Cro10,Oma13,Mah12].

### 6.2.4 Selective Preparation of Amorphous, Heptahydrate, and Tetrahydrate without Transformation

Fig. 6-3 shows solid phase concentration, solution concentration, particle size, and number of particles with elapsed time under various conditions. The equilibrium concentration of the amorphous solid was established immediately after the addition of anti-solvent. The solution concentration was 0.212 solute g/solvent g, and the amorphous solid concentration was 0.088 solute g/solvent g. It remained amorphous without transformation for 28 h. The particle size was 11  $\mu\text{m}$ , and the number of counts was constant at 22 300  $\# \text{ s}^{-1}$  (number count rate by FBRM).

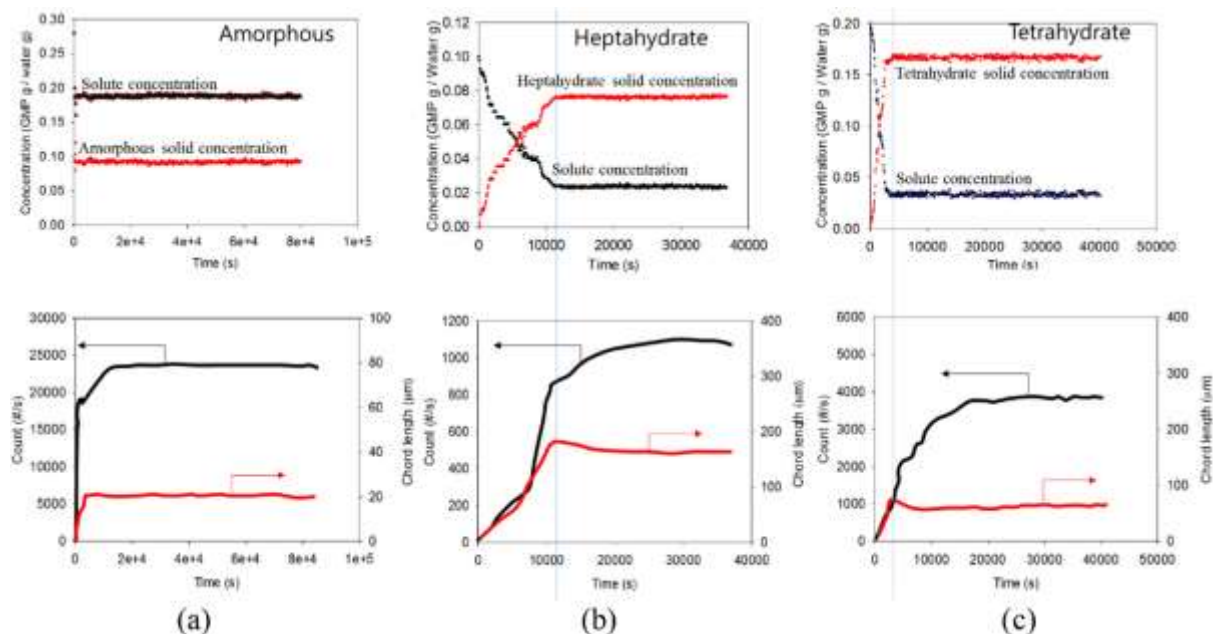


**Fig. 6-3: Preparation of amorphous, heptahydrate, and tetrahydrate without transformation. Top graphs were calculated by calibration of Raman peaks. a–c) Top graphs show a) amorphous solid concentration, b) heptahydrate solid concentration, and c) tetrahydrate solid concentration with solute concentration, respectively; bottom graphs show counts of particle and chord length of a) amorphous solids, b) heptahydrate solids, and c) tetrahydrate solids over time, respectively. Blue lines indicate completion point for crystal growth of heptahydrate and tetrahydrate by variation of solute concentration and particle size with time.**

Heptahydrate was crystallized immediately after the addition of the anti-solvent at an initial concentration of 0.1 solute g/solvent g. Over 11 000 s, the solution concentration decreased from 0.1 to 0.023 solute g/solvent g, and the heptahydrate solid concentration increased to 0.077 solute g/solvent g. Heptahydrate was maintained without transformation for 10 h. The particle size was 32  $\mu\text{m}$ , and the number of particles was constant at 9500  $\# \text{ s}^{-1}$ .

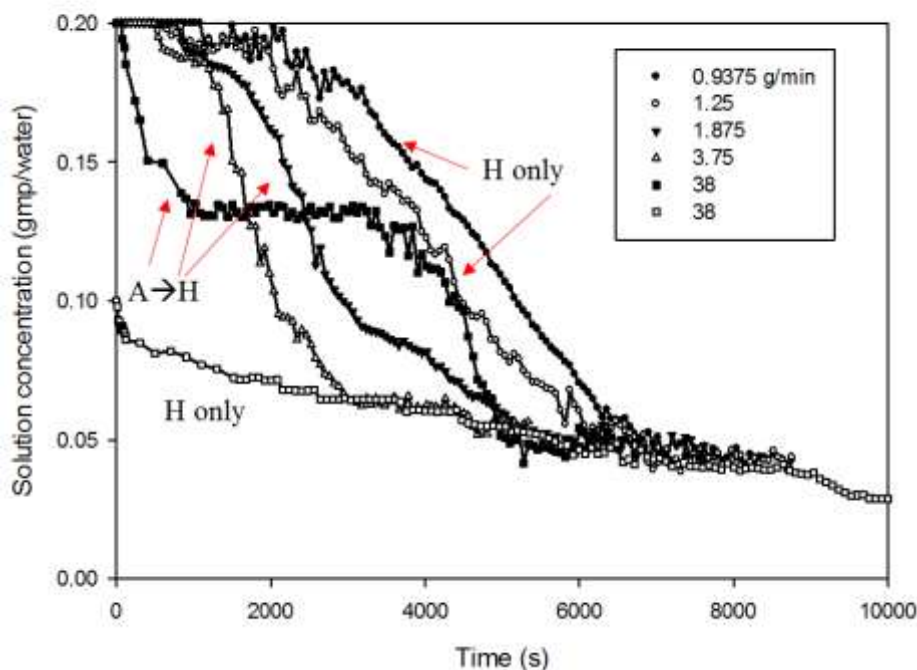
The tetrahydrate was crystallized immediately after the addition of the anti-solvent at a temperature of 50 °C and an initial concentration of 0.2 solute g/solvent g. Over a period of 3400 s, the solution concentration decreased from 0.2 to 0.032 solute g/solvent g, and the tetrahydrate solid concentration increased to 0.168 solute g/solvent g. The tetrahydrate was maintained without transformation for 10 h. The particle size was 72  $\mu\text{m}$ , and the number of

count was constant at  $3900 \text{ \# s}^{-1}$ .

Therefore in order to intentionally prepare either a metastable form or a stable form, the relationship between supersaturation and equilibrium concentration is necessary.

### 6.2.5 Effect of Anti-solvent Adding Rate

The screening of GMP forms using anti-solvent crystallization is affected by the anti-solvent-to-solvent ratio, anti-solvent feed rate, temperature, and initial concentration. Solution concentration–time profiles as a function of anti-solvent feed rate at 20 and 50 °C are shown in Figs. 6-4a and b, respectively. Nucleation, transformation, and growth were shown for the amorphous, heptahydrate, and tetrahydrate forms. Hydrates were formed at lower feed rates and lower concentrations. In some cases, the amorphous form was nucleated and then transformed to hydrate crystals. In the experiment at 20 °C, hydrates were grown by nucleation of heptahydrates at the anti-solvent feed rates of 0.9375 and 1.25  $\text{g min}^{-1}$  with a feed concentration of 0.2 solute  $\text{g/solvent g}$ , and at that of 38.0  $\text{g min}^{-1}$  with a feed concentration of 0.1 solute  $\text{g/solvent g}$ . Initially, amorphous solids were generated at 1.87–3.75  $\text{g min}^{-1}$ , and transformed to heptahydrates after 2000 s. When the anti-solvent feed rate is 38  $\text{g min}^{-1}$  at 0.2 solute  $\text{g/solvent g}$ , the amorphous form is first nucleated, and the solution concentration is maintained at the highest plateau for 4000 s, and then transformation into heptahydrate occurs. At 50 °C, pure amorphous solid was prepared without transformation at an initial concentration of 0.3 solute  $\text{g/solvent g}$  and an addition rate of 38.0  $\text{g min}^{-1}$ . Pure tetrahydrate solids were obtained with transformation at the methanol fraction of 0.67 (methanol  $\text{g/solvent mixture g}$ ). Heptahydrate-to-tetrahydrate and tetrahydrate-to-heptahydrate transformations were produced at methanol fractions of 0.33 and 0.5 (methanol  $\text{g/solvent mixture g}$ ), respectively.



(a)

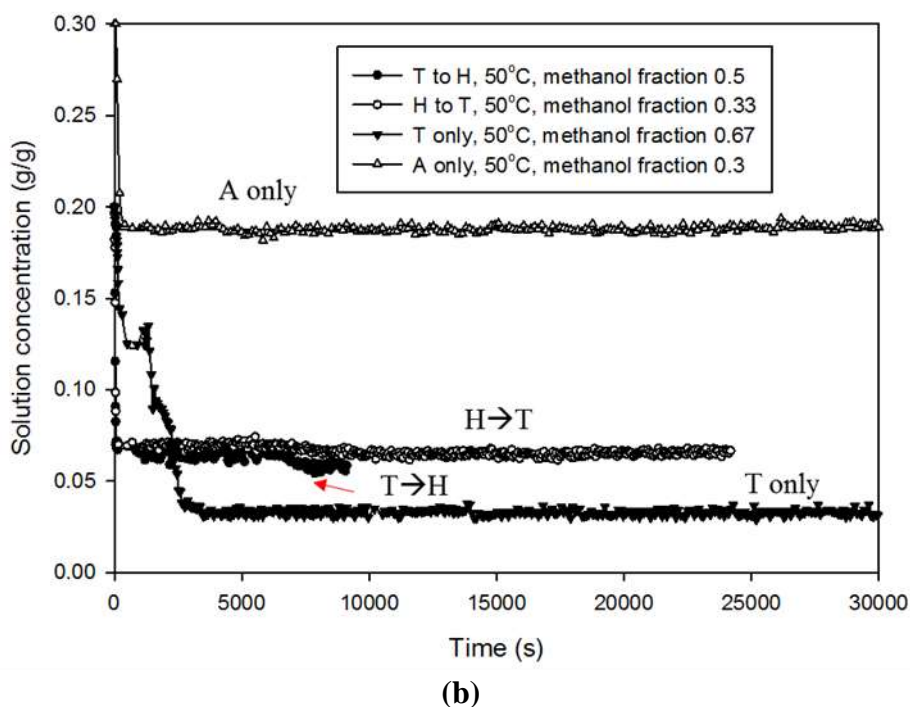
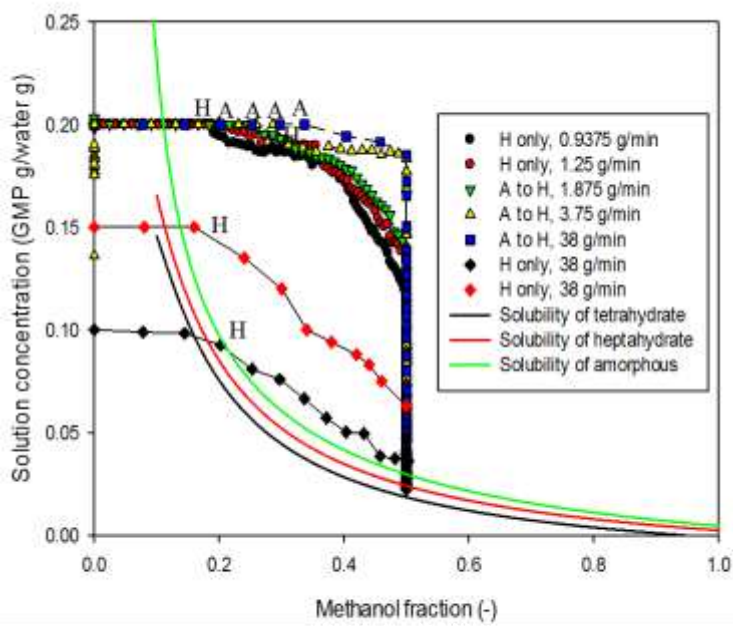
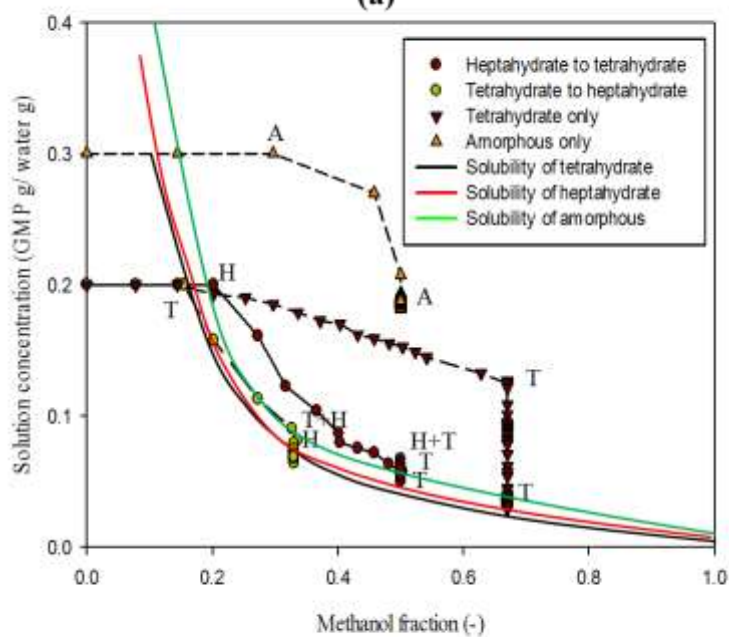


**Fig. 6-4: Variation of solution concentration with time for selective formation: a) 20 °C and b) 50 °C. (A, H, and T stand for amorphous, heptahydrate, and tetrahydrate, respectively).**

Figs. 6-5a and b shows the plots of solution concentration against the methanol fraction for methanol feed rates at 20 and 50 °C, respectively. As can be seen in Fig. 6-5a, heptahydrate was nucleated at a methanol fraction of 0.183, and 0.208 (methanol g/solvent mixture g) for anti-solvent addition rates of 0.9375 and 1.25 g min<sup>-1</sup>, respectively, and then grown without transformation. Despite highest addition rate (38 g min<sup>-1</sup>), at initial concentrations of 0.15 and 0.1 solute g/solvent g, nucleation of heptahydrate occurred at methanol fractions of 0.161 and 0.155 (methanol g/solvent mixture g), respectively. An amorphous solid was formed at a methanol fraction of 0.32, at an addition rate of 3.75 solute g/solvent g, and then transformed to heptahydrate at a methanol fraction of 0.50 (methanol g/solvent mixture g). After amorphous formation, the concentration decreased close to the solubility of heptahydrate by dissolution and growth. Heptahydrate was generated at an initial concentration of 0.1 solute g/solvent g and a methanol fraction of 0.26 (methanol g/solvent mixture g) without transformation.



(a)



(b)

**Fig. 6-5: Solution concentration against methanol fraction for amorphous, heptahydrate, and tetrahydrate formations: a) 20 °C and b) 50 °C (A, H, and T stand for amorphous, heptahydrate, and tetrahydrate, respectively).**

As can be seen in Fig. 6-5b, which is the result for 50 °C, the amorphous form was formed in a methanol fraction of 0.34 (methanol g/solvent mixture g), at an addition rate of 38 g min<sup>-1</sup>, and an initial concentration of 0.3 (GMP g/solvent g), and remained without transformation. The tetrahydrate was nucleated at a methanol fraction of 0.19 (methanol g/solvent mixture g) and at an addition rate of 3.8 g min<sup>-1</sup>, and was grown without transformation. The transformation from the heptahydrate form to the tetrahydrate form occurred at a methanol fraction of 0.20 (methanol g/solvent mixture g), and the transformation from the tetrahydrate to the heptahydrate form occurred at a methanol fraction of 0.14 (methanol g/solvent mixture g). These results were similar to the hydrate formation behavior of taltirelin in batch crystallization [Ngu15]. Finally from Figs. 6-4 and 6-5, the supersaturation can be calculated by the difference between the metastable concentration  $C_{met}$  and the solubility  $C^*$ . It is applicable for the selective preparation of amorphous, heptahydrate, and tetrahydrate solids. After nucleation, the concentration decreased to a more stable form of solubility due to the reduced supersaturation induced by crystal growth. The faster addition rate leads to the higher supersaturation. Thus, the amorphous form nucleated at a faster addition rate at the same solution concentration, whereas the hydrate crystals formed at a slower addition rate. The induction time was affected by supersaturation, which was related to the addition rate of anti-solvent.

### 6.3 Nucleation Study on Phase Transformation

#### 6.3.1 Metastable Zone Width and Supersaturation

Fig. 6-6 shows the variation of the solute concentration and the solid forms according to the mass fraction of methanol (operating line) with the solubility curves of the amorphous form and heptahydrate crystals. The experiment was carried out under Run 1 conditions. The solution is supersaturated by the increasing methanol fraction with respect to both solid forms. For systems which obey Ostwald's Rule [Ost97], the formation of the amorphous form will predominate, but it is expected that, even in such cases, nuclei of the heptahydrate crystal will appear only if the metastable zone of the heptahydrate ends within the metastable zone of the amorphous form. These will form the local conditions for the dissolution of the amorphous form and subsequent growth of the heptahydrate form.

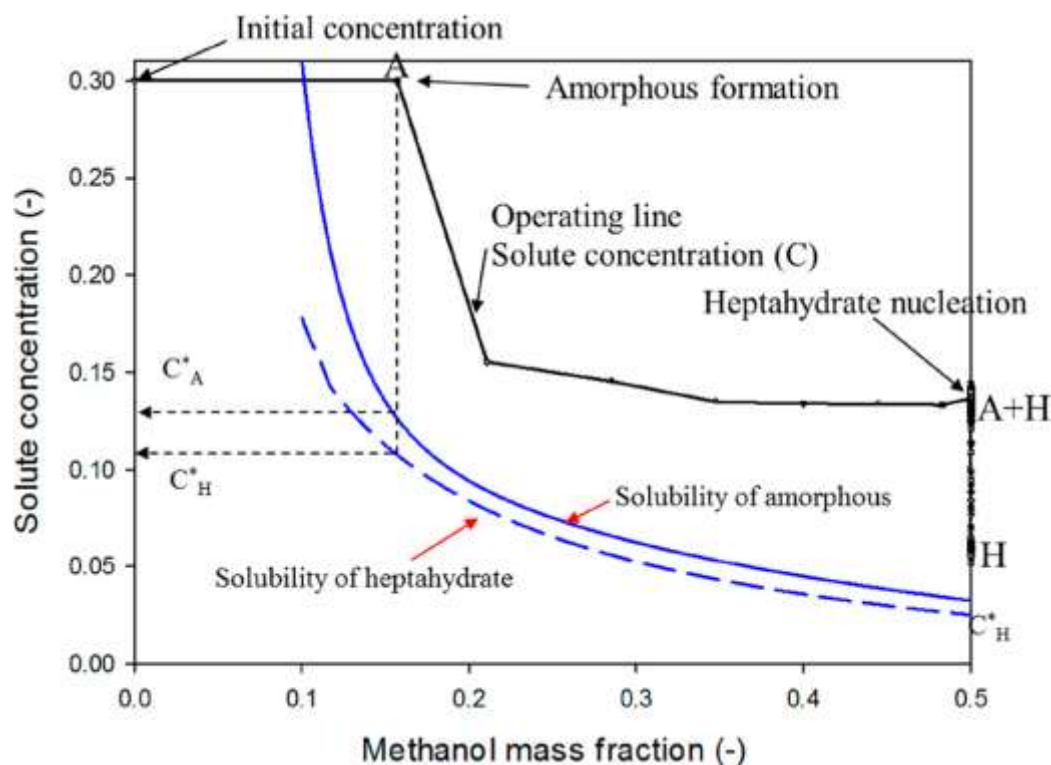


**Fig. 6-6: Variation of the solute concentration and the solid forms against the mass fraction of methanol, obtained at the experimental conditions of Run 1, with the solubility curves of the amorphous form and heptahydrate crystals [Kim22c].**

At point A in Fig. 6-6, the formation of the amorphous solid begins, and the solute concentration decreases sharply, as the methanol fraction increases. Heptahydrate crystals were formed in the slurry of amorphous particles at the point A+H. Here, the metastable zone for amorphous and heptahydrate production can be expressed by the excess amount of methanol (difference in methanol fractions between the equilibrium point and nucleation point) and the induction time,  $t_{ind}$ . The maximum supersaturation ratio for formation of the amorphous material is  $S_{met,A} = C_i/C_A^*$  (where  $C_i$  is the initial concentration), while the driving force of heptahydrate crystal nucleation  $S_{met,H}$  is  $C_A^*/C_H^*$  at the nucleation point. The concentration in the liquid phase increases slightly due to dissolution of the amorphous slurry. A higher initial supersaturation leads to a higher probability of amorphous particles appearing. This plot shows the steady-state plateau region identified by Cardew and Davey [Car85], while the crystal growth, supersaturation, and dissolution are all balanced.

Fig. 6-6 shows that the formation of amorphous solids occurred at a methanol fraction of 0.1675 (methanol g/solvent mixture g), with a solubility limit ( $C_A^*$ ) of 0.1303 GMP g/water g. About 25200 s (7 h) after the amorphous particle formation, the heptahydrate form was nucleated and grown until the solubility limit of the heptahydrate ( $C_H^*$ ) of 0.0324 (GMP g/water g) was reached. This figure may be used to determine the change in solid form, concentration, excess amount based on methanol fraction, transformation time, supersaturation of amorphous and heptahydrate forms, and induction time.

In the anti-solvent addition method, the characteristics of amorphous formation, crystalline nucleation, and transformation in solution depend on variables such as the initial concentration, addition rate, and anti-solvent fraction.

The nucleation rate can be expressed as [Oma06,Ulr03]:

$$J = A \exp(B) \quad (6-1)$$

where  $A$  is the pre-exponential factor, and  $B$  is the exponential term factor including the supersaturation ratio  $S$ :

$$B = -\frac{16\pi\gamma^3\nu^2}{3\kappa^3T^3(\ln S)^2} \quad (6-2)$$

where  $\gamma$  is the interfacial tension,  $\nu$  is the molecular volume,  $T$  is the temperature, and  $\kappa$  is the Boltzmann constant ( $1.3805 \times 10^{-23} \text{ J}\cdot\text{K}^{-1}$ ).

When the formation of a stable nucleus is the rate-limiting step, then the induction time,  $t_{ind}$ , is inversely related to the nucleation rate,  $J$ :

$$J \propto \frac{1}{t_{ind}} \quad (6-3)$$

The pre-exponential factor  $A$  in eq. 6-1 is expressed as [Kim01]:

$$A = 1.5D_{AB}(C_c N_A)^{5/3} \left(\frac{C}{C_c}\right)^{7/3} \sqrt{K \ln\left(\frac{C_c}{C^*}\right)} \quad (6-4)$$

where  $D_{AB}$  is the diffusion coefficient,  $C_c$  is the density of the solid, and  $C$  is the solute concentration.  $K$  is the slope of the log-log plot of the interfacial tension against  $C_c/C^*$ . The constant  $K = 0.333$  was derived from the experimental data [Kim01]. The pre-exponential term  $A$  depends on  $D_{AB}$  and the solute concentration when the temperature is constant. Since  $D_{AB}$  is inversely proportional to the viscosity, the pre-exponential term ( $A$ ) is proportional to the solute concentration and inversely proportional to the viscosity as:

$$A \propto \frac{C^{7/3}}{\eta} \quad (6-5)$$

where  $\eta$  is the viscosity. Therefore, the pre-exponential factor is affected by the concentration of the amorphous solid and the solute concentration due to the increased frequency of molecular attachment to sufficiently offset the decreasing driving force of the exponential term  $\exp B$ . Combining eqs. 6-2, 6-3, and 6-5 gives the following equation:

$$\frac{1}{t_{ind}} \propto \frac{C^{7/3}}{\eta} \exp(-(\ln S)^{-2}) \quad (6-6)$$

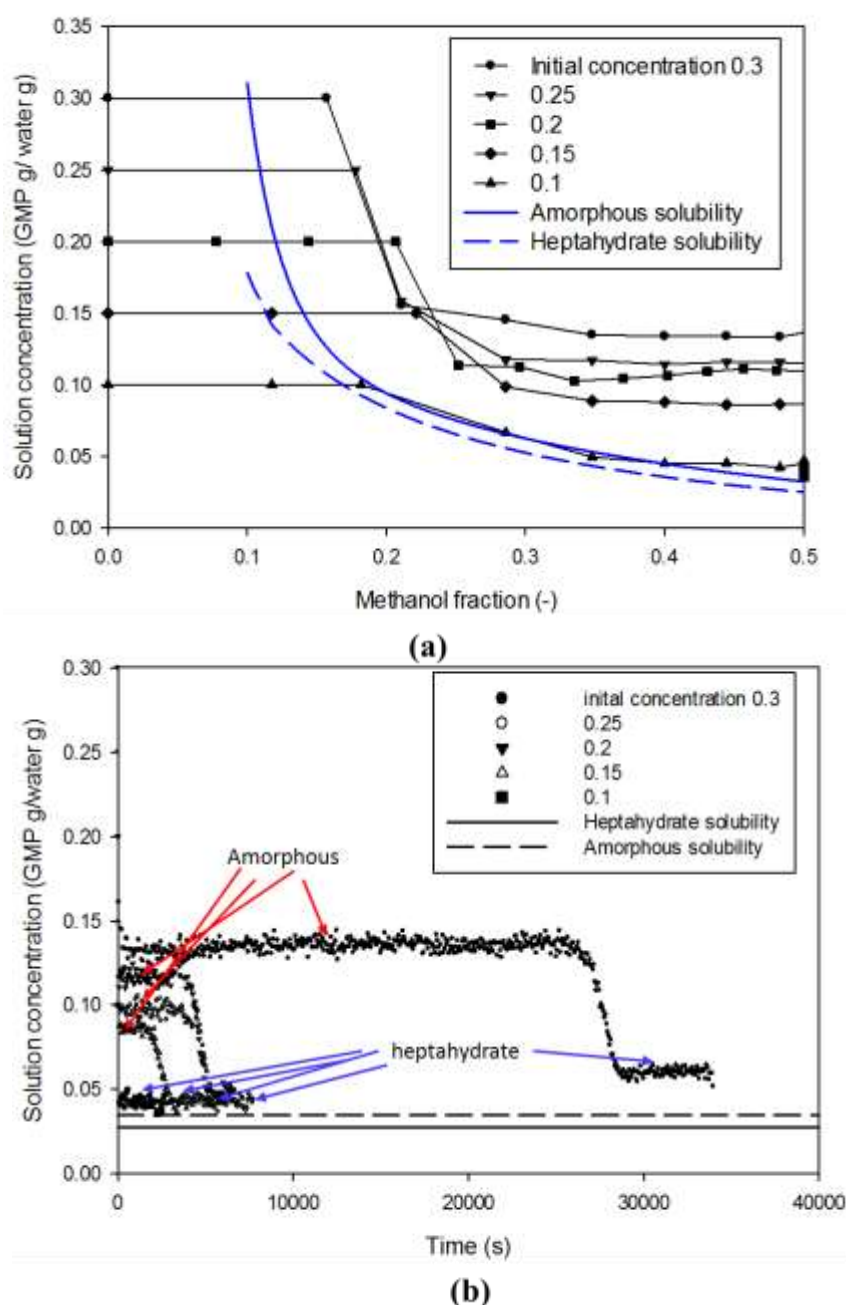
In the process of nucleation of the crystalline form after the formation of the amorphous form at a constant temperature and a supersaturation, the increase in the viscosity of the amorphous slurry causes an increase in the induction time of the crystalline form. On the other hand, if the viscosity is constant, the induction time increases with decreasing the supersaturation.

The pre-exponential factor  $A$  of eq. 6-1 includes the terms related to the solute concentration and the amorphous slurry concentration in the transformation process. In other words, it is greatly affected by the amorphous state due to the volume diffusion of the solute from the bulk solution to the nucleus. When the change in the supersaturation is larger than the pre-exponential factor, nucleation depends on the supersaturation of the exponential term.

### 6.3.2 Effect of the Initial Concentration

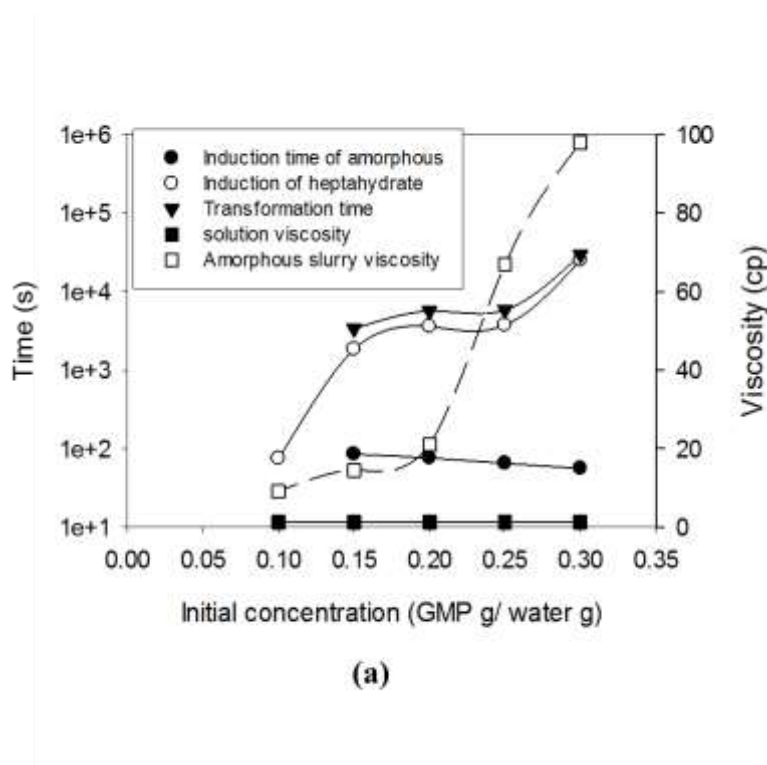
When the temperature, anti-solvent fraction, and addition rate are constant, the initial concentration affects not only supersaturation but also the pre-exponential factor in eq. 6-1. Fig.

6-7 shows the solute concentration-methanol fraction and the concentration–time profiles according to the initial concentration for the results of Runs 1–5 (also see Appendix). The operating conditions were set at a methanol fraction of 0.5 (methanol g/solvent mixture g), a methanol addition time < 1 min, and a temperature of 20 °C. From analysis of Figs 6-6 and 6-7, the results of Tabs. 5-3 and 5-4 were obtained.



**Fig. 6-7:** Plots of the solute concentration-methanol fraction and concentration–time according to the initial concentration for the results of Runs 1–5.

Fig. 6-8a shows the induction times of the amorphous and heptahydrate forms and the viscosities of the solution and the amorphous slurry according to the initial concentration. As the initial concentration increases, the induction time of the amorphous form decreases, while that of the heptahydrate form increases. According to the classical nucleation theory, the nucleation rate increases with supersaturation. This relationship applies because the amorphous form is formed from solution, but the nucleation of the heptahydrate form is impacted by the amorphous slurry state, in which the solution and the amorphous solid coexist. A previous study [Oma13] hypothesized that the surface of the metastable form promotes the nucleation of the stable form during the transformation process. In this study, nucleation was performed at 20 °C with a supersaturation ratio  $S$  ranging from 1.33 to 1.39 for the heptahydrate form. The transformation time from amorphous particles to heptahydrate crystals in Run 1 was 7.75 h at a supersaturation ratio of  $S=1.39$ . In the transformation process, the higher the concentration of the amorphous slurry, the lower the nucleation rate, which contradicts the result that the metastable particles activate the creation of the stable form [Oma13,Cro10]. When the initial concentration was 0.1 (GMP g/water g), the amorphous form was not formed, and a nucleation of a stable heptahydrate occurred. In the initial concentration range of 0.1 to 0.3 (GMP g/water g), the amorphous formation occurs at the  $S_A$  range of 1.75 to 2.47.



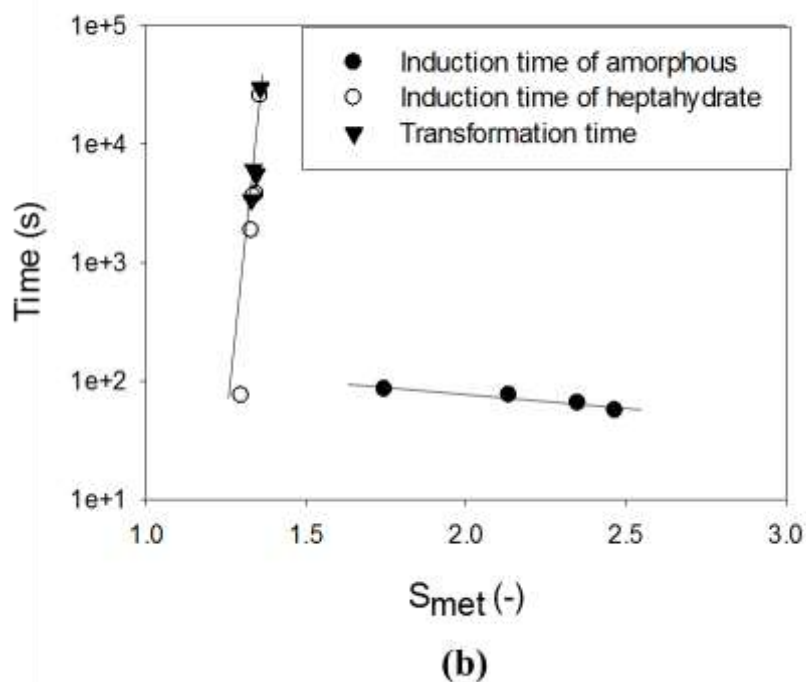


**Fig. 6-8: Effect of the initial concentration on the induction time, supersaturation, and viscosity: (a) induction times of the amorphous and heptahydrate forms and the viscosities of the solution and the amorphous slurry and (b) plot of the induction time against supersaturation.**

Fig. 6-8b shows an effect of supersaturation on the induction time for the results of Runs 1–5 at the maximum supersaturation ratios,  $S_{A,met}$  and  $S_{H,met}$ , and the mass fraction of methanol of 0.5 (methanol g/solvent mixture g). As seen in Tab. 5-3, supersaturations  $S_A$  and  $S_H$  increase with an increase in the initial concentration. As supersaturation increases, the induction time of the amorphous form decreases, while that of heptahydrate crystals increases. This contrary effect implies that the factors controlling the nucleation of heptahydrate cannot be explained by the supersaturation ratio. The contrary results of amorphous and crystalline forms can be grasped by the classical nucleation theory (eq. 6-1). It results in the formation of the amorphous material in solution and nucleation of heptahydrate crystals in the resulting amorphous slurry. As a result, the environments for the formation of the amorphous particles and the heptahydrate crystals are completely different. The remaining liquid in amorphous slurries has conditions without convection for the remaining liquid. The result correlates with the much higher viscosities than solid free liquids and consequently are much lower in diffusion coefficients. Also, the degree of supersaturation for the formation of the amorphous form is substantially higher than for the nucleation of the crystalline form. The induction time in eq. 6-6 is determined by the initial concentration, viscosity, and supersaturation. As a result, the pre-exponential factor is proportional to the initial concentration and inversely proportional to the viscosity. In eq. 6-2, the exponential term increases with increasing degree of supersaturation. As shown in Figs. 6-8a and b, the effect of the initial concentration on the induction time may

be interpreted by considering the viscosity. Previous experimental data [Qi17,Zou15] on the relationship between the induction time and supersaturation in transformation are analogous to the results of this study. The induction time in the transformation process from the amorphous to the crystalline form is determined by the pre-exponential term, while that of the amorphous form in the solution is determined by the exponential term. Consequently, the counts increase with increasing the initial concentration to follow the mass balance. FBRM counts of the amorphous particles are larger than that of heptahydrate crystals. At the end of the transformation, the mass of the heptahydrate crystals is higher than that of the amorphous particle due to its lower solubility. In Runs 1–5, the average size of amorphous particles and the heptahydrate crystalline form is in the range of 28–37  $\mu\text{m}$  and 46–55  $\mu\text{m}$ , respectively. Comparatively, the particle sizes for the crystalline form may be assumed to be similar because the supersaturation  $S_H$  is almost equivalent in all experiments.

The degree of supersaturation is not much different while transitioning from amorphous to crystalline forms. The effect of the exponential term in eq. 6-3 is minor, but there is a significant difference in the viscosity depending on the concentration of the amorphous slurry. As a result, the pre-exponential factor has a dominant influence. Fig. 6-8a shows the plateau solute concentration and the amorphous solid concentration along with the viscosity according to the initial concentration. The viscosities of the solution and the amorphous slurry were in the range of 0.0025–0.0043 Pa s and 0.015–0.098 Pa s, respectively, at the initial concentration investigated.

From this result, as shown in Fig. 5-8, the time required for transition from amorphous to heptahydrate crystal increases as the solute concentration increases. The number of particles in 300 g/L varied from 19302 #/s of amorphous to 7955 #/s of heptahydrate. As the initial concentration increases, counts of amorphous increase, while those of heptahydrate were almost constant. At 300, 250, 200 and 150 g/L, the transformation process took 29579, 5820, 5665, and 3383 s, respectively. The induction time of the crystalline heptahydrate form can be greatly increased in the presence of the amorphous form because the amorphous slurry solution lowers molecular diffusion, while the nucleation barrier of the heptahydrate crystal phase is increased.

### 6.3.3 Effect of Methanol Fraction

Fig. 6-9a shows the effects of the contents of methanol (mass fraction in the solvent mixture ranges from 0.3 to 0.8 (methanol g/solvent mixture g) on the induction time and supersaturation of amorphous and heptahydrate forms. It was studied under the conditions of an initial concentration of 0.2 (GMP g/water g), a temperature of 20 °C, and a rapid addition (Runs 14–18 in Tab. 5-5 and Appendix). The induction time of the amorphous form decreases as the methanol fraction increases, whereas it is increased for the heptahydrate form. With an increasing methanol fraction, supersaturation ratio  $S_A$  increased to around 0.9. A further increase in the methanol fraction leads to a decrease in the supersaturation. In addition, the supersaturation ratio  $S$  of amorphous and heptahydrate forms is in the range of 3.3–12.1 and 1.32–1.37, respectively, with respect to the methanol fraction of 0.33–0.72 (methanol g/solvent mixture g). The dependence of the methanol fraction on supersaturation is comparatively small in the heptahydrate form, while it is large in the amorphous form. The higher the content of methanol, the better the conditions were for the amorphous formation. According to eq. 6-6, the influence of both the exponential factor  $B$  and the pre-exponential factor  $A$  for homogeneous nucleation should be considered. The exponential factor is positively correlated with the supersaturation, and in consequence, it is also possible that the increase in the methanol

fraction leads to a decrease in the induction time of the amorphous form.

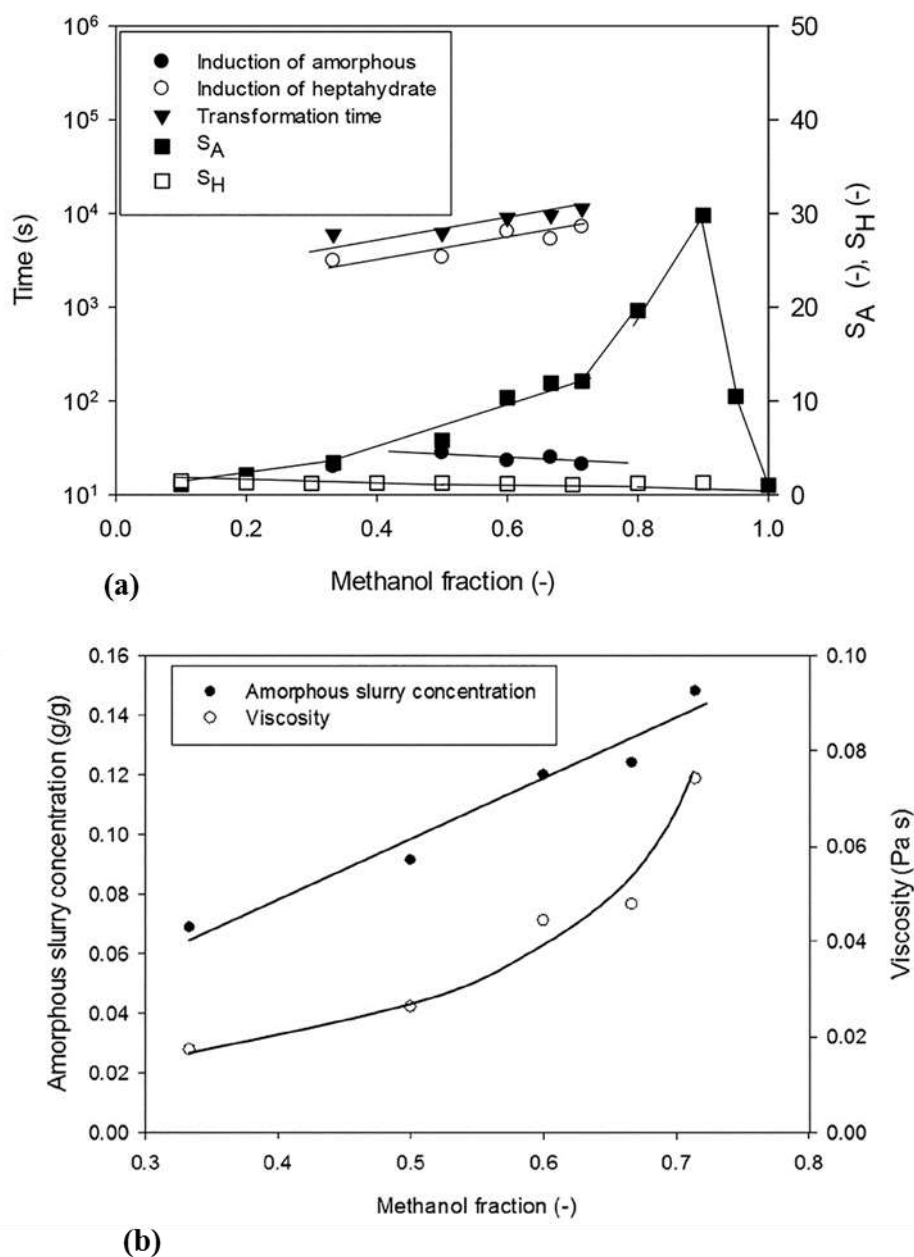


**Fig. 6-9: Effects of the contents of methanol on (a) the induction time and supersaturation of amorphous and heptahydrate forms and (b) the amorphous slurry concentration and viscosity.**

As a result, the supersaturation degree and solution properties are different for amorphous formation and heptahydrate nucleation. The solute concentration and viscosity of the amorphous slurry influence the nucleation of heptahydrate because it occurs in a slurry solution containing an amorphous solid and the difference in supersaturation is small. Therefore, the nucleation of heptahydrate is determined by the pre-exponential factor of eq. 6-5. As shown in Fig. 6-9b, as the methanol mass fraction increases from 0.33 to 0.72 (methanol g/solvent mixture g), the amorphous slurry concentration increases from 0.06 to 0.15 (amorphous GMP

g/water g), in which the viscosity increases from 0.0196 to 0.0775 Pa s. As a result, the induction time of heptahydrate increases with the methanol fraction.

#### 6.3.4 Effect of the Addition Rate

The addition rate is a key parameter to generate the supersaturation of the solution of the anti-solvent crystallization method. The nucleation kinetics is obtained by measuring the effect of the addition rate on the metastable zone width, which is expressed as the excess amount of the anti-solvent ( $\Delta A_a = A_a - A_a^*$ ) [Oci11,Ogr07,San10]]. The metastable zone width increases with an increase in the addition rate.

Figs. 6-10a and b shows the induction time, viscosity, and  $\Delta A_a$  for formation of the amorphous and heptahydrate forms according to the methanol addition rate. The results are listed in Runs 6–10 of Tabs 5-3 and 5-5 (also see the Appendix). As the addition rate increases, the induction time of the amorphous form decreases, whereas that of heptahydrate decreases up to 4 g/min and increases at high addition rates. As mentioned previously, the induction time of heptahydrate is affected by the viscosity of the amorphous slurry. At an addition rate < 4 g/min, there was a slight change of about 0.005 Pa s, but it increased to 0.021 Pa s at a high addition rate of 35 g/min. This suggests that the induction time at high addition rates is high due to a high viscosity of the amorphous slurry. Fig. 6-10b shows a log–log plot of  $\Delta A_{a,max}$  against the addition rate. These are plots to determine the nucleation kinetics in anti-solvent crystallization from the following relationship [Ogr07]:

$$\ln r = k_1 + n \ln(\Delta A_{a,max}) \quad (6-7)$$

From the slope and intercept of such plots, the values of  $n$  and  $k_1$  can be obtained using eq. 6-7. The plot of the solubility against the methanol fraction offers  $dC^*/dA_a = 0.017$  (solute g/anti-solvent g) [Kim22a].

The plots of Fig. 6-10b with eq. 6-7 give  $n = 3$  and  $k_1 = 4.6$  for the heptahydrate form and  $n = 3.8$  and  $k_1 = 6.3$  for the amorphous form. Crystallization of the heptahydrate form was observed without amorphous formation at a low addition rate (0.7 g/min).

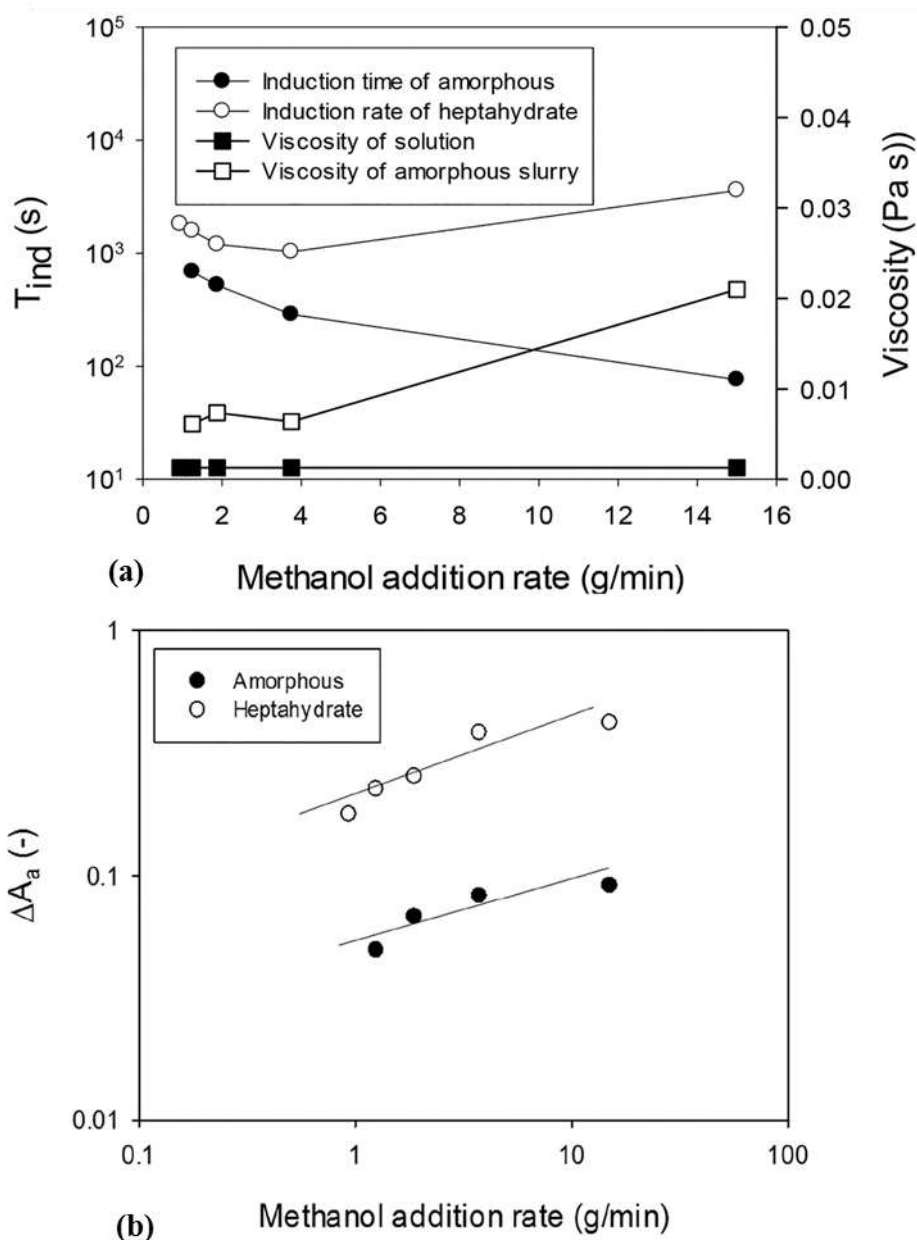


**Fig. 6-10: Effect of the addition rate on the induction time, viscosity, and  $\Delta A$  for formation of the amorphous and heptahydrate forms: (a) effect of the addition rate on the induction time and viscosity and (b) the plot of  $\Delta A$  against the addition rate.**

### 6.3.5 Screening of Solid Forms and the Kinetic Effect on Transformation

Fig. 6-11 shows the metastable zone limits of the amorphous and heptahydrate crystalline forms and their respective solubilities in a plot of the solute concentration versus the mass fraction of methanol in the mixed solvent. The amorphous form is depicted in the black circles. The red circles represent the nucleation regions of the heptahydrate. At methanol mass fractions of 0.33 and 0.72 (methanol g/solvent mixture g), amorphous forms are generated only at solute concentrations between the lower and upper limit lines, and heptahydrates can be obtained between the lower limit line and the heptahydrate solubility line. The two limit lines intersect

at a methanol fraction of 1.0 (methanol g/solvent mixture g). Therefore, amorphous and heptahydrate crystalline forms may be selectively prepared under all of the conditions of this study.

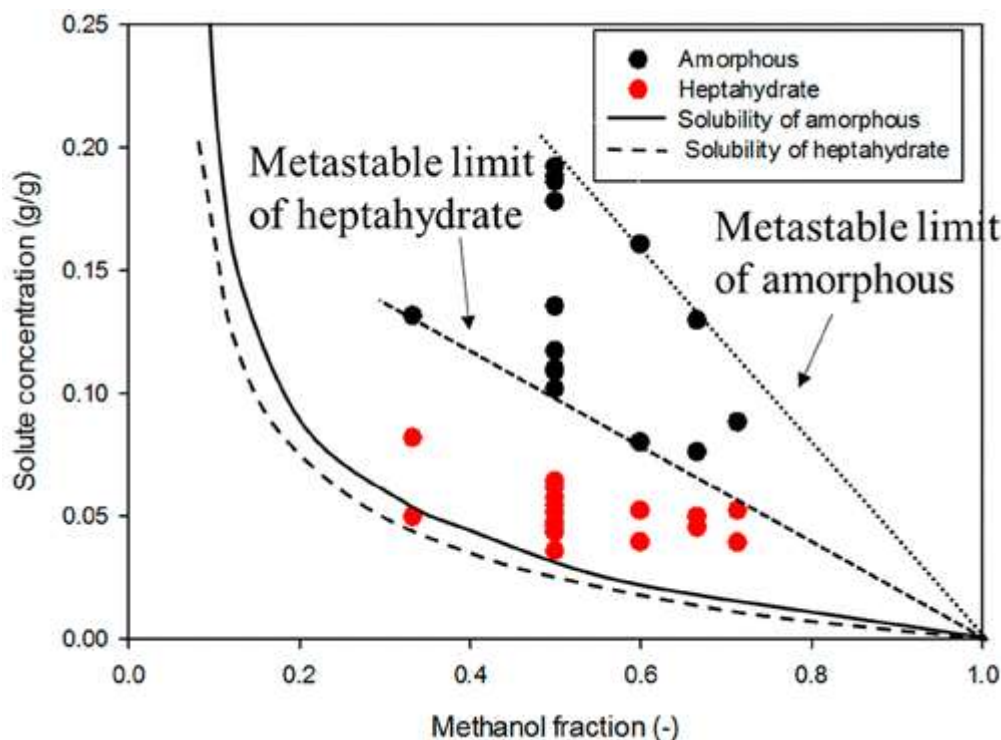
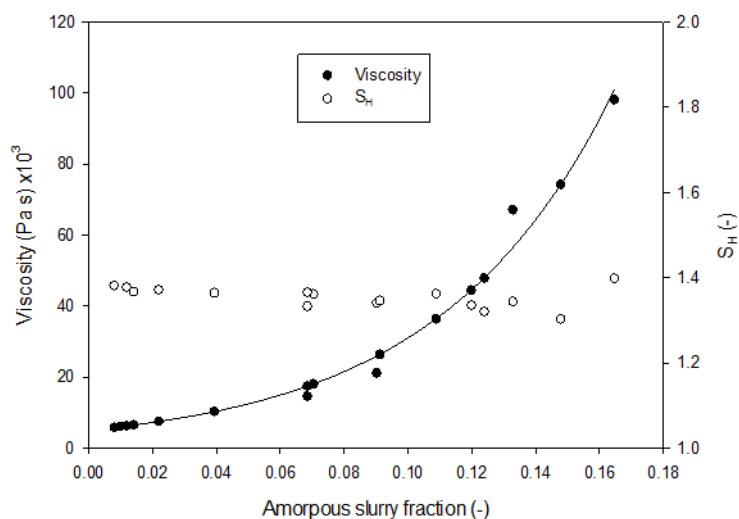
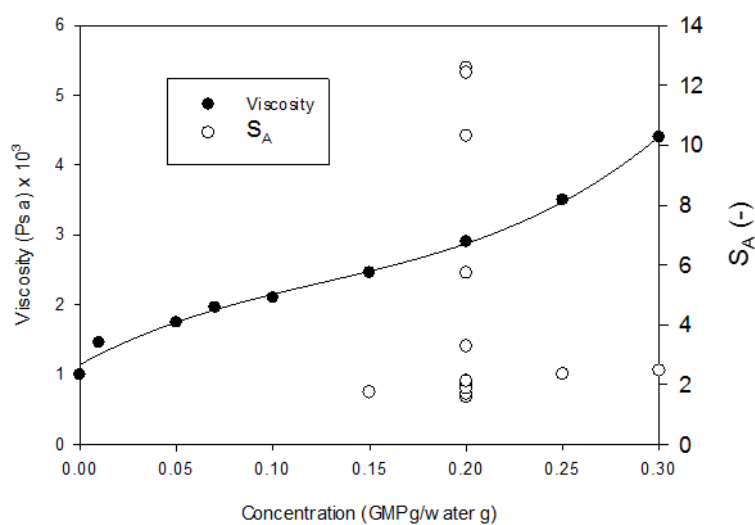


**Fig. 6-11: Metastable zone limits of the amorphous and heptahydrate crystalline forms and their respective solubilities in a plot of the solute concentration versus the mass fraction of methanol in the solvent mixture.**

The induction time and supersaturation of heptahydrates obtained at the conditions investigated were not related to each other. Therefore, it is necessary to consider the pre-exponential term of the nucleation theory described above for the induction time of heptahydrate. The effect of the pre-exponential term was considered because the difference in supersaturation between the amorphous and heptahydrate forms was not significant for heptahydrate formation. Fig. 6-12a shows the viscosity against the concentration of the amorphous slurry obtained from all experiments. When the amorphous slurry concentration is changed from 0.01 to 0.17 (amorphous GMP g/water g), the viscosity increases exponentially from 0.005 to 0.098 Pa s. The supersaturation ratio  $S$  of heptahydrate ranges from 1.33 to 1.40 in all of the experiments. Thus, the induction time of the heptahydrate correlates nicely with the viscosity of the amorphous slurry concentration. Fig. 6-12b shows the viscosity of the solute concentration and the supersaturation for the amorphous formation. The supersaturation  $S$  of the amorphous form ranges from 1.8 to 12.5 in all the experiments. The viscosity of the solution was 0.0021 to 0.0042 Pa s at initial concentrations of 0.1 to 0.3 (GMP g/water g), respectively (see Tab. 5-3), which is significantly lower compared to that of the amorphous slurry. Thus, the induction time of the amorphous form depends mainly on the supersaturation of the solute concentration.



(a)



(b)

**Fig. 6-12: Viscosity and supersaturation against (a) the concentration of the amorphous slurry and (b) solute concentration obtained at all the experiments.**

Fig. 6-13 shows the plot of  $1/t_{\text{ind}}$  against  $\eta^{-1}C^{7/3} \exp(-(\ln S)^2)$  for heptahydrate nucleation in eq. 6-6 for all data investigated. Both the pre-exponential factor and the exponential term were taken into account and applied to amorphous–crystalline transformation. This relationship was used to evaluate the heptahydrate formation experiments. It was determined that the pre-

exponential factor is the most important factor influencing transformation in the amorphous slurry. In the studied concentration and anti-solvent fraction, the heptahydrate form would be obtained at  $S < 1.4$ , while the amorphous form would be produced at a higher supersaturation level ( $S > 1.7$ ). Especially, at  $S_H < 1.3$ , heptahydrate was crystallized without transformation. The findings of this study would provide some guidance for the preparation of various pure forms by modifying the operating parameters, which impact supersaturation and viscosity. High supersaturation promotes the production of the amorphous form and can also cause the crystalline form to transform.

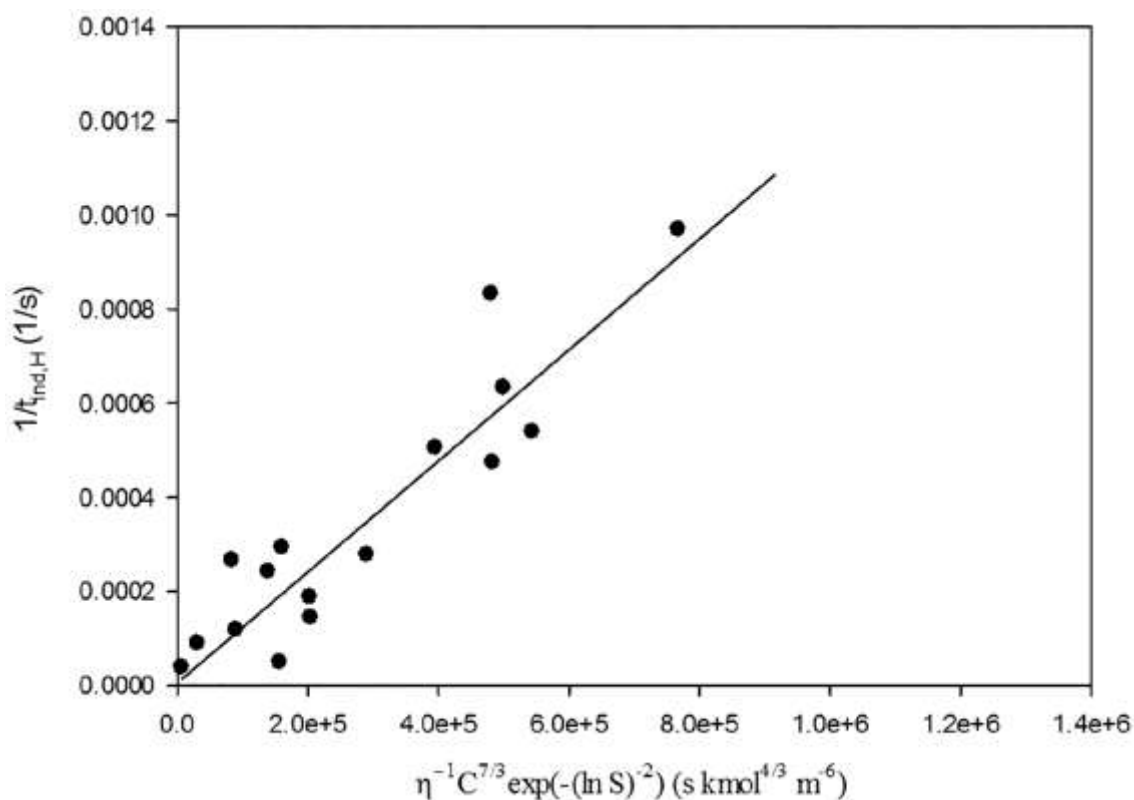


**Fig. 6-13: Plot of  $1/t_{ind}$  against  $\eta^{-1}C^{7/3} \exp(-(\ln S)^{-2})$  for heptahydrate nucleation in eq. 6-6 for all the data investigated.**

The proposed strategy for screening solid forms in case of GMP is shown in Fig. 6-14. A comprehensive screening strategy should highlight consideration of the solubility of the compounds and during crystallization in liquid different levels of supersaturation should be generated. Thus various screening techniques should be applied with this strategy. Consequently, in order to save time and resources, a screening strategy is proposed which consider the solubility and supersaturation. This provides information for the direct production of stable forms of substances and the preparation of stable forms by transformation after formation of metastable forms. Also, the production of a metastable form is usually challenging, but according to these strategies the proper selection of operating conditions to adjust the supersaturation and the solvent choice might enable to produce the desired (metastable) form.

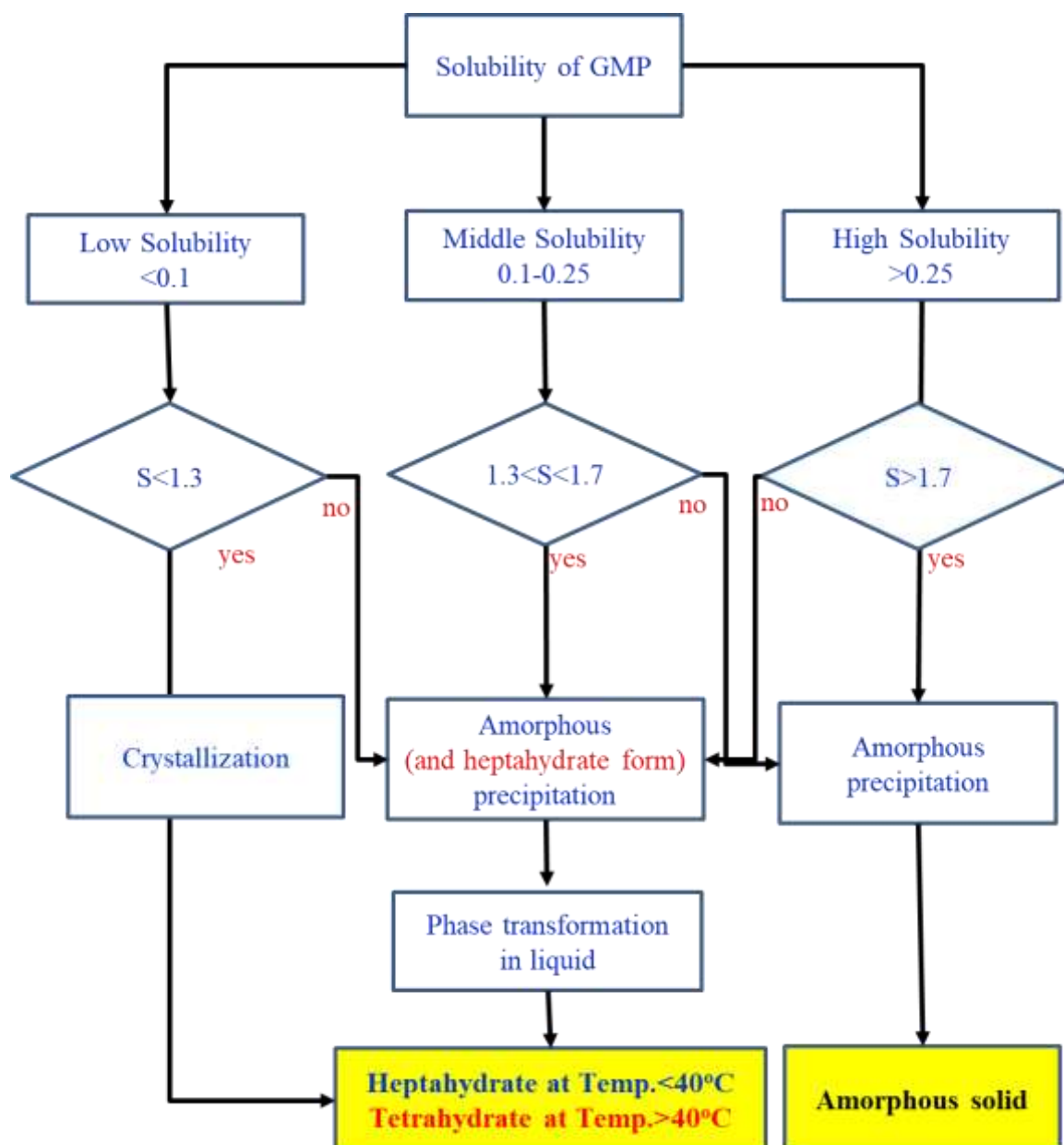


**Fig. 6-14:** Solid form screening strategy (in case of GMP)

## 6.4 Dissolution, Growth Kinetics and Controlling Step

### 6.4.1 Effect of Operating Parameters

The studies were carried out in several methanol–water mixed solvents (i.e., methanol fraction (methanol g/solvent mixture g) = 0.30–0.80) to investigate the influence of solvent composition on phase transformation. The solvent composition has a considerable impact on the process, and the results show that as the methanol fraction increases, so does the induction and transformation time.

The nucleation of the stable form is important for the transformation process. In general, the higher the solubility of a solute in a solvent, the higher the transformation rate should be [Das10]. However, it does not apply to the interpretation in this case. The solubility of amorphous material is higher in water/methanol mixtures with higher water content, but the transformation of amorphous material to the heptahydrate is slower. The rate of amorphous solid formation was affected by supersaturation. The concentration of the amorphous form produced affects the nucleation of the stable hydrate. The phase transformation process may be influenced by molecular diffusion, which is also reciprocal of the viscosity.

To investigate the effect of feed concentration on amorphous formation, different feed concentrations were supplied to the mixed solvent (methanol fraction = 0.50 (methanol g/solvent mixture g)) at 293.15 K. Kim and Ulrich [Kim22c] presented the induction and transformation times of heptahydrate increase as the feed concentration increases. The nucleation of the heptahydrate phase may have occurred on the surface of the amorphous phase [Jak16]. This effect is caused mostly by the increased local supersaturation degree at the amorphous solid dissolving surface. Because greater amorphous counts increase the number of heptahydrate nucleation sites, increasing the amorphous content can increase the nucleation rate. As the nucleation and growth of heptahydrate is a rate-determining step, the transformation rate is positively related to the amorphous amount.

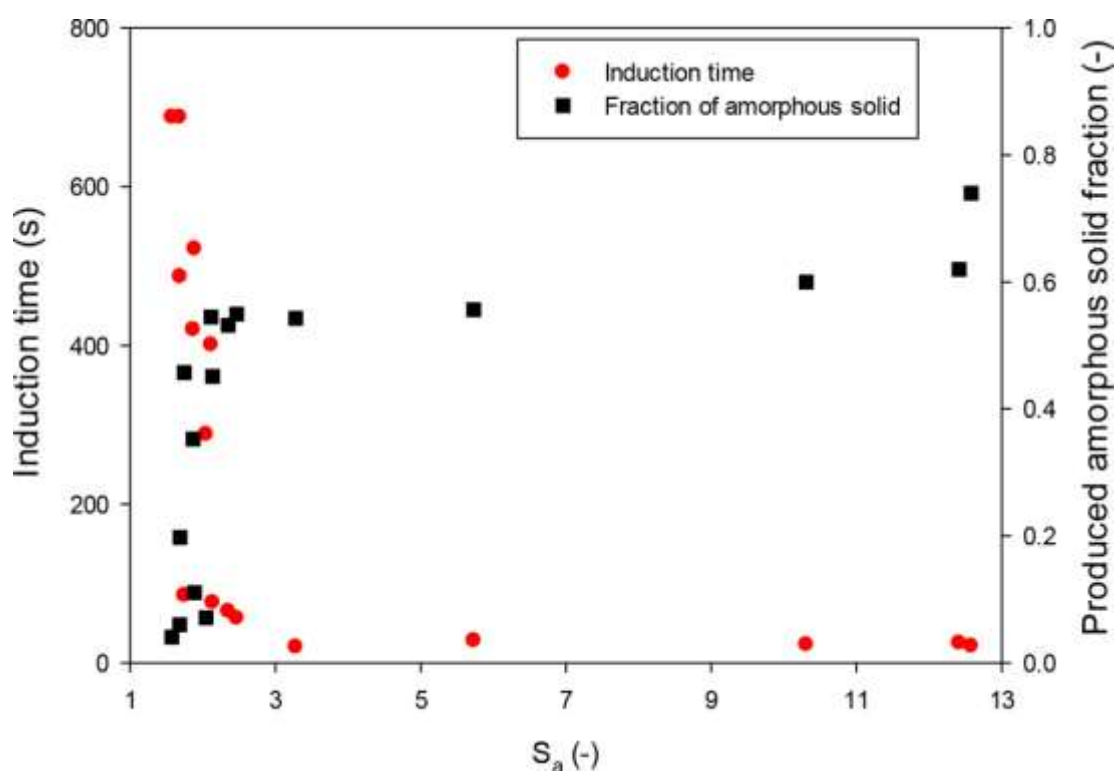


**Fig. 6-15: Effect of supersaturation for amorphous formation ( $S_a$ ) on induction time and produced amorphous solid fraction.**

As published [Kim22c], the induction period for the generation of a crystalline form from an amorphous slurry was longer when the concentration of the amorphous slurry was higher. Therefore, supersaturation, which is a control variable for amorphous formation, affects the induction period of the amorphous and amorphous fraction (Fig. 6-15). As the degree of supersaturation increased, the induction period decreased, and the amorphous fraction increased. As the concentration of the amorphous substance increased, the viscosity of

amorphous slurry increased, and molecular mobility decreased, resulting in a longer induction period for the formation of heptahydrate crystals. The condition for the formation of the metastable amorphous form affects the dissolution of the metastable form and the rate of formation of the stable form. The effect of the viscosity on the rate-limiting step was considered for all experimental results.

#### 6.4.2 Effect of Slurry Viscosity on Rate-Controlling Step

Tab. 6-2 shows the rate-controlling steps of the transformation process according to the operating conditions listed in Tab. 6-1. This is indicated by dividing the pattern into rate-limiting steps. The physical properties, especially, the diffusion coefficient of the metastable slurry where transformation occurs, influence the mass transfer rates of dissolution and growth, which determines the rate-controlling phase of transformation. Figs. 6-15a and b illustrates the influence of feed concentration and methanol fraction on the  $k_{da}/k_{gh}$  ratio, respectively. The  $k_{da}/k_{gh}$  ratio decreased as the feed concentration and methanol fraction increased. The dissolution rate-controlling step was dominant when the methanol fraction was  $> 0.71$  (methanol g/solvent mixture g) and the feed concentration was 0.2 (GMP g/water g). The growth rate-controlling step was dominant at a feed concentration  $< 0.3$  (GMP g/water g).

**Tab. 6-1: Experimental conditions of anti-solvent crystallization**

Run No.	Feed concentration	Methanol fraction	Addition time
	(GMP g/water g)	(g/g)	(min)
1	0.30	0.50	0.50
2	0.25	0.50	0.50
3	0.20	0.50	0.50
4	0.15	0.50	0.50
5	0.20	0.50	60.00
6	0.20	0.60	60.00
7	0.20	0.67	60.00
8	0.20	0.71	60.00
9	0.20	0.71	0.30
10	0.20	0.67	0.30
11	0.20	0.60	0.30
12	0.20	0.33	0.30
13	0.20	0.50	0.30

**Tab. 6-2: Experimental conditions, rate constants and rate-determining steps**

Run No.	Section I		Section II	
	$k_d \times 10^4$ [g/g s]	$k_g \times 10^4$ [g/g s]	$k_d \times 10^4$ [g/g s]	$k_g \times 10^4$ [g/g s]
1	0.425	0.524	3.783	5.970
2	3.448	3.729	9.864	7.971
3	3.189	3.487	8.833	5.269
4	5.052	5.923	21.413	10.661
5	5.147	0.178	14.815	4.500
6	0.579	0.970	2.218	1.087
7	0.672	0.549	1.004	0.842
8	5.682	0.550	7.067	4.052
9	1.765	2.378	4.398	4.517
10	0.689	1.556	4.117	3.170
11	1.719	2.949	11.380	7.911
12	1.125	0.693	4.144	3.464
13	3.115	0.675	7.905	5.938

Run No.	Overall stage		$k_d/k_g$ [-]	Controlled step			Pattern
	$k_d \times 10^4$ [g/g s]	$k_g \times 10^4$ [g/g s]		Section I	Section II	Overall	
1	2.664	4.155	0.641	D	D	D	A
2	6.108	5.488	1.113	D	G	G	B
3	5.021	4.065	1.235	D	G	G	C
4	8.656	6.967	1.242	D	G	G	B
5	10.219	2.446	4.178	G	G	G	C
6	1.163	1.012	1.150	D	G	G	C
7	0.822	0.682	1.206	G	G	G	B
8	6.889	3.600	1.913	G	D	G	C
9	3.641	3.902	0.933	D	D	D	C
10	2.338	2.332	1.002	D	G	G	B
11	4.395	4.323	1.017	D	G	G	B
12	3.318	2.705	1.226	G	G	G	C
13	4.785	2.510	1.906	G	G	G	C

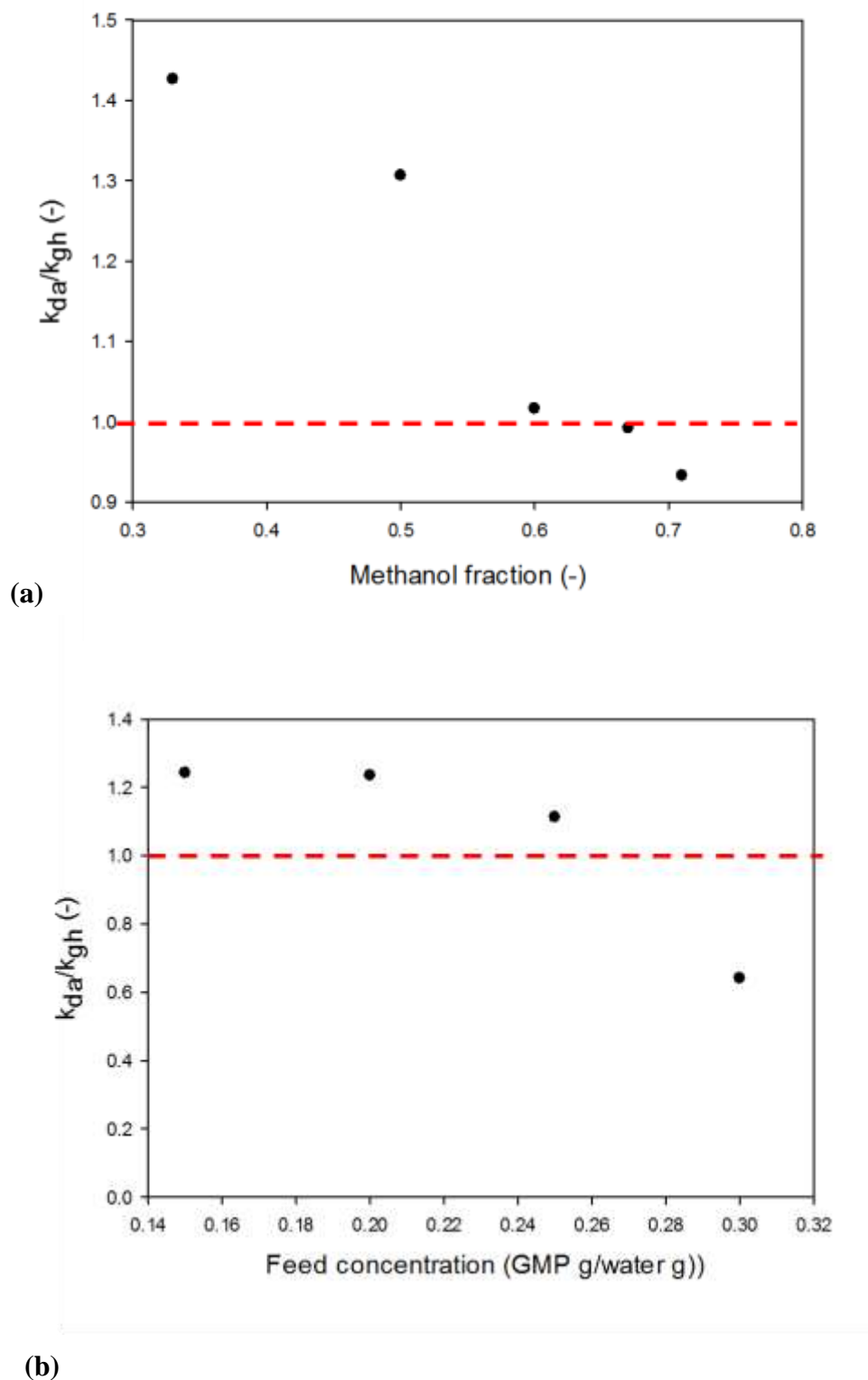


**Fig. 6-16: Plot of  $k_d/k_g$  ratio against operating conditions. (a) methanol fraction, (b) feed concentration.**

Fig. 6-15 shows the effect of supersaturation on the induction time of amorphous formation and the produced amorphous solid fraction for all experiments. Because the amorphous slurry's environment influences the rate-controlling step of the transformation process, the degree of supersaturation required for amorphous formation is important. Fig. 6-17 shows the  $k_{da}/k_{gh}$  ratio versus the viscosity of the amorphous slurry. As the viscosity increased, the  $k_{da}/k_{gh}$  ratio decreased. Even though this study was conducted at high supersaturation, the growth rate-controlling phase was observed when the slurry viscosity was below 70 cp. The dissolution rate-controlling step was consistent with Pattern A at 70 cp or higher.

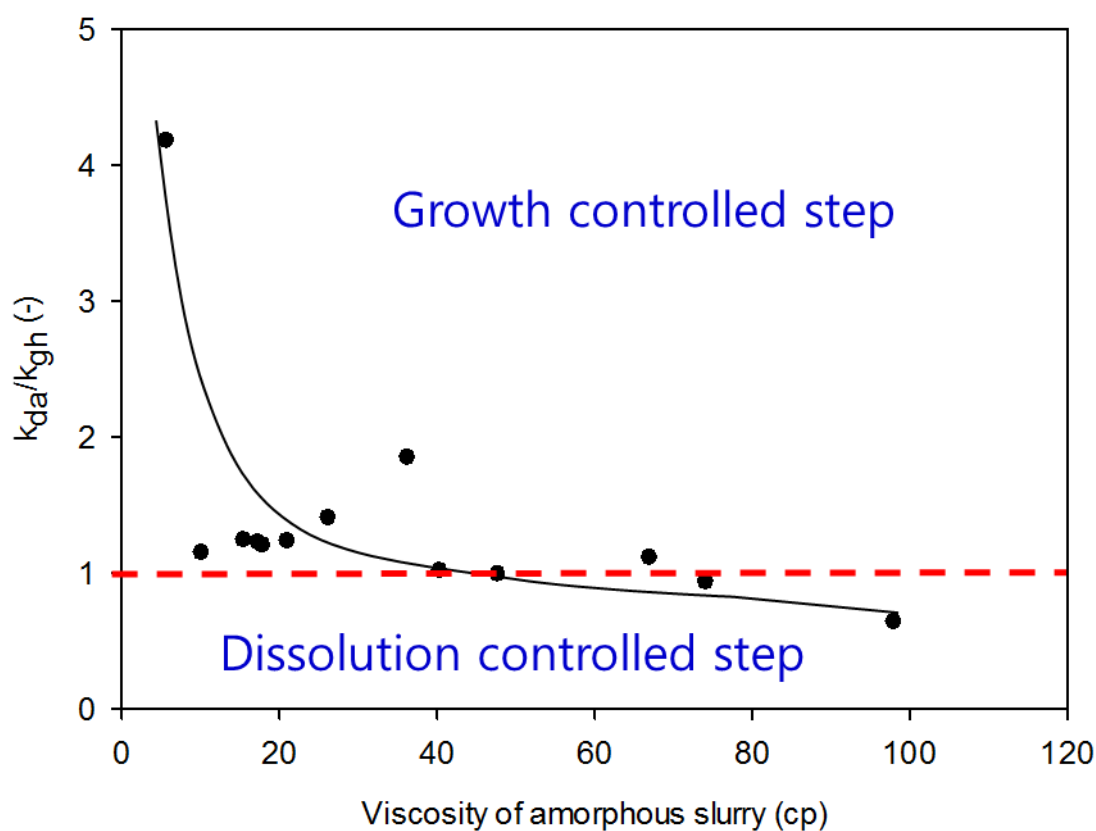


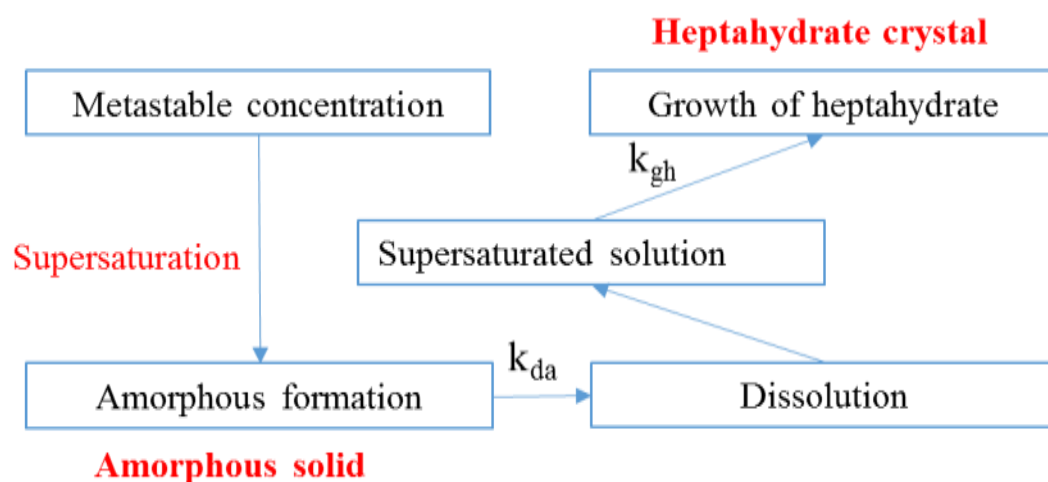
**Fig. 6-17: Effect of viscosity of amorphous on rate-determining step in all experiments.**

Although the experimental data are scattering, the dissolution control step is dominated in the area of high viscosity, while the growth control step is occupied when the viscosity is low. In the dissolution control stage, supersaturation is rapidly reduced, leading to the growth of the heptahydrate. On the other hand, the growth control step leads to the growth of heptahydrate because the dissolution rate is fast. The viscosity increases due to slurry intensity as the amorphous formation proceeds and, as a result, the molecular mobility decreases, and the apparent activation energy increases with time.

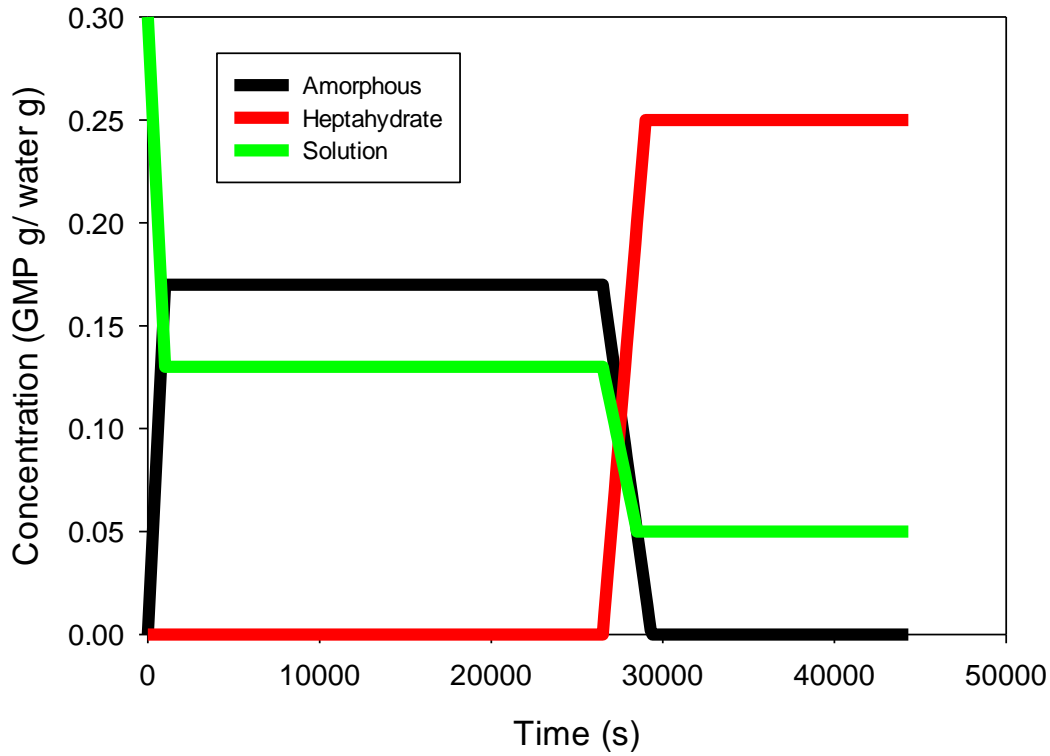
### 6.4.3 Model Presentation

The solute concentration–time plot provided some clear insights into the transformation’s rate-controlling mechanism. As a result, as shown in Fig. 5-12, the solute concentration directly monitored in all experiments was proven by applying a material balance to the concentrations of the amorphous and heptahydrate solids.

The schematic diagram of the transformation of solid forms by crystallization is shown in Fig. 6-18a. Because of supersaturation, the solution first approaches the metastable concentration limit, resulting in the amorphous form. The generated amorphous slurry was then dissolved at a rate equal to  $k_{da}$ , while the heptahydrate solid increases at a rate equal to  $k_{gh}$ . The relative values of  $k_{da}$  and  $k_{gh}$  were therefore used to determine the rate of transformation.



(a)



(b)

**Fig. 6-18: Model presentation of the transformation process of solid forms by crystallization: (a) Schematic diagram consisting of metastable formation and transformation, (b) Plot of concentration-time profile by modeling.**

Dissolution and growth are the two processes that describe the kinetics of a substance in solution or as a solid. According to eq. 6-8, these two elementary steps can explain the concentration–time profile of the solute and the quantity of solid.

$$\frac{dC}{dt} = G - D \quad (6-8)$$

Where,

$$D = \frac{dC_a}{dt} = k_{da}C_{ao} \quad (6-9)$$

and

$$G = \frac{dC_h}{dt} = k_{gh}C_{hf} \quad (6-10)$$

Concentrations of amorphous solids and heptahydrate solid are expressed by eqs. 6-11 and 6-12, respectively:

$$C_a = C_{ao} - k_{da}C_{ao}(t - t_o) \quad (6-11)$$

$$C_h = k_{gh}C_{hf}(t - t_o) \quad (6-12)$$

Material balance is as follows:

$$C = C_o - C_a - C_h \quad (6-13)$$

where  $C$ ,  $C_a$ , and  $C_h$  are the solute concentration, amorphous solid concentration, and heptahydrate solid concentration, respectively.  $C_{ao}$  and  $C_{hf}$  denote the concentrations of the initial amorphous solid and final heptahydrate solid, respectively,  $k_{ca}$  and  $k_{gh}$  represent the dissolution and growth rate constants, respectively, and  $t_o$  is the transformation starting time.

The current method for measuring the solute concentration is reliable because the solute concentration measurements provided a clear picture of the rate-controlling mechanism. Fig. 6-18b shows that the model's present range is within the plateau region, where the rate of dissolution is exactly balanced by the growth rate. Considering a ratio of the dissolution and growth rate constants reveals that the transformation is primarily controlled by the dissolution process, as the rate constants computed for the growth of the heptahydrate solids are significantly higher at a condition of Run 1. The pattern modeled from the rate constants for amorphous dissolution and heptahydrate growth obtained in Run 1 (corresponding to Pattern A) in Fig. 5-12a is shown in Fig. 6-18b. From the comparison of the two figures, the modeled pattern is very similar to that obtained in the experiment. This is consistent with observations made by others who investigated the phase transformation in many cases [Tur18, Jak16, Dha08].

Phase transformations in solution have been of great interest in different areas. The model proposed here offers the simple model allowing a straightforward interpretation of the process. The proposed parameters have a clear physical meaning and are comprehensible and easy to interpret. Its simplicity is applicable cases where two solid forms coexist. The combination of process analytical techniques and modeling would promote faster and deeper understanding of phase transformation processes. The methods presented in this work could also be applied to other systems.

## 6.5 Summary of Results

The following results were revealed in terms of thermodynamics, optimal operating conditions, nucleation, transformation, dissolution and growth kinetics for the selective preparation of amorphous and crystalline hydrate solid forms of GMP (the case study), which can be used for most similar cases. The bold fonts indicate the absolutely new and innovative facts which were found in this work. In brackets are given the corresponding aims of this thesis.

Thermodynamics and supersaturation:

- **The solubilities, supersaturated concentrations and metastable zone width for the amorphous, tetrahydrate, and heptahydrate forms of GMP were determined by in-situ measurement using Raman spectroscopy and FBRM. (see Chapter 3.2, No 1)**
- **The effects of the temperature and the solvent fraction on solubility for amorphous and crystalline forms in mixed solvent were investigated. (see Chapter 3.2, No 2)**
- **Calibrations between the concentrations and the Raman intensity were used to measure the solubility of GMP in binary solvent mixtures. (see Chapter 3.2, No 3)**
- **The concentrations of the solid forms of GMP were correlated with calibration by Raman spectroscopy. (see Chapter 3.2, No 3)**
- **The thermodynamic properties (dissolution enthalpy and entropy) and formation conditions for the amorphous, heptahydrate and tetrahydrate forms were revealed.**

(see Chapter 3.2, No 1)

- **Combined with the PXRD, Raman, SEM, and TGA-DSC results, it was concluded that amorphous GMP, tetrahydrate GMP, and heptahydrate GMP can all be well characterized. (see Chapter 3.2, No 3)**
- **The solubility and supersaturation limit for the tetrahydrate form crystallization were clarified. (see Chapter 3.2, No 1)**
- **The dependence of the relative stabilities of the amorphous, tetrahydrate, and heptahydrate solids on the solvent composition and temperature as well as thermodynamic properties such as the enthalpy and entropy of dissolution of GMP were estimated by plotting the solubility data and temperature using the van't Hoff equation. (see Chapter 3.2, No 1)**
- **The maximum supersaturation was highest for the amorphous material at 20-40°C, followed by heptahydrate and tetrahydrate crystals. These results clearly provide the solubility and maximum supersaturation to selectively produce the amorphous, heptahydrate and tetrahydrate forms. An amorphous solid form was produced at higher supersaturations compared to the hydrate. Heptahydrate crystallization was possible at 20–40 °C and methanol fractions of 0.15–0.6 (methanol g/solvent mixture g). Tetrahydrate was obtained in the entire range of solvent fractions at 45–60 °C and crystallized in the range of 20–40 °C even when the methanol fraction was greater than 0.8 (methanol g/solvent mixture g). The amorphous form was formed at a methanol fraction of less than 0.15 (methanol g/solvent mixture g) and no transformation occurred. (see Chapter 3.2, No 12)**

Finally, the maximum supersaturated concentrations and solubilities of amorphous and crystalline hydrated GMPs for different temperatures and solvent fractions were successfully determined by in-situ Raman spectroscopy and FBRM. From the thermodynamic study, the solid phase change, dissolution enthalpy, dissolution entropy, and solubility were provided, and information on the selectivity of the solid phase was obtained. It was shown that the use of these in-line tools can provide solubility and maximum supersaturation values to selectively produce amorphous, heptahydrate, and tetrahydrate solids. As a result, it is possible to provide the fundamental data for crystallization of the hydrates, enabling to screen the desired crystalline hydrate by measuring the solubility and supersaturation of the crystalline and amorphous forms using in-situ Raman and FBRM analysis.

Selective formation:

- **The formation of GMP solid forms was successfully monitored in-line by Raman spectroscopy and FBRM in an anti-solvent crystallization process. (see Chapter 3.2, No 3)**
- **The calibration and models built in this study can be used in other studies to measure the concentration of a solution and solid forms during crystallization and transformation. (see Chapter 3.2, No 2)**
- **Faster addition of the anti-solvent leads to a wider metastable zone as expected to favor the formation of the amorphous due to higher supersaturation. (see Chapter 3.2, No 7)**

- **Phase transformation, maximum supersaturation, and selective preparation of GMP solid forms were grasped. (see Chapter 3.2, No 7)**
- **By adjusting the concentration, temperature, and solvent/anti-solvent ratio, the preparation of the different solid forms with and without transformation was established. Therefore, a screening of amorphous, heptahydrate, and tetrahydrate of GMP was successfully established by knowing the metastable supersaturation of each of the forms. (see Chapter 3.2, No 6)**
- **The results demonstrate that amorphous–crystalline hydrate transformation consists of four stages, which are the nucleation of the amorphous form, pretransformation of the amorphous form, the nucleation of hydrate and dissolution of the amorphous form and the growth of hydrate crystal. (see Chapter 3.2, No 5)**
- **The rate-controlling step in amorphous-heptahydrate transformation is the dissolution of the amorphous form. The transformation between heptahydrate and tetrahydrate forms is a nucleation-growth-controlled step. (see Chapter 3.2, No 5)**
- **It was possible to control selectively the solid forms of GMP by referring to the supersaturation and the solubility data. This phenomenon requires a driving force for nucleation of tetrahydrate, because the difference in solubility between the two hydrates is very small. One possibility of explaining this is surface nucleation. The presence of a surface may be necessary to reduce the energy barrier for nucleation and to promote nucleation of the tetrahydrate. At this point, a higher concentration appears on the surface of the heptahydrate crystals that are dissolved compared to the solute concentration. As a result, nucleation of tetrahydrate on the surface of the heptahydrate can be activated. (see Chapter 3.2, No 9)**

This study provides a method for selective manufacturing of solid form by studying the formation and transformation of amorphous, heptahydrate, and tetrahydrate of GMP by combining FBRM and Raman information analyzed on-line over time. The supersaturation limit of anti-solvent crystallization was established according to the methanol/water ratio, initial concentration, anti-solvent feed rate and temperature. The controlling steps in the transformation of amorphous-to-hydrate solids and hydrate-to-hydrate crystals were studied. It was found that the solid form of disodium guanosine 5'-monophosphate can be selectively obtained by optimizing various conditions of anti-solvent crystallization by referring to the supersaturation and solubility data.

Nucleation kinetic:

- **The liquid-mediated phase transformation of the amorphous form to the crystalline heptahydrate form of guanosine 5'-monophosphate was studied in an anti-solvent crystallization using a methanol–water mixture as the solvent. (see Chapter 3.2, No 4)**
- **Three steps were monitored: amorphous material formation, amorphous material dissolution, and heptahydrate crystal growth using in-situ Raman spectroscopy, FBRM, and PVM, as well as off-line techniques such as viscosity, TGA, and PXRD. (see Chapter 3.2, No 8)**
- **Effects of the anti-solvent fraction, initial concentration, and addition rate on the transformation process were discussed. (see Chapter 3.2, No 6)**

- **In liquid-mediated transformation process, the parameters such as the solid form fraction, solute concentration, particle size, count numbers, induction time, metastable zone width, viscosity, dissolution rate, and crystal growth rate were measured. (see Chapter 3.2, No 4)**
- **At low initial concentrations, heptahydrate crystals were observed without transformation of the amorphous material. The induction time of the crystalline hydrate increases with the addition rate, anti-solvent fraction, and initial concentration. (see Chapter 3.2, No 7)**
- **Even at low anti-solvent fractions, heptahydrate nucleation occurs preferentially at very low addition rates. (see Chapter 3.2, No 8)**
- **The metastable zone limits of the amorphous and heptahydrate crystalline forms were established in a plot of the solute concentration versus methanol mass fraction in the mixed solvent. (see Chapter 3.2, No 12)**
- **Amorphous forms are generated exclusively at solute concentrations above 0.13 and 0.06 (GMP g/water g) at methanol mass fractions of 0.33 and 0.72 (methanol g/solvent mixture g), respectively, whereas heptahydrates can be produced below those values. (see Chapter 3.2, No 12)**
- **As a result, under all of the conditions of this investigation, amorphous and heptahydrate crystalline forms may be selectively generated. (see Chapter 3.2, No 7)**
- **The linear plot of  $1/t_{\text{ind}}$  against  $\eta^{-1}C^{7/3} \exp(-(\ln S)^{-2})$  for heptahydrate nucleation was established. Both the pre-exponential factor and the exponential term were applied successfully to comprehend the nucleation in the amorphous to crystalline transformation. (see Chapter 3.2, No 8)**
- **In the studied concentration and anti-solvent fractions, the heptahydrate form would be obtained at  $1.3 < S_H < 1.7$ , while the amorphous form would be produced at a higher supersaturation level ( $S_A > 1.7$ ). Especially, at  $S_H < 1.3$ , heptahydrate was crystallized without transformation. The results obtained in this work give some guidelines for the preparation of different pure forms by adjusting the operating conditions, which affect the supersaturation and viscosity. (see Chapter 3.2, No 9)**

It may be concluded that the pre-exponential factor of the classical nucleation rate equation contains the primary factors influencing the transformation of an amorphous slurry to crystalline heptahydrate. High supersaturation promotes the formation of the amorphous form, which can then be converted to the crystalline form. The pre-exponential factor of the nucleation rate equation holds great importance toward understanding the transformation of amorphous to crystalline material. This study gives a good understanding of the kinetics of nucleation of crystalline heptahydrate in the transformation from the amorphous slurry material.

Liquid-mediated phase transformation:

- **This kinetic study of the formation of an amorphous solid and the transformation of GMP from amorphous to heptahydrate revealed that various operating conditions influence the determination of the rate-controlling limits of the transformation. (see Chapter 3.2, No 5)**

- 
- An investigation of the effects of supersaturation, solvent composition, feed concentration, addition rate, and viscosity reveals that dissolution and growth clarify the rate-determining step in the overall kinetic constants. (see Chapter 3.2, No 11)
  - The transformation process consists of two sections, in which the rate of change of dissolution, growth, and supersaturation is divided into the initial and later sections of the transformation. (see Chapter 3.2, No 11)
  - The overall rate constants were calculated by combining the dissolution rate coefficient and the growth rate coefficient of each section. (see Chapter 3.2, No 11)
  - The dissolution and growth processes in the phase transformation of GMP from its amorphous to its heptahydrate form have been monitored using in situ Raman spectroscopy over various operating conditions and scattering experiments to quantitatively analyze kinetic parameters determining the phase transformation. (see Chapter 3.2, No 10)
  - Measuring concentration of solutions and solids allowed the determination of the rate-limiting processes during the transformation. (see Chapter 3.2, No 11)
  - The zero-order, first-order, and surface reaction equations as kinetic equations for the dissolution of the amorphous solids and the growth of the heptahydrate solids are highlighted and compared. (see Chapter 3.2, No 10)
  - The dissolution and growth steps of the transformation process, in terms of the solid concentration and solution concentration, were found. (see Chapter 3.2, No 11)
  - The dissolution of the metastable amorphous phase and the growth of the stable heptahydrate phase were found to fit a zero-order kinetics model. (see Chapter 3.2, No 10)
  - The calculated zero-order rate constants were found to be within the range of  $8.22 \times 10^{-5}$  to  $8.65 \times 10^{-4} \text{ s}^{-1}$  for dissolution of the amorphous phase and  $6.82 \times 10^{-5}$  to  $6.96 \times 10^{-4} \text{ wt \% s}^{-1}$  for growth of the heptahydrate phase. (see Chapter 3.2, No 10)
  - Amorphous formation, amorphous-hydrate transformation, and hydrate formation can be identified by plotting the metastable regions of amorphous and hydrate as the plot of concentrations against anti-solvent fractions. Polymorphs and solvates can be selectively obtained by obtaining information on the solubility and metastable zone of each polymorph and solvates (according to cooling rate or anti-solvent addition rate, initial concentration, temperature, and solvent/anti-solvent ratio). (see Chapter 3.2, No 12)
  - In the control of the anti-solvent crystallization process for the selective preparation of solid forms from compounds with amorphous and crystalline forms, addition rate, solute concentration, temperature, anti-solvent fraction and feed concentration affecting supersaturation played an important role in the transformation process. Using the developed method and the kinetic constants obtained in this work, it is possible to create an appropriate control strategy for producing the desired solid form in the final product. Finally, these results have important implications for process operations in the specialty chemical industry, where selecting the appropriate solid form of a substance can be a significant advantage. (see Chapter 3.2, No 12)

The transformation kinetics are clearly sensitive to both the solvent mixture composition and the feed concentration. From FBRM data, changes in particle size distribution, particle size, and counts were characterized during the phase transformation. In particular, the change in particle size distribution over time can determine the rate-controlling steps. A valid model has been developed and has been found to be reasonable by applying it to experimental data. As a result, experimental data obtained using Raman spectroscopy and FBRM were combined with dissolution and growth models to successfully identify and interpret phase transformations. The phase transformation is determined by the dissolution of the amorphous form and the nucleation and growth of the heptahydrate form. Three patterns according to the combination of dissolution, growth, and supersaturation were investigated. The dissolution rate-limiting step was dominated by a pattern in which both supersaturation and amorphous dissolution decreased simultaneously, and the growth rate-controlling step was shown in a pattern in which either supersaturation or amorphous dissolution was constant. It depends on the concentration, viscosity, solution concentration, and content of the amorphous slurry. Furthermore, the growth of heptahydrate crystals at a viscosity below 0.07 Pa s and the dissolution of the amorphous is the key determinant above it.

The effects of thermodynamic and kinetic properties on the selective crystallization of various categories of solid forms were investigated. Important information has been generated about the crystallization behavior with nucleation, growth, dissolution and transformation of hydrate compounds with amorphous and crystalline forms. This information helps to understand the principle of selective production of solid forms. This information could also guide the screening of new polymorphs, the control and development of solid forms. This will provide efficient process analysis technology in the production of solids in the solid chemical industry and contribute to the advancement of the quality of solid products.

## 7. Summary

Crystallization technology for intentionally preparing solid forms for compounds with amorphous and crystalline forms is a challenging task in the fine chemical and pharmaceutical industry sectors. In particular, in order to understand the screening of solid forms, the complex behavior of nucleation, growth, dissolution and transformation of a metastable to a stable form, and nucleation and growth of stable form must be studied. The selective preparation and purity of these solid forms is very important for the quality of the final solid product.

As a case study disodium guanosine 5'-monophosphate (GMP) was selected, because it was known that three solid forms such as amorphous solid and the crystalline tetrahydrate and heptahydrate crystals can be formed during a solid forming operation. The solubilities and maximum supersaturations for solid forms of GMP in water-methanol mixtures were measured in situ by Raman spectroscopy and focused beam reflectance measurement. The distinct Raman peaks of the amorphous form, crystalline hydrates, solution, and solvent were used for measurements of solubility and maximum supersaturation. Above 45 °C and at methanol fractions of 0.15–0.90 (methanol g/solvent mixture g), the tetrahydrate was the stable form, while below 40 °C and at methanol fractions of 0.15–0.60 (methanol g/solvent mixture g), the heptahydrate was the stable form. Especially, the tetrahydrate was stable in the methanol fraction > 0.7 (methanol g/solvent mixture g) at the temperature investigated. The solubility and supersaturated concentration values obtained here according to various conditions can be used as fundamental data to selectively produce amorphous, tetrahydrate and heptahydrate crystalline solids of GMP by an anti-solvent crystallization.

A screening of amorphous, heptahydrate, and tetrahydrate forms of GMP is investigated using an anti-solvent crystallization process with the aim to selectively produce each solid form. The concentrations of the solution and solid forms are monitored by in-situ Raman spectroscopy using a calibration tool. Concentrations of amorphous and hydrates phases are determined using in-line measurement techniques. The variables studied in anti-solvent crystallization are temperature, initial concentration, addition rate, and solvent fraction. The results demonstrate that transformation from amorphous to hydrate forms consists of four stages, which are the precipitation of the amorphous form, predissolution of amorphous form, the nucleation of hydrate crystal and dissolution of amorphous solid, and the growth of hydrate crystal. The rate-controlling step, in this case, is the dissolution of amorphous form. Transformation between heptahydrate to tetrahydrate crystals is a nucleation-growth-controlled step. It is possible to obtain selectively the solid forms of GMP by referring to the supersaturation and solubility data. This is an important result that can be applied as a technique for screening various solvates or polymorphs of compounds.

The liquid-mediated phase transformation of an amorphous form to a heptahydrate crystalline form of GMP was studied in an anti-solvent crystallization using methanol–water mixtures as solvents. Three steps were monitored: the formation of the amorphous form, dissolution of the amorphous form, and growth of the heptahydrate crystals using in-situ Raman spectroscopy, focused beam reflectance measurement (FBRM), and particle vision measurement (PVM) and off-line methods like viscosity, thermal gravimetric analysis (TGA), and powder X-ray diffraction (PXRD). Effects of the anti-solvent fraction, initial concentration, and addition rate of the anti-solvent on the transformation process were discussed. Solid forms, solute

---

concentration, particle size, counts, induction time, metastable zone width, solution viscosity, and amorphous slurry viscosity were all measured for 18 experimental runs. The influence of nucleation, transformation, and growth of solid forms on these parameters is an important information for industrial crystallization in relation to the operating conditions of the production process. The induction time of the crystalline hydrate increases with the supersaturation, but decreases with the increasing viscosity of the amorphous slurry. Both are not as expected. The induction time correlates nicely in the opposite direction with the viscosity of the amorphous slurry concentration. The amorphous slurry viscosity is about 20 times higher than the solution viscosity. Viscosity of the amorphous slurry was discovered to be a crucial factor influencing the transition of the amorphous slurry to the crystalline form in the pre-exponential component of the classical nucleation rate equation. The metastable zone boundaries of the amorphous and heptahydrate crystalline forms were shown in a plot of the solute concentration versus the mass fraction of methanol in the mixed solvent. The amorphous and heptahydrate crystalline forms can be selectively produced under all the conditions of this study. It was found that the pre-exponential factor of the nucleation rate equation factor is very crucial in comprehending the transformation from an amorphous to a crystalline state.

The kinetics of the formation of amorphous GMP and its transformation to the heptahydrate phase were studied under various operating conditions. Supersaturation, solvent composition, feed concentration, addition rate, and viscosity were shown to affect the rate-determining steps of the transformation. The rate-controlling mechanisms in the overall kinetics have been confirmed. The observation of the slurry viscosity of the suspension of the amorphous phase shows the option to observe the phase transformation. The transformation process was affected by the dissolution, growth, and supersaturation in which the rate-controlling step was divided into two sections, such as the initial and later sections of the transformation. The overall rate constants were determined by combining the constants of the dissolution rate and the growth rates of each section. In-situ Raman spectroscopy examination of the concentration of solution and solids can determine the rate-limiting processes during the transformation. The zero-order, first-order, and surface reaction equations as kinetic equations are highlighted and compared for the dissolution of the amorphous solids and the growth of the heptahydrate crystals. The dissolution of the amorphous (metastable form) and the growth of the heptahydrate (stable form) were found to be best fitted to the zero-order kinetic model. In particular, the variation of particle size distribution over time can give the rate-determining steps. These results suggest that the data measured by Raman spectroscopy and FBRM can be successfully coupled into a dissolution and growth model to further grasp and interpret the phase transformation. A dissolution rate-controlling step was dominated by a pattern in which both supersaturation and amorphous dissolution decreased simultaneously, and the growth rate-controlling step was shown in a pattern in which either supersaturation or amorphous dissolution was constant. Furthermore, the growth of heptahydrate crystals at a viscosity of the suspension with the amorphous solids below 0.07 Pa s and the dissolution of the amorphous solids above it can be used as the key determinant. Using the method developed and the kinetic constants obtained in this work, it is possible to create an appropriate control strategy to produce the desired form (amorphous or hydrate) in the final product.

## 8. Abbreviations, Symbols and Units

### Abbreviations

A	amorphous
CLD	chord length distribution
FBRM	focused beam reflectance measurement
GMP	disodium guanosine 5'-monophosphate
H	heptahydrate
MS	metastable phase
PVM	particle vision microscope
PXRD	powder X-ray diffraction
S	stable phase
SEM	scanning electron microscopy
T	tetrahydrate
TGA	thermogravimetric analyzer
US	unstable phase

### Symbols

A	pre-exponential constant in eq. 2-14	$\#/m^3s$
$A_a$	amount of the anti-solvent	kg/kg
$A_a^*$	amount of the anti-solvent in equilibrium	kg/kg
$\Delta A_a$	$A_a - A_a^*$ , the excess amount of the anti-solvent	kg/kg
B	exponential term factor in eq. 6-2	-
C, c	concentration	kg/kg solvent
$C_c$	molar density of the solid	$kmol/m^3$
$d_m$	molecular diameter	m
D	diffusion coefficient	$m^2/s$
$D_i$	dissolution rate	kg/kg s
$E_a$	activation energy	J/mol
$\Delta G, G$	Gibbs free energy	J/mol
$G_i$	growth rate	kg/kg s
$\Delta H$	enthalpy	J/mol
J	nucleation rate	$\#/m^3s$
$k_G$	rate constants of the growth	1/s
$k_D$	rate constants of the dissolution	1/s
$k_1$	constant in eq. 6-7	-
$N_A$	Avogadro's number	1/mol
n	constant in eq. 6-7	-
R	gas constant	J/mol K
r	addition rate	Kg/s
$\Delta S_d$	entropy of dissolution	J/mol K
S	supersaturation ratio, $C/C^*$	-
T	temperature	K or $^{\circ}C$
$t_{ind}$	induction time	s
t	time	s
X, x	mole fraction, mass fraction	-

$X_a$	fractional conversion of amorphous phase	-
$X_h$	fractional conversion of heptahydrate phase	-

### Greek letters

$\eta$	viscosity	Pa s
$\Delta$	difference	-
$\mu$	chemical potential	J/mol
$\gamma$	interfacial energy	J/m <sup>2</sup>
$\kappa$	Boltzmann constant	J/K
$v_m$	molar volume	m <sup>3</sup> /mol

### Subscripts

a	amorphous
h	heptahydrate
i	component i
m	melting point
met	metastable zone limit
ms, MS	metastable phase
o	initial state
f	final state
s, S, ST	stable polymorph
t	tetrahydrate

### Superscripts

*	equilibrium state
---	-------------------

## 9. References

- [Aal09] Aaltonena, J., Allesøb, M., Mirzac, S., Koradiab, V., Gordond, K. C. Rantanen, J. Solid form Screening – A Review, *European Journal of Pharmaceutics and Biopharmaceutics* 2009, 71, 1, 23-37.
- [Alj02] Al-Jibbouri, S., Ulrich, J. The Growth and Dissolution of Sodium Chloride in a Fluidized Bed Crystallizer, *Journal of Crystal Growth* 2002, 234, 1, 237-246.
- [Ama88] Amathieu, L., Boistelle, R. Crystallization Kinetics of Gypsum from Dense Suspension of Hemihydrate in Water, *J. Cryst. Growth* 1988, 88, 183-192.
- [An16] An, J-H., Jin, F., Kim, H. S., Ryu, H. C., Kim, J. S., Kim, H. M., Kim, K. H., Kiyong, A. N., Jung, K. Investigation of the Polymorphic Transformation of the Active Pharmaceutical Ingredient Clopidogrel Bisulfate Using the Ionic Liquid AEImBF<sub>4</sub>, *Cryst. Growth Des.* 2016, 16, 4, 1829–1836.
- [Bab11] Babu, N. J., Nangia, A. Solubility Advantage of Amorphous Drugs and Pharmaceutical Cocrystals, *Cryst. Growth Des.* 2011, 11, 2662–2679.
- [Bar08] Barthe, S. C., Grover, M. A., Rousseau, R. W. Observation of Polymorphic Change through Analysis of FBRM Data: Transformation of Paracetamol from Form II to Form I, *Cryst. Growth Des.* 2008, 8, 3316-3322.
- [Bar82] Barnes C. L., Hawkinson, S. W. Structure of Disodium Guanosine 5'-Phosphate Heptahydrate, *Acta Cryst.* 1982, B38, 812-817.
- [Bec01] Bechtloff B, Nordhoff S, Ulrich J. Pseudopolymorphs in Industrial Use, *Cryst. Res. Technol.*, 2001, 36, 1315-1328.
- [Bec96] Beckmann, W., Otto, W. H. Occurrence, Stability, Kinetics of Crystallization and Polymorphic Transition of the A, B and C Modification of Abecarnil - Influence of Supersaturation, Temperature, Solvents and Impurities, *Chem. Eng. Res. Des.* 1996, 74, 750-757.
- [Ber99] Bernstein, J., Davey, R. J., Henck, J.-O. Concomitant Polymorphs, *Angewandte Chemie* 1999, 38(23), 3440-3461.
- [Bla05] Blanco, M., Valdés, D., Llorente, I., Bayod, M. Application of NIR Spectroscopy in Polymorphic Analysis: Study of Pseudo-Polymorphs Stability, *Journal of Pharmaceutical Sciences* 2005, 94, 1336-1342.
- [Boi92] Boistelle, R., Astier, J. P., Marchis-Mouren, G., Desseaux, V., Haser, R. Solubility, Phase Transition, Kinetic Ripening and Growth Rates of Porcine Pancreatic  $\alpha$ -Amylase Isoenzymes, *J. Cryst. Growth* 1992, 123, 109-120.
- [Buc14] Bučar, D.-K., Rodger F. Henry, Zhang, G. Z., MacGillivray, L. R. Synthon Hierarchies in Crystal Forms Composed of Theophylline and Hydroxybenzoic Acids: Cocrystal Screening via Solution-Mediated Phase Transformation, *Cryst. Growth Des.* 2014, 14, 10, 5318–5328.
- [Buc98] Buchauer, K. A Comparison of Two Simple Titration Procedures to Determine Volatile Fatty Acids in Influent to Wastewater and Sludge Treatment Processes, *Water Saffetoria* 1998, 24, 49– 56.
- [Bur79] Burger, A., Ramberger, R. On the Polymorphism of Pharmaceuticals and Other Molecular Crystals., *Mikrochim. Acta* 1979, 2, 273-316.
- [Cai08] Caillet, A., Puel, F., Fevotte, G. Quantitative in Situ Monitoring of Citric Acid Phase Transition in Water Using Raman Spectroscopy, *Chem. Eng. Process.: Process Intensification* 2008, 47, 377-382.
- [Car85] Cardew, P. T., Davey, R. J. The Kinetics of Solvent-Mediated Phase Transformations, *Proc. R. Soc. A-Math. Phys.* 1985, 398, 415– 428.

- [Cha18] Chattopadhyay, B., Jacobs, L., Panini, P., Salzmann, I., Resel, R., Geerts, Y. Accessing Phase-Pure and Stable Acetaminophen Polymorphs by Thermal Gradient Crystallization, *Cryst. Growth Des.* 2018, 18 (3), 1272–1277.
- [Che18] Chen, Q., Zou, F., Yang P., Zhou J., Wu, J., Zhuang W., Ying H. Transformation of Microstructure and Phase of Disodium Guanosine 5'-Monophosphate: Thermodynamic Perspectives, *Chinese Journal of Chemical Engineering* 2018, 26, 2112-2120.
- [Cro10] Croker, D., Hodnett, B.K. Mechanistic Features of Polymorphic Transformations: the Role of Surfaces, *Crystal Growth & Design* 2010, 10, 6, 2806–2816.
- [Cui07] Cui, Y. A Material Science Perspective of Pharmaceutical Solids, *International Journal of Pharmaceutics* 2007, 339, 3–18.
- [Dan09] Dang, L., Yang, H., Black, S., Wei, H. The Effect of Temperature and Solvent Composition on Transformation of  $\beta$ - to  $\alpha$ -Glycine as Monitored in Situ by FBRM and PVM, *Org. Process Res. Dev.* 2009, 13(6), 1301–1306.
- [Dan16] Dang, L. T. N., Kim, K.-J. Solvent-Mediated Polymorphic Transformation of  $\alpha$ -Taltirelin by Seeded Crystallization, *Chem Eng Technol* 2016, 39, 7, 1281-1288.
- [Das10] Dashi, S., Murthy, P. N., Nath, L., Chowdhury, P. Kinetic Modeling on Drug Release from Controlled Drug Delivery Systems, *Acta Poloniae Pharmaceutica Drug Research* 2010, 67(3), 217-223.
- [Dav02] Davey, R. J., Blagden, N., Righini, S., Alison, H., Ferrari, E. S. Nucleation Control in Solution Mediated Polymorphic Phase Transformations: The Case of 2,6-Dihydroxybenzoic Acid, *J. Phys. Chem. B* 2002, 106, 1954-1959.
- [Dav86] Davey, R. J., Cardew, P. T., McEwan, D., Sadler, D. E. Rate Controlling Processes in Solvent-Mediated Phase Transformations, *Journal of Crystal Growth* 1986, 79(2), 648-653.
- [Dha08] Dharmayat, S., Hammond, R., Lai, B. X., Ma, C., Purba, E., Roberts, K. J., Chen, Z.-P., Martin, E., Morris, J., Bytheway, R. An Examination of the Kinetics of the Solution-Mediated Polymorphic Phase Transformation Between  $\alpha$ - and  $\beta$ -Forms of L-Glutamic Acid as Determined Using Online Powder X-Ray Diffraction, *Cryst. Growth Des.* 2008, 8(7), 2205–2216.
- [Fan15] Fang, Z., Zhang, L., Maob, S., Rohani, S., Ulrich J., Lu, J. Solubility Measurement and Prediction of Clopidogrel Hydrogen Sulfate Polymorphs in Isopropanol and Ethyl Acetate, *J. Chem. Thermodynamics* 2015, 90, 71–78.
- [Fer03] Ferrari, E. S., Davey, R. J., Cross, W. I., Gillon, A. L., Towler, C. S. Crystallization in Polymorphic Systems: The Solution-Mediated Transformation of  $\beta$  to  $\alpha$  Glycine, *Cryst. Growth Des.* 2003, 3, 53-60.
- [Fev04] Févotte, G., Calas, J., Puel, F., Hoff, C. Applications of NIR Spectroscopy to Monitoring and Analyzing the Solid State During Industrial Crystallization Processes, *Int. J. Pharm.* 2004, 273, 159-169.
- [Flo13] Flood, A. E., Wantha, L. Population Balance Modeling of the Solution Mediated Transformation of Polymorphs: Limitations and Future Trends, *Journal of Crystal Growth* 2013, 373, 7-12.
- [Gar02] Garcia, E., Hoff, C., Veesler, S. Dissolution and Phase Transition of Pharmaceutical Compounds, *J. Cryst. Growth* 2002, 237-239, 2233-2239.
- [Gre10] Greco, K., Bogner, R. Crystallization of Amorphous Indomethacin during Dissolution: Effect of Processing and Annealing, *Mol. Pharmaceutics* 2010, 7, 1406–1418.
- [Gru96] Grunenberg, A., Henck, J.-O., Siesler, H.W. Theoretical Derivation and Practical Application of Energy/Temperature Diagrams as an Instrument in Preformulation Studies of Polymorphic Drug Substances, *Int.J.Pharm.* 1996, 129, 147-158.

- [Gu01] Gu, C.-H., Young Jr., V., Grant, D. J.W. Polymorph Screening: Influence of Solvents on the Rate of Solvent-Mediated Polymorphic Transformation, *Journal of Pharmaceutical Sciences* 2001, 90(11), 1878-1890.
- [Guo10] Guo, J., Jones, M. J., Ulrich, J. Polymorphism of 3,3'-Dihydroxy-b,b-Carotene-4,4'-dione (Astaxanthin), *Chemical Engineering Research and Design* 2010, 88, 1648-1652.
- [Guo18] Guo, N., Hou, B., Wang, N., Xiao, Y., Huang, J., Guo, Y., Zong, S., Hao, H. In Situ Monitoring and Modeling of the Solution-Mediated Polymorphic Transformation of Rifampicin: From form II to form I, *Journal of Pharmaceutical Sciences* 2018, 107(1), 344-352.
- [Gut18] Guthrie, S. M., Smilgies, D.-M., Giri, G. Controlling Polymorphism in Pharmaceutical Compounds Using Solution Shearing, *Cryst. Growth Des.* 2018, 18, 2, 602-606.
- [Har09] Haruki, M., Kobayashi, F., Kishimoto, K., Kihara, S.-I., Takishima, S. Measurement of the Solubility of Metal Complexes in Supercritical Carbon Dioxide Using a UV-Vis spectrometer, *Fluid Phase Equilib.* 2009, 280, 49-55.
- [Har16] Hartwig, A., Ulrich, J. Influences of Ethanol on the Thermodynamics and Kinetics in the Crystallization of Xylitol, *Crystal Research & Technology* 2016, 51, 6, 405-408.
- [Hea17] Healy, A. M., Worku, Z. A., Kumar, D., Madi, A. M. Pharmaceutical Solvates, Hydrates and Amorphous Forms: A Special Emphasis on Crystals, *Adv. Drug Delivery Rev.* 2017, 117, 25-46.
- [Hei12] Heinrich, J., Ulrich, J. Application of Laser-Backscattering Instruments for In Situ Monitoring of Crystallization Processes – A Review, *Chem. Eng. Technol* 2012, 35, 6, 967-979.
- [Hel13a] Hellstén, S., Han, B., Mäkilä, E., Niemi, H., Salonen, J., Lehto, V.-P., Stelzer, T., Louhi-Kultanen, M., Ulrich, J. Insights into the Evaporation Kinetics of Indomethacin Solutions, *Chem Eng Technol* 2013, 36, 8, 1300-1306.
- [Hel13b] Helmdach, L., Feth, M. P., Ulrich, J. Integration of Process Analytical Technology Tools in Pilot-Plant Setups for the Real-Time Monitoring of Crystallizations and Phase Transitions, *Org. Process Res. Dev.* 2013, 17, 3, 585-598.
- [Hel15] Helmdach, L., Feth, M. P., Ulrich, J. Application of Ultrasound Measurements as PAT Tools for Industrial Crystallization Process Development of Pharmaceutical Compounds *Org. Process Res. Dev.* 2015, 19, 1, 110-121.
- [Her12] Herman, C., Haut, B., Douieb, S., Larcy, A., Vermylen, V., Leysens, T. Use of in Situ Raman, FBRM, and ATR-FTIR Probes for the Understanding of the Solvent-Mediated Polymorphic Transformation of II-I Etiracetam in Methanol, *Org. Process Res. Dev.* 2012, 16, 49-56.
- [Hix31] Hixson, A.W., Crowell, J. H. Dependence of Reaction Velocity upon Surface and Agitation, *Ind. Eng. Chem.* 1931, 23(8), 923-931.
- [Hu05] Hu, Y., Liang, J. K., Myerson, A. S., Taylor, L. S. Crystallization Monitoring by Raman Spectroscopy: Simultaneous Measurement of Desupersaturation Profile and Polymorphic Form in Flufenamic Acid Systems, *Ind. Eng. Chem. Res.* 2005, 44, 1233-1240.
- [Jak16a] Jakubiak P, Wagner B, Grimm H. P., Petrig-Schaffland J, Schuler F, Alvarez-Sanchez R. Development of a Unified Dissolution and Precipitation Model and Its Use for the Prediction of Oral Drug Absorption, *Mol Pharm.* 2016, 13(2), 586-598.
- [Jak16b] Jakubiak, P., Schuler, F., Alvarez-Sánchez, R. Extension of the Dissolution-Precipitation Model for Kinetic Elucidation of Solvent-Mediated Polymorphic Transformations, *European Journal of Pharmaceutics and Biopharmaceutics* 2016, 109, 43-48.

- [Jin10] Jin, Y. S., Ulrich, J. New Crystalline Solvates of Atorvastatin Calcium, *Chemical Engineering technology* 2010, 33, 5, 839-844.
- [Jor02] Jørgensen, A., Rantanen, J., Karjalainen, M., Khriachtchev, L., Räsänen, E., Yliruusi, J. Hydrate Formation During Wet Granulation Studied by Spectroscopic Methods and Multivariate Analysis, *Pharm. Res.* 2002, 19, 1285-1291.
- [Jou02] Jourani, A., Bounahmidi, T. Kinetics of Hydroxyapatite Heterogeneous Nucleation and Crystal Growth During Spontaneous Calcium Phosphate Precipitation in Sugar Solutions, *Chem. Eng. J.* 2002, 89, 185-192.
- [Jub16] Jubana, A., Briançona, S., Puel, F. Processing-Induced-Transformations (PITs) During Direct Compression: Impact of Tablet Composition and Compression Load on Phase Transition of Caffeine, *International Journal of Pharmaceutics* 2016, 501, 253-264.
- [Jun05] Lu, J. J., Ulrich, J. The Influence of Supersaturation on Crystal Morphology – Experimental and Theoretical Study, *Crystal Research and Technology* 2005, 40, 839-846.
- [Kam67] Kamio, H., Nakamachi, H. Water of Crystallization in Disodium 5'-Inosinate and Disodium 5'-Guanylate and Their Mixed Crystal Formation, *Yakugaku Zasshi.* 1967, 87, 1436-1441.
- [Kan15] Kanajia, P., Poovizhi, P., Ng, W. K., Tan, R. B. H. Amorphous Formulations for Dissolution and Bioavailability Enhancement of Poorly Soluble APIs, *Powder Technol.* 2015, 285, 2–15.
- [Kat80] Katti, S., Seshadri, T., Viswamitra, M. Structure and Conformation of Disodium Guanosine-5'-Phosphate Heptahydrate  $C_{10}H_{13}N_5O_8PNa_2 \cdot 7H_2O$ , *Curr. Sci.* 1980, 49 (14), 533– 535.
- [Kel09] Kelly, R. C., Rodríguez-Hornedo, N. Solvent Effects on the Crystallization and Preferential Nucleation of Carbamazepine Anhydrous Polymorphs: A Molecular Recognition Perspective, *Org. Process Res. Dev.* 2009, 13, 6, 1291–1300.
- [Kes13] Kestur, U. S., Ivanovic, I., Alonzo, D. E., Taylor, L. S. Influence of Particle Size on the Crystallization Kinetics of Amorphous Felodipine Powders, *Powder Technol.* 2013, 236, 197-204.
- [Kim01] Kim, K.-J., Mersmann, A. Estimation of Metastable Zone Width in Different Nucleation Processes, *Chem. Eng. Sci.* 2001, 56, 2315-2323.
- [Kim15] Kim, K. J., Doherty, M. F. Crystallization of Selective Polymorph using Relationship between Supersaturation and Solubility, *AIChE* 2015, 61, 1372–1379.
- [Kim22a] Kim, J., Ulrich, J. Thermodynamic Study on Amorphous Form and Crystalline Hydrates by in Situ Raman and FBRM, *Chem. Eng. Technol.* 2022, 45, 291–301.
- [Kim22b] Kim, J., Ulrich, J. Finding Conditions to Process Hydrate Crystals and Amorphous Solids of Disodium Guanosine 5'-Monophosphate by an Anti-solvent Crystallization Process, *Cryst. Res. Technol.* 2022, 57, 2100176, 1-14.
- [Kim22c] Kim, J., Ulrich, J. Nucleation Behavior in a Transformation of Amorphous State to Crystalline State during Anti-solvent Crystallization, *Ind. Eng. Chem. Res.*, 2022, 61(20), 7052–7066.
- [Kim22d] Kim, J., Ulrich, J. Dissolution and Growth Kinetics and the Rate-Controlling Step in Transformation of Amorphous to Crystalline Phase Using Antisolvent Crystallization, *Ind. Eng. Chem. Res.*, 2022, 61 (39), 14609–14625.
- [Kit09] Kitamura, M. Strategy for Control of Crystallization of Polymorphs, *CrystEngComm*, 2009, 11, 949–964.
- [Kit13] Kitamura, M., Horimoto, K. Role of Kinetic Process in the Solvent Effect on Crystallization of BPT Propyl Ester Polymorph, *Journal of Crystal Growth* 2013, 373,

- 151-155.
- [Kit93] Kitamura, M. Crystallization Behavior and Transformation Kinetics of L-histidine Polymorphs, *J. Chem. Eng. of Japan* 1993, 26(3), 303-307.
- [Lee11] Lee, S., Choi, A., Kim, W.-S., Myerson, A. S. Phase Transformation of Sulfamerazine Using a Taylor Vortex, *Cryst. Growth Des.* 2011, 11, 11, 5019–5029.
- [Lew01] Lewiner, F., Klein, J. P., Puel, F., Fe´votte, G. On-line ATR FTIR Measurement of Supersaturation During Solution Crystallization Processes. Calibration and Applications on Three Solute/Solvent Systems, *Chem. Eng. Sci.* 2001, 56, 2069-2084.
- [Lie11] Liu B. S., Sun H., Wang J.K., Yin Q. X. Solubility of disodium 5'-guanylate heptahydrate in aqueous methanol mixtures, *Food Chemistry* 2011, 128, 218-221.
- [Lok13] Lokhandwala, H., Deshpande, A., Deshpande, S. Kinetic Modeling and Dissolution Profiles Comparison: An Overview, *Int J Pharm. Bio. Sci.* 2013, 4(1), 728 – 737.
- [Lu05] Lu, J. J., Ulrich, J. The Influence of Supersaturation on Crystal Morphology – Experimental and Theoretical Study, *Crystal Research and Technology* 2005, 40, 9, 839-846.
- [Mah12] Maher, A., Croker, D. M., Rasmuson, A. C., Hodnett, B. K. Solution Mediated Polymorphic Transformation: Form II to Form III Piracetam in Ethanol, *Cryst. Growth Des.* 2012, 12, 12, 6151–6157.
- [Mah14] Maher, D., Croker, M., Seaton, C. C., Rasmuson, Å. C., Hodnett, B. K. Solution-mediated Polymorphic Transformation: Form II to Form III Piracetam in Organic Solvents, *Crystal Growth Des.* 2014, 14, 3967–3974.
- [Man09] Mangin, D., Puel, F., Veesler, S. Polymorphism in Processes of Crystallization in Solution: A Practical Review, *Org. Process Res. Dev.* 2009, 13, 6, 1241–1253.
- [Mar99] Maruyama, S., Ooshima, H., Kato, J. Crystal Structures and Solvent-Mediated Transformation of Taltireline Polymorphs, *Chemical Engineering Journal* 1999, 75(3), 193-200.
- [Mer01] Mersmann, A. *Crystallization Technology Handbook*, M. Dekker: New York, 2001.
- [Mik04] Mikhailenko, M. A. Growth of Large Single Crystals of the Orthorhombic Paracetamol, *J. Cryst. Growth* 2004, 265 (3-4), 616– 618.
- [Mor15] Mori, Y., Maruyama, M., Takahashi, Y., Ikeda, K., Fukukita, S., Yoshikawa, H. Y., Okada, S., Adachi, H., Sugiyama, S., Takano, K. Selective Crystallization of Metastable Phase of Acetaminophen by Ultrasonic Irradiation, *Appl. Phys. Express* 2015, 8 (6), 065501.
- [Mos14] Mostafavi, M., Petersen, S., Ulrich, J. Effect of Particle Shape on Inline Particle Size Measurement Techniques *Chem. Eng. Technol* 2014, 37, 10, 1721-1728.
- [Mul93] Mullin, J. W. *Crystallization*, Butterworth-Heinemann Ltd.: Oxford, 1993.
- [Mun14] Munroe, A., Croker, D. M., Rasmuson, A. C., Hodnett, B. K. Solution-Mediated Polymorphic Transformation of FV Sulphathiazole, *Cryst. Growth Des.* 2014, 14, 7, 3466–3471.
- [Mur02] Murphy, D, Rodríguez-Cintrón F, Langevin B, Kelly R.C., Rodríguez-Hornedo N, Solution-Mediated Phase Transformation of Anhydrous to Dihydrate Carbamazepine and the Effect of Lattice Disorder, *International Journal of Pharmaceutics* 2002, 246, 121-134.
- [Ngu08] Nguyen, TNP, Kim K. J., Kinetic Study on Hemipenta Hydrate Risedronate Monosodium in Batch Crystallization by Cooling Mode, *International Journal of Pharmaceutics* 2008, 364, 1–8.
- [Ngu11] Nguyen, A. T., Kang, J. K., Choi, G. J., Kim, W. S. Phase Transformation of Guanosine 5'-Monophosphate in Drowning-out Crystallization: Comparison of

- Experimental Results with Mathematical Modeling, *Cryst. Res. Technol.* 2011, 46 (1) 53–60.
- [Ngu15] Nguyen, D. L. T., Kim, K. J. Inline Monitoring of Taltirelin Crystallization in Batch Cooling Mode Using Raman Spectroscopy, *Chem. Eng. Technol.* 2015, 38, 1059-1067.
- [Oci11] O’Ciardhá, C. T., Frawley, P. J., Mitchell, N. A. Estimation of the Nucleation Kinetics for the Anti-solvent Crystallisation of Paracetamol in Methanol/Water Solutions, *J. Cryst. Growth* 2011, 328 (1), 50–57.
- [Ogr07] O’Grady, D., Barrett, M., Casey, E., Glennon, B. The Effect of Mixing on the Metastable Zone Width and Nucleation Kinetics in the Anti-Solvent Crystallization of Benzoic Acid, *Chem. Eng. Res. Des.* 2007, 85, 945–952.
- [Oma06a] Omar, W., Mohnicke, M., Ulrich, J. Determination of the Solid Liquid Interfacial Energy and Thereby the Critical Nucleus Size of Paracetamol in Different Solvents, *Cryst. Res. Technol.* 2006, 41, 337–343.
- [Oma06b] Omar, W., Ulrich, J. Solid Liquid Equilibrium, Metastable Zone, and Nucleation Parameters of the Oxalic Acid–Water system, *Cryst. Growth Des.* 2006, 6(8), 1927–1930.
- [Oma07] Omar, W. Ulrich, J. Determination of Nucleation Parameters and the Solid Liquid Interfacial Energy of the KCl-Ethanol-Water System, *Crystal Research & Technology* 42, 2007, 432-439.
- [Oma08] Omar, W., Al-Sayed, S., Sultan, A., Ulrich, J. Growth Rate of Single Acetaminophen Crystals in Supersaturated Aqueous Solution under Different Operating Conditions, *Cryst. Res. & Technol.* 2008, 43, 22-27.
- [Oma12] O’Mahony, M. A., Maher, A., Croker, D. M., Rasmuson, A. C., Hodnett, B. K. Examining Solution and Solid State Composition for the Solution-Mediated Polymorphic Transformation of Carbamazepine and Piracetam, *Cryst. Growth Des.* 2012, 12, 4, 1925–1932.
- [Oma13] O’Mahony, M. A., Seaton, C. C., Croker, D. M., Veessler, S., Rasmuson, Å. C., Hodnett, K. Investigation into the Mechanism of Solution-Mediated Transformation from FI to FIII Carbamazepine: The Role of Dissolution and the Interaction Between Polymorph Surfaces, *Cryst. Growth Des.* 2013, 13(5), 1861-1871.
- [Ono04] Ono, T., Ter Horst, J. H., Jansens, P. J. Quantitative Measurement of the Polymorphic Transformation of L-Glutamic Acid Using In-Situ Raman Spectroscopy, *Cryst. Growth Des.* 2004, 4, 465-469.
- [Ost97] Ostwald, W. Studien Ueber Die Bildung und Umwandlung Fester Koerper, *Z Physik Chem.* 1897, 22, 289–330.
- [Ouy21] Ouyang, J., Chen, J., Rosbottom, I., Chen, W., Guob M., Heng, J. Y. Supersaturation and Solvent Dependent Nucleation of Carbamazepine Polymorphs During Rapid Cooling Crystallization, *Cryst. Eng. Comm.*, 2021, 23, 813-823.
- [Pan18] Pana, B., Wei, H., Jiang, J., Zong, S., Lv, P., Dang, L. Solution-Mediated Polymorphic Transformation of CL-20: An Approach to Prepare Purified Form  $\epsilon$  Particles, *Journal of Molecular Liquids* 2018, 265, 216-225.
- [Par19] Park, I.H., Yang, H. O., Kim, J. H., Kim, K. J., Solubility Measurement Study on a Metastable Polymorph of  $\beta$ -2,4,6,8,10,12-Hexanitro-2,4,6,8,10,12-Hexaazaisowurtzitane by Raman Spectroscopy, *Cryst. Growth Des.* 2019, 19, 4990–5004.
- [Pin05] Pinho, S. P., Macedo, E. A. Solubility of NaCl, NaBr, and KCl in Water, Methanol, Ethanol, and Their Mixed Solvents, *J. Chem. Eng. Data* 2005, 50, 29–32.
- [Pok06] Pokharkar, V. B., Mandpe, L. P., Padamwar, M. N., Ambike, A. A., Mahadik, K. R.,

- Paradkar, A. Development, Characterization and Stabilization of Amorphous Form of a Low Tg Drug, *Powder Technol.* 2006, 167, 20–25.
- [Qi17] Qi, M.-H., Chen, W.-S., Zhou, H., Chen, J.-Y., Ren, G.-B. Solution-mediated Polymorphic Transformation of Amorphous Form to Form I of Olmesartan Medoxomil in Methanol-Water Mixture Solvents, *Cryst. Res. & Technol.* 2017, 52, 1700038.
- [Qu06a] Qu, H., Louhi-Kultanen, M., Rantanen, J., Kallas, J. Solvent-Mediated Phase Transformation Kinetics of an Anhydrate/Hydrate System, *Cryst. Growth Des.* 2006, 6, 2053-2060.
- [Qu06b] Qu, H., Louhi-Kultanen, M., Kallas, J. Solubility and Stability of Anhydrate/Hydrate in Solvent Mixtures, *International Journal of Pharmaceutics* 2006, 321, 101–107.
- [Reu06] Reutzel-Edens, S. M. Achieving Polymorph Selectivity in the Crystallization of Pharmaceutical Solids: Basic Considerations and Recent Advances, *Current Opinion in Drug Discovery & Development* 2006, 9(6), 806-815.
- [Rod99] Rodríguez-Hornedo, N., Murphy, D. Significance of Controlling Crystallization Mechanisms and Kinetics in Pharmaceutical Systems, *J. Pharm. Sci.* 1999, 88, 651– 660.
- [Ryu 12] Ryu, B., Ulrich, J. Controlled Nucleation and Growth of Protein Crystals by Solvent Freeze-Out, *Cryst. Growth Des.* 2012, 12, 12, 6126–6133.
- [Sal98] Salari, A., Young, R. E. Application of Attenuated Total Reflectance FTIR Spectroscopy to the Analysis of Mixtures of Pharmaceutical Polymorphs, *International Journal of Pharmaceutics* 1998, 163, 157-166.
- [San10] Sangwal, K. On the Interpretation of Metastable Zone Width in Anti-Solvent Crystallization, *Cryst. Res. Technol.* 2010, 45, 909–919.
- [Sch06] Scholl, J., Bonalumi, D., Vicum, L., Mazzotti, M., Muller, M. In Situ Monitoring and Modeling of the Solvent-Mediated Polymorphic Transformation of L-Glutamic Acid, *Cryst. Growth Des.* 2006, 6, 881-891.
- [Sch11] Schuster, A., Stelzer, T., Ulrich, J. Generation of Crystalline Hollow Needles: New Approach by Liquid-Liquid Phase Transformation, *Chem. Eng. Technol.* 2011, 34(4), 599-603.
- [Sei15] Seidel, J., Ulrich, J. Generation of Crystalline Microcontainers of Salicylic Acid, *Chem. Eng. Technol.* 2015, 38(6), 984-990.
- [Sha14] Shah, J. C., Deshpande, A. Kinetic Modeling and Comparison of in Vitro Dissolution Profiles, *World J. Pharm. Sci.* 2014, 2(4), 302-309.
- [Shi21] Shi, G., Li, S., Shi, P., Gong, J., Zhang, M., Tanga, W. Distinct Pathways of Solid-to-Solid Phase Transitions Induced by Defects: the Case of DL-Methionine, *IUCrJ* 2021, 4, 584-594.
- [Sot19] Soto, R., Rasmuson, Å. C. Crystal Growth Kinetics of Piracetam Polymorphs in Ethanol and Isopropanol, *Cryst. Growth Des.* 2019, 19(8), 4273–4286.
- [Sto05] Stoica, C., Tinnemans, P., Meekes, H., Vlieg, E., Van Hoof, P. J. C. M., Kaspersen, F. M. Epitaxial 2D Nucleation of Metastable Polymorphs: A 2D Version of Ostwald's Rule of Stages, *Cryst. Growth Des.* 2005, 5, 975-981.
- [Su10] Su, W., Hao, H., Barrett, M., Glennon, B. The Impact of Operating Parameters on the Polymorphic Transformation of d-Mannitol Characterized in Situ with Raman Spectroscopy, FBRM and PVM, *Org. Process Res. Dev.* 2010, 14, 1432– 1437.
- [Su13] Su, W., Hao, H., Glennon, B. Barrett, M. Spontaneous Polymorphic Nucleation of d-Mannitol in Aqueous Solution Monitored with Raman Spectroscopy and FBRM, *Cryst. Growth Des.* 2013, 13(12), 5179–5187.
- [Tak12] Takiyama, H. Supersaturation Operation for Quality Control of Crystalline Particles

- in Solution Crystallization, *Advanced Powder Technology* 2012, 23( 3), 273-278.
- [Tak16] Takeguchi, K., Obitsu, K., Hirasawa, S., Orii, R., Ieda, S., Okada, M., Takiyama, H. Effect of Temperature and Solvent of Solvent-Mediated Polymorph Transformation on ASP3026 Polymorphs and Scale-up, *Org. Process Res. Dev.* 2016, 20(5), 970–976.
- [Tan20] Tang, W., Sima, A. D., Gong, J., Wang, J., Li, T. Kinetic Difference between Concomitant Polymorphism and Solvent-Mediated Phase Transformation: a Case of Tolfenamic Acid, *Cryst. Growth Des.* 2020, 20(3), 1779–1788.
- [Tao07] Tao, J., Jones, K.J., Yu, L. Cross-Nucleation between d-Mannitol Polymorphs in Seeded Crystallization, *Cryst. Growth Des.* 2007, 7, 12, 2410–2414.
- [Tey08] Teychené, S., Biscans, B. Nucleation Kinetics of Polymorphs: Induction Period and Interfacial Energy Measurements, *Cryst. Growth Des.* 2008, 8, 4, 1133–1139.
- [Thr00] Threlfall, T. Crystallisation of Polymorphs: Thermodynamic Insight into the Role of Solvent, *Org. Proc. Res. Dev.* 2000, 4, 5, 384–390.
- [Tie16] Tieger, E., Kiss, V., Pokol, G., Finta, Z., Dušek, M., Rohlíček, J., Skořepová, E., Brázda, P. Studies on the Crystal Structure and Arrangement of Water in Sitagliptin L-Tartrate Hydrates, *Cryst. Eng. Comm.* 2016, 18, 3819-3831.
- [Tit03] Titiz-Sargut, S., Ulrich J. Application of a Protected Ultrasound Sensor for the Determination of the Width of the Metastable Zone, *Chemical Engineering and Processing: Process Intensification* 2003, 42, 11, 841-846.
- [Tsu18] Tsubonoya, M., Murofushi, A., Yamamura S., Sugawara, Y. Crystal Structure and Sequential Dehydration Transitions of Disodium Guanosine 5'-Monophosphate Tetrahydrate, *Structural Chemistry* 2018, 74, 1153-1159.
- [Tur18] Turner, T. D., Caddick, S., Hammond, R. B., Roberts, K. J., La, X. Kinetics of the Aqueous-Ethanol Solution Mediated Transformation between the Beta and Alpha Polymorphs of p-Aminobenzoic acid, *Cryst. Growth Des.* 2018, 18(2), 1117–1125.
- [Ulr02] Ulrich, J., Strege, C. Some Aspects of the Importance of Metastable Zone Width and Nucleation in Industrial Crystallizers, *Journal of Crystal Growth* 2002, 237, 2130-2135.
- [Ulr03] Ulrich, J. Solution Crystallization-Development and New Trends, *Chem. Eng. Technol.* 2003, 26, 832–835.
- [Ulr04] Ulrich, J., Jones, M.J. Industrial Crystallization: Developments in Research and Technology, *Chemical Engineering Research and Design* 2004, 82, 12, 1567-1570.
- [Ulr15] Ulrich, J., Pietzsch, M. What is a Protein Crystal? Can We Apply the Terminology of Classical Industrial Crystallization to Them? *Cryst. Res. Technol.* 2015, 50, 7, 560-565.
- [Vau06] Vaughn, J. M., McConville, J. T., Crisp, M. T., Johnston, K. P., Williams III, R. O. Supersaturation Produces High Bioavailability of Amorphous Danazol Particles Formed by Evaporative Precipitation into Aqueous Solution and Spray Freezing into Liquid Technologies, *Drug Dev. Ind. Pharm.* 2006, 32, 559-567.
- [Vee03] Veessler, S., Lafferrere, L., Garcia, E., Hoff, C. Phase Transitions in Supersaturated Drug Solution, *Org. Process Res. DeV.* 2003, 7, 983-989.
- [Wan00] Wang, F., Wachter, J. A., Antosz, F. J., Berglund, K. A. An Investigation of Solvent-Mediated Polymorphic Transformation of Progesterone Using in Situ Raman Spectroscopy, *Org. Process Res. DeV.* 2000, 4, 391-395.
- [Wan11] Wang, N., Fu, Q., Yang, G. Determination of the Solubility, Dissolution Enthalpy and Entropy of Icariin in Water, Ethanol, and Methanol, *Fluid Phase Equilibria.* 2011, 306, 171-174.
- [Wan13] Wantha L., Flood A. E. Population Balance Modeling of the Solution-Mediated Transformation of DL-Methionine Polymorphs, *Chem. Eng. Technol.* 2013, 36(8), 1313-1319.

- [Wan15] Wang, G., Ma, Y., Wang, Y., Hao, H., Jiang, Y. Investigation of Solution-Mediated Phase Transformation of Cefuroxime Acid to its Acetonitrile Solvate, *Org. Process Res. Dev.* 2015, 19(12), 1820-1825.
- [Wan17] Wang, Y., Sun, P., Xu, S., Du, S., Zhang, T., Yu, B., Zhang, S., Wang, Y., Gong, J. Solution-Mediated Phase Transformation of Argatroban: Ternary Phase Diagram, Rate-Determining Step, and Transformation Kinetics, *Ind. Eng. Chem. Res.* 2017, 56(15), 4539–4548.
- [Wan18] Wantha, L. Kinetics of the Solution-Mediated Polymorphic Transformation of Organic Compounds, *Current Pharmaceutical Design* 2018, 24, 21, 2383-2393.
- [Wil06] Wildfong, P.L., Morris, K.R., Anderson, C.A., Short, S.M. Demonstration of a Shear-Based Solid-State Phase Transformation in a Small Molecular Organic System: Chlorpropamide, *J. Pharm. Sci.* 2007, 96, 1100-1113.
- [Wol89] Wolff, S. D., Yancey, P. H., Stanton, T. S., Balaban, R. S. A Simple HPLC Method for Quantitating Major Organic Solutes of Renal Medulla, *American Journal of Physiology-Renal Physiology* 1989, 256, F954– F956.
- [Wu06] Wu, T. Yu, L. Surface Crystallization of Indomethacin below T<sub>g</sub>, *Pharm. Res.* 2006, 23, 2350-2355.
- [Xu12] Xu, J., Tian, Y., Liu, Y., Zhang, H., Shu, Y., Sun, J. Polymorphism in Hexanitrohexaazaisowurtzitane Crystallized from Solution, *Journal of Crystal Growth* 2012, 354(1), 13-19.
- [Yam02] Yamanobe, M., Takiyama, H., Matsuoka, M. Polymorphic Transformation of DL-Methionine Crystals in Aqueous Solutions, *J. Cryst. Growth* 2002, 237-239, 2221-2226.
- [Yan20] Yang, H. O., Kim, J. H., Kim, K. J., Study on the Crystallization Rates of  $\beta$ - and  $\epsilon$ -form HNIW in in-situ Raman Spectroscopy and FBRM, *Propellants Explos. Pyrotech.* 2020, 45, 422-430.
- [Yu14] Yu, X., Wang, J., Ulrich, J. Purification of Lysozyme from Protein Mixtures by Solvent-Freeze-Out Technology, *Chem Eng Technol* 2014, 37, 8, 1353-1357.
- [Zha04] Zhang, G.G., Law, D., Schmitt, E.A., Qiu, Y. Phase Transformation Considerations During Process Development and Manufacture of Solid Oral Dosage Forms, *Adv. Drug Deliv. Rev.* 2004, 56, 371-390.
- [Zha11] Zhang, R., Ma, J., Li, J., Jiang, Y., Zheng, M. Effect of pH, Temperature and Solvent Mole Ratio on Solubility of Disodium 5'-Guanylate in Water + Ethanol System, *Fluid Phase Equilibria.* 2011, 303, 35-39.
- [Zhu19] Zhu, M., Wang, Y., Li, F., Bao, Y., Huang, X., Shi, H., Hao, H. Theoretical Model and Experimental Investigations on Solution-Mediated Polymorphic Transformation of Theophylline: from Polymorph I to Polymorph II, *Crystals* 2019, 9(5), 260-273.
- [Zim76] Zimmerman, S. B. X-ray Study by Fiber Diffraction Methods of a Self-Aggregate of Guanosine-5'-Phosphate with the Same Helical Parameters as Poly (rG), *J. Mol. Biol.* 1976, 106 (3), 663– 672.
- [Zon19] Zong, S., Wang, J., Xiao, Y., Sakoth, B., Wu, H., Liu, Q., Zhou, Y., Huang, X., Hao, H. Thermodynamic and Population Balance Models for Solvent-Mediated Phase Transformation of Lansoprazole, *Chemical Engineering Science* 2019, 207, 247-257.
- [Zon19] Zong, S., Wang, J., Xiao, Y., Sakoth, B., Wu, H., Liu, Q., Zhou, Y., Huang, X., Hao, H. Thermodynamic and Population Balance Models for Solvent-Mediated Phase Transformation of Lansoprazole, *Chemical Engineering Science* 2019, 207, 247-257.
- [Zou15] Zou, F., Zhuang, W., Wu, J., Zhou, J., Yang, P., Liu, Q., Chen, Y., Ying, H. Determination of Metastable Zone Widths and the Primary Nucleation and Growth Mechanisms for the Crystallization of Disodium Guanosine 5'-Monophosphate from a

- 
- Water–Ethanol System, *Ind. Eng. Chem. Res.* 2015, 54, 137–145.
- [Zou16] Zou, F., Zhuang, W., Chen, Q., Yang, P. P., Lin, C., Jiao, P., Zhou, J., Wu, J., Ying, H. Solvent Effects on Nucleation of Disodium Guanosine 5'-Monophosphate in Anti-Solvent/Water Mixtures, *Cryst. Eng. Comm.* 2016,18, 6653-6663.
- [Zou17] Zou F., Chen Q., Yang, P., Zhou, J., Wu, J., Zhuang, W., Ying, H. Solution-Mediated Polymorphic Transformation: From Amorphous to Crystals of Disodium Guanosine 5'-Monophosphate in Ethanol, *Ind. Eng. Chem. Res.* 2017, 56, 8274–8282.

## 10. Appendix

Run 2

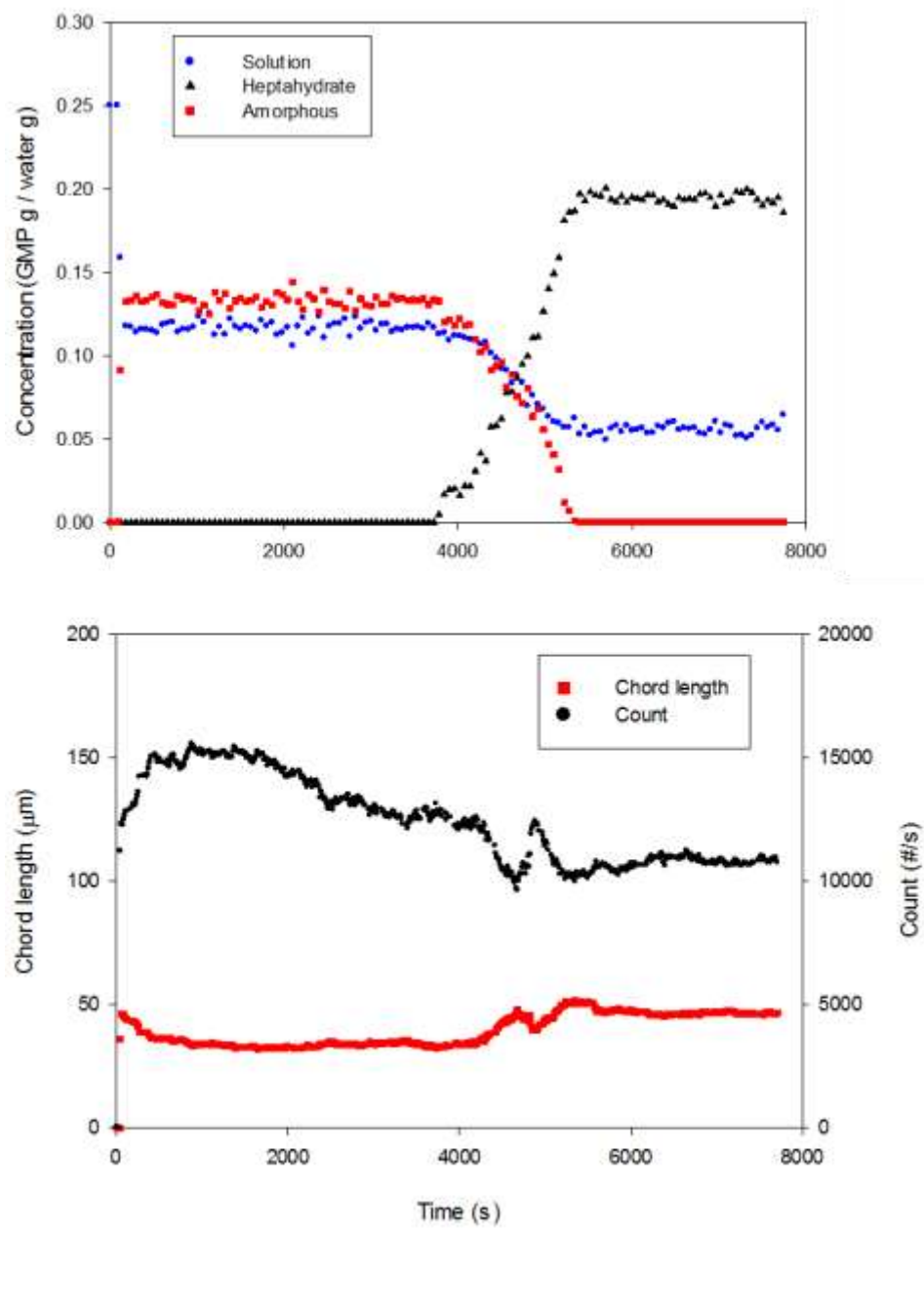
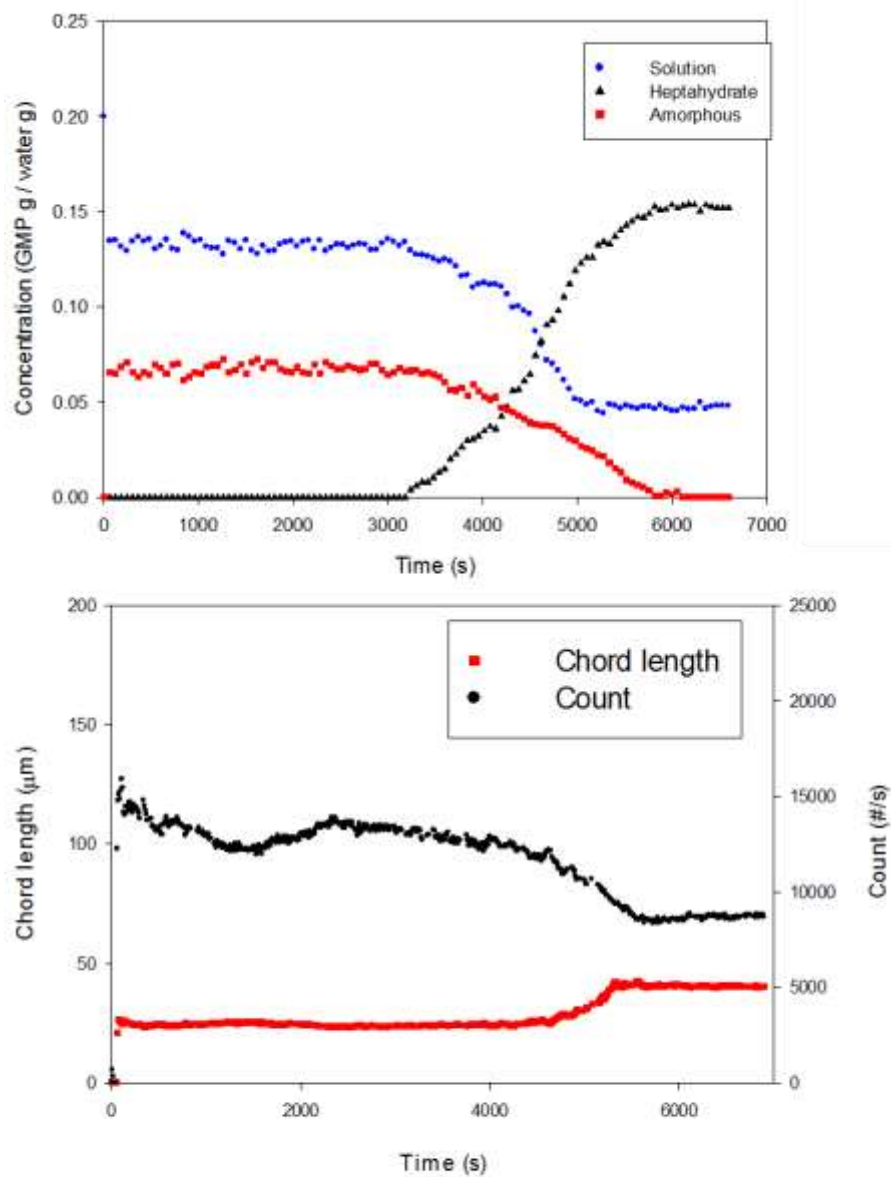
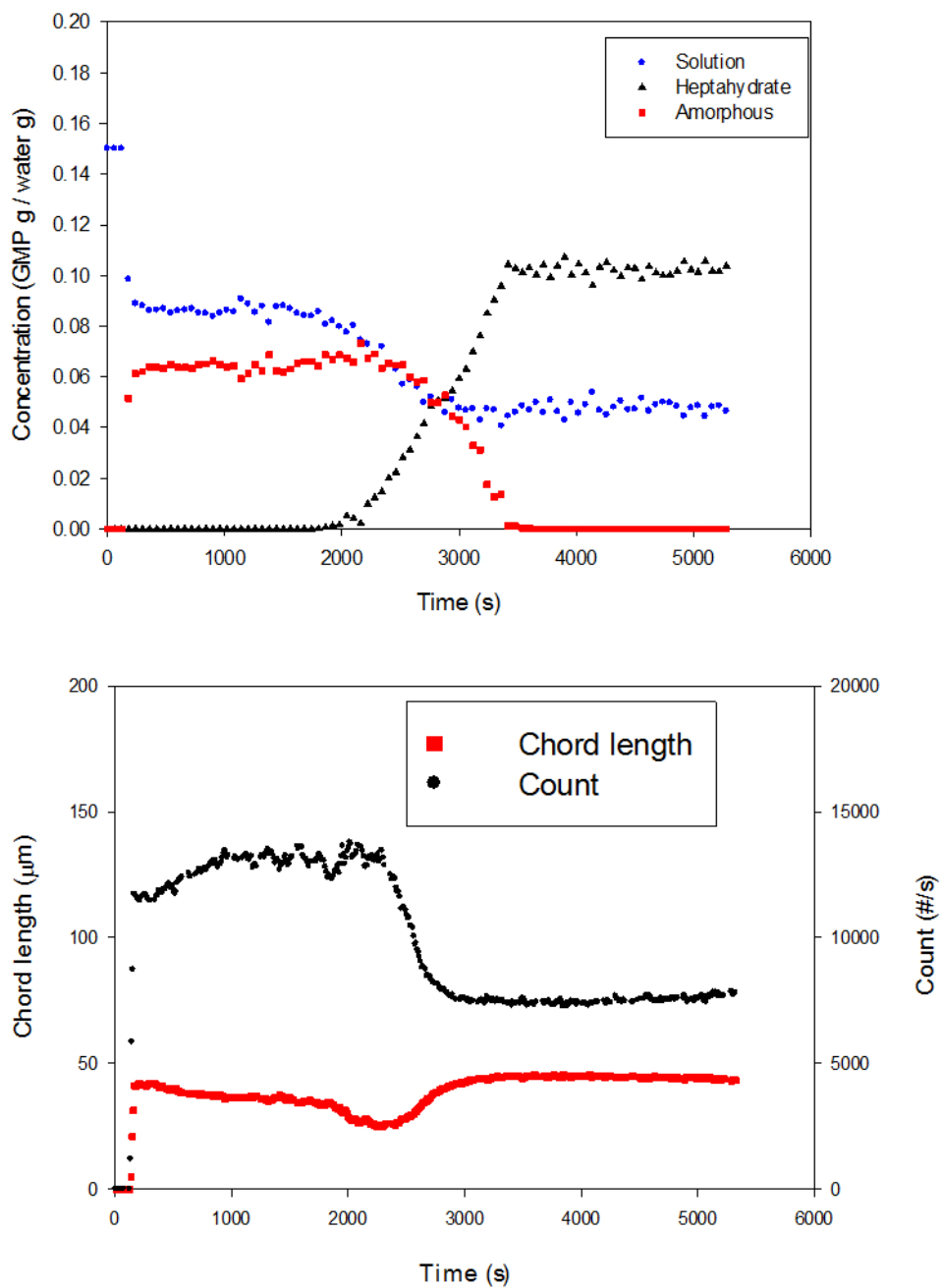


Fig. 10-1: Measurement by in situ Raman spectroscopy and FBRM for Run 2.

Run 3

**Fig. 10-2: Measurement by in situ Raman spectroscopy and FBRM for Run 3.**

## Run 4



**Fig. 10-3: Measurement by in situ Raman spectroscopy and FBRM for Run 4.**

## Run 5

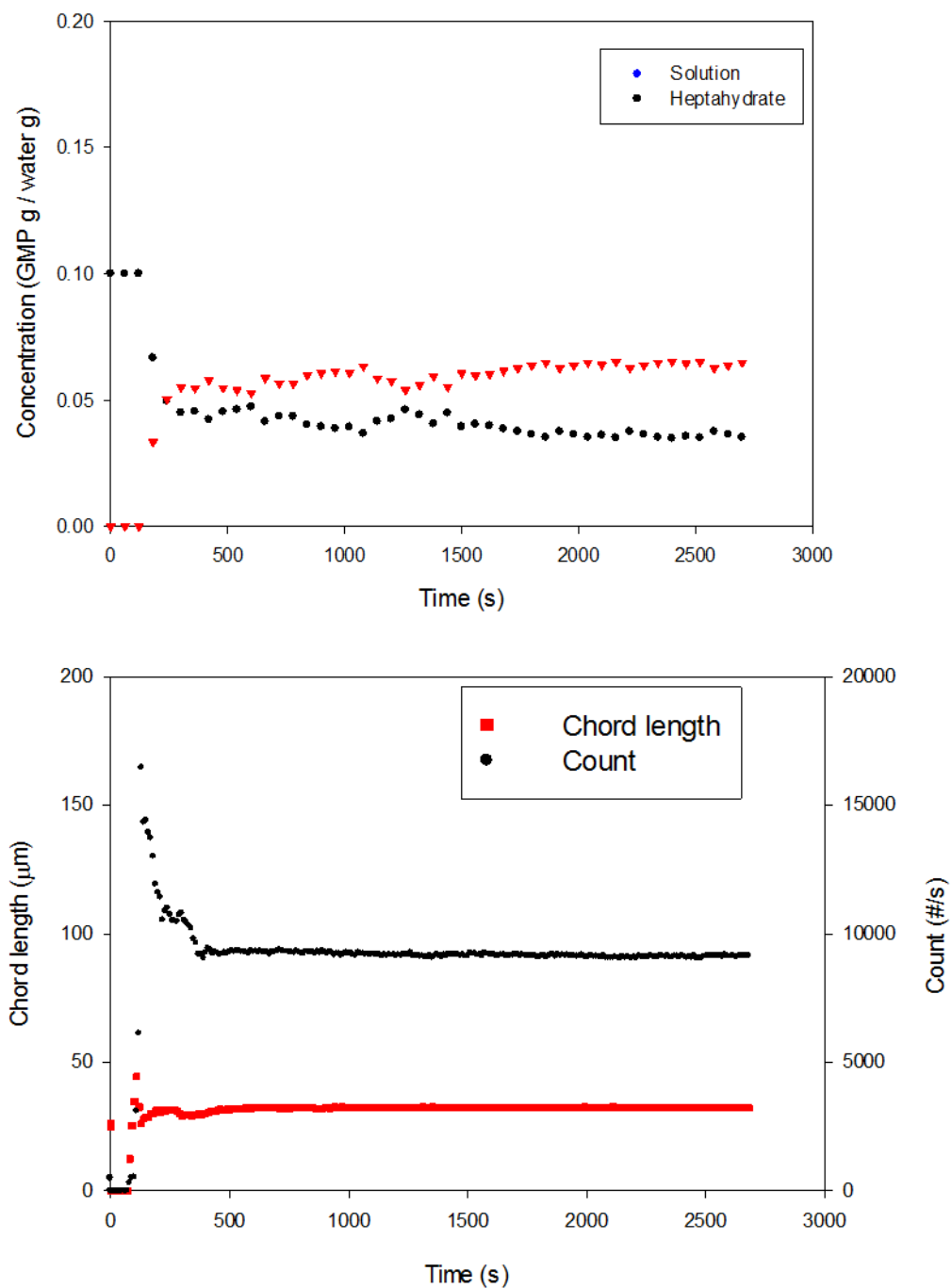


**Fig. 10-4: Measurement by in situ Raman spectroscopy and FBRM for Run 5.**

## Run 6

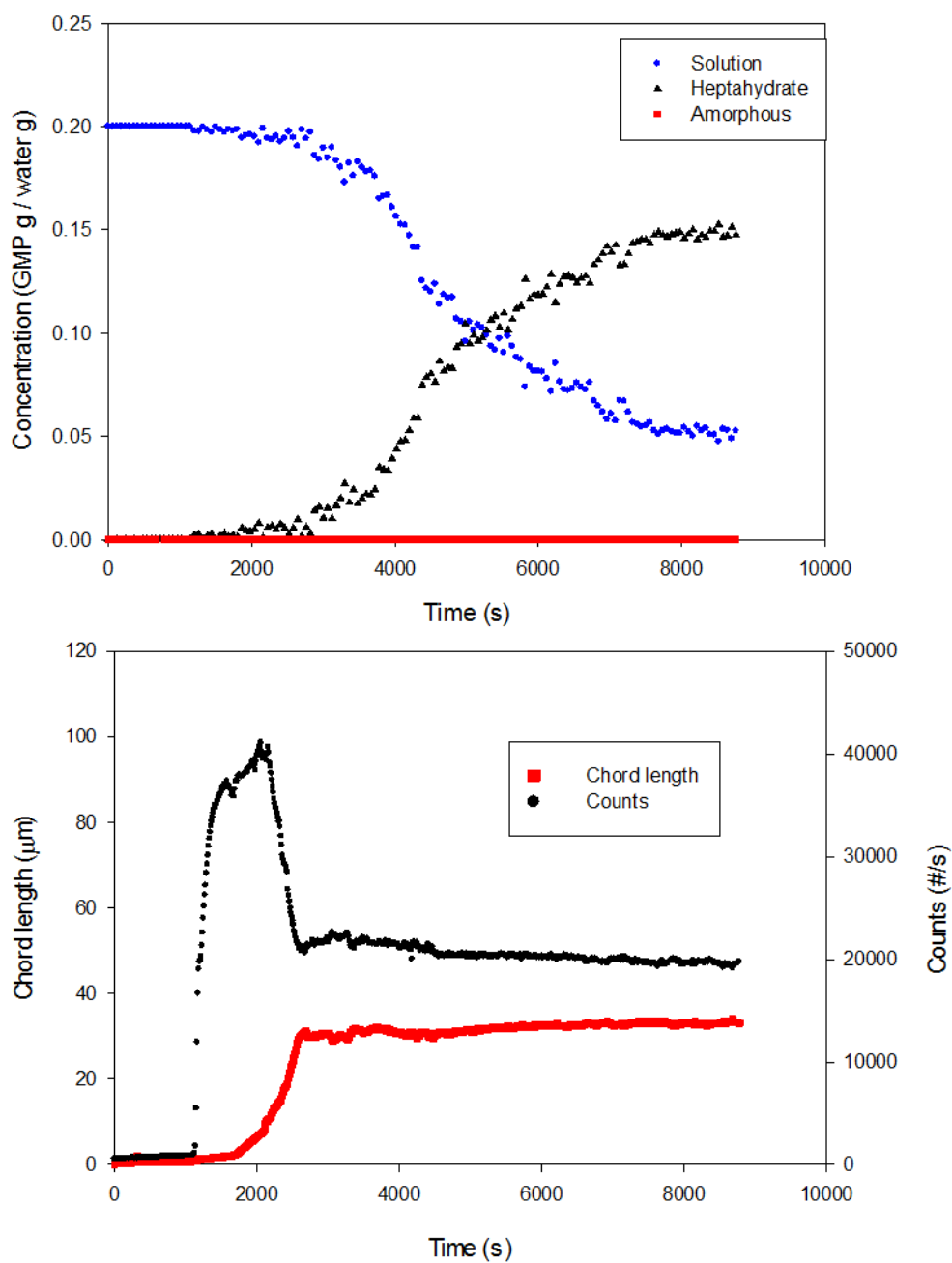


Fig. 10-5: Measurement by in situ Raman spectroscopy and FBRM for Run 6.

## Run 7

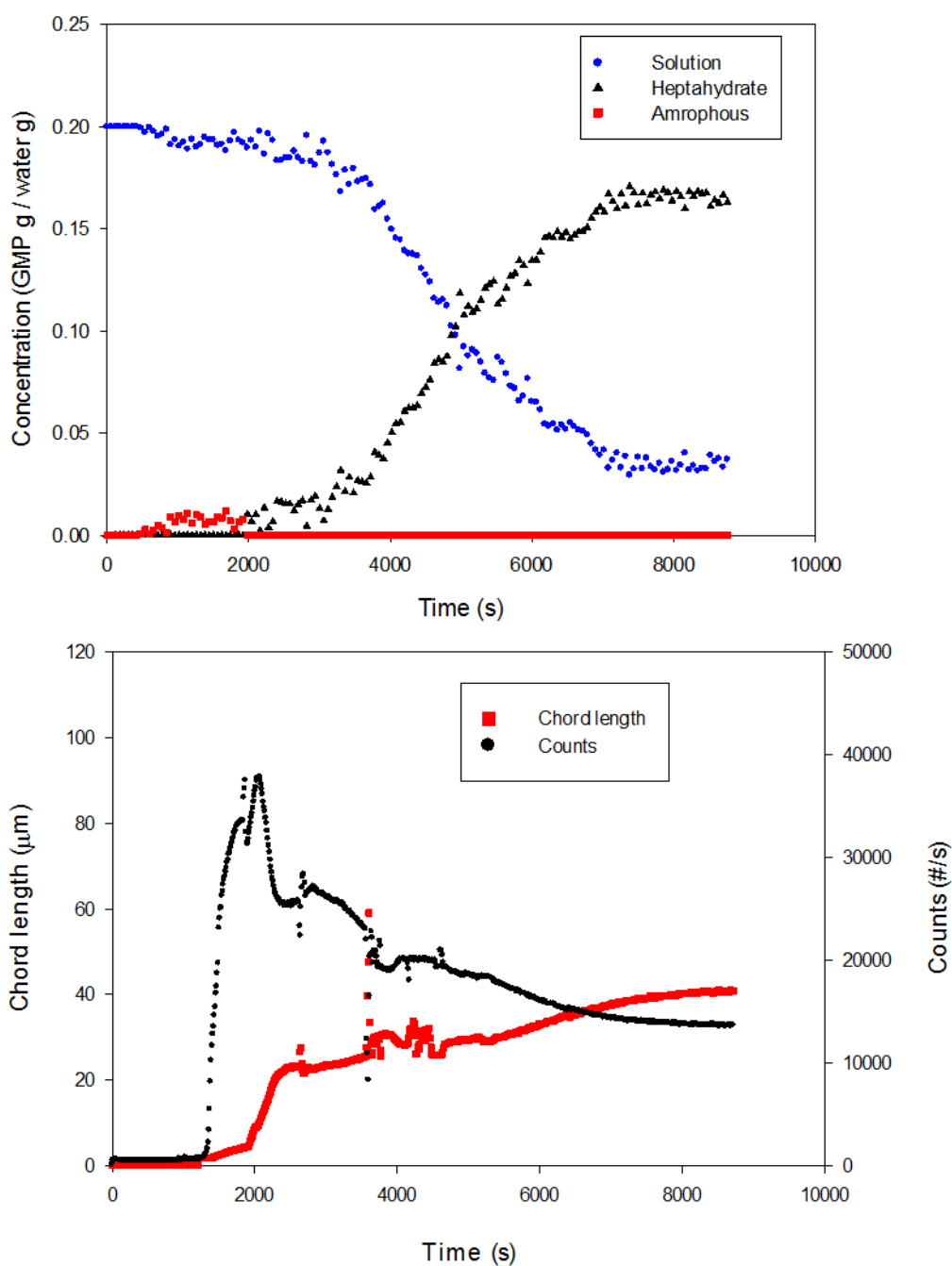


Fig. 10-6: Measurement by in situ Raman spectroscopy and FBRM for Run 7.

Run 8

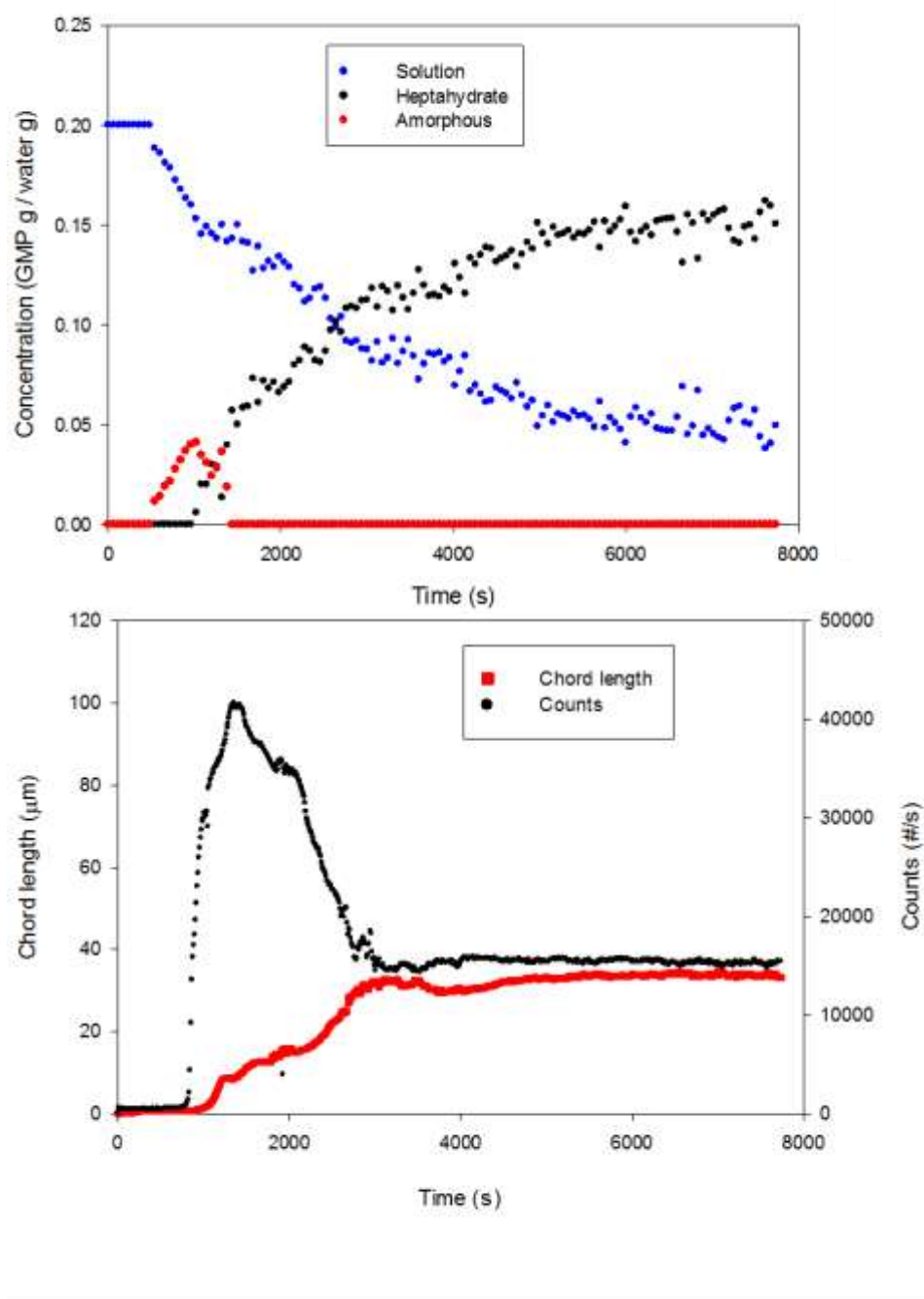


Fig. 10-7: Measurement by in situ Raman spectroscopy and FBRM for Run 8.

## Run 9

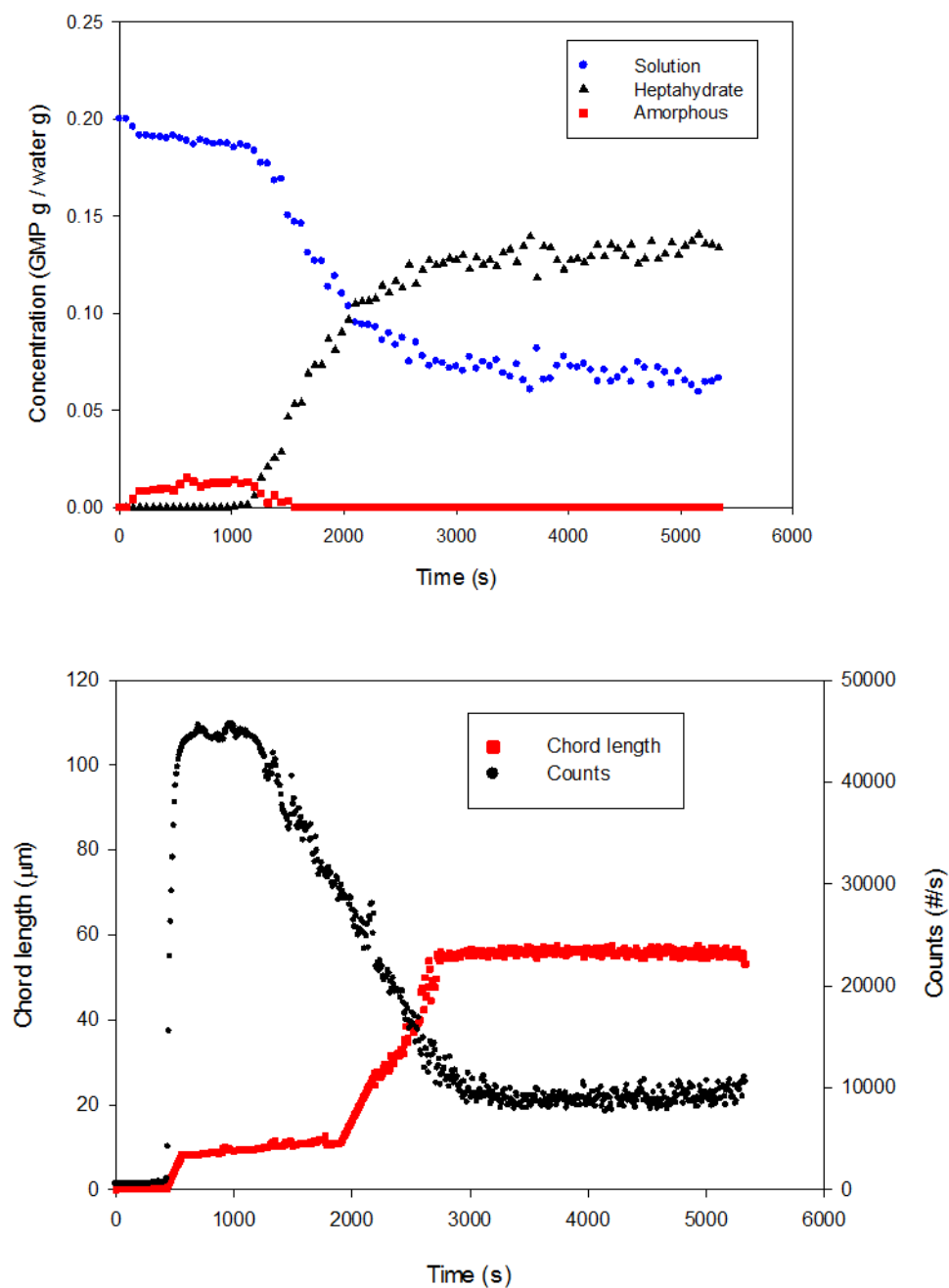
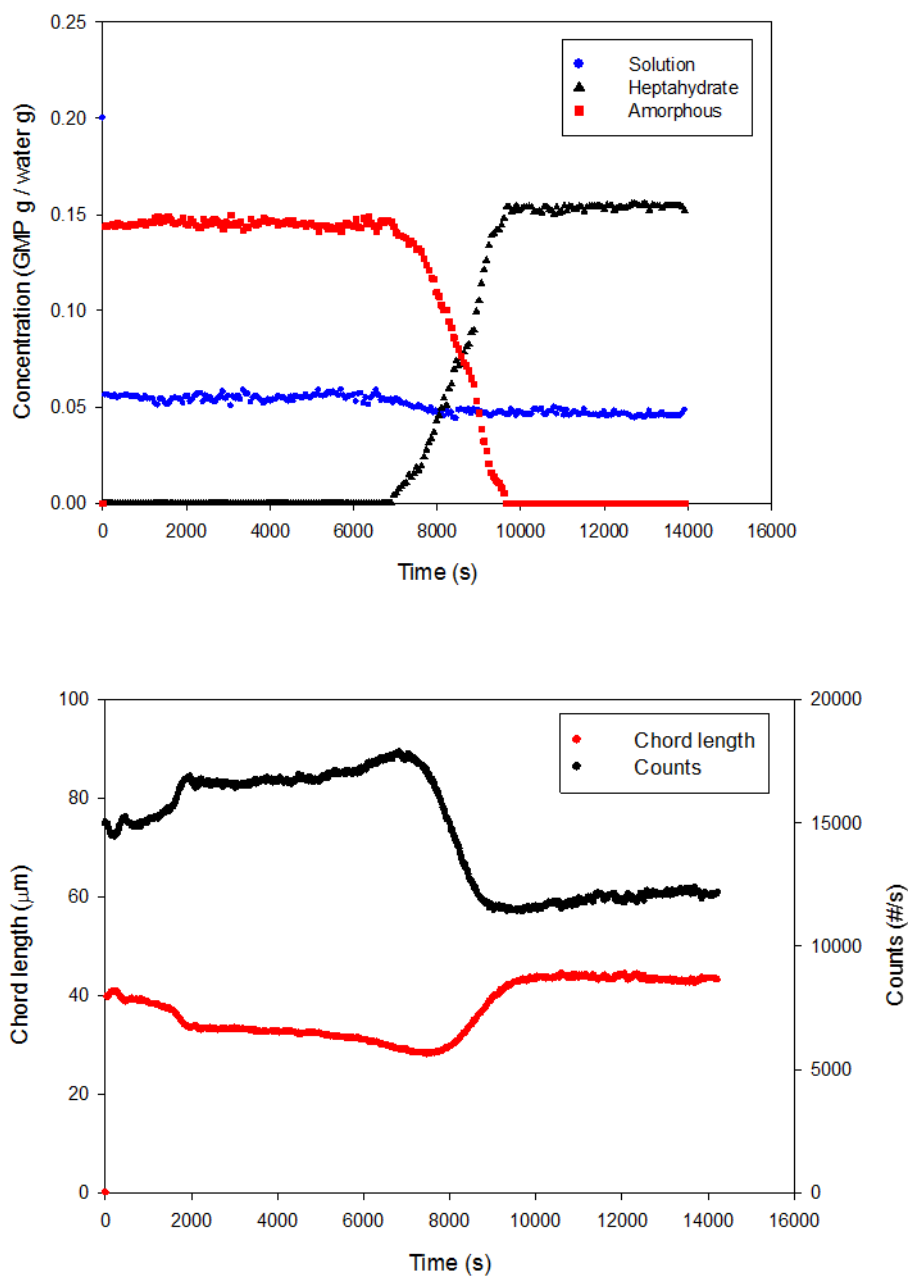
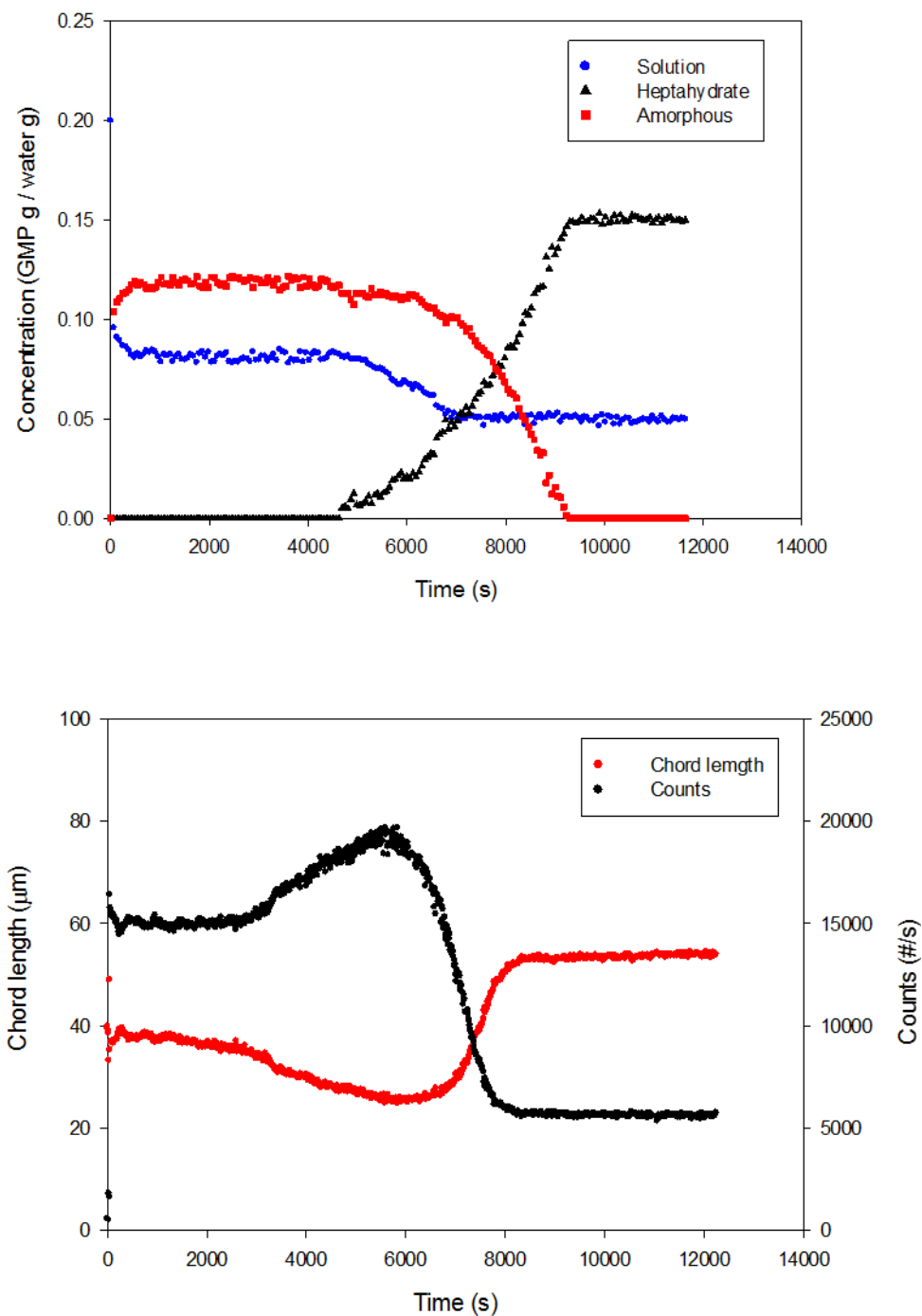


Fig. 10-8: Measurement by in situ Raman spectroscopy and FBRM for Run 9.

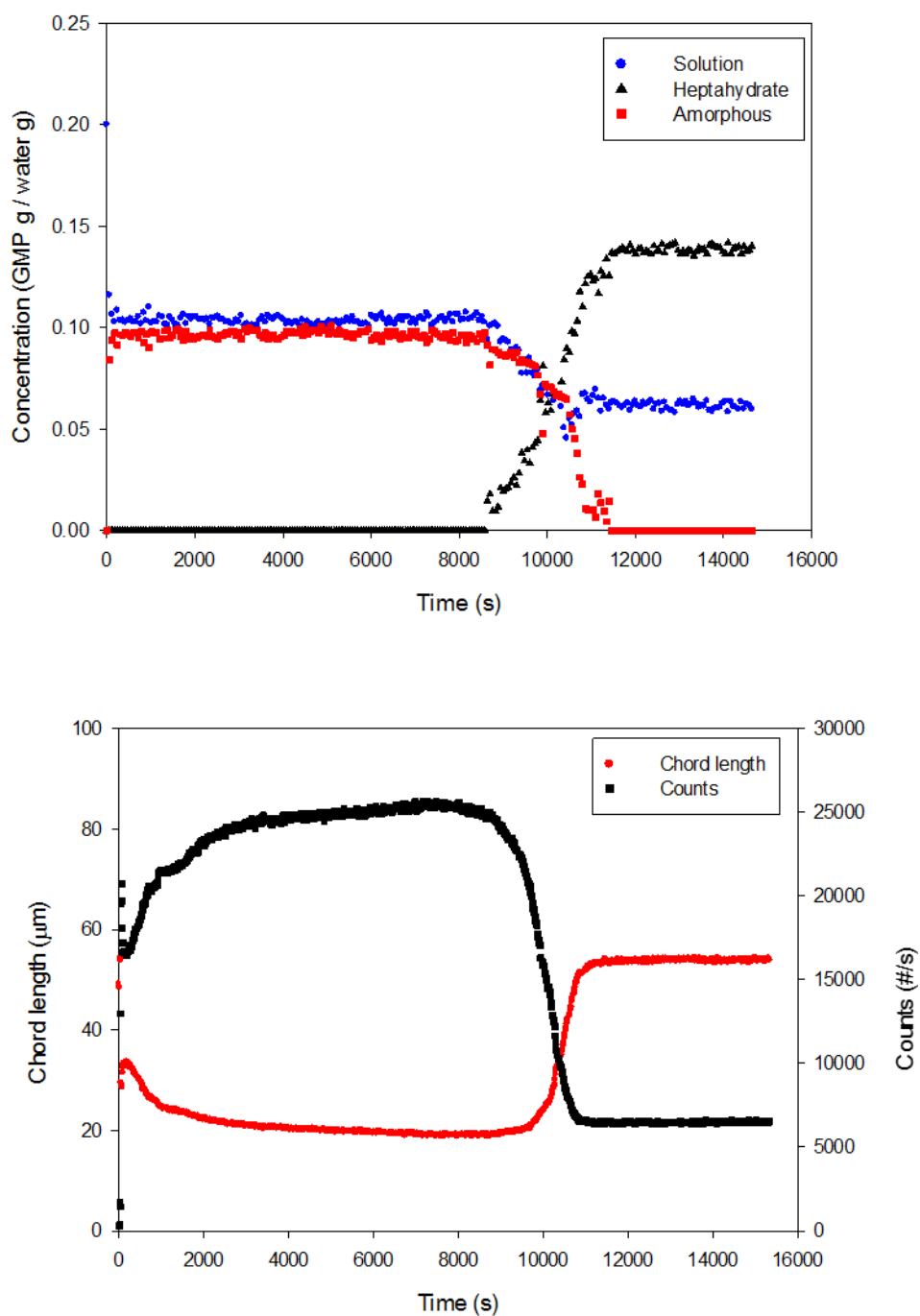
Run 14

**Fig. 10-9: Measurement by in situ Raman spectroscopy and FBRM for Run 14.**

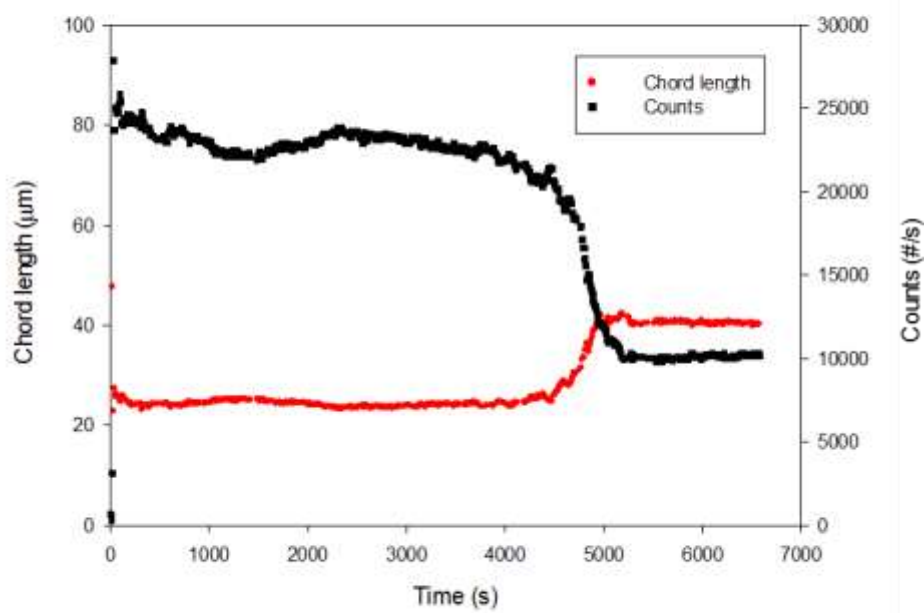
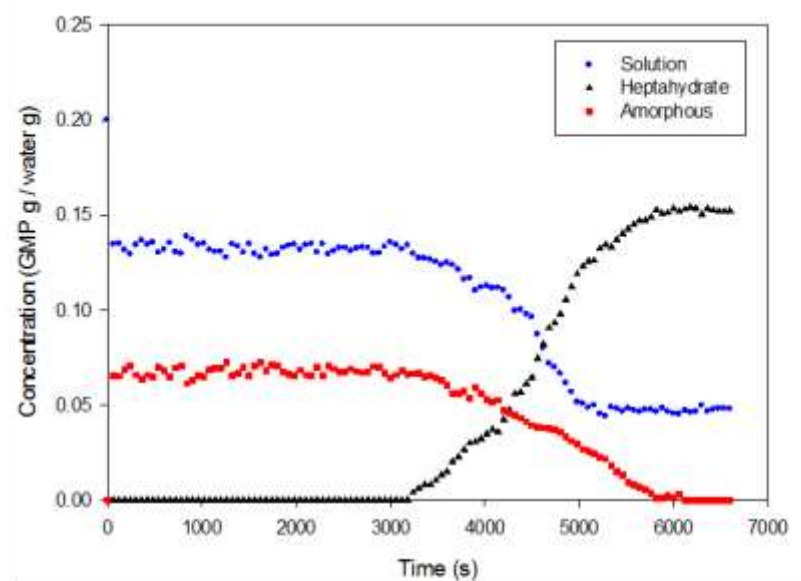
Run 15

**Fig. 10-10: Measurement by in situ Raman spectroscopy and FBRM for Run 15.**

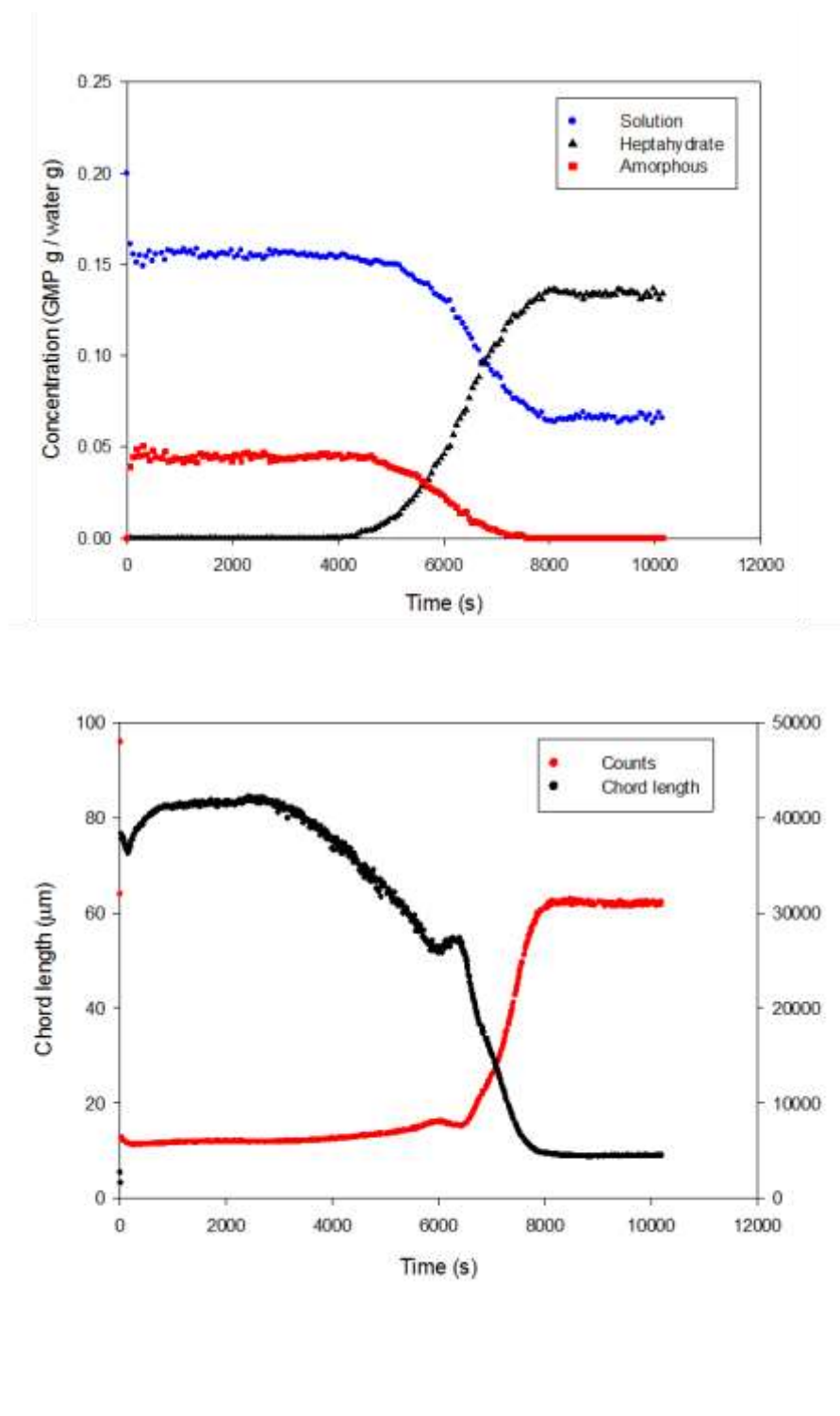
Run 16

**Fig. 10-11: Measurement by in situ Raman spectroscopy and FBRM for Run16.**

Run 17

**Fig. 10-12: Measurement by in situ Raman spectroscopy and FBRM for Run 17.**

Run 18

**Fig. 10-13: Measurement by in situ Raman spectroscopy and FBRM for Run18.**

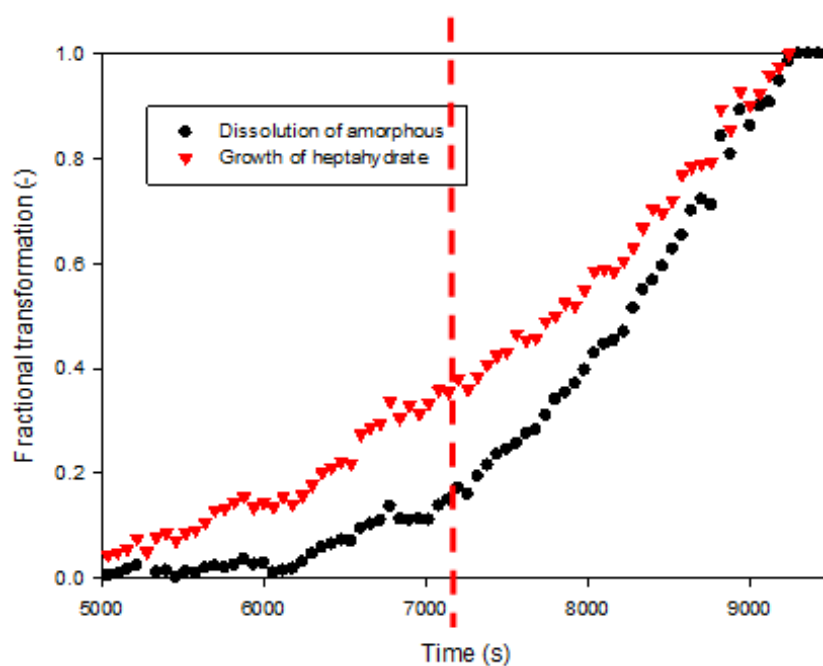


**Fig. 10-14: Calculation of rate constants of dissolution and growth from plot of fractional concentration against time during transformation for Run 10.**

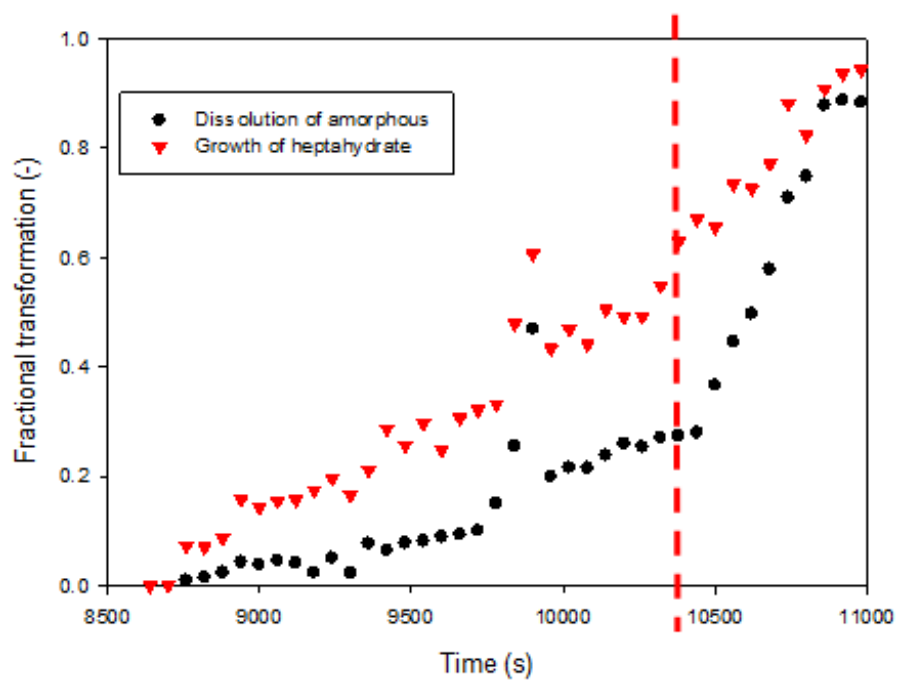


**Fig. 10-15: Calculation of rate constants of dissolution and growth from plot of fractional concentration against time during transformation for Run 11.**

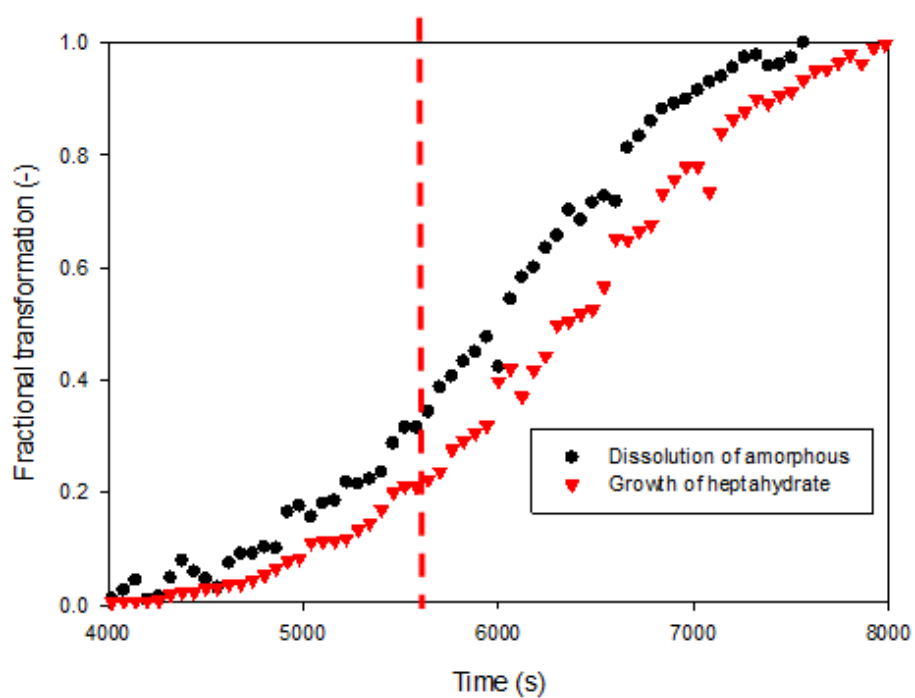


**Fig. 10-16: Calculation of rate constants of dissolution and growth from plot of fractional concentration against time during transformation for Run 12.**

## **Statement of Authorship**

Declaration under Oath

I declare under oath that this thesis is my own work entirely and has been written without any help from other people. I used only the sources mentioned and included all the citations correctly both in word or content.

05/20/2023

Jungsuk Kim

---

## Curriculum Vitae

### Jungsuk Kim

---

First Name: Jungsuk

Last Name: Kim

Date of birth: July 23, 1986 in Deajeon, South Korea

Nationality: Korean

E-mail: click7031@naver.com, jungsuk.kim@natfak1.uni-halle.de

Mobile Number: (+82)10-3434-1320

---

### **Career and Education**

08/2022 – Present	LG Energy Solution, Battery Cell Development, Senior Researcher, Daejeon, Korea
06/2022 – 08/2022	Time out for PhD-research
09/2019 – Present	Supervised by Prof. Dr. J. Ulrich, Chair of Thermal Process Technology, Martin Luther University Halle-Wittenberg, Germany
07/2020 – 05/2022	Korea Electrical Power Research Institute, Hydrogen Fuel Cell, Researcher (contracted), Deajeon, Korea
09/2019 – 06/2020	Crystallization Technology Laboratory, Research Assistance, Deajeon, Korea
05/2018 – Present	PhD Work
06/2016 – 08/2019	Korea Research Institute of Electrical Power, Hydrogen Fuel Cell Catalyst and MEA Development, Researcher, Deajeon, Korea
02/2016	M.Sc. Degree in Chemical Engineering at Sogang University, Korea Master Thesis Entitled: A Study on the Synthesis of P-Phenylenediamine (PPD) from P-Diodobenzene (PDIB) Using Coper( I )
03/2014 – 02/2016	M.Sc. Study in Chemical Engineering at Sogang University, Korea
01/2013 – 09/2013	Korea Research Institute of Chemical Technology, Research Assistance, Practical Work
02/2014	B.Sc. Degree in Chemical Engineering at Daejeon University, Korea
03/2006 – 02/2014	B.Sc. Study in Chemical Engineering at Deajeon University, Korea
03/2002 – 02/2005	Yusung High School in Deajeon, Korea
03/1999 – 02/2002	Eun Middle School in Deajeon, Korea
03/1993 – 02/1999	Eun Elementary School in Deajeon, Korea

---

## Publications

**Kim, J.**, Ulrich, J. Thermodynamic Study on Amorphous Form and Crystalline Hydrates by in Situ Raman and FBRM, *Chem. Eng. Technol.* 2022, 45, 291–301.

**Kim, J.**, Ulrich, J. Finding Conditions to Process Hydrate Crystals and Amorphous Solids of Disodium Guanosine 5'-Monophosphate by an Anti-solvent Crystallization Process, *Cryst. Res. Technol.* 2022, 57, 2100176, 1-14.

**Kim, J.**, Ulrich, J. Nucleation Behavior in a Transformation of Amorphous State to Crystalline State during Anti-solvent Crystallization, *Ind. Eng. Chem. Res.* 2022, 61(20), 7052–7066.

**Kim, J.**, Ulrich, J. Dissolution and Growth Kinetics and the Rate-Controlling Step in Transformation of Amorphous to Crystalline Phase Using Antisolvent Crystallization, *Ind. Eng. Chem. Res.* 2022, 61 (39), 14609–14625.

Yang, S., **Kim, J.**, Choi, M., Kim, Y. Energy Management Technology Development for an Independent Fuel Cell-Battery Hybrid System Using for a Household, *Trans. of Korean Hydrogen and New Energy Society* 2019, 30, 2, 155-162.

Chung, S., Shin, D., Choun, M., **Kim, J.**, Yang, S., Choi, M., Kim, J. W., Lee, J. Overcome Mass Transfer Limitation of PEMFC Cathode via Incorporation of Hydrophobic Carbon Nanostructure, *ECS Transactions* 2018, 85 (13), 475-487.

**Kim, J.**, Lee, J., Lee, S. Y., Choi, W. C., Kang, N. Y., Park, S., Kim, K., Lim, J. S., Park, Y.-K., Seo, H. A Study on the Synthesis of p-Phenylenediamine (PPD) Using Copper Catalyst, *Korean Chemical Engineering Research* 2016, 54, 3, 425-430.

Kim, O.-H., Oh, S.-H., Ahn, C.-Y., Kim, S., Kim, J. K., **Kim, J.**, Yang, S., Choi, M., Cho, Y.-H., Sung, Y.-E., Enhanced Performance of Ionomer Binder with Shorter Side-Chains, Higher Dispersibility, and Lower Equivalent Weight, *Fuel Cells* 2018, 18(6), 71-72.

Ou, K., Yuan, W. W., Choi, M., **Kim, J.**, Kim, Y.-B., Development of New Energy Management Strategy for a Household Fuel Cell/Battery Hybrid System, *Int. J of Energy Research* 2019, 43, 4686-4700.

Lee, S.-Y., **Kim, J.**, Seo, H., Kang, N. Y., Choi, W. C., Park, S., Park, Y.-K., Synthesis of p-Phenylenediamine (PPD) from p-Diiodobenzene Using Copper(I) Catalyst, *The Korean Society of Industrial and Engineering Chemistry*, Vol.2015, 36-36, 2015.

Choi M., Yang S., **Kim, J.**, Jin, H.-J., Rhee, C.-K., Development of 200W Class Direct Formic Acid Fuel Cell Stack using Bi-Modified Pt/C Catalyst by Irreversible Adsorption, 232nd ECS Meeting, October 1-5, 2017.

Han, D., **Kim J.**, Yang, S., Choi, M., Fuel cell (PEMFC) Performance and Optimization According to Outer Quantity, *The Korean Society of Industrial and Engineering Chemistry*, Vol. 2017, 25-25, 2017.